DESIGN, MODELING, AND CONTROL OF AUTOMOTIVE POWER TRANSMISSION SYSTEMS

A DISSERTATION

SUBMITTED TO THE FACULTY OF THE GRADUATE SCHOOL

OF THE UNIVERSITY OF MINNESOTA

BY

Xingyong Song

IN PARTIAL FULFILLMENT OF THE REQUIREMENTS

FOR THE DEGREE OF

DOCTOR OF PHILOSOPHY

Professor Zongxuan Sun, Advisor

June, 2011

Acknowledgement

I would like to express my sincere gratitude to the people who made a significant difference in the successful completion of my doctoral study at the University of Minnesota.

First and foremost, I would like to thank my advisor, Professor Zongxuan Sun, for the extraordinary vision, competence, dedication, generosity, knowledge and guidance he provided me throughout my time at the University of Minnesota. I feel forever grateful to be his first Ph.D. student. His energy and consistent support encouraged me towards completion of my doctoral study. I sincerely appreciate the invaluable insights and continuous inspiration provided by him. What's more, I will never forget the time he spent in reviewing my research outcome, checking the technical details and proof reading the paper drafts. Step by step, he taught me how to express logically and concisely, and demonstrated to me how to become an independent researcher.

I would also like to extend my thanks to my other committee members, Professor Perry Li, Professor Tryphon Georgiou, and Professor Rajesh Rajamani. I'm sincerely grateful to Professor Li for his invaluable advice during my research and coursework, and to Professor Georgiou for his patience whenever I asked questions in his control theory lecture, and to Professor Rajamani for his very helpful advice when I just came to University of Minnesota for graduate study. In addition, I also would like to thank Professor Kim Stelson for serving as my Preliminary exam committee and his time for evaluating my research proposal. Besides, I also want to thank Dr. Pete Seiler for the technical discussion on *LPV* control.

I would also like to acknowledge the financial supports from General Motors Research Center. And I would like to express my sincere gratitude to Dr. Kumar Hebbale and Dr. Chi-Kuan Kao in General Motors Research Center for their constructive comments on my research results.

Besides, I also want to thank my friends and colleagues in my lab, with whom I had the privilege to work and spend time together, including but not limited to Zhen Zhang,

Yu Wang, Pradeep Gillella, Azrin Zulkefli, Chien-Shin Wu, Ke Li, Adam Heinzen, Ali Sadighi, and Matt McCuen, etc. I am grateful for their friendship which made my life easier, happier, and warmer during the long-lasting Minnesota winters

Last but certainly not least, my greatest gratitude goes to my family for their love and long-lasting support. From my parents, Zhenyuan Song and Lanying Cui, I received the most encouragement and strength whenever challenges arose. I'm sincerely grateful for all these years together, and all the happiness we have enjoyed. In addition, my deepest and sincerest gratitude go to my beloved wife, Shuang Li, for her love, understanding, devotions, supports, and encouragements during my study. She has always been an irreplaceable resource of wisdom and strength for me. I feel extremely fortunate to meet and go through all these incredible years with her together.

Abstract

This thesis focuses on investigating the design, modeling and control methodologies, which can enable smooth and energy efficient power transmission for conventional, hybrid and future automotive propulsion systems.

The fundamental requirements of the modern power transmission system are: (1). It should be able to shift the torque transmission ratio efficiently and smoothly to enable the fuel efficient operation of the power source. (2). It should be able to reject/damp out the power source torque oscillation in an energy saving fashion to avoid rough torque transfer to the driveline. Critical factors determining the successful power transmission include the appropriate control of the power transfer key components (clutches), the optimal power transmission coordination with the automotive driveline system, and the capability to smooth out the power source input oscillation in a fuel efficient fashion. To meet these resolutions, this thesis will investigate the enabling design and control methodologies for power transmission in three levels: the fundamental clutch level, the intermediate driveline level, and the entire propulsion system level.

First, the clutch level design is investigated in two categories: open loop control and closed loop control. For the open loop, two key issues are addressed. One is to ensure the consistent initial condition with optimal valve structure design, and the other is the clutch fill process optimization using a customized dynamic programming with reduced computational cost for stiff hydraulic system. For the closed loop control case, the solutions are further divided into two groups. One is to enable feedback with pressure sensor measurement, and the other is to close the control loop without any sensor. Through experiments, both methods are shown to enable precise, fast and robust clutch actuation.

Second, the driveline level design considers optimizing the power transmission coordination with the driveline. Optimal conditions to achieve efficient and smooth torque transfer are formulated. The nonlinear optimization is then solved using the Dynamic Programming.

Finally, in the propulsion system level, the engine start/stop torque oscillation rejection problem for hybrid vehicle and future advanced combustion system is discussed. Through proper formulation, this problem can be treated as disturbance rejection for a linear parameter varying (*LPV*) system under the internal model principle. To experimentally implement the state of the art controller design, two problems should be solved. First, the vibration signal is periodic with changing magnitude, whose generating dynamics has not been studied before and needs to be derived. Second, the current linear time varying internal model control is lack of robustness, and the design method of a low order yet robust internal model stabilizer is still unavailable. This thesis proposes promising approaches to address this fundamental bottleneck issue in the time varying internal model control theory, which is one of the key contributions in this thesis. The proposed stabilizer synthesis method is treated in a general form, and can potentially be applied to other applications beyond the automotive field as well. Experimental results are also shown to validate the effectiveness of the proposed algorithm.

In summary, the contributions of this thesis span from the control applications to the fundamental control theory. Application wise, this thesis formulates the smooth and efficient power transmission design and control problem in three levels, and proposes design, dynamics analysis and control methodologies to address the critical challenges in each level respectively. For control theory, a robust and low order stabilizer synthesis method is proposed to enable reference tracking/disturbance rejection based on linear time varying internal model principle. This stabilizer design addresses one of the most critical issues in the linear time varying internal model control synthesis, which facilitates experimental investigation of the internal model controller in the *LTV* setting.

Contents

List of Tables

List of Figures

Chapter 1

Introduction

1.1 Background and Motivation

This thesis focuses on investigating the design, modeling and control methodologies, which can enable smooth and energy efficient power transmission for conventional, hybrid and future automotive propulsion systems.

Automotive propulsion system typically involves power generation [1-2][1] and power transmission [3-5]. The fundamental requirement of any type of automotive propulsion is smooth propulsion performance, high energy efficiency and low emissions. To fulfill these requirements, the main challenges are to enable the clean energy conversion of the power source, and at the same time transfer the power to the driveline in an efficient and smooth fashion. First, the efficient power generation highly depends on the operation condition of the power source [1-2]. The typical optimal operation condition of an engine lies in a small range of torque and speed [4]. While the performance criteria of the propulsion system require a wide driveline torque output and speed range, it is inevitable to have an intermediary mechanism [3-8] between the power source (engine) and the automotive driveline to enable different operating conditions. Second, the modern and future automotive propulsion systems seek an aggressive energy management strategy and advanced energy conversion technique [1-2]. These technologies often result in higher torque oscillation and thus bring in great challenges to the smooth torque transfer. For example, the optimal energy management strategy for hybrid powertrain requires frequent start and stop of the engine [9, 10], which could generate large engine torque pulses and thus cause driveline vibration. Similarly, many advanced fuel efficient combustion technologies with a short combustion duration, such as homogenous charge compression ignition (HCCI) [1-2] for future automotive propulsion, will generate large torque pulsations and have the same issue for triggering

[1] The reference number refers to the reference lists at the end of each chapter. This applys to all the reference numbers throughout the thesis.

driveline vibrations. Clearly, without a smooth power transmission means, those advanced technologies cannot be effectively implemented.

Therefore, the fundamental requirements of the modern power transmission system are: (1). It should be able to shift the torque transmission ratio efficiently and smoothly to enable the fuel efficient operation of the power source. (2). It should be able to reject/damp out the power source torque oscillation in an energy efficient fashion to avoid rough torque transfer to the driveline. To meet these two objectives, various kinds of power transmission devices have been developed. Emerging technologies [3, 4] such as six or more speeds automatic transmission (AT), continuously variable transmission (CVT), dual clutch transmission (DCT), automated manual transmission (AMT), and electrically variable transmission (EVT) have appeared in the market. The newly developed hybrid power train technology is in fact an electrically variable transmission, which can optimize the engine operation condition with the aid of electric motors/generators. However, with these transmission technologies, the system dynamics become much more complicated. What's more, the advanced combustion (HCCI, etc) of current liquid fuel or even the alternative fuel will bring in more critical control challenges on the future power transmission. Therefore, with the stringent emission and fuel economy requirements, it becomes increasingly important to incorporate appropriate feedback control methodologies in the system propulsion and power transfer. This incorporation not only lies in the appropriate control algorithm, but could also be the mechanical/hydraulic design aided by the feedback control concept.

1.2 Research Objectives

A successful power transmission is determined by many factors. Specifically, it depends on the operation of its enabling and most fundamental mechanism, such as transmission clutches; it depends on its optimal coordination with the automotive driveline system; it also depends on the capability to smooth out the power source input in a fuel efficient fashion, such as input torque oscillation rejection. In other words, the actuation of the clutch system itself should be smooth and efficient; the power transmission coordination with the driveline should be smooth and efficient; and the power source oscillation rejection should be smooth and efficient as well. Considering

these factors, this thesis will investigate the enabling design and control methodologies for power transmission in three different levels: the fundamental clutch level, the intermediate driveline level, and the entire propulsion system level. The problems in each level are unique, but also interconnected.

First of all, as a complex mechanical system, the power transmission system should maintain the optimal operation itself. This further requires the proper function of the key components enabling the power transmission. The clutch is one of the critical components for most power transfer devices, such as the automatic transmission [4-8], the automated manual transmission [11], dual clutch transmission [12] and even some hybrid vehicle transmissions [13-15]. They are connected to the engine and the driveline respectively and the surfaces are covered with friction material. By engaging or disengaging the clutches, the power source will be either connected or separated from the driveline. A smooth and efficient control of the clutch actuation is critical; otherwise it will cause driveline vibration. This thesis will discuss the clutch level design and control based on a specific example: the clutch to clutch shift problem in a six speed automatic transmission, while the principle and approaches can be applied to many other types of transmissions like multi-mode hybrid transmissions. Specifically, we will investigate the clutch control methods in two categories: open loop and closed loop control.

The benefits of the open loop clutch control are its hardware compactness and low cost. Its main challenges lie in two aspects: consistent initial condition and optimal control process. First, typically the clutch motion happens in an extremely short time (about 0.2 second). To precisely control the optimal process from the start in open loop, it is crucial to ensure consistent initial condition. It is observed that the design of a so called ball capsule system is crucial to ensure the initial condition reliability. In this thesis, the ball capsule system structure and dynamics are analyzed and optimally designed. Second, to realize the clutch to clutch shift in open loop, the pre-shift process called clutch fill, which highly affects the later shift and engagement, should be optimized. The optimization process is challenging as stiff hydraulic dynamics result in computational intensive optimization. This thesis then presents a customized dynamic programming algorithm, which can successfully avoid the stiffness problem.

In addition, for the closed loop clutch control, the main challenges are to form a feedback loop in a structurally compact, precise and robust fashion. Two different approaches are proposed. One method is to close the control loop with a pressure sensor, while the other method is to form the feedback without any sensor at all. For the pressure sensor based control, the sensor is mounted in the clutch chamber and then the clutch motion and torque transfer are controlled based on the pressure regulation using a sliding mode controller and an observer. For the feedback control with no sensor measurement, a new clutch control hydra-mechanical mechanism, which includes an internal feedback structure, is proposed. The closed loop control is based on pure hydra-mechanical components, and is proved to be precise, robust, and cost efficient.

Second, a successful clutch actuation alone is not enough. Its coordination with the driveline is another critical factor. Failure in coordination will result in a less efficient or perturbed power transmission. Specifically, the desired clutch and driveline coordination should ensure smooth vehicle launch and gearshift without lurch, and minimize energy loss due to the clutch slip. To achieve this goal, we applied Dynamic Programming method to design the optimal clutch and engine velocity/torque trajectory during gearshift. The method is shown to provide optimal solution given non-quadratic cost function and the nonlinear dynamic model. In particular, in this thesis, we will study the driveline level control based on the automated manual transmission (AMT) optimal clutch engagement problem.

Finally, beyond the self regulation, a successful power transmission design should also enable the efficient operation of the power source and reject the potential driveline vibration triggered by the input torque pulses. To be specific, the aggressive energy management of the hybrid powertrain, the advanced clean combustion like HCCI and etc require a power transmission mechanism with efficient vibration rejection capability. To realize this, it is necessary to understand the torque output characteristic from the power source and the driveline resonance dynamics as well. In other words, the oscillation rejection needs to be investigated from the integrated system level point of view with an appropriate understanding of the whole propulsion system. As a representative example, the power split hybrid system [16] is studied in this thesis. The fuel efficient operation of

the hybrid vehicle requires frequent start and stop of the engine, which will induce large engine torque pulses and can easily cause driveline vibration. Thus the power transfer control with the energy efficient vibration reduction is crucial. Through proper formulation, this problem can be treated as disturbance rejection for a linear parameter varying (*LPV*) system under the internal model principle. To experimentally implement the state of the art controller design method, two problems should be solved. First, the vibration signal is periodic with changing magnitude, whose generating dynamics has not been studied before and needs to be derived. Second, the current state-of-the-art linear parameter varying (*LPV)* internal model based control design is lack of robustness, and the robust internal model stabilizer synthesis is still unavailable. This thesis proposes promising approaches to address this fundamental issue in the time varying internal model control theory, which is one of the key contributions in this thesis. The proposed stabilizer synthesis method is treated in a general form, and can potentially be applied to other applications beyond the automotive field as well.

1.3 Dissertation Organization and Overview

In summary, this thesis proposes design, dynamics analysis and control methodologies, which can enable smooth and energy efficient propulsion and power transfer. The proposed approaches are presented based on specific examples in three consecutive levels: clutch level, driveline level and propulsion system level. First, the clutch level design is presented from chapter 2 to chapter 5. Chapter 2 discusses the consistent initial condition for open loop clutch control. Chapter 3 presents the open loop clutch control process optimization. Chapter 4 shows the closed loop clutch control with only pressure feedback. And Chapter 5 introduces a closed loop clutch control method without any sensor measurement. Second, the driveline level design is presented in Chapter 6 using the automated manual transmission driveline coordination as an example. Finally,

The organization of this thesis will be presented in detailed as the following.

Chapter 2: Clutch Level Design (Clutch Fill Initial Condition Control): Ball Capsule Dynamics Analysis and Optimal Design

In this chapter, the ball capsule dynamics is modeled, in which the derivation of the ball capsule throttling area is considered novel and critical because of its asymmetrical nature. Following this, the ball capsule's intrinsic positive feedback structure is also revealed, which is considered to be the key to realize a fast response. Moreover, through the system dynamics analysis, the slope angle of the capsule is found to be an effective control parameter for system performance and robustness. To this end, the optimal shape of the capsule is designed using Dynamic Programming to achieve the desired performance.

Chapter 3: Clutch Level Design (Open Loop Clutch Control Process Optimization): Optimal Clutch Fill Control Using a Customized Dynamic Programming

In this chapter, we present a systematic approach to evaluate the clutch fill dynamics and synthesize the optimal pressure profile. First, a clutch fill dynamic model, which captures the key dynamics in the clutch fill process, is constructed and analyzed. Second, the applicability of the conventional numerical Dynamic Programming (DP) method to the clutch fill control problem, which has a stiff dynamic model, is explored and shown to be inefficient. Thus we developed a new customized DP method to obtain the optimal and robust pressure profile subject to specified constraints. The customized DP method not only reduces the computational burden significantly, but also improves the accuracy of the result by eliminating the interpolation errors. To validate the proposed method, a transmission clutch fixture has been designed and built in the laboratory. Both simulation and experimental results demonstrate that the proposed customized DP approach is effective, efficient and robust for solving the clutch fill optimal control problem.

Chapter 4: Clutch Level Design (Closed Loop Control With Pressure Feedback) :Pressure Based Clutch Control for Automotive Transmissions

In this chapter, we investigated the closed loop clutch control enabled by a pressure sensor in the clutch chamber. The main challenges of the pressure based clutch control lie in the complex dynamics due to the interactions between the fluid and the mechanical systems, the on/off behavior of the clutch assembly, the time varying clutch loading condition, and the required short time duration for a clutch shift. To enable precise pressure based control, this chapter presents the contributions in three aspects. First, a

clutch dynamic model is constructed and validated, which precisely captures the system dynamics in a wide pressure range. Second, a sliding mode controller is designed to achieve robust pressure control while avoiding the chattering effect. Finally, an observer is constructed to estimate the clutch piston motion, which is not only a necessary term in the nonlinear controller design but also a diagnosis tool for the clutch fill process. The experimental results demonstrate the effectiveness and robustness of the proposed controller and observer.

Chapter 5: Clutch Level Design (Closed Loop Control Without Sensor Measurement): Hydra-mechanical Based Internal Feedback Mechanism Development for Clutch Control

This chapter considers the closed loop clutch control without electronic sensor measurement. To address this problem, a new clutch actuation mechanism is proposed, which realizes an internal feedback structure. The proposed mechanism is novel as it embeds all the control elements in the orifice area regulation, which successfully solves the precise and robust control of the hydraulic system with nonlinear dynamics. In this paper, we first present the working principle of the new clutch actuation mechanism. Then, the mechanical system design is shown and the system dynamic model is built. To this end, the proposed internal feedback control mechanism is fabricated and validated in a transmission testing fixture. The new mechanism performance is finally presented through a series of simulation and experimental results.

Chapter 6: Driveline Level Design: Automated Manual Transmission Optimal Clutch Engagement Analysis

In this chapter, the optimal clutch engagement problem for the automated manual transmission system is formulated. To realize an energy efficient and smooth clutch engagement, the possibility of using the Dynamic Programming method to generate the optimal clutch and engine torque control inputs is investigated. In particular, the controllability of the AMT system is studied to determine the number of control inputs necessary for the optimal control, and the Dynamic Programming is applied to solve the optimization problem.

Chapter 7: Propulsion System Level: Hybrid Vehicle Vibration Rejection Using Angle Based Time Varying Repetitive Control

This chapter presents the hybrid vehicle vibration rejection problem. The key contributions are to formulate the internal model control approach for periodic signal with magnitude variation, and then apply the angle based repetitive control for *LPV* plant to fulfill the energy efficient vibration rejection. By proper formulation, the oscillation disturbance signal is periodic with magnitude variation. As will be revealed in this chapter, the generating dynamics of this kind of signals is time varying, and thus simply embedding its generating dynamics as the internal model controller will no longer ensure asymptotic performance. To enable successful vibration reduction, the generating dynamics of this unique signal is first derived, and then its corresponding controller design method is presented. After a series of simulations and case studies, the proposed control framework is demonstrated to be a promising solution for the hybrid powertrain vibration reduction problem.

Chapter 8: Propulsion System Level: Robust Stabilizer Design for Linear Parameter Varying (LPV) Internal Model Control System

This chapter focuses on a low order robust stabilizer synthesis for a general linear parameter varying internal model control problem. The existing stabilization approaches are either lack of robustness or results in too high stabilizer order, which limit the further studies in experiments. The method proposed in this chapter overcomes this bottleneck by taking advantage of the unique structure of the time varying internal model control system. Instead of using a dynamic stabilizer with high order, the approach using a sequence of time varying gains will be presented. A critical issue addressed is to avoid the non-convex optimization associated with the time varying gain synthesis and then convert the stabilizer design into a series of Linear Matrix Inequality (LMI) constraints. Experimental studies are then conducted on the hydrostatic dynamometer system and prove the robustness and computational efficiency of the proposed approach.

References in Chapter 1

[1] T. Kuo. Valve and fueling strategy for operating a controlled auto-ignition combustion engine. In SAE 2006 Homogeneous Charge Compression Ignition Symposium, pp. 11-24, San Ramon, CA, 2006.

[2] T. Kuo, Z. Sun, J. Eng, B. Brown, P. Najt, J. Kang, C. Chang, and M. Chang. Method of HCCI and SI combustion control for a direct injection internal combustion engine. U.S. patent 7,275,514, 2007.

[3] Wagner, G., "Application of Transmission Systems for Different Driveline Configurations in Passenger Cars", SAE Technical Paper 2001-01-0882.

[4] Sun, Z. and Hebbale, K., "Challenges and Opportunities in Automotive Transmission Control", Proceedings of 2005 American Control Conference, Portland, OR, USA, June 8-10, 2005.

[5] Lee, C.J., Hebbale, K.V. and Bai, S., "Control of a Friction Launch Automatic Transmission Using a Range Clutch". Proceedings of the 2006 ASME International Mechanical Engineering Congress and Exposition, Chicago, Illinois, 2006.

[6] Hebbale, K.V. and Kao, C.-K., "Adaptive Control of Shifts in Automatic Transmissions". Proceedings of the 1995 ASME International Mechanical Engineering Congress and Exposition, San Francisco, CA, 1995.

[7] Bai, S., Moses, R.L, Schanz, Todd and Gorman, M.J. "Development of A New Clutch-to-Clutch Shift Control Technology". SAE Technical Paper 2002-01-1252.

[8] Marano, J.E, Moorman, S.P., Whitton, M.D., and Williams, R.L. "Clutch to Clutch Transmission Control Strategy". SAE Technical Paper 2007-01-1313/

[9] S. Tomura, Y. Ito, K. Kamichi, and A. Yamanaka. Development of vibration reduction motor control for series-parallel hybrid system. In SAE Technical Paper Series 2006-01-1125, 2006.

[10] S. Kim, J. Park, J. Hong, M. Lee and H. Sim. Transient control strategy of hybrid electric vehicle during mode change. In SAE Technical Paper Series 2009-01-0228, 2009

[11] Glielmo, L. Iannelli, L. Vacca, V. and Vasca, F. “Gearshift Control for Automated Manual Transmissions”, IEEE/ASME Transactions on Mechatronics, VOL 11, No. 1, Feb., 2006.

[12] Zhang, Y., Chen, X., Zhang, X., Jiang, H., and Tobler, W., “Dynamic Modeling and Simulation of a Dual-Clutch Automated Lay-Shaft Transmission”, ASME Journal of Mechanical Design Vol. 127, Issue. 2, pp. 302-307, March, 2005.

[13] T. Goro, et al. Development of the hybrid system for the Saturn VUE hybrid. SAE technical paper 2006-01-1502.

[14] M. Levin, et. al. Hybrid powertrain with an engine-disconnection clutch. In SAE Technical Paper Series 2002-01-0930, 2002.

[15] T. Grewe, B. Conlon, and A. Holmes. Defining the General Motors 2-Mode Hybrid Transmission. SAE technical paper 2007-01-0273.

[16] J. Liu, and H. Peng. Modeling and control of a power-split hybrid vehicle. IEEE Transactions on Control Systems Technology, vol. 16 (6) pp. 1242-1251, 2008.

Chapter 2

The Clutch Level Design--Modeling, Analysis and Optimal Design of the Automotive Transmission Ball Capsule System

This chapter investigates the initial condition control for open loop clutch operation. To have a precise open loop actuation, it is critical that the initial conditions of the clutch fill process do not change from cycle to cycle. It will be revealed that the initial condition consistency depends on a small valve system called ball capsule system. In the following the modeling, dynamics analysis and optimal design of this miniature valve system will be presented in detail.

2.1. Introduction

To reduce vehicle fuel consumption and tailpipe emissions, automotive manufacturers have been developing new technologies for powertrain systems. In the transmission area, emerging technologies [1, 2] such as six or more speeds automatic transmission (AT), continuously variable transmission (CVT), dual clutch transmission (DCT), automated manual transmission (AMT), and electrically variable transmission (EVT) have appeared in the market. The basic function of any type of automotive transmissions is to transfer the engine torque to the vehicle with the desired ratio smoothly and efficiently. The commonly used actuation device for gear shifts in transmissions is electro-hydraulically actuated clutch. In automatic and hybrid transmissions, the most common configuration is to use wet clutches with hydraulically actuated pistons. This is mainly due to the high power density of electro-hydraulic systems.

Recently with the introduction of six or more speeds automatic transmissions, the clutch to clutch shift control technology [3-6] has once again attracted a lot of research and development efforts. This clutch shift control technology is the key enabler for a compact, light, and low cost automatic transmission design. This technology uses pressure control valves to control the clutch engagement and disengagement processes of the oncoming and off-going clutches. A critical challenge for the clutch shift control is the

synchronization of the oncoming and off-going clutches, which is highly dependent on the oncoming clutch fill time.

A schematic diagram of the transmission clutch system is shown in Figure 2.1. To engage the clutch, high pressure fluid flows into the clutch chamber and pushes the piston towards the clutch pack until they are in contact. This process is called the clutch fill. At the end of the clutch fill process, the clutch pack is ready to be engaged to transfer the engine toque to the vehicle driveline. The difficulty in realizing a precise clutch fill time lies in the fact that a pressure feedback control loop could not be formed due to the lack of a pressure sensor inside of the clutch chamber. Therefore, it is necessary to control the clutch fill in an open loop fashion, which highly depends on the initial conditions of the clutch system. To control the clutch fill process precisely, it is therefore critical that the initial conditions of the clutch fill process do not change from cycle to cycle. However, as the whole clutch system rotates around the central shaft (Figure 2.1), the centrifugal force will keep a certain amount of fluid at the ceiling of the clutch chamber. The fluid pressure induced by the rotation of the leftover fluid will push on the piston and will therefore affect the initial conditions of the clutch fill process in the following cycle. To dissipate the leftover fluid and subsequently release the centrifugal force induced pressure, a ball capsule system is introduced and mounted on the clutch chamber as shown in Figure 2.1.

The ball capsule system consists of a ball and a capsule. Together with the whole clutch system, the capsule rotates around the central shaft (Figure 2.1). The centrifugal force acting on the ball keeps the ball in contact with the capsule ceiling, so that the ball can rotate along the capsule inner wall between the open position and the closed position. The opening and closing of the ball capsule system is controlled by the fluid pressure inside the clutch chamber and the centrifugal force. When the fluid pressure inside the chamber is below a specific level, the sum of moments acting on the ball at the contact point will push the ball to rotate along the capsule inner wall from the closed position to the open position. The fluid inside the clutch chamber then can flow out to the exhaust through the opening area between the ball and the inner wall of the capsule. On the other hand, when the fluid pressure inside the chamber is high enough, the ball will rotate to the closed position and seal off the exhaust port.

The performance of the ball capsule system is crucial for clutch engagement and disengagement processes. As shown in Figure 2.1, when the clutch disengages, the piston is pushed to the left by the spring force, and the fluid inside the clutch chamber is dissipated through the inlet orifice. At this time, the pressure inside the clutch chamber drops, and the ball capsule needs to open to allow the fluid held by the centrifugal force at the ceiling of the chamber to flow out to the exhaust. When the clutch fill process starts, the pressurized fluid enters the clutch chamber through the inlet orifice. When this happens, the ball needs to close quickly in order to build up the pressure inside of the clutch chamber. In addition to these requirements, the system also needs to be robust and able to avoid undesirable ball chattering between the open and closed positions. In this chapter, the dynamics of the ball capsule system will be modeled and the stability of the system will be analyzed, in order to provide the optimal capsule design to achieve the desired performance.

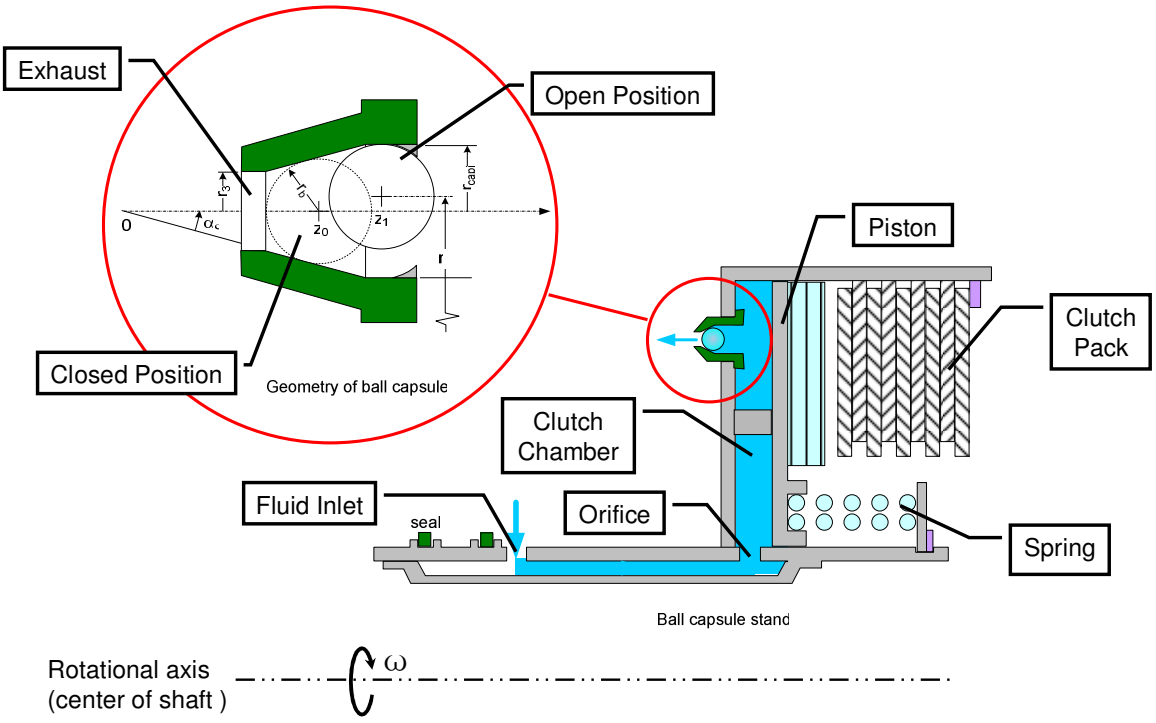

Figure 2.1. Automotive Transmission Clutch and Ball Capsule System

One of the objectives of this study is to realize swift response of the ball capsule system during clutch engagement and disengagement. Since the clutch fill process usually takes a fraction of a second [2], the response of the ball capsule system must be

fast enough to allow pressure to build up inside the clutch chamber. In order to understand and characterize the ball dynamics in such a short time period and its effects on the clutch chamber pressure, the dynamics of the ball capsule system is modeled. The main challenge in building the dynamic model is deriving the fluid throttling area, which is the opening area between the ball and the capsule inner wall. Based on the dynamic model, an intrinsic positive feedback structure in the system is found. This is in fact desirable since the unstable characteristic of the ball capsule system results in the exponential increase of the ball rotational speed, which ensures quick response.

Another objective of the ball capsule design is to prevent high impact speed when the ball closes the exhaust, which will otherwise cause noise and wears. In addition, the ball capsule system must be robust, in other words, once the exhaust is closed, it should remain closed until the clutch is disengaged. If there are pressure variations inside of the chamber, the ball capsule should not open and the ball must not chatter between the open and closed positions, which will otherwise adversely influence the clutch fill process. By analyzing the dynamics of the system, it is found that the desired performance can be realized by a proper design of the capsule inner wall profile. To this end, a robust design for the ball capsule system with variable slope angles using the dynamic programming method is proposed.

The rest of this chapter is organized as follows. Section 2.2 presents the system dynamic model. Section 2.3 analyzes the intrinsic positive feedback structure of the ball capsule system. Section 2.4 presents the discrete model of the system and formulates the ball capsule design problem as an optimization problem. To this end, the Dynamic Programming method is applied to redesign the shape of the ball capsule inner wall. Section 2.5 presents case studies and simulation results.

2.2. System Modeling

Figure 2.2 shows the schematic diagram of the ball capsule system. The capsule rotates around the central shaft (see Figure 2.1) together with the clutch system. The centrifugal force acting on the ball F_c induced by the rotational motion, keeps the ball in contact with the capsule ceiling. Since the centrifugal force is normally much larger than the weight of the ball, the following modeling will be based on the assumption that the

ball "rolls" without sliding on the capsule wall. When clutch fill starts, the transmission fluid with pressure P_S from the pump enters the clutch chamber through an orifice, $A_{orf.}$. P_1 is the fluid pressure inside the chamber V_1 between the orifice A_{orf} and the throttling area A_{th}. A_{th} is the smallest opening area between the ball and the capsule inner wall, which changes with the motion of the ball. P_2 is the fluid pressure inside the chamber V_2 between the throttling area A_{th} and the exhaust orifice A_{ex}. If large enough, the pressure difference between P_1 and P_2 will overcome the torque induced by the centrifugal force F_c and pushes the ball to rotate along the capsule inner wall towards the exhaust port which is the closed position. P_c is the fluid centrifugal pressure induced by the rotation of the chamber, and the fluid pressure outside of the exhaust is assumed to be atmospheric, P_{atm}.

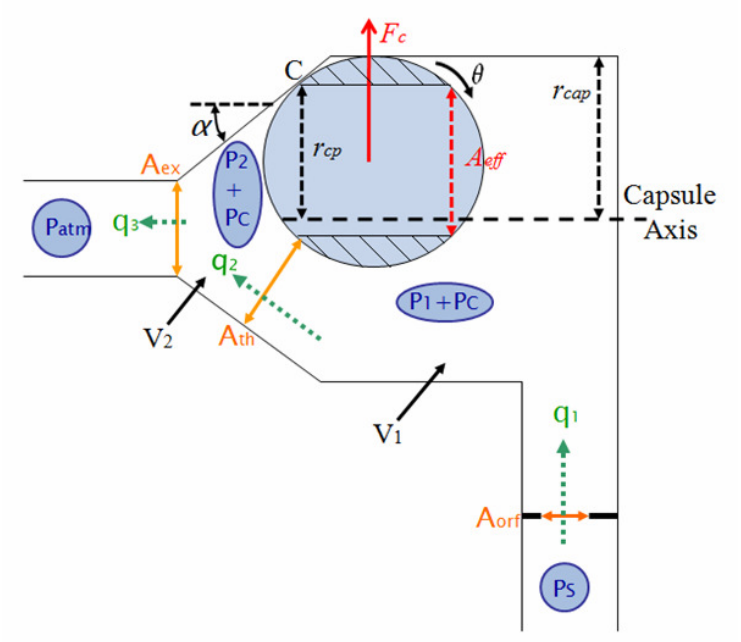

Figure 2.2. Schematic Diagram of the Ball Capsule System

2.2.1 Dynamic Model

The ball capsule system model could be expressed as:

$$
\begin{aligned}
&\dot{\theta} = v \\
&J\dot{v} = (P_1 + P_c)A_{eff}\, r_b \cos(\alpha) - (P_2 + P_c)A_{eff}\, r_b \cos(\alpha) - F_c r_b \sin(\alpha) \\
&\dot{P}_1 = \frac{\beta}{V_1}(q_1 - q_2) \\
&\dot{P}_2 = \frac{\beta}{V_2}(q_2 - q_3)
\end{aligned}
\tag{2.1}
$$

where

$$q_1 = C_d A_{orf} \sqrt{\frac{2}{\rho_{oil}}(P_S - P_1)} \tag{2.2}$$

$$q_2 = C_d A_{th} \sqrt{\frac{2}{\rho_{oil}}(P_1 - P_2)} \tag{2.3}$$

$$q_3 = C_d A_{ex} \sqrt{\frac{2}{\rho_{oil}}(P_2 + P_c - P_{atm})} \tag{2.4}$$

$$A_{eff} = \pi\left(r_b \cos(\alpha)\right)^2 \tag{2.5}$$

$$F_c = \frac{4}{3}\pi r_b^3 \left(\rho_{steel} - \rho_{oil}\right) r_c \omega^2 \tag{2.6}$$

$$r_{cp} = r_{cap} - r_b + r_b \cos(\alpha) - r_b \theta \sin(\alpha) \tag{2.7}$$

$$
\begin{aligned}
A_{th} = \pi \cdot \left(r_b + \frac{x_{lift}}{2} \sin\alpha \right) \sin(2\alpha) \cdot x_{lift} + \pi \cdot \left(1 - \frac{\sin^2\alpha}{2} \right) \sin\alpha \tan\alpha \cdot x_{lift}^2 \\
- \frac{\pi (x_{lift} \tan\alpha)^2}{2 r_b \cos\alpha} \left(x_{lift} + \frac{r_b}{\sin\alpha} \right) \sin(2\alpha) \cos(\alpha)
\end{aligned}
\tag{2.8}
$$

$$x_{lift} = \frac{\left[r_{cp} - r_b \times \cos(\alpha) \right]}{\tan(\alpha)} = \frac{\left[r_{cap} - r_b + r_b \cos(\alpha) - r_b \theta \sin(\alpha) - r_b \times \cos(\alpha) \right]}{\tan(\alpha)} \tag{2.9}$$

θ is the rotational angle of the ball, v is the ball rotational velocity, r_b is the radius of the ball, and α is the angle of the capsule wall. q_1, q_2 and q_3 are the flow rates at the corresponding orifices. ω is the clutch system rotational speed, r_c is the distance from the center of the ball to the axis of the transmission (shown in Figure 2.3), r_{cp} is the distance between the contact point C and the capsule axis, and r_{cap} is the capsule radius shown in Figure 2.2. A_{eff} in Eq(2.5) is the area on the ball where the forces acting on the ball due to pressures P_1 and P_2 are in effect. This is because, the border line between V_1 and V_2 on the ball is assumed to be the vertical line that lies on the points where the radius of the ball is perpendicular to the surface of the capsule ramp. As a result, the sum of P_1 and P_C acts on both sides of the shaded surfaces of the ball in Figure 2.2, thus cancelling the forces acting on both sides of the surfaces. The remaining area, called A_{eff}, is therefore the effective area on which P_1 and P_2 act against each other. Eq(2.6) is the centrifugal force acting on the ball due to the rotation of the clutch system. The second equation in Eq(2.1) is the net moment acting on the ball at the contact point of the ball with the capsule ramp, denoted as point C. The third equation in Eq(2.1) corresponds to the transient pressure dynamics of P_1 in volume V_1, as a result of the flow rate in, q_1 through A_{orf} shown in Eq(2.2) and the flow rate out, q_2 through A_{th} shown in Eq(2.3). Similarly, the fourth equation in Eq(2.1) is the transient pressure dynamics of P_2 in volume V_2. Eq (2.8) and (2.9) are equations to calculate the throttling area A_{th}, the derivation of which will be presented in the next session.

Suppose at the initial condition, the ball is at the top corner of the inner surface of the capsule (Figure 2.3) and the value of r_c at this position is $r_{c\_initial}$. By trigonometry, r_c can be expressed as:

$$r_c = r_{c\_initial} - h = r_{c\_initial} - r_b\theta\sin(\alpha) \tag{2.10}$$

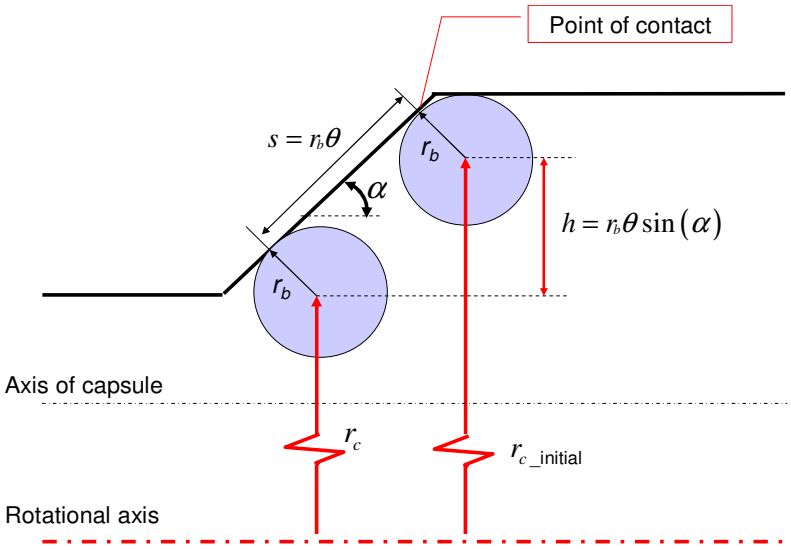

Figure 2.3. Schematic Diagram of the Ball Capsule System

The centrifugal fluid pressure P_c, shown in Figure 2.4, due to the centrifugal force is a function of r_c and can be expressed as:

$$P_c = \frac{\rho_{oil}}{2}\omega^2\left(r_c^2 - r_{st}^2\right)$$

where r_{st} is the starting level of the fluid. Considering that the size of the capsule system is relatively small compared to the transmission system, P_c could be assumed to be constant.

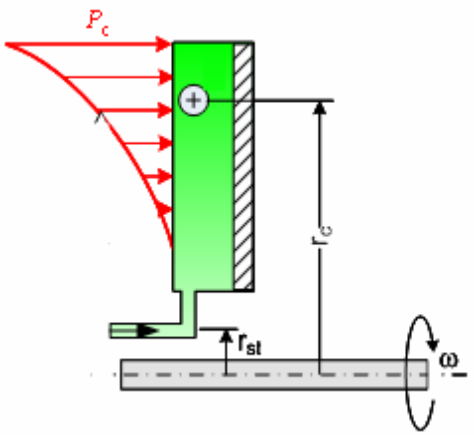

Figure 2.4. Fluid centrifugal pressure

2.2.2 Derivation of the Throttling Area

Most of the throttling areas in fluid system modeling are symmetric [7]. However, in the ball capsule system, the derivation of the throttling area A_{th} between the ball and the capsule inner surface is not straightforward because the ball is not concentric with the conical capsule.

As shown in Figure 2.5(a), the capsule surface is a cone surface and could be represented using cone geometry function as:

$$\text{Cone surface:} \qquad y^2 + z^2 = x^2 \tan^2 \alpha \tag{2.11}$$

Similarly, the ball surface is a sphere surface centered at O_i $(x_i, y_i, 0)$, and could be represented as:

$$\text{Sphere surface:} \qquad (x - x_i)^2 + (y - y_i)^2 + z^2 = r_b^2 \tag{2.12}$$

The y-component and z-component of a line *OP* along the cone surface (Figure. 2.5(a)) can be described in terms of the x-component by using the two equations,

$$\text{Line } OP: \qquad y = x \tan \alpha \cos \beta \tag{2.13}$$

$$z = x \tan \alpha \sin \beta \tag{2.14}$$

To find the throttling area A_{th}, which is the smallest area between the ball (sphere surface) and the capsule (cone surface), first the minimum distance from the line *OP* on the cone surface to the sphere surface need to be obtained. The shortest distance from a line to a sphere is also the shortest distance from the sphere center to the line minus the sphere radius (line *AD* in Figure. 2.5(b)).

As the ball rotates along the ball capsule surface, its center trajectory is represented as:

$$y_i = x_i \tan \alpha - r_b \sec \alpha \tag{2.15}$$

The squared distance between point (x, y, z) on line *OP* and the center of the ball $(x_i, y_i, 0)$ is

$$d^2 = (x - x_i)^2 + (y - y_i)^2 + z^2 = (x - x_i)^2 + (x\tan\alpha\cos\beta - y_i)^2 + (x\tan\alpha\sin\beta)^2 \quad (2.16)$$

Differentiating equation (2.16) and equating it to zero leads to the nearest point on the line *OP* to the center of the ball

$$x = (x_i + y_i \tan\alpha\cos\beta)\cos^2\alpha \quad (2.17)$$

$$y = (x_i + y_i \tan\alpha\cos\beta)\sin\alpha\cos\alpha\cos\beta \quad (2.18)$$

$$z = (x_i + y_i \tan\alpha\cos\beta)\sin\alpha\cos\alpha\sin\beta \quad (2.19)$$

The nearest point is denoted as point *D*, and the shortest distance as O_iD.

Substituting equations (2.17-2.19) into (2.16) yields

$$O_iD^2 = x_i^2\sin^2\alpha - 2x_iy_i\sin\alpha\cos\alpha\cos\beta + y_i^2(1 - \sin^2\alpha\cos^2\beta) \quad (2.20)$$

Subtracting the radius of the ball from O_iD results in the shortest distance from the line OP to the surface of the sphere

$$AD = O_iD - r_b \quad (2.21)$$

The throttling area, which is shown as the shaded area in Figure 2.5(b), can be divided into infinitely many trapezoidal elements as illustrated by *ADEF* in Figure 2.5(b). The lengths of the arcs *AF* and *DE* are:

$$\widehat{AF} = r_b\cos\alpha \cdot d\varphi \quad \text{and} \quad \widehat{DE} = (O_iD)\cos\alpha \cdot d\varphi$$

Therefore the area of the trapezoidal element *ADEF* can be calculated as

$$dA = (AD)\cdot\frac{\widehat{DE} + \widehat{AF}}{2} = (AD)\cdot\frac{(O_iD)\cos\alpha + r_b\cos\alpha}{2}\cdot d\varphi \quad (2.22)$$

Since O_iD is a function of β, the relationship between β and φ need to be derived to integrate d*A*. The relationship between the angle β and φ is shown in Figure 2.5(c).

BB' is the cross sectional view of the ball capsule system at point *A*, which is perpendicular to the *x* axis. The inner circle on *BB'* represents the cross sectional surface of the ball, and the outer circle is the cross section of the cone. According to sines law, in triangle $O'O'_iA$

$$\frac{\sin(\varphi-\beta)}{O'O_i'}=\frac{\sin(\beta)}{O_i'A}$$

Since *O'* and O'_i are very close in the ball capsule system, φ-β is small. Therefore the following approximation can be made

$$\sin(\varphi-\beta)=(\varphi-\beta)$$

$$d(\frac{\sin(\varphi-\beta)}{O'O_i'})=d(\frac{\varphi-\beta}{O'O_i'})=d(\frac{\sin(\beta)}{O_i'A})$$

Consequently

$$\frac{d\varphi-d\beta}{O'O_i'}=\cos(\beta)\frac{d\beta}{O_i'A}$$

Hence

$$d\varphi=[\cos(\beta)\frac{O'O_i'}{O_i'A}+1]d\beta$$

From equation (2.22)

$$dA=(AD)\cdot\frac{\widehat{DE}+\widehat{AF}}{2}=(AD)\cdot\frac{(O_iD)\cos\alpha+r_b\cos\alpha}{2}\cdot[\cos(\beta)\frac{O'O_i'}{O_i'A}+1]\cdot d\beta$$

The throttling area then can be calculated as the convolution of *dA* about the x-axis,

$$A_{th}=\int dA=\pi\cdot\left(r_b+\frac{x_{lift}}{2}\sin\alpha\right)\sin(2\alpha)\cdot x_{lift}+\pi\cdot\left(1-\frac{\sin^2\alpha}{2}\right)\sin\alpha\tan\alpha\cdot x_{lift}^2$$
$$-\frac{\pi(x_{lift}\tan\alpha)^2}{2r_b\cos\alpha}(x_{lift}+\frac{r_b}{\sin\alpha})\sin(2\alpha)\cos(\alpha)$$

Where

$$x_{lift}=x_i-r_b\csc\alpha=x_{in}-r_b\theta\cos(\alpha)-r_b\csc\alpha$$

x_i is the distance between the cone vertex O and the ball center O_i along the x-axis, x_{in} is x_i value at the initial position and θ is the rotational angle of the ball. By representing x_{in} using r_{cap} and r_b, the above equation for x_{lift} can be transformed into equation (2.9).

To verify the above formula, the throttling areas are drawn and measured in Pro-Engineer software. Figure 2.6 shows a good match between the A_{th} values obtained from ProE and those from Equation (2.8), where y_i is the vertical coordinate of the ball center defined in Equation (2.15).

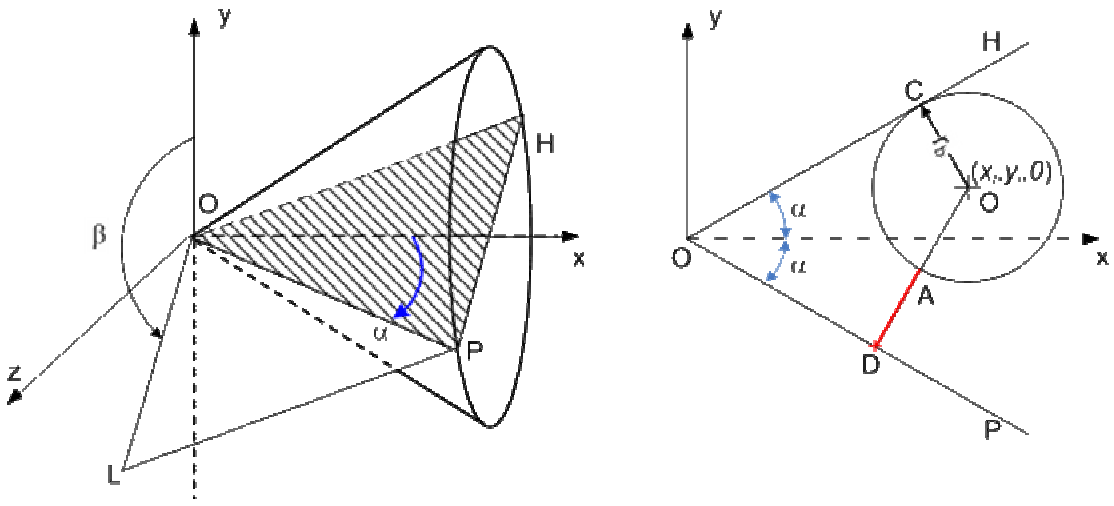

(a) Capsule and Ball Geometries

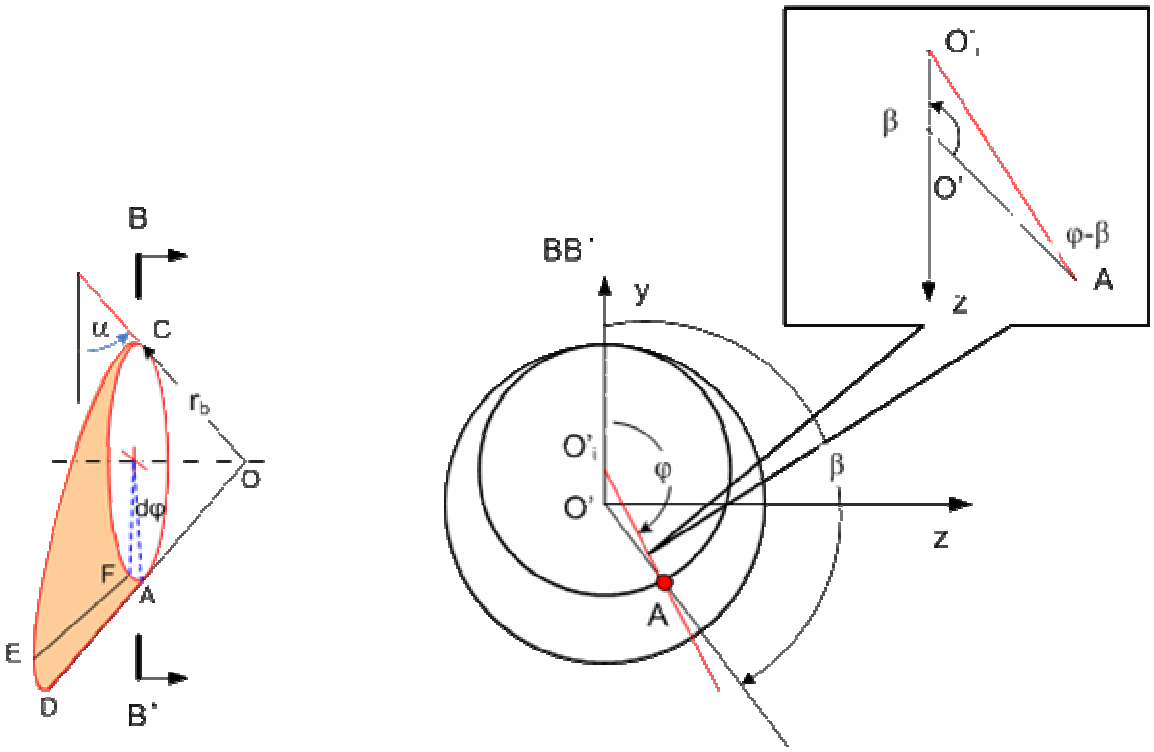

(b) Integration of the minimum distance

(c) β and ϕ relationship

Figure 2.5. Geometric representation of the ball capsule system

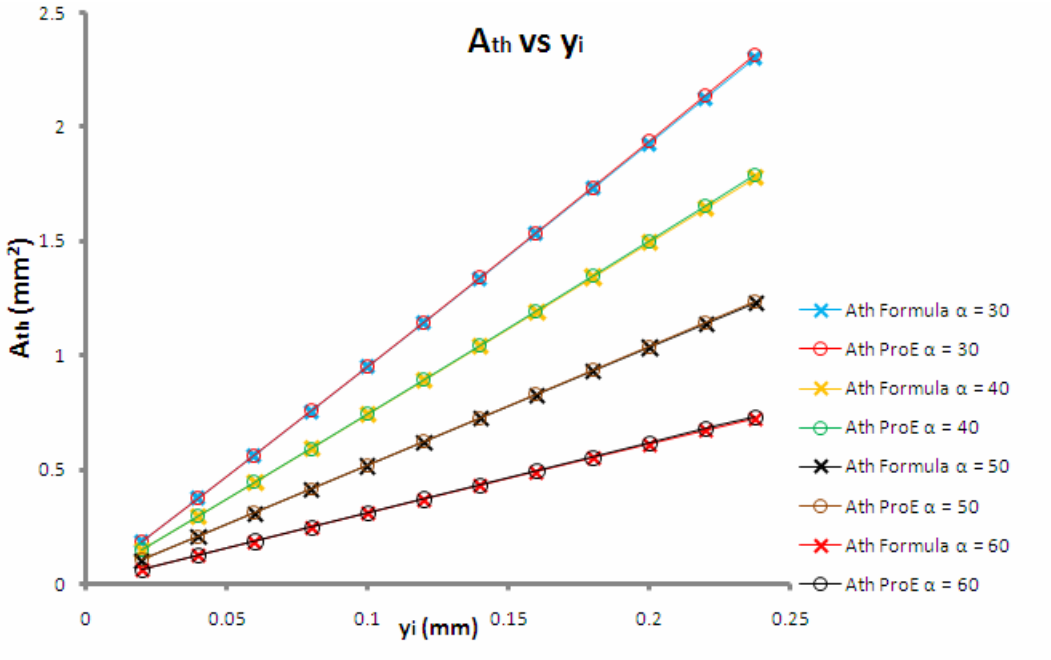

Figure 2.6. Theoretical and ProE A_{th} values comparisons

2.2.3 Reduced Order Model

By now, the dynamic modeling for the ball capsule system is completed. However, the Dynamic Programming method, which will be used for the capsule inner wall profile design later would suffer from heavy computational burden if the order of the system is high. Thus, it is desirable to reduce the order of the model while still capturing the main dynamics of the system. Since the bulk modulus of the fluid is significantly larger compared to the fluid volume, it is reasonable to assume that the volumetric flow rates are the same across the whole capsule from the orifice to the exhaust (q_1=q_2=q_3), resulting in a second order model which can be expressed as:

$$\begin{aligned} \dot{\theta} &= v \\ J\dot{v} &= (P_1 - P_2)A_{eff} r_b \cos(\alpha) - F_c r_b \sin(\alpha) \end{aligned} \tag{2.23}$$

where

$$\begin{aligned} P_1 &= \frac{1}{\left[\frac{A_{th}^2}{A_{th}^2 + A_{ex}^2} + \left(\frac{A_{orf}}{A_{ex}}\right)^2\right]}\left[\left(\frac{A_{orf}}{A_{ex}}\right)^2 P_s + \left(\frac{A_{th}^2}{A_{th}^2 + A_{ex}^2}\right)(P_{atm} - P_c)\right] \\ &= P_s - \frac{1}{\left[\frac{A_{th}^2}{A_{th}^2 + A_{ex}^2} + \left(\frac{A_{orf}}{A_{ex}}\right)^2\right]}\left[\left(\frac{A_{th}^2}{A_{th}^2 + A_{ex}^2}\right)(P_s - (P_{atm} - P_c))\right] \\ &= P_s - \frac{1}{\left[1 + \left(\frac{A_{orf}}{A_{ex}}\right)^2 (1 + \frac{A_{ex}^2}{A_{th}^2})\right]}\left[(P_s - P_{atm} + P_c)\right] \end{aligned} \tag{2.24}$$

$$P_2 = \left(\frac{A_{orf}}{A_{ex}}\right)^2 (P_s - P_1) + P_{atm} - P_c \tag{25}$$

As validated by a series of simulation results (see Figure 2.7), the second order ball capsule model has been shown to be a good approximation of the fourth order ball capsule model, and therefore will be used in the following analysis and design sections.

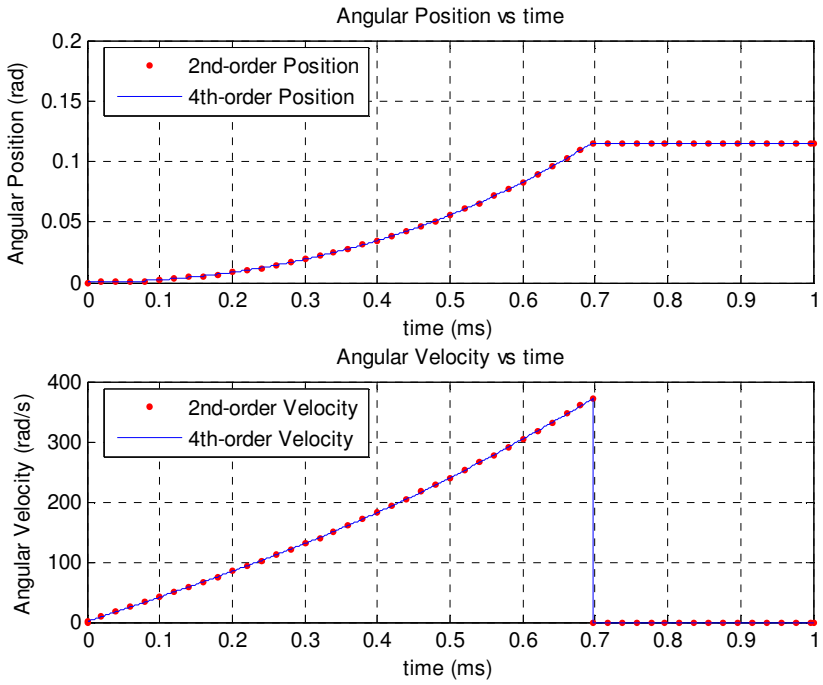

Figure 2.7. Simulation result comparison between 2nd and 4th order model

2.3. System Dynamics Analysis

In this section the stability of the ball capsule system is analyzed as it will provide insight on the design of the system. As can be seen from Figure 2.7, the rotational speed of the ball continues to increase, which results in a quick response of the ball capsule system. The reason for the exponentially increasing velocity is due to an intrinsic positive feedback structure of the system, and the unstable characteristic is the key enabler of the quick response of the ball capsule system.

2.3.1 Analysis for System with Constant Capsule Angle

In this section only the capsule with a single slope angle is considered (as shown in Figure 2.2), which is the simplest way to design the capsule system. Since P_1 and P_2 both depend on the throttling area A_{th}, which in turn is determined by θ, the ball capsule system can be represented as a closed loop feedback system shown in Figure 2.8.

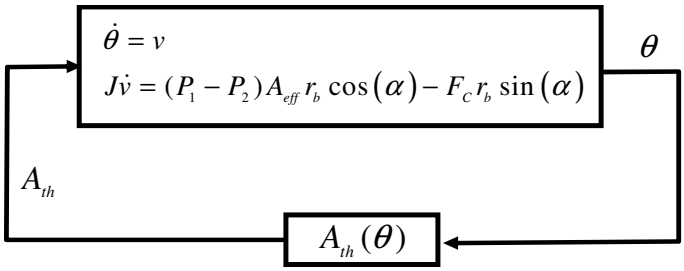

Figure 2.8. System dynamics of ball capsule system

Suppose the rotational angle θ increases when the ball rotates clockwise to the exhaust, and decreases when rotating counterclockwise (see Figure 2.2). As θ increases, A_{th} decreases (Eq. 2.8 and Eq. 2.9), and consequently P_1 goes up (Eq. 2.24), while P_2 drops (Eq. 2.25), resulting in the rise of (P_1-P_2). Furthermore, the centrifugal force F_c will drop due to the decrease of r_c. P_c is assumed to be constant during this process. Based on the above analysis, it can be seen that the angular acceleration of the ball will increase (Eq. 2.23), which further propels the increase of v and θ. Therefore v and θ will keep increasing until the ball reaches the exhaust port. This reveals the physical mechanism of the unstable dynamics of the ball capsule system, and a proof based on Chetaev's theorem [8] is given as follows.

Given a fixed input pressure P_s and a fixed α value, by solving

$$\begin{aligned} &\dot{\theta} = v = 0 \\ &J\dot{v} = (P_1 - P_2)A_{eff} r_b \cos(\alpha) - F_c r_b \sin(\alpha) = 0 \end{aligned} \tag{2.26}$$

we can get an equilibrium point:

$$x_{eq} = \begin{bmatrix} \theta_0 \\ 0 \end{bmatrix}$$

Assume $\theta_0 > 0$.

For the ball capsule system described by (2.23), define a continuously differentiable function

$$V(x) = (\theta - \theta_0)v \tag{2.27}$$

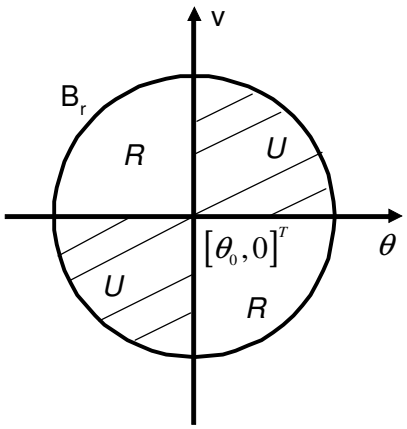

Figure 2.9. Region for U

As shown in Figure 2.9, the circle B_r is a region on the state space around the equilibrium point $[\theta_0, 0]^T$ with a radius of r, which can be as large as possible. Let the set $U = \{x \in B_r \mid V(x) > 0$ except at $[\theta_0, 0]^T\}$, containing the first and third quadrants on the coordinates. The boundary of U is the two coordinate axes, on which $V(x)=0$. Next, let the set $R = \{x \in B_r \mid V(x) < 0\}$, containing the second and fourth quadrant.

Theorem 1: For every point x inside the state space except the origin $[\theta_0, 0]^T$,

$$\dot{V}(x) = \dot{\theta}v + \dot{v}(\theta - \theta_0) = v^2 + \dot{v}(\theta - \theta_0) > 0 \tag{2.28}$$

Proof: if $\theta > \theta_0$, based on Equations (2.8) and (2.9), $A_{th}(\theta) < A_{th}(\theta_0)$. From Equation (2.24), $P_1(\theta) > P_1(\theta_0)$, and from Equation (2.25) $P_2(\theta) < P_2(\theta_0)$. Therefore,

$$[P_1(\theta) - P_2(\theta)] > [P_1(\theta_0) - P_2(\theta_0)] \tag{2.29}$$

In addition, from Equation (2.10), $r_c(\theta) < r_c(\theta_0)$. Then based on Equation (2.6),

$$F_c(\theta) < F_c(\theta_0) \tag{2.30}$$

From Equations (2.23), (2.29) and (2.30), it can be concluded that

$$J\dot{v}(\theta) > J\dot{v}(\theta_0) = 0$$

Therefore

$$\dot{v}(\theta) > 0 \ , \quad \text{and } \dot{V}(x) = \dot{\theta}v + \dot{v}(\theta - \theta_0) = v^2 + \dot{v}(\theta - \theta_0) > 0$$

If $\theta < \theta_0$, using the same approach gives

$\dot{v}(\theta) < 0$, and $(\theta - \theta_0) < 0$

so $\dot{V}(x) = \dot{\theta} v + \dot{v}(\theta - \theta_0) = v^2 + \dot{v}(\theta - \theta_0) > 0$

If $\theta = \theta_0$, $\dot{V}(x) = \dot{\theta} v + \dot{v}(\theta_0 - \theta_0) = v^2 > 0$ if v is not equal to zero. If v=0, then $\dot{V}(x) = 0$. Therefore, $\dot{V}(x) > 0$ for every x in the state space except the origin $[\theta_0, 0]^T$. ■

Theorem 2: If the initial state is in region U as shown in Figure 2.9, then the state trajectory $x(t)$ will leave U through the circle B_r. If the initial state starts at the axes, then $x(t)$ will enter region U. If the state is at region R, then $x(t)$ will have three possible trajectories depending on the system dynamics. It will eventually enter the first quadrant, or the third quadrant, or stop at the origin $[\theta_0, 0]^T$, which is the equilibrium point.

Proof: As $V(x)$ is continuously differentiable in the set U and $\dot{V}(x) > 0$ in U, according to Chetaev's theorem [8], any state trajectory $x(t)$ starting in U must leave U through the circle B_r and therefore be unbounded. Hence the origin is unstable.

The trajectory of the state $x(t)$ can also be analyzed if the initial state x_0 lies outside of the region U. Suppose the initial state starts on the axis excluding the origin $[\theta_0, 0]^T$. In this case, $V(x_0)=0$ and $\dot{V}(x) > 0$, then

$$V(x(t)) = V(x_0) + \int_0^t \dot{V}(x(\tau)) d\tau > 0 \tag{2.31}$$

indicates that $x(t)$ will not stay on the axis where $V(x)=0$ or enter the region R where $V(x)<0$. $x(t)$ will then enter the region U where $V(x)>0$.

If the initial position x_0 starts in the second or the fourth quadrant (region R where $V(x)<0$), the dynamic state $x(t)$ must leave this region as well. In this case,

$$V(x_0) = (\theta - \theta_0) v < 0 \tag{2.32}$$

Define a compact set $\{x \in R \text{ and } V(x) \le -a\}$, and then the continuous function $\dot{V}(x)$ has a minimum over the compact set, i.e. $\dot{V}(x) = v^2 + \dot{v}(\theta - \theta_0) \ge \gamma > 0$ [8], where a, γ are positive numbers. Therefore

$$V(x(t)) = V(x_0) + \int_0^t \dot{V}(x(\tau)) d\tau \ge V(x_0) + \gamma t \tag{2.33}$$

This indicates that *x(t)* will eventually leave the above defined compact set. Since this can happen for an arbitrarily small number a, and also noting that the acceleration $\dot{v}$ and the displacement $(\theta - \theta_0)$ have the same sign (as shown in Theorem 1), *x(t)* will eventually enter the first quadrant, or the third quadrant, or stop at the origin. ■

The ball capsule system is shown to be unstable from the above analysis. In fact, the unstable characteristic is crucial for the ball capsule system performance because it ensures quick response and fast closure of the ball capsule system. Once the input pressure *Ps* is large enough, the ball starts to rotate, and will continue with increasing speed until it stops at the exhaust. However, as the rotational speed continues to increase, the speed could get too high when the ball reaches the exhaust and causes collision that may result in wears and noise.

In addition, the ball capsule system should be robust, which means that once it is closed it should remain closed until the clutch is disengaged. If the pressure inside the chamber oscillates, the ball capsule should not open and chatter between the open and closed positions, which otherwise will adversely influence the clutch fill process. When the ball is at the open position, the input pressure P_S required to rotate the ball towards the exhaust depends on the slope angle of the capsule at the open position. Similarly, at the closed position, the pressure P_1 required to hold the ball in place is also a function of the capsule slope angle at the exhaust port. To avoid ball chattering, it is desirable to have different capsule slope angles. Thus, a capsule shape with variable capsule slope angle is proposed.

2.3.2 Analysis for System with Variable Capsule Slope Angle

If the angle of the capsule inner wall is not constant, then the system will have multiple equilibrium points as shown in Figure 2.10(a). The multiple equilibrium points on the state space are shown in Figure 2.10(b). When the ball rotates in region I as shown in Figure 2.10(a), its states $[\theta, v]^T$ lie in region I of the state space as shown in Figure 2.10(b). Similarly, when the ball enters region II on the capsule, its states move to region II of the state space. Region I and Region II are divided into four quadrants respectively based on the locations of the equilibrium points O_1 and O_2.

Suppose the initial state x_0 is on the axis of θ shown in Figure 2.10(b), which means that the velocity of the ball is zero at the initial condition, then based on theorem 2 the trajectory of $x(t)$ will move to quadrant 1 with increasing θ and v, which equally means that the ball rotates in the positive direction with positive velocity in region I of the capsule. Eventually the ball will leave region I and reach region II as shown in Figure 2.10(a), which corresponds to the state $x(t)$ arriving at point A in Figure 2.10(b). The angle of the capsule changes, and so does the location of equilibrium point. Therefore the trajectory of $x(t)$ in region II need to be considered based on the position of the equilibrium point O_2 shown in Figure 2.10(b). As a result, $x(t)$ arrives in the second quadrant of region II. Then according to Theorem 2, there will be three possible trajectories of the state $x(t)$, depending on the position of the equilibrium point O_2.

Trajectory 1: Based on the analysis in Theorem 2, if $x(t)$ reaches the equilibrium point O_2, then it will stay there assuming no disturbance. In this case, the ball will stay at the equilibrium point in region II, which is not desirable because the ball would not close the capsule.

Trajectory 2: If the state $x(t)$ does not stay at the equilibrium point, then $x(t)$ will either move to the first quadrant or the third quadrant of region II depending on the location of the equilibrium point O_2. If designed properly, $x(t)$ will enter the first quadrant of region II and continue with increasing speed until the ball reaches the exhaust, and the final velocity of the ball could be controlled by choosing the position of equilibrium point O_2. This is the desirable trajectory because the equilibrium points can be chosen by designing the capsule inner wall profile to control the final velocity of the ball before it reaches the exhaust.

Trajectory 3: If $x(t)$ enters the third quadrant of region II, then based on Theorem 2 it will eventually go back to region I, which means that the ball will rotate backward to region I on the capsule. Again, the trajectory of $x(t)$ in region I need to be considered based on the location of O_1. Similar to previous analysis, $x(t)$ enters the fourth quadrant of region I, and may later go to either point E (a point in the first quadrant), point F (a point in the third quadrant) or the equilibrium point O_1, all of which are undesirable as the ball will not close the exhaust. In particular, if the state $x(t)$ goes to point E, it will

move in the first quadrant of region I again, and repeat the paths analyzed previously. This is the case where the ball oscillates between region I and region II.

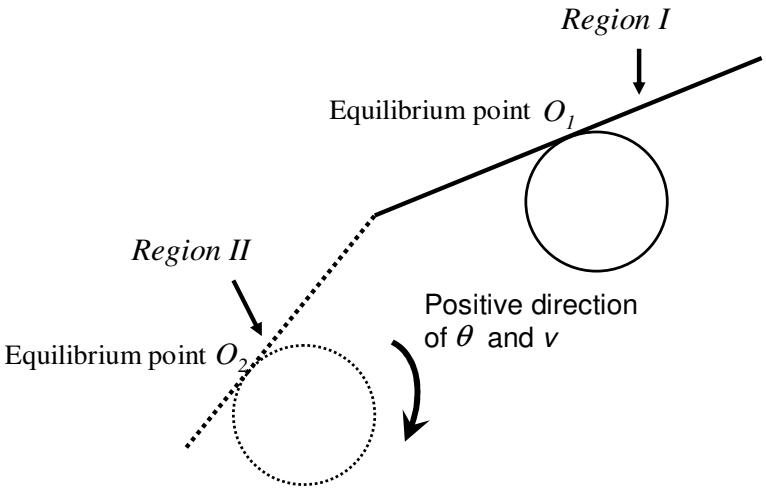

(a) A capsule system with two different slope angles.

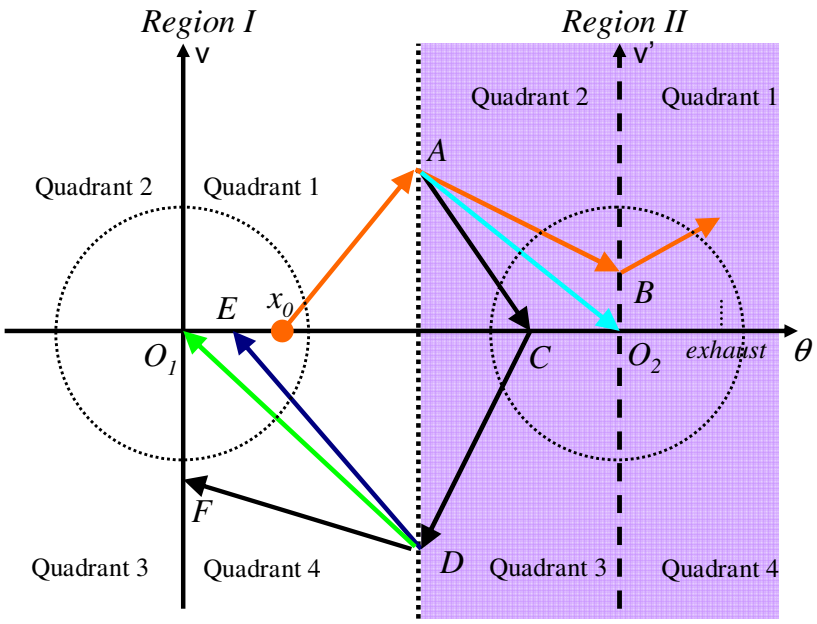

(b) Coordinates of the state space and the state transit portrait

Figure 2.10. Ball Capsule System with Multiple Slope Angles

From the analyses above, the trajectory of *x(t)* is determined by the location of the equilibrium points. According to equation (2.26), the equilibrium point is related to the

capsule angle α. Therefore the dynamics of the ball capsule system can be affected by the capsule slope angle α. In other words, the capsule slope angle α could be regarded as a control input to the ball capsule dynamic system. Subsequently, it is proposed that the angle and shape of the capsule are redesigned to obtain the desired performance.

2.4. Optimal Design For the Ball Capsule System

So far, the ball capsule system dynamics have been modeled and analyzed. To achieve the desired performance, there have to be control means to affect its dynamic behavior. As shown before, one of the control means is to design the capsule inner wall profile. In this section, the capsule profile design problem is converted into a nonlinear optimization problem, and then the Dynamic Programming method is applied to solve it.

2.4.1 Formulation of Ball Capsule Optimal Design Problem

To achieve the desired ball capsule performance, the optimal design is constrained by the appropriate choice of the initial conditions X_{initial} and final conditions X_{final}, which are chosen to meet specific design requirements. Additionally, among all the ball capsule profiles satisfying the above constraints, the one that has the minimum change of capsule slope angle is desirable. This will result in a smooth shape of the capsule wall, which in turn reduces the manufacturing cost. The total time T_{final} for the ball to move from the open position to the closed position is also preferred to be as small as possible.

$N=T_{final}/\Delta t$ is defined as the number of steps from the initial state to the final state. Note that T_{final} is not predetermined, but needs to be optimized. Now, the ball capsule design problem is ready to be formulated as an optimization problem that will achieve the above objectives. The cost function of the optimization problem is:

$$g = \lambda_1 \sum_{k=1}^{N} (\alpha(k) - \alpha(k-1))^2 + \lambda_2 (X(0) - X_{initial})^2 + \lambda_3 (X(N) - X_{final})^2 + \lambda_4 (T_{final}) \quad (2.34)$$

In particular, the first term of the cost function ensures the increment of the capsule slope angle to be as small as possible at each time step. The last three terms ensures that the system will start from the specified initial conditions and reach the desired final conditions at minimal time T_{final}. λ_1, λ_2, λ_3 and λ_4 are the weighting factors. Consequently,

the optimal control problem is to find an optimal sequence of the capsule slope angle α to minimize the cost function while satisfying the initial and final constraints.

A systematic solution to the above optimization problem can be determined recursively via Bellman's Dynamic Programming [9-10]. Since the system model (2.23) is nonlinear, analytical solution cannot be obtained. Instead numerical solution will be provided. However, first the system model needs to be discretized to carry out the numerical Dynamic Programming method.

2.4.2 System Model Discretization

To enable the design of variable slope angle for the capsule, the states of the system and the capsule slope angle α need to be discretized as shown in Figure 2.11.

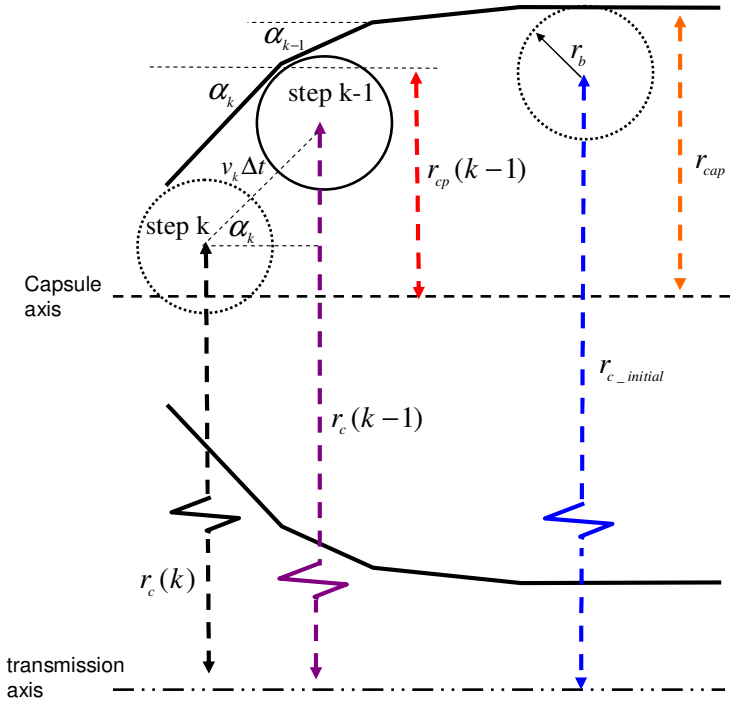

Figure 2.11. Geometry of the discrete capsule system.

The system equation (2.23) can be discretized as:

$$J\frac{v_k - v_{k-1}}{\Delta t} = (P_1(k-1) - P_2(k-1))\pi(r_b\cos(\alpha_k))^3 - F_c(k-1)r_b\sin(\alpha_k) \tag{2.35}$$

where Δt refers to the sampling time interval. Therefore the discrete state model could be written as:

$$v_k = v_{k-1} + \frac{\Delta t}{J}[(P_1(k-1) - P_2(k-1))\pi(r_b\cos(\alpha_k))^3 - F_c(k-1)r_b\sin(\alpha_k)] \tag{2.36}$$

$$\theta_k = \theta_{k-1} + v_k\Delta t \tag{2.37}$$

where

$$P_1(k-1) = \frac{1}{\left[\left(\frac{A_{th}^2(k-1)}{A_{th}^2(k-1)+A_{ex}^2}\right)+\left(\frac{A_{orf}}{A_{ex}}\right)^2\right]}[\left(\frac{A_{orf}}{A_{ex}}\right)^2 P_S + \left(\frac{A_{th}^2(k-1)}{A_{th}^2(k-1)+A_{ex}^2}\right)(P_{atm} - P_c)] \tag{2.38}$$

$$\begin{aligned} A_{th}(k-1) = {} & \pi\cdot\left(r_b + \frac{x_{lift}(k-1)}{2}\sin\alpha_k\right)\sin(2\alpha_k)\cdot x_{lift}(k-1) \\ & + \pi\cdot\left(1-\frac{\sin^2\alpha_k}{2}\right)\sin\alpha_k\tan\alpha_k\cdot x_{lift}^2(k-1) \\ & - \frac{\pi[x_{lift}(k-1)\tan\alpha_k]^2}{2r_b\cos\alpha_k}(x_{lift}(k-1) + \frac{r_b}{\sin\alpha_k})\sin(2\alpha_k)\cos(\alpha_k) \end{aligned} \tag{2.39}$$

$$r_{cp}(k-1) = r_c(k-1) + r_b\cos(\alpha_k) - (r_{c\_initial} + r_b - r_{cap}) \tag{2.40}$$

$$x_{lift}(k-1) = \frac{\left[r_{cp}(k-1) - r_b\times\cos(\alpha_k)\right]}{\tan(\alpha_k)}$$

where $r_c(k\text{-}1)$ is the distance from the center of the ball to the transmission axis at step k-1.

Similarly,

$$P_2(k-1) = \left(\frac{A_{orf}}{A_{ex}}\right)^2\left(P_S - P_1(k-1)\right) + (P_{atm} - P_c) \tag{2.41}$$

$$F_c(k-1) = \frac{4}{3}\pi \cdot r_b^3(\rho_{stl} - \rho_{oil}) r_c(k-1)\omega^2 \tag{2.42}$$

Finally, $r_c(k)$, which is the distance between the center of the ball to the transmission axis at step k, could be derived if the slope angle α_k at step k is known:

$$r_c(k) = r_c(k-1) - (v_k \Delta t)\sin(\alpha_k) \tag{2.43}$$

In the discrete model, $r_c(k)$ is used to represent the position of the ball.

In summary, equation (2.36) and equation (2.43) together could be expressed as

$$[r_c(k), v_k] = f(r_c(k-1), v_{k-1}, \alpha_k) \tag{2.44}$$

The variable α_k, which is the slope angle of the capsule at step k, could be regarded as the control input.

2.4.3 Optimal Design Using the Dynamic Programming Method

Since in this problem the initial condition is specified instead of the final conditions (T_{final} needs to be determined), the forward dynamic programming [11], which is a dual approach to backward dynamic programming [12] is used. The standard numerical Dynamic Programming approach requires state space discretization and interpolation, which brings in high computational burden. Therefore the discrete forward dynamic programming method introduced in [11] is implemented and at the same time the state space is discretized into regions, which has been presented in [13].

First, at each step k, α is discretized into L discrete values $\{\alpha_k{}^0, \alpha_k{}^1, \ldots \alpha_k{}^j \ldots \alpha_k{}^L\}$ as shown in Figure 2.12. In addition, for each discrete value of α_k, discrete regions can be generated on the plane of r_c and v shown as the black and white blocks. According to equation (2.44), only the predetermined discrete values for α_k at each step need to be generated, and then the values of $r_c(k-1)$, v_{k-1} from previous step together with α_k will be used to obtain the values for $r_c(k)$, v_k. Then, $X(k)=[\alpha_k, r_c(k), v_k]^T$ is defined. As shown in Figure 2.12, $\{X^0(k-1), X^1(k-1), \ldots X^i(k-1), \ldots X^{L_{k-1}}(k-1)\}$ are the possible discrete states calculated from step k-1. Then suppose from

$$[r_c^i(k), v_k^i] = f(X^i(k-1), \alpha^j(k)) \tag{2.45}$$

$r_c^i(k)$ and v_k^i are found and suppose that $[\alpha_k^j, r_c^i(k), v_k^i]^T$ lies in region *A* in Figure 2.12. Subsequently, the vector $[\alpha_k^j, r_c^i(k), v_k^i]^T$ can be assigned as the value for region *A*, and $[\alpha_k^j, r_c^i(k), v_k^i]^T$ is memorized as one of the discrete states for step *k*. Moreover, the cost function can be calculated based on $[\alpha_k^j, r_c^i(k), v_k^i]^T$ as:

$$J_k(\alpha_k^j, r_c^i(k), v_k^i) = [\lambda_1(\alpha_k^j - \alpha_{k-1}^i)^2 + \hat{J}_{k-1}(X^i(k-1)] \tag{2.46}$$

In the subsequent calculation, if $[\alpha_k^j, r_c^{i+c}(k), v_k^{i+c}]^T$ obtained from $f(X^{i+c}(k-1), \alpha_k^j)$ also falls into region *A*, then the cost function is recalculated again based on $[\alpha_k^j, r_c^{i+c}(k), v_k^{i+c}]^T$ as:

$$J_k(\alpha_k^j, r_c^{i+c}(k), v_k^{i+c}) = [\lambda_1(\alpha_k^j - \alpha_{k-1}^{i+c})^2 + \hat{J}_{k-1}(X^{i+c}(k-1)] \tag{2.47}$$

Then if $J_k(\alpha_k^j, r_c^i(k), v_k^i)$ is larger than $J_k(\alpha_k^j, r_c^{i+c}(k), v_k^{i+c})$, the value of region *A* should be reassigned as $[\alpha_k^j, r_c^{i+c}(k), v_k^{i+c}]^T$, and at the same time $[\alpha_k^j, r_c^i(k), v_k^i]^T$ in the discrete value space would be replaced by $[\alpha_k^j, r_c^{i+c}(k), v_k^{i+c}]^T$. But if $J_k(\alpha_k^j, r_c^i(k), v_k^i)$ is smaller than $J_k(\alpha_k^j, r_c^{i+c}(k), v_k^{i+c})$, $[\alpha_k^j, r_c^{i+c}(k), v_k^{i+c}]^T$ would be discarded and the process resumes.

Finally, after the minimum cost function for each state has been obtained, it is easy to get the optimal sequence of capsule slope angle $\alpha=[\alpha_0, \ldots, \alpha_N]$ which will minimize the total cost value.

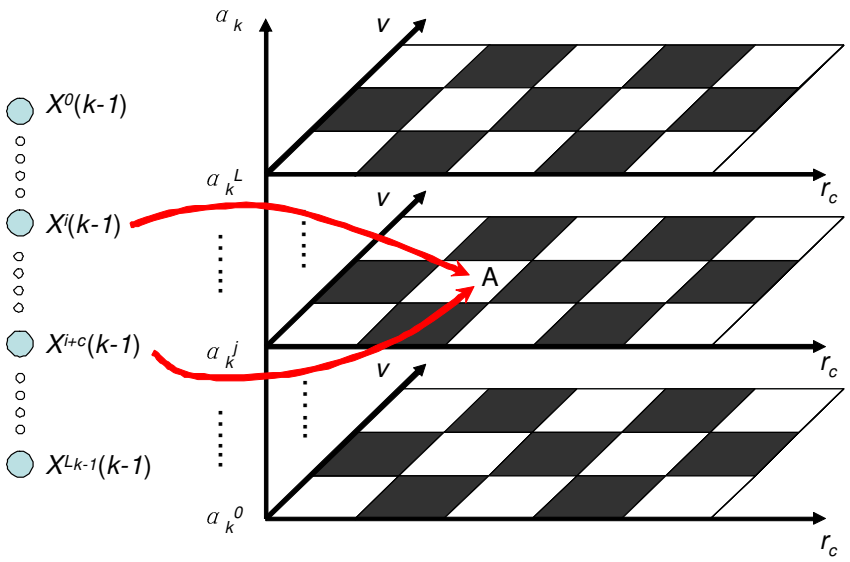

Figure 2.12. State space quantization for DP

2.5. Case Studies And Simulation Results

In this section, three possible capsule designs are considered and simulation results are provided for comparison. The system dynamic model is constructed in Matlab/SIMULINK environment, and the parameters of the model are shown in Table 2.1.

Table 2.1. Parameter Values of System Dynamic Model

β	17000(bar)	ρ_{oil}	813.79 (kg/ m^3)
C_d	0.7	r_{st}	37.3126 (mm)
ρ_{steel}	7778.05(kg/m^3)	$A_{orifice}$	3.0434 (mm^2)
r_b	1.9812(mm)	ω	2000 (rpm)
P_{atm}	1(bar)	$r_{c\_initial}$	56.947 (mm)
A_{ex}	5.8(mm^2)	r_{c_final}	56.832 (mm)
r_{cap}	2.1 (mm)		

The three capsule design profiles are shown in Figure 2.13. The design in Figure 2.13(a), which is the current design of the ball capsule, has a flat surface at the ceiling

and an angled wall near the exhaust to hold the ball. Note that, this design can be considered as a special case of the variable slope angle ball capsule system analyzed in section 2.3.2. Figure 2.13(b) presents a single slope capsule design， which is analyzed in section 2.3.1. Figure 2.13(c) shows the optimal capsule design using the Dynamic Programming method.

The input pressure P_s used in the simulation is 1.2×10^5 Pa. Figure 2.14 shows the angular velocity of the ball as it rotates towards the closed position. Figure 2.15 presents the change of the distance r_c , which is the distance between the center of the ball to the transmission rotational axis, with respect to time. Note that r_c at the opening position is 56.947 mm for all three designs, and is 56.832 mm at the exhaust. Figure 2.16 shows the actuation torque acting on the ball versus time. The actuation torque is defined as

$$Tor = (P_1 - P_2)A_{eff} r_b \cos(\alpha) - F_c r_b \sin(\alpha). \tag{2.48}$$

If the actuation torque is negative at the exhaust, the ball cannot be held at the closed position and will rotate backward. Figure 2.17 shows the throttling area during the ball motion.

2.5.1 Case Study I: The Current Capsule Design

For the current capsule design, as shown in Figure 2.14, the ball angular velocity jumps to a high value, and closes the exhaust quickly. However, at the closed position, the actuation torque *Tor* (2.48) is negative as shown in Figure 2.16, which means the ball could not be held at the exhaust. Thus the ball will rotate backwards, and keep chattering between the closed position and the open position, which is undesirable for the clutch fill process. The cause of this chattering phenomenon is the improper design of the slope angles at the opening position and the closed position. According to the previous analysis of the system dynamics, the slope angle at the opening position determines the minimum input pressure P_s (triggering pressure) required to start the ball motion toward the exhaust, and the slope angle at the closed position determines the minimum input pressure P_s (holding pressure) required to hold the ball at the exhaust. Figure 2.18 shows the triggering pressure and holding pressure as a function of the slope angle. It can be seen that a relatively small input pressure can trigger the start of the ball motion toward

the exhaust if the capsule slope angle at the opening position is small (0 degree for current design). However, if the slope angle at the closed position is large (36.73 degrees for current design), then the small input pressure will not be enough to hold the ball at the exhaust, which causes chattering and is exactly the problem associated with the current capsule design.

2.5.2 Case Study II: The Capsule Design with Single Slope Angle

For the capsule with single slope angle, the ball angular velocity goes up quickly as shown in Figure 2.14. The angular velocity reaches its peak value before closing off the exhaust. Note that during the closing process, the throttling area A_{th} continues to drop, which acts as the intrinsic feedback to the system dynamics and explains the fast response of the ball capsule system. Once the capsule is closed, the ball will be held at the closing position because the actuation torque *Tor* (2.48) is positive as shown in Figure 2.16. Therefore this design avoids the chattering problem.

Even though the chattering problem is avoided, the single slope capsule design does not have any flexibility of controlling the ball capsule system dynamics. If the slope angle is small, then the ball angular velocity may increase too fast and cause high impact at the exhaust. In addition, the added length of the capsule due to the small slope angle is also a concern for packaging. Moreover, as shown in Figure 2.18, if the slope angle is too large, the triggering pressure will be high, which will waste a lot flow before the ball capsule can be closed. Another drawback of this design is that, although the single slope capsule avoids the chattering problem when the input pressure is constant, it does not ensure robust performance. As shown in Figure 2.18, the difference between the triggering pressure and the holding pressure is insignificant. Therefore, if there are some perturbations in the input pressure P_s, the ball will oscillate between the open and closed positions. Consequently, to add control means to the ball angular velocity and also to improve system robustness, the capsule design with multiple slope angles is proposed.

2.5.3 Case Study III: The Capsule Design with Multiple Slope Angles

To ensure robust performance, the capsule angles at the opening position and at the exhaust need to be designed appropriately. The capsule angle at the closed position (Region C in Figure (2.13c)) is designed to be smaller than that at the open position (Region A in Figure (2.13c)). As shown in Figure (2.18), this design will raise the gap between minimum triggering pressure and the minimum holding pressure, and thus increase system robustness. In addition, to avoid noise and wears at the exhaust, the impact speed at the exhaust is designed to be 200 rad/sec, which is another constraint in our optimal design. Furthermore, to make manufacturing easier, the number of different slope angles should be as small as possible. The weighting values selected for the Dynamic Programming cost function are: λ_1=100, λ_2=1, λ_3=1, λ_4=15. Based on the above constraints, the Dynamic Programming method is used to obtain the optimal values for the slope angles and the length of each angled section as shown in Figure 2.13 (c).

For the capsule design shown in Figure 2.13 (c), when the ball is closing the capsule, the ball angular velocity increases initially in region A, because the actuation torque *Tor* (2.48) at the beginning is positive as shown in Figure 2.16. When the ball enters region B, the actuation torque becomes negative due to the large slope angle of region B, resulting in a decrease in the angular velocity, which is actually the case analyzed in section 2.3.2. Finally, the ball enters region C and stops at the exhaust. The final angular velocity could be controlled by designing the slope angles. In addition, as shown in Figure 2.15, the ball is held at the exhaust, which is ensured by proper design of the slope angles at the open and closed positions. Again, the intrinsic feedback of the throttling area A_{th} ensures the fast closing of the capsule as shown in Figure 2.17.

During clutch disengagement, when the fluid is released from the clutch chamber, the pressure inside the chamber will drop. When the pressure inside of the clutch chamber is lower than the minimum pressure to hold the ball at the exhaust, the ball will rotate back towards the open position. The opening process is also unstable and the rotating speed of the ball will increase as well. Once the ball reaches the open position (region A), the centrifugal force will hold the ball at the open position. Since the slope angle at the open position is designed to be larger than that at the exhaust, the moment from the

centrifugal force at the open position will be larger. Moreover, the pressure in the clutch chamber will be low during the clutch disengagement. Therefore, the centrifugal force will be large enough to hold the ball still at the open position to avoid ball chattering.

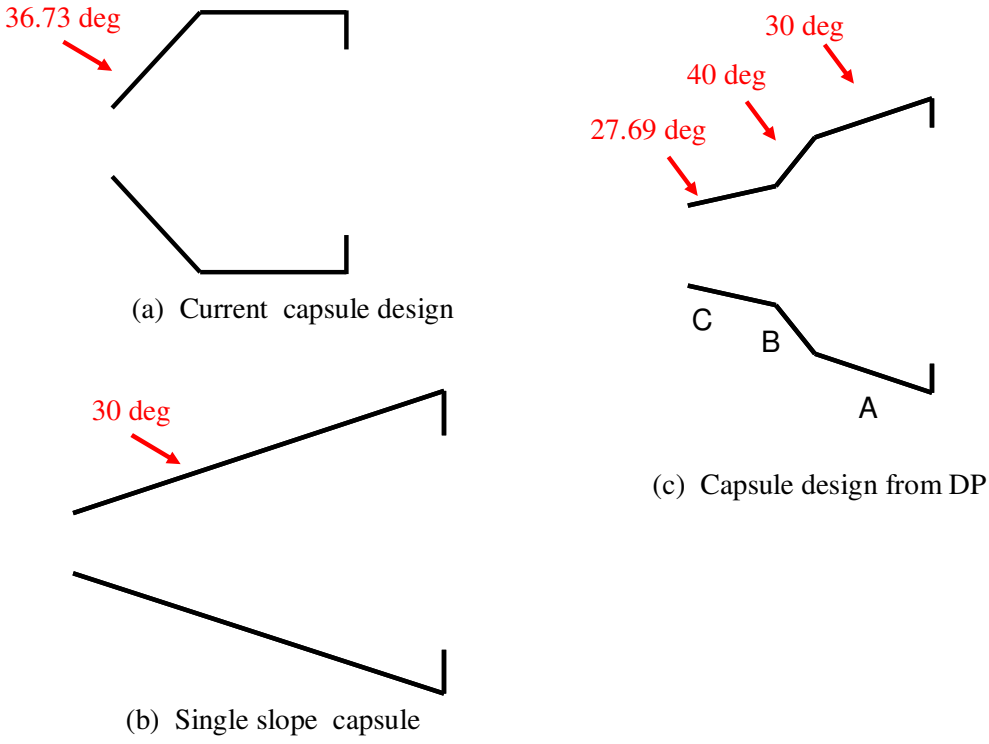

Figure 2.13. Ball Capsule Design

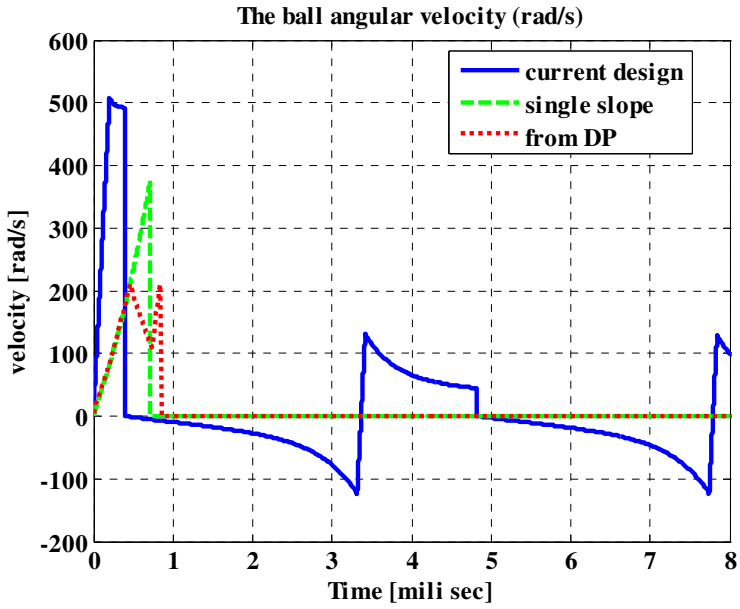

Figure 2.14. Angular velocity of the ball

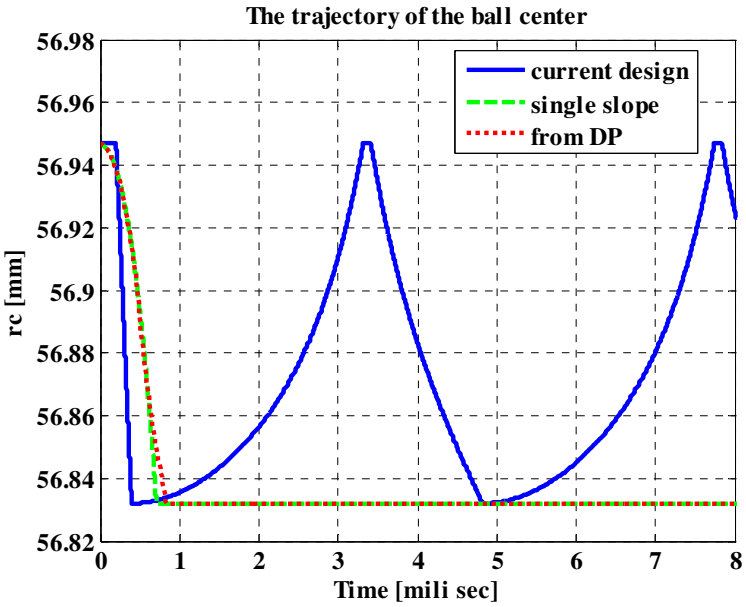

Figure 2.15. The trajectory of the ball center r_c

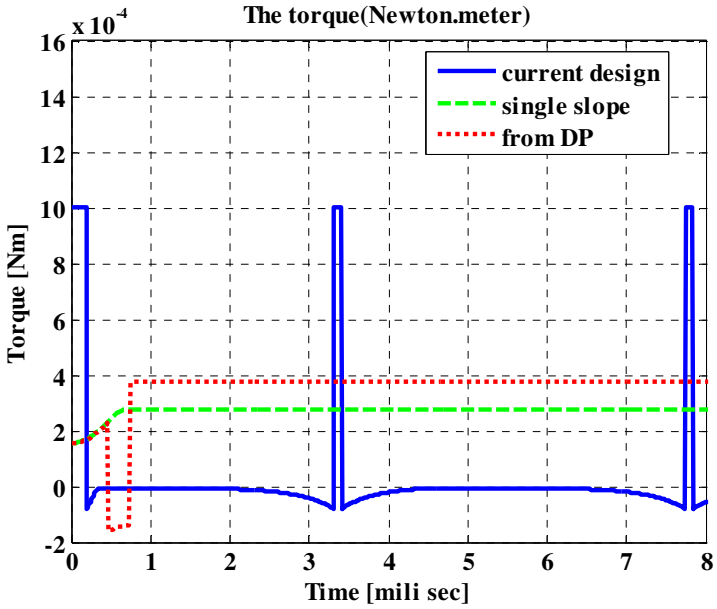

Figure 2.16. Actuation torque on the ball

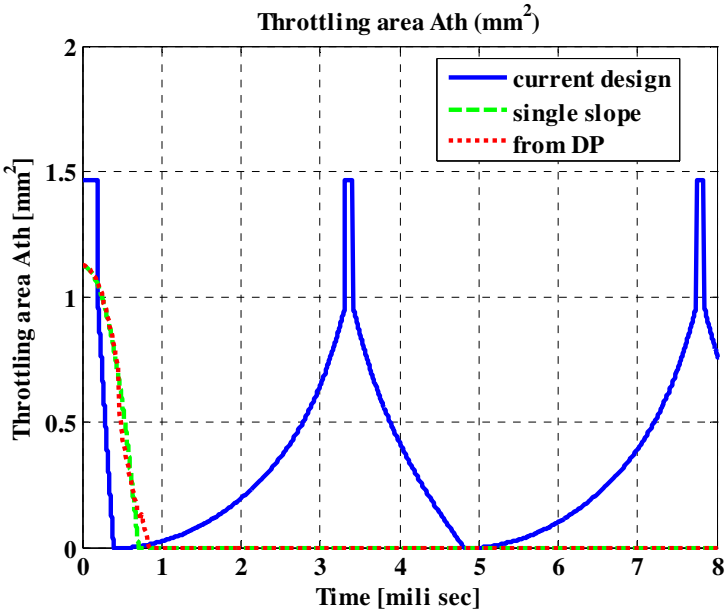

Figure 2.17. The throttling area A_{th}

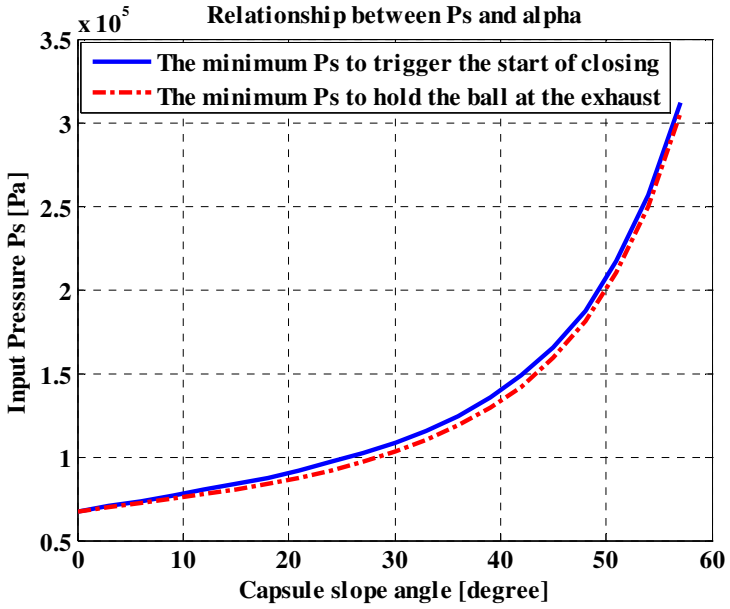

Figure 2.18. The closing and holding input pressure

2.6. Conclusion

This chapter presents the modeling, analysis, and optimal design of the ball capsule system for automotive transmissions. A dynamic model of the ball capsule is first constructed. The derivation of the ball capsule throttling area is considered novel and critical because of its asymmetric nature. Further analysis of the system dynamics

reveals that the ball capsule contains an intrinsic positive feedback structure, and thus is unstable. This unique and interesting property is the key to ensure a fast response. In addition, it is found that the shape of the capsule is an effective control parameter for the performance and robustness of the ball capsule system, and that the capsule with multiple slope angles rather than the current design could render desired performance. To provide an optimal design of the ball capsule, the problem is then formulated as a constrained optimization problem and is solved using Dynamic Programming method. Case studies and simulation results show the effectiveness of the proposed design methods.

References In Chapter 2

[24] Song, X., Zulkefli, A., Sun, Z. and Miao, H., "Transmission Clutch Fill Control Using A Customized Dynamic Programming Method", Proceedings of the 2008 ASME Dynamic System and Control Conference, DSCC 2008-2166, Ann Arbor, Michigan, 2008.

[1] Wagner, G., "Application of Transmission Systems for Different Driveline Configurations in Passenger Cars", SAE Technical Paper 2001-01-0882.

[2] Sun, Z. and Hebbale, K., "Challenges and Opportunities in Automotive Transmission Control", Proceedings of 2005 American Control Conference, Portland, OR, USA, June 8-10, 2005.

[3] Hebbale, K. and Kao, C, "Adaptive Control of Shifts in Automatic Transmissions", Proceedings of the 1995 ASME International Mechanical Engineering Congress and Exposition, San Francisco, CA, 1995.

[4] Bai, S., Moses, R., Schanz, T. and Gorman, M. "Development of A New Clutch-to-Clutch Shift Control Technology", SAE Technical Paper 2002-01-1252.

[5] Marano, J., Moorman, S., Whitton, M., and Williams, R. "Clutch to Clutch Transmission Control Strategy", SAE Technical Paper 2007-01-1313.

[6] Han, W. and Yi, S., "A Study of Shift Control Using the Clutch Pressure Pattern in Automatic Transmission", Proceedings of the IMechE, Part D: Journal of Automobile Engineering, Volume 217, Number 4/2003, pp 289-298.

[7] Manring, N., 2005, Hydraulic Control Systems, John Wiley & Sons, Hoboken, New Jersey.

[8] Khalil, H., 2002, Nonlinear Systems (Third Edition), Prentice-Hall Inc., New Jersey.

[9] Bellman, R., 1957, Dynamic Programming, Princeton University Press, New Jersey.

[10] Bellman, R. and Dreyfus, S., 1962, Applied Dynamic Programming, Princeton University Press, New Jersey.

[11] John, H. and Lapidus, L., “Aspects of the Forward Dynamic Programming Algorithm”, I&EC Process Design and Development, 1968.

[12] Larson, R. and Casti, J., 1978, Principles of Dynamic Programming: Basic Analytical and Computational Methods, Marcel Dekker Inc., New York and Basel.

[13] Song, X., Zulkefli, A., Sun, Z. and Miao, H., “Transmission Clutch Fill Control Using A Customized Dynamic Programming Method”, Proceedings of the 2008 ASME Dynamic System and Control Conference, DSCC 2008-2166, Ann Arbor, Michigan, 2008.

Chapter 3

The Clutch Level Design-- Transmission Clutch Fill Control Using a Customized Dynamic Programming Method

After maintaining a consistent initial condition as presented in Chapter 2, the second critical factor for the efficient open loop clutch control is the clutch fill actuation process optimization. In this chapter, we present a systematic approach to evaluate the clutch fill dynamics and synthesize the optimal control pressure profile.

3.1. Introduction

The automotive transmission, as a key component of the vehicle propulsion system [1], is designed to transfer the engine torque to the vehicle driveline with desired ratio smoothly and efficiently. The main components of a typical automatic transmission include the torque converter, the planetary gear set and the clutch system. The power transfer and gearshift is in fact realized by engaging and disengaging the clutch systems. Figure 3.1 shows a simplified schematic diagram of a six speed automatic transmission [2], with five sets of clutch packs. Clutches are connected to specific gears of the planetary gear set, and different gear ratio is realized by engaging the corresponding clutches. During the gear shift, one set of clutch (on-coming clutch) needs to be engaged and another set (off-going clutch) needs to be disengaged [2], which is called clutch to clutch shift [3-7]. For a smooth clutch to clutch shift, precise synchronization of the on-coming clutch and off-going clutch is critical, which otherwise will cause undesirable torque interruption and oscillation [3]. To ensure precise synchronization, before clutch engagement, it is necessary to actuate the oncoming clutch to a position where the clutch packs are just in contact. This process is called clutch fill and plays an important role for the clutch to clutch shift technology.

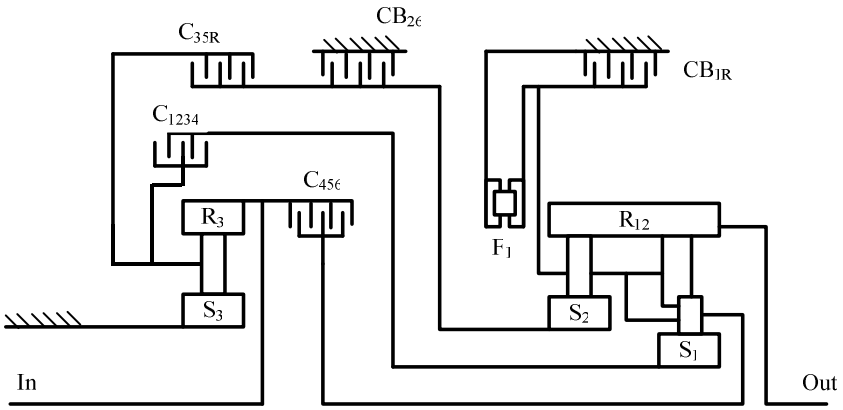

Figure 3.1. Scheme diagram of a six speed automatic transmission

The commonly used clutch actuation devices in transmissions are electro-hydraulically actuated clutches. This attributes mainly to the high power density of electro-hydraulic systems. A schematic diagram of a typical transmission clutch actuation system is shown in Figure 3.2. Once the clutch is to be engaged, pressurized fluid flows into the clutch chamber and pushes the clutch piston towards the clutch packs until they are in contact (clutch fill). At the end of the clutch fill process, the input pressure P_s is further increased, which then squeezes the clutch piston to the clutch packs and transfers the engine toque to the vehicle driveline. It is imperative to control the clutch piston to reach the clutch packs within a specified clutch fill time because an improper clutch fill process can result in either an *under-fill* or an *over-fill* [3], both of which can cause the failure of the clutch shift synchronization and therefore negatively affect the clutch shift quality. Therefore, designing the clutch fill pressure command is critical to achieve a fast and precise clutch fill and a smooth start to the clutch engagement process. Moreover, it is desirable to synthesize the clutch fill pressure to reduce the peak flow demand during the clutch fill process. This feature would enable a smaller transmission pump to improve vehicle fuel economy [8]. However, there are two main challenges associated with the clutch fill control design. First, even small errors in calculating the clutch fill pressure and fill time could lead to an over-fill or an under-fill, which will adversely impact the shift quality. Second, currently there is no pressure sensor inside the clutch chamber, and consequently a pressure feedback control loop could not be formed. Therefore, it is necessary to design an open loop pressure control

profile, which should be optimal in the sense of peak flow demand and also robust in terms of clutch fill time. Clearly, the traditional approach based on manual calibration is not effective to achieve the above objectives. In this chapter, we will present a systematic approach to solve this problem.

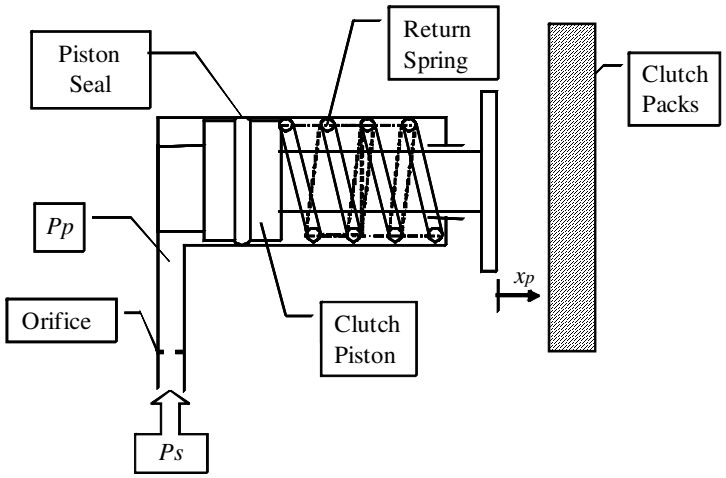

Figure 3.2. Schematic diagram of a clutch mechanism

To enable a systematic and model based control design, a precise clutch fill dynamic model is necessary. It should capture the key dynamics of the clutch fill process, which are not identical to those of the clutch engagement process [9-11]. Based on the clutch fill dynamic model, a systematic approach for this control problem can be determined recursively via Bellman's Dynamic Programming (DP) method [12-13]. Researchers in vehicle control field have successfully applied Dynamic Programming to various optimal control problems [14-16]. For example, Kim and co-authors [15] used Dynamic Programming (DP) method to obtain the optimal gear shift and throttle control that maximizes fuel economy while satisfying the power demand. Kang and co-authors [16] have applied optimal control method to lean burn engines using numerical DP approach. However, different from applications above, the clutch actuation system contains high frequency and stiff dynamics [10, 11], which requires a very fast sampling rate for the discretized model. As a result, the large number of steps, along with the curse of dimensionality [17] associated with conventional numerical DP method, prohibits its efficient implementation for the clutch fill control problem. Furthermore, the conventional numeric DP algorithm suffers from interpolation errors, which will affect the accuracy of the final results. Therefore, we have proposed a customized numerical

Dynamic Programming approach, which has successfully solved the above problems and generated satisfactory results. The customized DP method transforms the stiff dynamic model into a non-stiff one by a unique model structure transformation and state discretization, and thus enables the reduction of the discrete sampling steps. Furthermore, by discretizing the state space into regions rather than discrete nodes, the interpolation error is avoided. Finally, the customized DP only searches the optimal solution within the reachable discrete states, which dramatically reduces the searching space and therefore mitigates the curse of dimensionality problem [17].

To validate the proposed control methodology, a transmission clutch fixture and hydraulic control circuit are designed and built to facilitate the experimental investigation of the optimal clutch fill control. Through a series of experiments, the dynamic model parameters are identified. To this end, the optimal clutch fill input pressure designed by the customized dynamic programming is implemented to achieve the optimal clutch fill performance.

The rest of the chapter is organized as follows. Section 3.2 presents the system model and formulates the clutch fill control problem as an optimization problem. Section 3.3 first investigates the applicability of conventional numerical Dynamic Programming approach and then presents the customized numeric DP method. Experimental setup, system identification and the clutch fill experimental results are presented in section 3.4. Conclusion is provided in section 3.5.

3.2. Problem description

In this section, we first model the transmission clutch actuation system and then formulate the clutch fill control problem as an optimization problem.

3.2.1 System Modeling

As shown in Figure 3.2, p_s is the supply pressure command and also the control input to the system, p_p is the pressure inside the clutch chamber, and x_p is the clutch piston displacement. The pressurized fluid flows into the clutch chamber and pushes the clutch piston to the right, and finally contacts the clutch pack. We call this process clutch fill. The dynamics associated with clutch fill can be modeled as:

$$\dot{x}_1 = x_2 \tag{3.1}$$

$$\dot{x}_2 = \frac{1}{M_p}[A_p \times (x_3 + P_c - P_{atm}) - D_p x_2 - F_{drag}(x_3 + P_c, x_2) - K_p \times (x_1 + x_{p0})] \tag{3.2}$$

$$\dot{x}_3 = \frac{\beta}{V_0 + A_p x_1}[sign(u - x_3) C_d A_{orifice} \sqrt{\frac{2|u - x_3|}{\rho}} - A_p x_2] \tag{3.3}$$

$$\text{where} \begin{bmatrix} x_1 = x_p \\ x_2 = \dot{x}_p \\ x_3 = p_p \\ u = p_s \end{bmatrix} \text{ and } \begin{bmatrix} x_1(0) \\ x_2(0) \\ x_3(0) \end{bmatrix} = \begin{bmatrix} 0 \\ 0 \\ u(0) \end{bmatrix}$$

where x_1 *is* the clutch piston displacement, x_2 is the clutch piston velocity, x_3 is the clutch chamber pressure, u is the supply pressure control input, M_p is the effective mass of the piston, A_p is the piston surface area, D_p is the clutch damping coefficient, P_{atm} is the atmospheric pressure, K_p is the return spring constant, x_{p0} is the return spring preload, β is the fluid bulk modulus, V_0 is the chamber volume, C_d is the discharge coefficient, $A_{orifice}$ is the orifice area, and ρ is the fluid density. F_{drag} is the piston seal drag force, which is dependent on the piston motion. It is modeled as:

$$F_{drag} = \begin{cases} \left[k_m (x_3 + P_c) + c_m\right] \times \tanh\left(\frac{x_2}{\alpha}\right) & (x_2 \neq 0) \\ F_{stick} & (x_2 = 0) \end{cases} \tag{3.4}$$

where k_m and c_m are constant, α is the piston seal damping coefficient, and F_{stick} is the static stick friction force from the Kanopp's stick-slip model [18]. The stick friction is often neglected in the clutch dynamic models for engagement [9-11], as it is relatively small comparing with the clutch engagement force. But due to the lower operating pressure during the clutch fill, the stick friction force becomes critical. For numerical stability, it is assumed that the drag force is F_{stick} when the piston velocity x_2 is within a small interval around zero [18], which is called the stick region as shown in Figure 3.3. When the velocity is in this region, the value of F_{stick} is to balance the net force and the piston acceleration is assumed to be zero. Moreover, there is a maximum value

constraint for the stick friction. If the net force exceeds the maximum stick friction, the piston will accelerate. The maximum stick friction, which is noted as F_{static}, is proportional to the clutch chamber pressure and can be modeled as:

$$F_{static} = k_s \left(x_3 + P_c \right) + c_s \tag{3.5}$$

where k_s and c_s are constant.

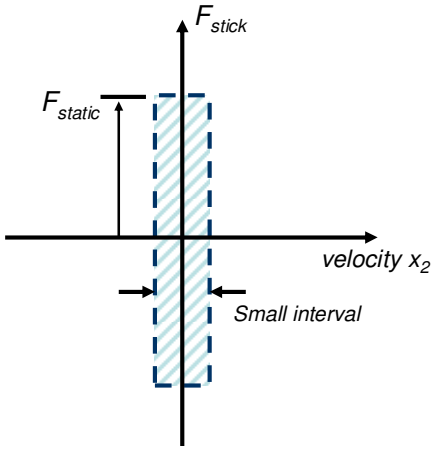

Figure 3.3. Stick friction diagram

In addition, P_c is the centrifugal force induced pressure generated from the rotation of the clutch assembly [19]. The fluid pressure distribution P_{ct} due to the centrifugal force at any radius r can be expressed as:

$$P_{ct} = \frac{\rho}{2} \omega^2 \left(r^2 - r_{st}^2 \right) \tag{3.6}$$

where ω is the clutch system rotational speed and r_{st} is the starting fluid level [20]. The average fluid centrifugal pressure P_c on the effective piston area A_p can be expressed as:

$$P_c = \frac{\int_{r_{pi}}^{r_{po}} P_{ct} \cdot 2\pi r dr}{A_p} \tag{3.7}$$

where r_{pi} and r_{po} are the piston inner and outer radius respectively.

3.2.2 Formulation of the Clutch Fill Control Problem

To enable a fast and precise clutch fill, the clutch piston must travel exactly the distance d, which is required for the piston to contact the clutch pack, in the desired clutch fill time T. Also, at time T, the piston velocity x_2 should be zero, and the pressure force inside the chamber must be equal to the spring force in order to keep the piston in contact with the clutch pack. These requirements can translate into a set of final conditions that the system must satisfy:

$$x_1(T) = d\,, \qquad x_2(T) = 0 \quad and \quad x_3(T) = \frac{K_p \times (d + x_{p0})}{A_p} + P_{atm} - P_c \tag{3.8}$$

where d is the desired clutch stroke, and $x_1(T)$, $x_2(T)$ and $x_3(T)$ are the final states.

Among the controls that can bring the clutch from initial states to the final states (3.8), we would like to take the one that has minimum peak flow demand. This will enable a smaller displacement transmission pump, which in turn will improve the vehicle fuel economy and reduce cost [8]. To reduce the peak flow demand, we need to minimize the peak value of the piston velocity x_2 during the clutch fill process since the clutch fill flow is proportional to the piston velocity. Therefore, x_2 should quickly approach the average velocity, and stay at the average velocity as long as possible, and at the end goes to the final state conditions as shown in Figure 3.4. Note that the total area enclosed by the x_2 trajectory should be the piston displacement d.

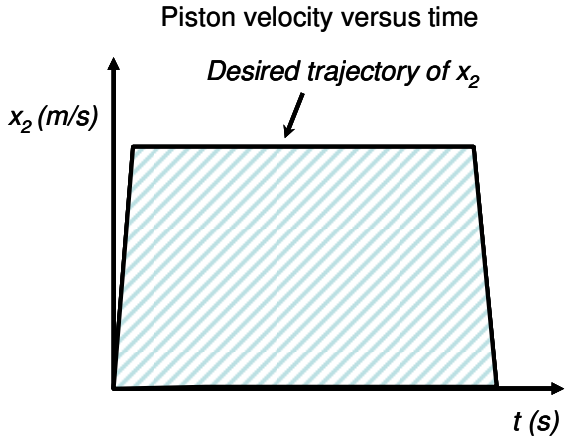

Figure 3.4. Desired trajectory of x_2

In addition, the piston velocity can not increase too fast at the beginning of the clutch fill. Before the clutch starts moving, the clutch chamber pressure increases and therefore the stick friction on the clutch piston also increases. The stick friction will reach its maximum value F_{static} and then the clutch piston will move. Once moving, the piston drag force will switch from stick friction to drag force in motion, which is smaller than the F_{static}. This friction force transient is non-smooth and nonlinear [18], which makes it difficult to track and control a fast changing piston velocity profile given the fact that currently there is no feedback sensor for the clutch fill process. Therefore, in Figure 3.5, the initial velocity of the clutch fill is designed to be small for a short duration and then rise quickly to its peak value.

However, the above considerations have not taken system robustness into account. In particular, the solenoid valve, which is used to generate the input pressure command u, has time delay and subsequently results in the shift of x_2 trajectory as shown in Figure 3.5. Note that the final time T is fixed, so the piston could not travel to the desired distance d due to the shift and the difference between the desired trajectory and the shifted one will be:

$$\Delta d = \int_{T-\Delta T}^{T} x_2(t)dt \tag{3.9}$$

Therefore, to minimize Δd, the value of $x_2(t)$ between time T-ΔT and T should be as small as possible as shown in Figure 3.5, and we can claim that the unique trajectory of x_2 will enhance the robustness of the system for time delay. In addition, from (3.8), we can see that the clutch fill final states are determined by the spring stiffness K_p, the piston area A_p, the spring preload x_{po} and the centrifugal pressure P_c. K_p, A_p, and x_{po} can be measured accurately and will not change much with the environment. P_c can also be accurately determined based on the transmission rotational speed, and it in fact has less influence on the final condition due to its small magnitude comparing with the other forces. Therefore the final states of the clutch fill system are quite robust.

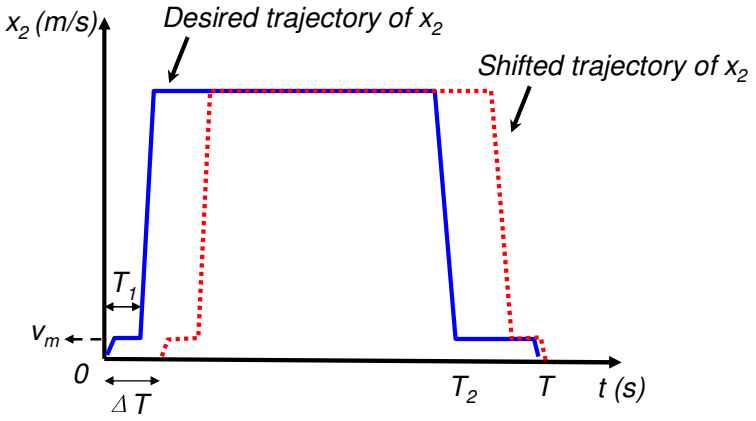

Figure 3.5. Shifted trajectory of x_2

Now we are ready to formulate the clutch fill control as an optimization problem. The cost function of the optimization problem is:

$$g = \int_0^{T_1} [x_2(t) - v_m]^2 dt + \lambda_1 \int_{T_1}^{T_2} [x_2(t) - \frac{d}{T}]^2 dt + \lambda_2 \int_{T_2}^{T} [x_2(t) - v_m]^2 dt + \lambda_3 [x_1(T) - d]^2$$
$$+ \lambda_4 [x_2(T) - 0]^2 + \lambda_5 \{x_3(T) - [\frac{K_p(d + x_{p0})}{A_p} + P_{atm} - P_c]\}^2 \quad (3.10)$$

In particular, the first term of the cost function ensures the piston to start with a low velocity v_m. The second term ensures that the velocity x_2 remains close to the average velocity d/T, which will minimize the peak value of x_2 and therefore the peak flow demand. The third term ensures x_2 to be as small as possible (close to zero) from time T_2 to final time T, which will enhance system robustness. The last three terms ensures that the system will reach the specified final conditions in the required time T. λ_1, λ_2, λ_3, λ_4, and λ_5 are the weighting factors.

3.3. Optimal Control design

A systematic solution to the above optimization problem can be determined recursively via Bellman's Dynamic Programming. Since the system model (3.1-3.3) is nonlinear, analytical solution cannot be obtained. Instead numerical solution will be provided. But first we need to discretize the system model to carry out the numerical Dynamic Programming method.

3.3.1 System Model Discretization

We discretize the system model (3.1-3.3) as follows:

$$x_1(k+1) = \Delta t x_2(k) + x_1(k) \tag{3.11}$$

$$\begin{aligned} x_2(k+1) = x_2(k) + \frac{\Delta t}{M_p}\{A_p[x_3(k) + P_c - P_{atm}] - D_p x_2(k) - \\ F_{drag}\left[x_3(k) + P_c, x_2(k)\right] - K_p \times [x_1(k) + x_{p0}]\} \end{aligned} \tag{3.12}$$

$$x_3(k+1) = \frac{\Delta t \beta}{V_0 + A_p x_1(k)}\{sign\left[u(k) - x_3(k)\right] \times C_d A_{orifice}\sqrt{\frac{2\left|u(k) - x_3(k)\right|}{\rho}} - A_p x_2(k)\} + x_3(k) \tag{3.13}$$

where Δt refers to the sampling time interval. For presentation simplicity, define f as the simple representation of the state space model (3.11-3.13), and define $X(k)=[x_1(k), x_2(k), x_3(k)]^T$.

We define $N=T/\Delta t$ as the number of steps from the initial state to the final state. And the cost function (3.10) becomes:

$$\begin{aligned} g(X) = \sum_{k=0}^{N_1}[x_2(k) - v_m]^2 \Delta t + \lambda_1 \sum_{k=N_1+1}^{N_2}[x_2(k) - \frac{d}{T}]^2 \Delta t + \lambda_2 \sum_{k=N_2+1}^{N-1}[x_2(k) - v_m]^2 \Delta t + \\ \lambda_3[x_1(N) - d]^2 + \lambda_4[x_2(N) - 0]^2 + \lambda_5\{x_3(N) - [\frac{K_p(d + x_{p0})}{A_p} + P_{atm} - P_c]\}^2 \end{aligned} \tag{3.14}$$

Consequently, the optimal control problem is to find an optimal control input u to minimize the cost function

$$J(X) = \min_{u \in U} g(X) \tag{3.15}$$

where $X=[X(0), \ldots. X(N)]$, $u=[u(0), \ldots., u(N)]$, and U represents the set of feasible control inputs.

3.3.2 Applicability of Conventional Numerical Dynamic Programming to the Optimal Clutch Fill Control

In this section, the applicability of conventional numeric Dynamic Programming for

the clutch fill control problem is explored. To convert the Dynamic Programming into a finite computational problem, the standard method is to use state space quantization and interpolation [12, 13, 16]. Though widely applied in numerical DP applications, the conventional numerical DP algorithm is not suitable for solving the clutch fill control problem. The system model (3.11-3.13) includes stiff dynamic equations [21], which is a typical feature having the presence of rapidly changing transients [21]. The stiffness of the system can be manifested mathematically by evaluating the Jacobian matrix of the linearized form of the dynamic model (11-13) along its state trajectories [21]. This stiffness feature will require DP to have a very high sampling rate. Typical ways to deal with stiff dynamic equations like *A*-stable method [22] and newton's iterative method are not desirable in this application.

Besides, the conventional numerical Dynamic Programming also requires state space discretization and interpolation, which also results in high computational burden. In addition, the possible states for each step are discretized before the Dynamic Programming process, but some of those are not reachable at all [16]. This is because the system dynamics have already set constraints between $x_1(k)$, $x_2(k)$, x_3 (k) and $x_1(k+1)$, $x_2(k+1)$ and x_3 $(k+1)$, so the states can be reached only if they satisfy the specific dynamic relationship. Consequently, certain quantified discrete states are actually not needed in the Dynamic Programming process. Furthermore, the interpolation [16] used to calculate the cost function will cause approximation errors. And the approximation errors will propagate as the time step increases. It has been indicated that the interpolation error tends to increase almost linearly [17].

3.3.3 Optimal Control Using a Customized Dynamic Programming Method

As shown above, the conventional numerical DP algorithm with interpolation is not suitable to solve the clutch fill control problem. In this section, we present a customized numerical Dynamic Programming method, which can generate an accurate optimal control sequence with much reduced computational burden.

First, it is desirable to avoid the stiffness and sampling interval constraint associated with the clutch fill dynamic model. One possible way to realize this is to have a proper

inversion of the model structure and therefore change its stiff characteristic. Given the structure of the system model (11-13), if $x_1(k+1)$, $x_2(k+1)$, $x_3(k+1)$, and $x_2(k)$ are known, we can calculate the values of $x_1(k)$, $x_3(k)$ and the input $u(k)$ as follows:

$$x_1(k) = x_1(k+1) - \Delta t x_2(k) = R_1(k) \tag{3.16}$$

$$x_3(k) = R_2(k) \tag{3.17}$$

$$u(k) = sign(W)\left(\frac{W}{C_d A_{orifice}}\right)^2 \frac{\rho}{2} + x_3(k) = R_3(k) \tag{3.18}$$

where

$$W = [x_3(k+1) - x_3(k)] \times \frac{[V_0 + A_p x_1(k)]}{\Delta t \beta} + A_p x_2(k)$$

The equation $R_2(k)$ determines the in-chamber pressure $x_3(k)$ in the step k and involves the drag force F_{drag} term, which has different models depending on the piston velocity x_2. When $x_2(k)$ is not zero, F_{drag} can be obtained from equation (3.4) and $R_2(k)$ is:

$$R_2(k) = \frac{1}{A_p - k_m \times \tanh[\frac{x_2(k)}{\alpha}]} \times \{[x_2(k+1) - x_2(k)] \times \frac{M_p}{\Delta t} -$$
$$A_p(P_c - P_{atm}) + D_p x_2(k) + K_p[x_1(k) + x_{p0}] + (c_m + k_m P_c)\tanh[\frac{x_2(k)}{\alpha}]\}$$

When $x_2(k)$ is zero but $x_2(k+1)$ is nonzero, which means that the piston starts moving, the F_{drag} is assumed to be the maximum static friction F_{static} in (3.5) and $R_2(k)$ becomes:

$$R_2(k) = \frac{1}{A_p - k_s} \times \{[x_2(k+1) - x_2(k)] \times \frac{M_p}{\Delta t} -$$
$$A_p(P_c - P_{atm}) + D_p x_2(k) + K_p[x_1(k) + x_{p0}] + (c_s + k_s P_c)\}$$

When both $x_2(k)$ and $x_2(k+1)$ are zero, which means that the piston stays static, the chamber pressure $x_3(k)$ variation is assumed to be small and $R_2(k)$ becomes:

$$R_2(k) = x_3(k+1)$$

For notation simplicity, we can denote Eq. (3.16), (3.17) and (3.18) as [$x_1(k)$, $x_3(k)$,

$u(k)]=R[x_1(k+1), x_2(k+1), x_3(k+1), x_2(k)]$. Note that as $x_2(k)$ is now predetermined in the inverse dynamic model (3.16-3.18), it could be regarded as an input, and the new unknown states become $[x_1(k), x_3(k), u(k)]$. Therefore, the Jacobian matrix of (3.16-3.18) during clutch motion becomes:

$$\frac{\partial[R_1(k), R_2(k), R_3(k)]^T}{\partial[x_1(k+1), x_3(k+1), u(k+1)]^T} = \begin{bmatrix} 1 & 0 & 0 \\ \dfrac{\partial R_2(k)}{\partial x_1(k+1)} & 0 & 0 \\ \dfrac{\partial R_3(k)}{\partial x_1(k+1)} & \dfrac{\partial R_3(k)}{\partial x_3(k+1)} & 0 \end{bmatrix} \tag{3.19}$$

The eigenvalues of (19) are always inside or on the unit circle regardless of the value of Δt, which means the dynamic model (3.16-3.18) is not stiff [21] and therefore the sampling interval constraint can be avoided. Note that the above model transformation still requires the predetermined value for $x_1(k+1)$, $x_2(k+1)$, $x_3(k+1)$, and $x_2(k)$. Interestingly, as the Dynamic Programming is implemented in a backward fashion, $x_1(k+1)$, $x_2(k+1)$ and $x_3(k+1)$ were calculated in the previous step, and $x_2(k)$ can be discretized into finite grids and predetermined in advance. Note that not all model inversion will result in non-stiff dynamics. For example, the inverse model $X(k)= X(k+1)-f\ [X(k+1),u(k)] \times \Delta t$ (f is the dynamic model (3.11-3.13)) using the backward Euler method is still stiff [22].

Therefore, instead of making combinations of predetermined discrete values of $x_1(k)$, $x_2(k)$ and $x_3(k)$ in the conventional DP [16], we only need to generate the predetermined discrete values for $x_2(k)$ at each step, and then use the values of $x_1(k+1)$, $x_2(k+1)$, $x_3(k+1)$ from previous step together with $x_2(k)$ to obtain the values for $x_1(k)$ and $x_3(k)$. Consequently, unlike the conventional DP, which searches the entire quantified discrete state space (the combinations of predetermined discrete grids) [16], the discrete states to search are determined by the system dynamics (3.16-3.18), and therefore all the discrete states searched in the DP computation are reachable.

However, although the discrete states generated by the above method are all reachable, the number of discrete states will increase from step to step. Suppose the

number of discrete states at step k+1 is L_{k+1}, and the number of discrete values of $x_2(k)$ at step k is L, then the total number of discrete states generated for step k would be $L_k=L_{k+1}\times L$. So the number of states will grow very quickly after N steps. To avoid this problem, instead of discretizing the state space into specific discrete values, the customized Dynamic Programming algorithm divides the state space into several regions. As shown in Figure 3.6, $\{x_2^0(k), x_2^1(k),\ldots x_2^j(k)\ldots x_2^L(k)\}$ are the discrete values of x_2 at step k, and $\{X^0(k+1), X^1(k+1),\ldots X^i(k+1),\ldots X^{L_{k+1}}(k+1)\}$ are the possible discrete states calculated from step k+1. In addition, for each discrete value of $x_2(k)$, we can generate several discrete regions on the plane of x_1 and x_3 shown as the black and white blocks in Figure 3.6. Then suppose from

$$[x_1^i(k), x_3^i(k), u^i(k)] = R[X^i(k+1), x_2^j(k)] \tag{3.20}$$

we get $x_1^i(k)$ and $x_3^i(k)$, and suppose that $[x_1^i(k), x_2^j(k), x_3^i(k)]^T$ lies in region A in Figure 3.6. Subsequently, we can assign the vector $[x_1^i(k), x_2^j(k), x_3^i(k)]^T$ as the value of region A, and also memorize $[x_1^i(k), x_2^j(k), x_3^i(k)]^T$ as one of the discrete states for step k. Moreover, we can calculate the cost function based on $[x_1^i(k), x_2^j(k), x_3^i(k)]^T$ as:

$$J_k[x_1^i(k), x_2^j(k), x_3^i(k)] = \lambda_e[x_2^j(k) - v]^2 + \hat{J}_{k+1}[X^i(k+1)] \tag{3.21}$$

where $\hat{J}_{k+1}$ is the cost function of state $X^i(k+1)$ at step k+1. Here we also define two symbols v and λ_e, which are equal to v_m in (3.10) and 1 respectively when step $k \le N_1$, are equal to d/T and λ_1 respectively when step $k \le N_2$, and are equal to v_m and λ_2 respectively when $k > N_2$.

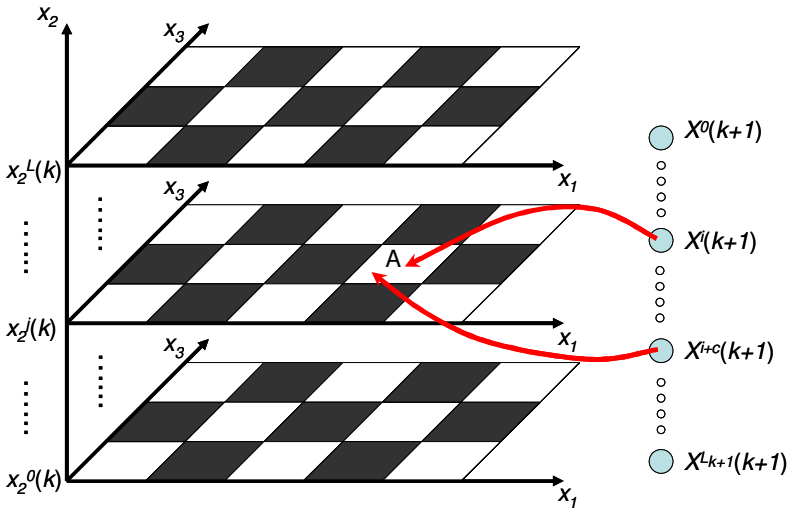

Figure 3.6. State space quantization

In the following calculation, if $[x_1^{i+c}(k), x_2^j(k), x_3^{i+c}(k)]^T$ obtained from $R[X^{i+c}(k+1), x_2^j(k)]$ also lies in region A, we then calculate the cost function again based on $[x_1^{i+c}(k), x_2^j(k), x_3^{i+c}(k)]^T$ as:

$$J_k[x_1^{i+c}(k), x_2^j(k), x_3^{i+c}(k)] = \lambda_e[x_2^j(k) - v]^2 + \hat{J}_{k+1}[X^{i+c}(k+1)] \tag{3.22}$$

If $J_k[x_1^i(k), x_2^j(k), x_3^i(k)]$ is larger than $J_k[x_1^{i+c}(k), x_2^j(k), x_3^{i+c}(k)]$, we should reassign the value of region A as $[x_1^{i+c}(k), x_2^j(k), x_3^{i+c}(k)]^T$, and at the same time $[x_1^i(k), x_2^j(k), x_3^i(k)]^T$ in the discrete space will be replaced by $[x_1^{i+c}(k), x_2^j(k), x_3^{i+c}(k)]^T$. But if $J_k[x_1^i(k), x_2^j(k), x_3^i(k)]$ is smaller than $J_k[x_1^{i+c}(k), x_2^j(k), x_3^{i+c}(k)]$, $[x_1^{i+c}(k), x_2^j(k), x_3^{i+c}(k)]^T$ will be disregarded and the process goes on.

We summarize the proposed customized Dynamic Programming algorithm as follows:

First, $x_2(k)$ is discretized into a finite grid with size L, and the x_1 and x_3 plane corresponding to each discrete $x_2^j(k)$ is discretized into $L \times L$ regions.

$$\begin{cases} x_2(k) \in \{x_2^1(k), x_2^2(k), ..., x_2^j(k), ..., x_2^L(k)\} \\ region_j(k) \in \{reg_j^1(k), reg_j^2(k), ...reg_j^h(k), ..., reg_j^{L \times L}(k)\} \end{cases} \tag{3.23}$$

where $region_j(k)$ refers to the discrete regions on x_1--x_3 plane corresponding to specific $x_2^j(k)$. Also define λ as a diagonal matrix whose diagonal elements are the weighting

factors λ_3, λ_4, λ_5 in Eq (3.14).

Step N-1, **for** $1 \le j \le L$,

$$[x_1(N-1), x_3(N-1), u(N-1)] = R[X\_final, x_2^j(N-1)] \tag{3.24}$$

$$X^j(N-1) = [x_1(N-1), x_2^j(N-1), x_3(N-1)] \tag{3.25}$$

$$\begin{aligned} &J_{N-1}[X^j(N-1)] = \lambda_2[x_2^j(N-1) - v_m]^2 + \\ &\{f[X^j(N-1), u(N-1)] - X_{final}\}^T \lambda \{f[X^j(N-1), u(N-1)] - X_{final}\} \end{aligned} \tag{3.26}$$

Step k, **for** $0 \le k < N-1$, **for** $1 \le j \le L$, **and for** $1 \le i \le L_{k+1}$

$$[x_1(k), x_3(k), u(k)] = R[X^i(k+1), x_2^j(k)] \tag{3.27}$$

$$X_{temp} = [x_1(k), x_2^j(k), x_3(k)] \tag{3.28}$$

If $X_{temp} \in reg_j^h(k)$, **then**

$$J_{k\_temp} = \lambda_e[x_2^j(k) - v]^2 + J_{k+1}[X^i(k+1)] \tag{3.29}$$

If $J_{k\_temp} < J_k[x_2^j(k), reg_j^h(k)]$, **then**

$$J_k[x_2^j(k), reg_j^h(k)] = J_{k\_temp} \tag{3.30}$$

$$X_j^h(k) = X_{temp} = [x_1(k), x_2^j(k), x_3(k)] \tag{3.31}$$

Finally, after we have obtained the minimum cost function for each reachable state, we can easily get the optimal sequence of control input u=[$u(0)$,…., $u(N)$] which would minimize the total cost function.

In summary, the proposed algorithm has three advantages over the conventional numerical DP algorithm. First, the system dynamic model is transformed from stiff equations into non-stiff equations. Thus, we can use a smaller number of steps (N=800 in our simulation) for DP. Second, all the states in the process are reachable, so by getting states $x_1(k)$ and $x_3(k)$ directly from $x_1(k+1)$, $x_2(k+1)$, $x_3(k+1)$ and $x_2(k)$ using Eq (3.20), $\hat{J}_{k+1}$ in (3.21) can be directly matched with $J_{k+1}[x_1(k+1), x_2(k+1), x_3(k+1)]$, therefore eliminating the approximation errors caused by interpolation in the conventional

Dynamic Programming [16]. Third, as not all the discrete regions need to be considered during the process, the curse of dimensionality [17] problem is mitigated.

3.4. Simulation and Experimental results

3.4.1 Experimental Setup

To validate the proposed optimal clutch fill control, a transmission clutch fixture is designed and built as shown in Figure 3.7. The main parts include a servo motor, an automotive transmission pump, a pilot-operated proportional relief valve, a proportional reducing/relieving valve, two pressure sensors, a clutch mounting device/fixture, two displacement sensors, a flow meter, a power supply unit with servo amplifier and an XPC-target real time control system.

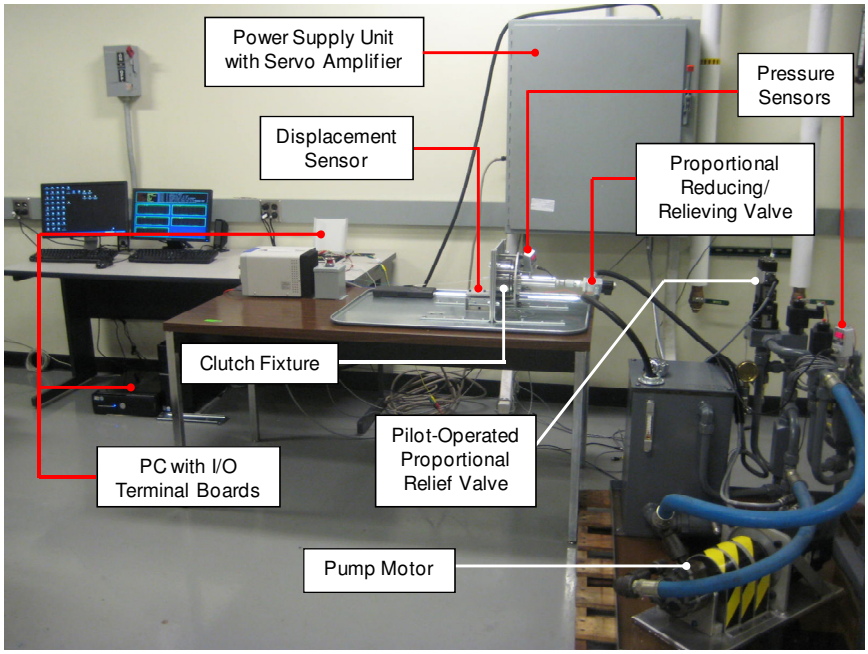

Figure 3.7: Clutch fill experimental setup

The hydraulic circuit diagram is shown in Figure 3.8. A pump with a 2-stage pilot operated relief valve provides the high pressure fluid. A servo amplifier unit controls the speed of the pump motor. A proportional reducing/relieving valve is used to control the fluid to the clutch chamber.

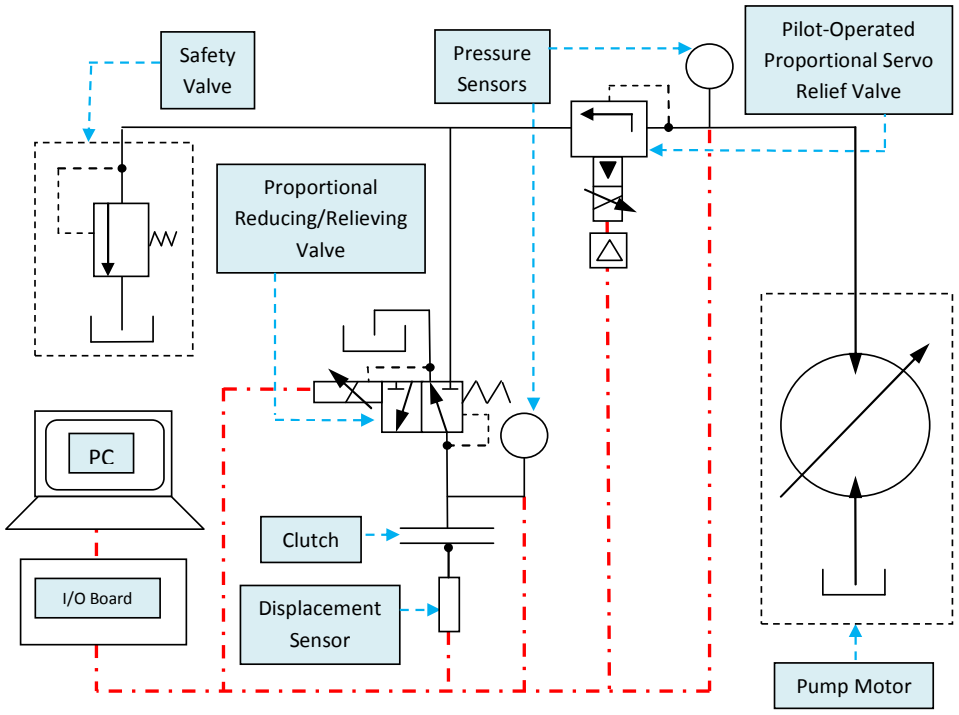

Figure 3.8. The hydraulic circuit scheme diagram

To measure the motion of the clutch fill process, the clutch system has been instrumented with displacement, pressure and flow sensors. The clutch piston displacement is measured by two different displacement sensors 180 degrees apart. A micro gauging differential variable reluctance transducer (MGDVRT) is mounted on one location of the clutch piston and a laser sensor is mounted 180 degree apart. Due to the rubber sealing and manufacturing tolerance, the friction around the circular piston is not necessarily balanced. This may cause the piston to twist around the shaft while moving. Therefore it is necessary to measure the piston motion at different locations simultaneously and calculate the average piston displacement. In addition, the clutch system input pressure is measured using an Omega pressure sensor *PX209-030G5V* with measurement range from 0 to 30 *psi* and the resolution of 0.075 *psi*, and a Max-machinery flow meter *G015* with the range from 0.15 to 15 *lpm* and the time constant of 1.7 *ms* is used to measure the input flow rate.

3.4.2. System identification

To implement the dynamic programming and optimal control, the parameters of the clutch system model (1-3) need to be identified. The effective mass of the piston M_p, the

piston surface area A_p, the return spring constant K_p, the preload distance of the return spring x_{p0}, the stick friction peak value F_{static}, the orifice area $A_{orifice}$, the fluid density ρ, the discharge coefficient C_d, the bulk modulus β and the clutch chamber volume V_0 can be measured or obtained directly. As the clutch is not rotating in the lab experimental setup, the centrifugal pressure P_c is zero.

The F_{static}, which is the maximum drag force when the clutch stays static, is measured by recording the clutch chamber pressure at the start of the piston motion. In the experiment, the clutch piston is kept static at the specific travel distance and then moves to the next position as shown in Figure 3.9. The minimum pressure P_{min} required to move the piston at the specified position is obtained as pointed by the arrow in Figure 3.9. Therefore F_{static} in the corresponding chamber pressure can be calculated by

$$F_{static} = P_{\min} \times A_p - K_p \times (x_1 + x_{po}) \tag{3.32}$$

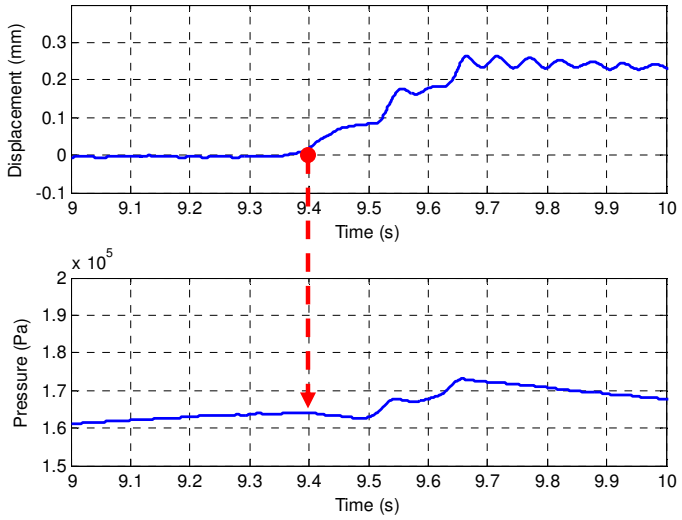

Figure 3.9. Experiments for measuring the stick friction F_{static}

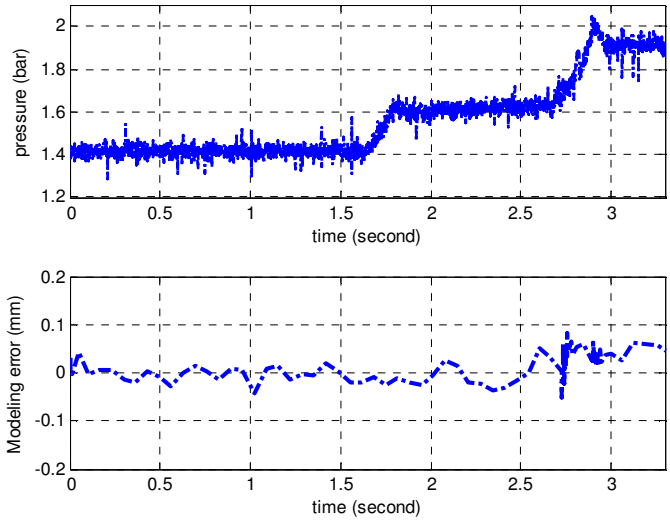

(a) Input pressure profile. (b) Modeling error.

Figure 3.10. System identification model verification

The remaining model parameters, the damping coefficient D_p, the piston seal damping coefficient α, and the piston seal drag force F_{drag} while the piston is moving, are identified using the least square estimation approach [23]. The identified model is then compared with the experimental data using the input pressure profile shown in Figure 3.10(a), and the modeling error is shown in Figure 3.10 (b). Finally, the measured and identified parameter values are presented in Table 3.1.

3.4.3. Clutch Fill Simulation and Experimental Results

In this section, both simulation and experimental results are reported to validate the proposed control method. An optimal input pressure is derived to achieve the desired clutch fill velocity profile using the customized dynamic programming method. The desired final state conditions are $x_1(T)=d=0.000725$ (m), $x_2(T)=0$ (m/s), $x_3(T)=1.91\times 10^5$ (Pa). Figure 3.11 (solid red line) shows the optimal control input. The total steps for DP is 800. The number of discrete values for $x_2(k)$ at each step is 100, and the number of discrete regions for each discrete $x_2(k)$ value is 100×100. For the customized DP method, we only evaluate the states that can be reached. The computation time for the customized DP method is 22 minutes with a 1.86GHZ computer.

TABLE 3.1. PARAMETER VALUES OF THE SYSTEM DYNAMIC MODEL

M_p	0.4 (kg)	T	0.3 (s)
x_{p0}	1.5928 (mm)	Δt	0.000375 (s)
K_p	242640 (N/m)	$A_{orifice}$	2.0442e-5 (m^2)
D_p	135.4 (N/m/s)	ρ	880 (kg/ m^3)
A_p	0.00628 (m^2)	C_d	0.7
α	4.1054e-6(m/s)	P_{atm}	1 (bar)
V_0	7.8e-5 (m^3)	β	1625 (bar)
k_m	0.001517 (m^2)	k_s	0.00153(m^2)
c_m	5.22 (N)	c_s	5.26(N)

The resulting optimal control input pressure is then implemented in the experiment to verify its performance as shown Figure 3.11 (dashed blue line). Due to the short time duration (0.3 second) and total displacement (0.725 mm), precise pressure and motion control of the clutch fill process is very challenging. In addition, the clutch mechanism is extremely sensitive to pressure rise in the clutch chamber when the clutch piston starts to move which adds up to the intricacy of controlling the clutch piston motion. This is because the current clutch design behaves as an on/off switch during the clutch fill process, where the input pressure required to start the piston motion is only 0.3 bar lower than the final pressure (see Figure 3.11). Despite of these challenges, the clutch piston displacement, velocity and the input flow profiles from the experiments exhibit optimal shape as shown in Figure 3.12. The experimental velocity profile in Figure 3.12 (b) is obtained by numerical differentiation of the displacement data, and its optimal shape can be further verified by the smooth input flow rate shown in Figure 3.12 (c).

The repeatability issue is also verified using multiple experiments with the same desired pressure inputs shown in Figure 3.11. The experimental results in Figure 3.13 exhibits good repeatability. Specifically, Figure 3.13 (a) presents the piston displacements from five groups of experiments, which clearly show that all the displacement trajectories have similar optimal shape and can overlap each other. Figure 3.13 (b) shows the error histogram of all the data points in the five trajectories comparing

with the desired one, which again exhibits good repeatability.

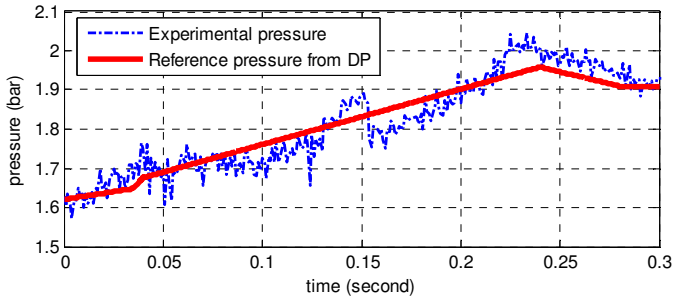

Figure 3.11. Optimal input pressure and the experimental tracking results

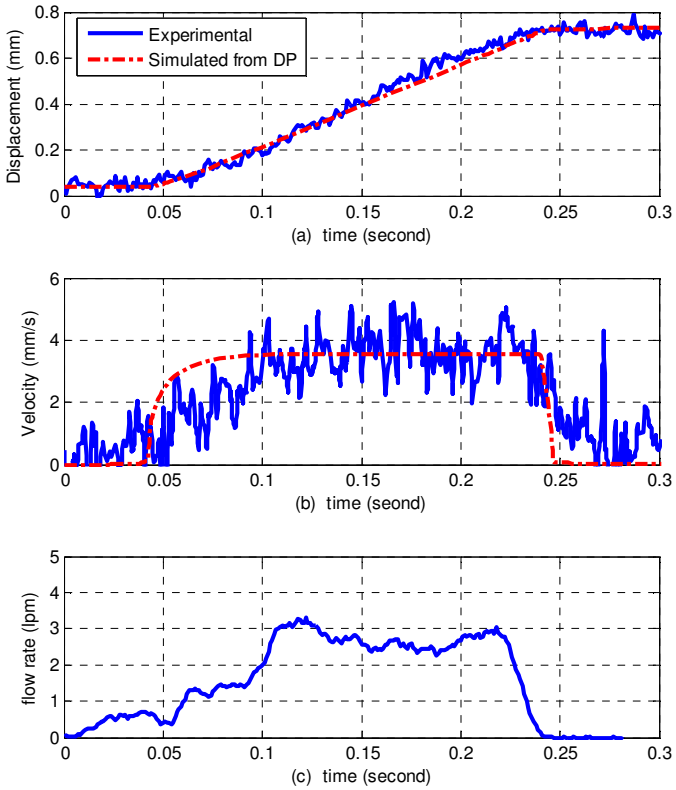

Figure 3.12. Experimental results for clutch displacement, velocity and input flow rate

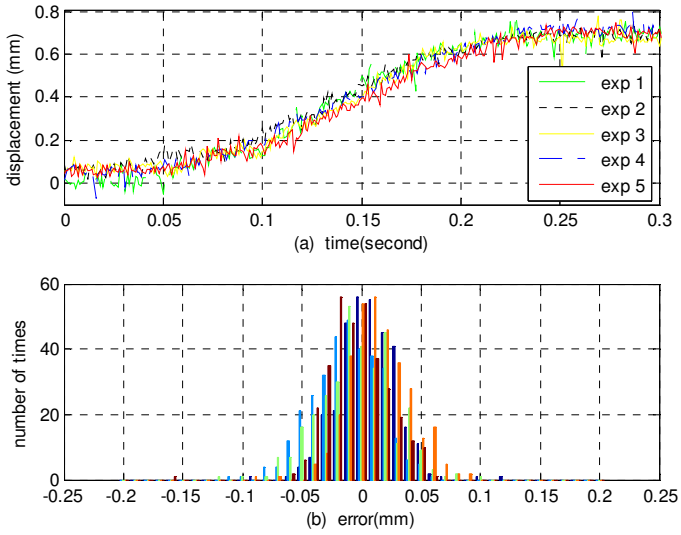

Figure 3.13. Clutch fill repeatability test (a). five groups of displacement profiles. (b) histogram of data error comparing with optimal trajectory

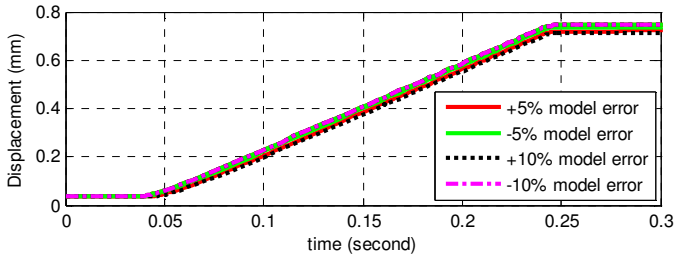

(Piston displacement trajectories with 5% perturbation (red solid line), 10% parameter perturbation (black dotted line),-5% parameter perturbation (green solid line), and -10% perturbation (dashed purple line).)

Figure 3.14. Clutch fill robustness test

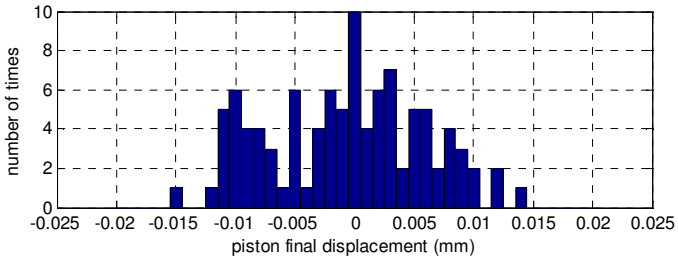

Figure 3.15. Histogram of clutch fill piston final position

We also added ±5% and ±10% perturbations to the dynamic model parameters (D_p, α, β, F_{drag}, ρ, V_o, $A_{orifice}$) and simulated the system performance using the designed control

input in Figure 3.11. The trajectories shown in Figure 3.14 arrived in acceptable intervals around the desired final states and thus demonstrated system robustness against those model parameter variations. In addition, random perturbations within ±10% interval are also added to those model parameters, and the resulted piston final displacements at the end of the clutch fill are collected through 100 tests. The clutch fill final piston position errors are then projected into a histogram shown in Figure 3.15. The histogram shows that most of the clutch trajectories finally arrive within a small interval around 0.725mm, which is the desired displacement of the clutch fill.

The influence of the time delay caused by the solenoid valve was explored as well. The desired optimal clutch fill piston displacement is compared to that with solenoid valve delay in Figure 3.16. Because of the unique velocity profile proposed in Figure 3.5, the clutch fill with solenoid delay can still reach the final position within the required clutch fill duration (0.3 second).

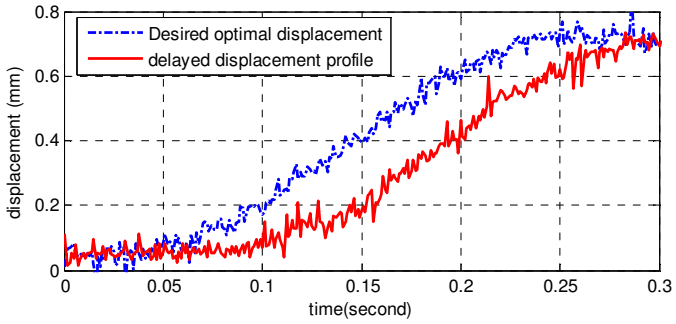

Figure 3.16. Experimental data demonstrating clutch fill robustness on time delay

Comparison with a non-optimal clutch fill process is also shown in Figure 3.17. It can be seen that the non-optimal approach results in a high clutch piston velocity spike, which represent the high peak flow demand that could only be met with a larger and less fuel efficient pump.

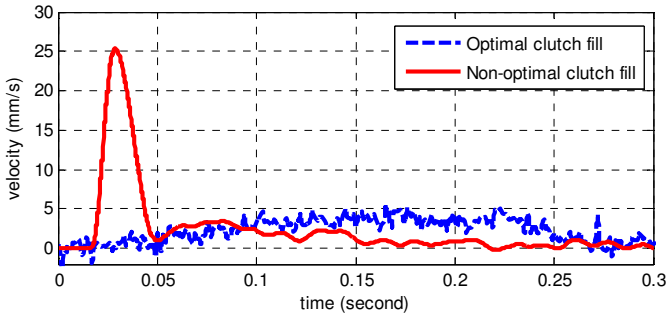

Figure 3.17. Optimal and non-optimal clutch fill velocities profile comparison

3.5. Conclusion

This chapter presents a systematic approach for transmission clutch fill control using a new customized Dynamic Programming method. The objective of the clutch fill control is to enable a fast and precise clutch fill and reduce the peak flow demand. We formulated this problem into a constrained optimization problem. To reduce the computational burden and eliminate the interpolation errors in the conventional numerical DP method, a customized Dynamic Programming method was proposed. The customized DP algorithm transforms the original stiff system dynamic model to a non-stiff one and thus avoids the large number of steps required by the sampling time of the discretized clutch model. Furthermore, comparing with the conventional DP, it is free of interpolation error and reduces the computational burden by selectively searching the reachable states. To validate the optimal control, a transmission clutch fixture is designed and built for experimental investigation. A dynamic model that captures the key clutch fill dynamics is constructed and identified with the experimental data. Finally, simulation and experimental results show the effectiveness of the proposed control method.

References in Chapter 3

[1] Wagner, G., "Application of Transmission Systems for Different Driveline Configurations in Passenger Cars". SAE Technical Paper 2001-01-0882.

[2] Lee, C.J., Hebbale, K.V. and Bai, S., "Control of a Friction Launch Automatic Transmission Using a Range Clutch". Proceedings of the 2006 ASME International Mechanical Engineering Congress and Exposition, Chicago, Illinois, 2006.

[3] Sun, Z. and Kumar, H., "Challenges and opportunities in automotive transmission control". Proceedings of 2005 American Control Conference, Portland, OR, USA, June 8-10, 2005.

[4] Hebbale, K.V. and Kao, C.-K., "Adaptive Control of Shifts in Automatic Transmissions". Proceedings of the 1995 ASME International Mechanical Engineering Congress and Exposition, San Francisco, CA, 1995.

[5] Bai, S., Moses, R.L, Schanz, Todd and Gorman, M.J. "Development of A New Clutch-to-Clutch Shift Control Technology". SAE Technical Paper 2002-01-1252.

[6] Marano, J.E, Moorman, S.P., Whitton, M.D., and Williams, R.L. "Clutch to Clutch Transmission Control Strategy". SAE Technical Paper 2007-01-1313

[7] Han, W. and Yi, S.J., "A Study of Shift Control Using the Clutch Pressure Pattern in Automatic Transmission." Proc. Instn Mech. Engrs Part D: Journal of Automobile Engineering. Volume 217, Number 4/2003, pp 289-298

[8] Miao, H., Sun, Z., Fair, J., Lehrmann, J., Harbin, S. "Modeling and Analysis of the Hydraulic System for Oil Budget in an Automotive Transmission". Proceedings of ASME 2008 Dynamic Systems and Control Conference, Ann Arbor, Michigan, USA, October 20-22, 2008

[9] Montanari, M., Ronchi, F., Rossi, C., Tilli, A., Tonielli, A., "Control and Performance Evaluation of a Clutch Servo System With Hydraulic Actuation", Journal of Control Engineering Practice, Vol. 12, Issue 11, pp. 1369-1379, Nov, 2004

[10] Horn, J., Bamberger, J., Michau, P., Pindl, S., "Flatness-based Clutch Control for Automated Manual Transmissions", Journal of Control Engineering Practice, Vol. 11, Issue 12, pp. 1353-1359, Dec, 2003

[11] Glielmo, L., Iannelli, L., Vacca, V., "Gearshift Control for Automated Manual Transmissions", IEEE/ASME Transactions on Mechatronics, Vol. 11, No.1, pp. 17-26, Feb., 2006.

[12] Bellman, R. E. (1957). Dynamic programming. Princeton University Press, New Jersey.

[13] Bellman, R. E. and Dreyfus, S. E. (1962). Applied dynamic programming. Princeton University Press, New Jersey.

[14] I. Kolamanovsky, I. Siverguina, and B. Lygoe, "Optimization of Powertrain Operating Policy for Feasibility Assessment and Calibration: Stochastic Dynamic Programming Approach," Proceedings of the American Control Conference, Anchorage, AK, pp 1425-1430, May 8-10, 2002

[15] Daekyun Kim, Huei Peng, Shushan Bai, and Joel M. Maguire. "Control of Integrated Powertrain with Electronic Throttle and Automatic Transmission." IEEE Transactions on Control Systems Technology, Vol. 15, Issue 3, pp. 474 – 482, May 2007

[16] J.M. Kang, I. Kolmanovsky and J.W. Grizzle, "Dynamic Optimization of Lean Burn Engine Aftertreatment." ASME Transactions on Journal of Dynamic Systems, Measurement, and Control, Vol. 123/153, pp. 153-160, June 2001

[17] De Madrid, A.P. Dormido, S., and Morilla, F., "Reduction of the Dimensionality of Dynamic Programming: A Case Study," Pro. Of 1999 American Control Conference, pp 2852-2856, June 1999

[18] Karnopp, D., "Computer Simulation of Stick-Slip Friction in Mechanical Dynamic Systems", ASME Transactions on Journal of Dynamic Systems, Measurement, and Control, Vol. 107, No. 1, pp. 100-103, March 1985

[19] Song, X., Zulkefli, A., Sun, Z. and Miao, H., "Modeling, Analysis, and Optimal Design of the Automotive Transmission Ball Capsule System", ASME Transactions

on Journal of Dynamic Systems, Measurement and Control, Vol. 132, 021003, March, 2010.

[20] Song, X., Sun, Z., Yang, X., Zhu, G., "Modeling, Control and Hardware-in-the-Loop Simulation of an Automated Manual Transmission", Proc. Instn Mech. Engrs Part D: Journal of Automobile Engineering, Vol. 224, No. 2, pp.143-160, 2010.

[21] Hairer, E., Wanner, G., 1996. Solving Ordinary Differential Equations II (second edition), Springer Series in Computational Mathematics

[22] Gautschi, W., 1997. Numerical Analysis: An Introduction, Birkhauser Boston

[23] Crassidis, J.L. and Junkins, J.L. "Optimal Estimation of Dynamic Systems". Chapman and Hall/CRC Applied Mathematics and Nonlinear Science Series, CRC Express LLC, 2004.

NOMENCLATURE IN CHAPTER 3

C_{35R}: clutch corresponding to gear ratio 3, 5, and reverse gear.

CB_{26}: clutch corresponding to gear ratio 2 and 6.

CB_{1R}: clutch corresponding to gear 1 and reverse gear.

C_{1234}: clutch corresponding to gear 1, 2,3 and 4.

C_{456}: clutch corresponding to gear 4, 5, and 6.

S_1, S_2, S_3: sun gear in the planetary gear set.

R_3, R_{12}: ring gear in the planetary gear set.

p_s: supply pressure

p_p: pressure inside the clutch chamber

x_p: clutch piston displacement

u: input pressure, = p_s

x_1: state, clutch piston displacement, = x_p

x_2: state, clutch piston velocity

x_3: state, pressure inside the clutch chamber, = p_p

X: =$[x_1(k), x_2(k), x_3(k)]^T$

X_final: clutch fill final states

M_p: effective mass of the piston

A_p: piston surface area

D_p: clutch damping coefficient

P_{atm}: atmosphere pressure

K_p: return spring constant

x_{p0}: return spring preload

β: the fluid bulk modulus

V_0 : the clutch chamber volume

C_d: discharge coefficient

$A_{orifice}$: the orifice area

ρ: the fluid density

F_{drag} is the piston seal drag force

k_m: drag force equation constant

c_m: drag force equation constant

k_s: static friction equation constant

c_s: static friction equation constant

α : the piston seal damping coefficient

F_{stick} : the static stick friction force

F_{static} : maximum stick friction

P_c: centrifugal pressure

r_{pi} and r_{po} : the piston inner and outer radius respectively

d: desired clutch stroke

ΔT: valve time delay

T: final time

λ_1, λ_2, λ_3, λ_4, and λ_5 : the weighting factors for cost function

v & λ_e: two symbols defined under Eq (21).

N: number of steps in dynamic programming

g: total cost function

J: minimized cost function

v_m: a reference low velocity in Eq (10)

f: discrete state space model

R: customized DP transformation function.

reg: customized DP discretized region.

L: number of discretized values for a single state in DP

Δt: discrete dynamics time step interval

Chapter 4

The Clutch Level Design-- Pressure Based Closed Loop Clutch Control

Both Chapters 1 and 2 investigate the clutch control approaches in an open loop fashion. This is a viable solution in most of the current automatic transmission clutch systems due to cost and compactness concern. With the increasing demand of transmission efficiency and performance, and also to enable aggressive mode shifts for multi-mode hybrid transmission, a more precise clutch shift control is necessary, which calls for the closed loop clutch control. This chapter will be devoted to exploring the possible robust clutch control means based on potential feedback sensors.

4.1 Introduction

With the increasing demand for fuel efficiency and reduced emissions, new technologies have emerged in the automotive transmission systems [1-3]. Clutch to clutch shift control [3-7] is a key enabler for fuel efficient, compact and low cost transmission designs, including automatic transmissions [3], dual clutch transmissions [8], and hybrid transmissions [9-11]. Specifically, Figure 1(a) shows a simplified schematic diagram of a six speed automatic transmission [2], with five sets of clutch packs and three planetary gear sets. During the gear shift, one clutch (on-coming clutch) needs to be engaged while another (off-going clutch) needs to be disengaged [2]. This process is called clutch-to-clutch shift [4-7]. For a smooth clutch-to-clutch shift, proper control of two consecutive processes is necessary. First, precise coordination of the on-coming clutch and off-going clutch is critical, which otherwise will cause undesirable torque interruption and oscillations [3]. To ensure precise synchronization, before clutch engagement, it is necessary to fill the oncoming clutch to a position where the clutch packs are just in contact. This process is called clutch fill. Second, during the clutch engagement process, which typically occurs right after the clutch fill, smooth and precise torque control is crucial.

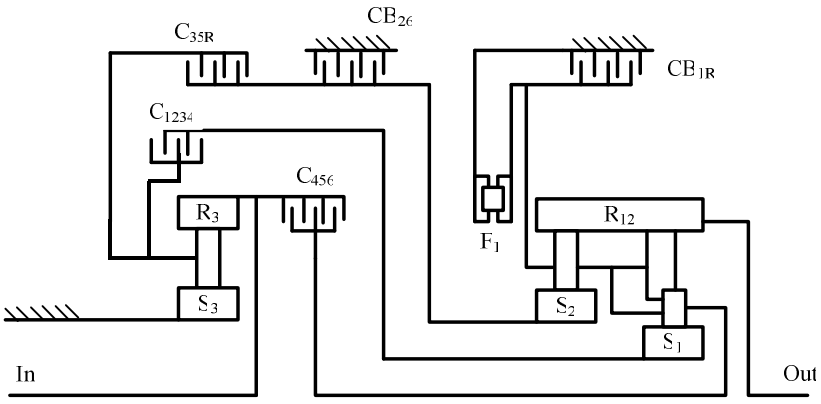

(a). Scheme diagram of a six speed automatic transmission

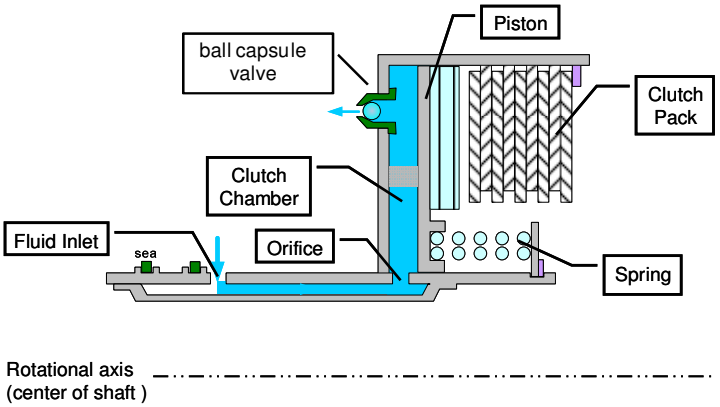

(b). Clutch actuation mechanism

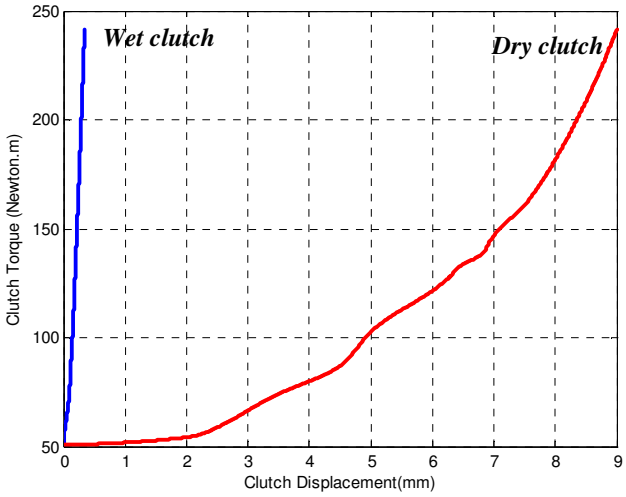

(c). Schematic clutch characteristic curves for dry and wet clutches

Fig. 4.1. Clutch system diagrams

The commonly used clutch actuation device in transmissions is an electro-hydraulically actuated clutch. Figure 4.1(b) shows a schematic diagram of a typical transmission clutch actuation system. When the clutch is to be engaged, pressurized fluid will flow into the clutch chamber and pushes the clutch piston forward until they are in contact (clutch fill). At the end of the clutch fill, the input pressure is further increased, which then squeezes the clutch piston to the clutch packs. It is important to control the clutch piston to reach the clutch packs within a specified time because an improper clutch fill can cause the failure of the clutch shift synchronization and then affect shift quality.

In this chapter, we will specifically study the hydraulically actuated "wet" clutch, which is widely applied in the planetary gear automatic transmissions [3] and hybrid transmissions [9-11]. This attributes mainly to the high power density of electro-hydraulic systems and the heat dissipation ability of "wet" clutches. The control of "wet" clutches is unique comparing with its counterpart "dry" clutch, which will be further analyzed in the following paragraphs. Currently there is no pressure sensor inside the clutch chamber, and therefore the clutch control in the automatic transmissions is either in an open loop fashion or controlled using speed signal as the feedback. However, the speed signal can only be used as the feedback variable during the clutch engagement, but not for the clutch fill. With the increasing demand of transmission efficiency and performance, a more precise clutch shift control is necessary, which calls for a more effective closed loop clutch control. There are two possible ways of measuring the clutch motion directly: by measuring the clutch piston displacement or measuring the pressure inside the clutch chamber. In this chapter, the pressure feedback is selected for "wet" clutch control due to three reasons. First, although the transferred torque can be calculated from the clutch pack displacement, the displacement *vs* torque curve for "wet" clutch is very steep comparing with "dry" clutch [12,27] as shown in Figure 4.1(c), which makes it difficult to obtain an accurate torque estimate from the displacement. In contrast, the pressure based information can be directly related to the transferred torque during the clutch engagement. Second, with a compact transmission design, it is very difficult to package a displacement sensor that moves with the clutch piston. Third, for the wet clutch used in automatic transmissions, the total displacement of the clutch piston

is about 1~2 mm, and a high resolution displacement sensor for such a small range is usually cost prohibitive for mass production.

Previous research works [12-15] on clutch control mainly focus on the "dry" clutch engagement control, which has a longer clutch piston stroke comparing with the "wet" clutch. Reference [12] introduces the automated manual transmission control with a PID controller. Ref [13] presents a switching approach between a local controller and a global controller with a pneumatic actuator and an on/off valve. Ref [14] considers dry clutch engagement position tracking problem using dynamics inversion and backstepping. In reference [15], a flatness based displacement tracking controller is designed for automated manual transmission dry clutch engagement based on the fact that the relative degree of its nonlinear system is equal to the system order. Although showing promising results, approaches used in [12-15] focus on engagement control and all require displacement feedback, and therefore cannot be directly applied to wet clutch fill and engagement control. In addition, reference [16] presents an *H*-infinity control design for regulating clutch rotational slipping speed and its implementation with a virtual clutch model. Reference [17] and [18] report the backstepping design and a reduced order nonlinear observer respectively for the clutch slipping control using the clutch rotational speed as the feedback signal. Both references [17] and [18] report interesting simulation results. However, slip speed feedback [16-18] cannot be used for the clutch fill phase, and it is not a direct feedback on the transferred torque comparing with the pressure feedback.

This chapter focuses on pressure based control for the clutch fill and engagement of "wet" clutch packs in automatic or hybrid transmissions. Comparing with the intensively researched "dry" clutch displacement based engagement control [12-15], this control has several challenges. First, the "wet" clutch system has a much shorter stroke, which demands for very precise position and pressure (torque) control. On the one hand, the dynamics modeling from the beginning of the clutch fill (low pressure) to the end of the clutch engagement (intermediate to high pressure) covers a wider pressure range, which results in several unique dynamic phenomena. On the other hand, the clutch fill process has a very short stroke and it demonstrates an on/off behavior, where the activating pressure is very close to the final pressure. With a small difference in pressure range and less than 1 *mm* of clutch piston travel, precise control of the piston motion to avoid either

"over-fill" or "under-fill" [3] becomes very challenging. Second, the modeled system dynamics are highly nonlinear with a single relative degree and second order internal dynamics, and applying a systematic nonlinear robust control to achieve precise pressure tracking is challenging. Although the sliding mode control is a potential candidate for the robust control design with this specific dynamic structure, its chattering effect due to high gain is still troublesome in reality. Therefore a systematic approach to design the gain for this application is necessary. Third, only measuring the pressure without the piston displacement makes the control difficult. On the one hand, it is hard to diagnose the clutch fill process, which usually requires the piston position data. On the other hand, a higher sliding mode gain is necessary due to the lack of the internal dynamics state information (piston displacement and velocity), as otherwise a dynamic loading variation caused by the start of the piston motion will result in a sudden pressure drop and subsequently the pressure tracking failure during this transient. Clearly an appropriate method of estimating the piston motion is required.

To address the above challenges, this chapter presents a systematic approach for modeling and controlling of wet clutches with pressure feedback. First, the system dynamic model is explored. Specifically, the proportional pressure reducing valve dynamics, the mechanical actuator dynamics, and the wet clutch pressure dynamics are constructed and validated with extensive experiments. Several unique phenomena are revealed for the system dynamics. Due to the wide range of pressure change, variation of the bulk modulus is critical. Due to the design of the clutch piston assembly, it is observed that the clutch piston may twist around the shaft, which presents a challenge for measuring the piston displacement at one location. This observation is critical for the dynamics modeling to decide the start of the piston motion. Second, a sliding mode controller is designed to regulate the clutch chamber pressure. To avoid the chattering effect, precise and less conservative estimation of the system unmodeled dynamics is crucial. This can be obtained from the experimental data in the first step. The gain of the sliding mode control is then designed based on the bounds of the unmodeled dynamics to ensure robust tracking while avoid chattering. Finally, an observer for piston motion is built based on the pressure measurement. The piston displacement and velocity estimation is not only a necessary compensation term to alleviate the sliding mode

controller high gain demand, but also a diagnosis tool for detecting the start and end of the clutch fill process.

To validate the proposed modeling and control approach, a transmission clutch fixture and hydraulic control circuit are designed and built. Through a series of experiments, the dynamic model parameters are identified. To this end, the robust pressure controller and observer are designed and implemented. Experimental results show the precise tracking performance of the clutch chamber pressure, as well as comparisons with various control configurations.

The rest of the chapter is organized as follows. Section 4.2 presents the system dynamics modeling. Section 4.3 presents the sliding mode based nonlinear control and the observer design. Section 4.4 describes the experimental system setup and the dynamic model identification. Experimental results demonstrating the control performance are shown in section 4.5. Conclusion is provided in section 4.6.

4.2 System Dynamics Modeling

Figure 4.2 shows a simplified schematic diagram of the clutch actuation system. The main components include a pump, hydraulic control valves, a clutch assembly, pressure and displacement sensors. The proportional pressure reducing valve controls the flow in and out of the clutch chamber. When the clutch fill begins, the valve will connect the clutch chamber to the high pressure source, which is regulated by a relief valve, and the high pressure fluid flows into the chamber and pushes the piston towards the clutch pack. Once the clutch fill ends, the valve will control the chamber pressure to further increase until the clutch packs are fully engaged. When the clutch is disengaged, the proportional pressure reducing valve connects the clutch chamber to the tank, and the clutch return spring pushes the clutch piston back to the disengaged position. The clutch dynamic model consists of the valve dynamics, the clutch mechanical actuator dynamics, and the clutch chamber pressure dynamics, which will be presented in the following sessions.

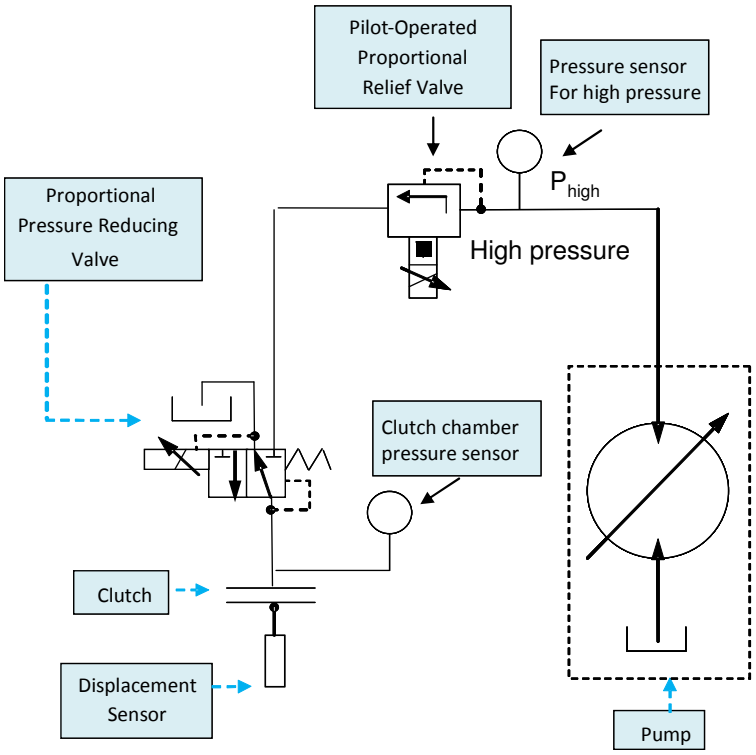

Fig. 4.2. Hydraulic circuit diagram of the clutch actuation system

4.2.1 Modeling of the proportional pressure reducing valve

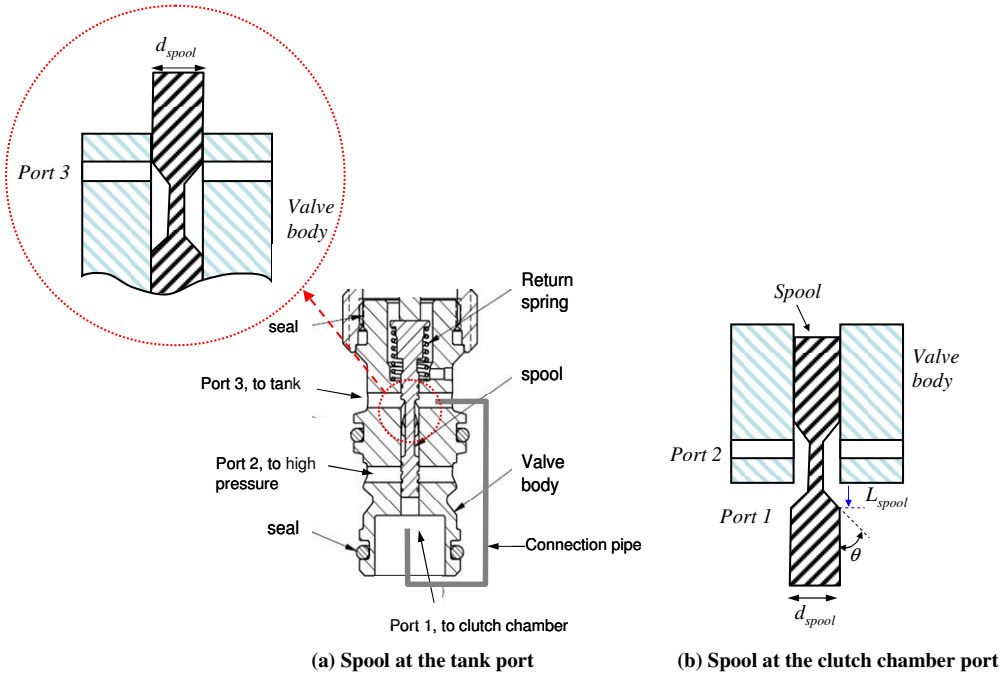

(a) Spool at the tank port **(b) Spool at the clutch chamber port**

Fig. 4.3. Cross sectional view of the proportional pressure reducing valve

The valve used to control the clutch chamber pressure is a three way two position proportional pressure reducing valve. Figure 4.3 (a) shows its cross section. Port 1 is connected to the clutch chamber with pressure P_r, port 2 is connected to the supply pressure P_{high}, and port 3 is connected to the tank. The orifice between the clutch chamber (port 1) and the supply pressure (port 2) is determined by the spool position, which is controlled by the input voltage.

When there is no control voltage, the spool is kept at the top position by the return spring. At this position port 3 is connected to port 1. Therefore the fluid inside the clutch chamber will flow to the tank. When a positive voltage is exerted on the magnetic coil, the induced magnetic force will push the spool towards port 1. As the spool connects port 1 to port 2, the high pressure fluid will flow into the clutch chamber. The increased pressure in port 1 will push the spool upward and eventually close the orifice between port 1and port 2. Clearly, the spool position is determined by the magnetic force F_{mag}, the returning spring force F_{spring}, and the chamber pressure P_r.

The spool dynamics can be described as:

$$\begin{aligned} \dot{L}_{spool} &= v_{spool} \\ \dot{v}_{spool} &= \frac{1}{M_{spool}}[F_{mag}(Vol) - K_{spring}(L_{spool} + L_{pre-load}) \\ &\quad - D_{spool} v_{spool} - A_{spool} P_r] \end{aligned} \tag{4.1}$$

$$\text{where } F_{mag}(Vol) = K_f \times i = K_f \times (\frac{i_{\max} - i_{\min}}{Vol_{\max}} Vol + i_{\min}) \tag{4.2}$$

L_{spool} is the spool position, v_{spool} is the spool velocity, M_{spool} is the spool mass, K_{spring} is the spool spring constant, A_{spool} is the cross sectional area of the spool, and D_{spool} is the damping coefficient. $L_{pre\text{-}load}$ is the spool position where the orifice between port 1 and port 2 is just closed. F_{mag} is the magnetic force, which is determined by the coil magnetic constant K_f and the current i. The current i is generated by the power amplifier and can be calculated using the input voltage Vol. i_{max} and i_{min} are the maximum and minimum current that can be generated from the power amplifier, and Vol_{max} is the maximum control voltage corresponding to i_{max}.

As shown in Figure 4.3 (b), given the spool position L_{spool}, the orifice area $A_{orifice}$ between the high pressure port 2 and chamber pressure port 1 is:

$$A_{orifice}(L_{spool}) = \pi L_{spool} \sin(\theta) \times \left(d_{spool} - L_{spool} \sin\theta \cos\theta \right) \tag{4.3}$$

where d_{spool} is the diameter of the spool, and θ is the spool surface slant angle as shown in Figure 3(b).

Similarly, as shown in Figure 4.3 (a), the orifice area A_{dump} between the tank port 3 and the pressure port 1 is:

$$A_{dump}(L_{spool}) = -\pi L_{spool} \sin(\theta) \times \left(d_{spool} + L_{spool} \sin\theta \cos\theta \right) \tag{4.4}$$

Then the flow dynamics across the valve orifice is:

$$Q(L_{spool}, P_r) = \begin{cases} sign(P_h - P_r) C_d \sqrt{\dfrac{2|P_h - P_r|}{\rho}} A_{orifice}(L_{spool}), & L_{spool} > 0 \\ 0, & L_{spool} = 0 \\ -C_d \sqrt{\dfrac{2|P_r|}{\rho}} A_{dump}(L_{spool}), & L_{spool} < 0 \end{cases} \tag{4.5}$$

where ρ is the fluid density, C_d is the discharge coefficient, $A_{orifice}$ is the orifice area connecting the clutch chamber (port 1) and the supply pressure (port 2), and A_{dump} is the orifice area connecting the clutch chamber (port 1) and the tank (port 3). When the spool position $L_{spool} > 0$, the clutch chamber is connected to the high pressure. When the spool position $L_{spool} < 0$, the clutch chamber is connected to the tank.

4.2.2 Mechanical System Modeling

The dynamics of clutch motion can be modeled as [20]:

$$\dot{x}_1 = x_2 \tag{4.6}$$

$$\dot{x}_2 = \frac{1}{M_p} \times [A_p \times (P_r + P_c - P_{atm}) - D_p x_2 - F_{drag}(P_r + P_c, x_2) - F_{res}(x_1 + x_{p0})] \tag{4.7}$$

where x_1 *is* the clutch piston displacement, x_2 is the clutch piston velocity, M_p is the effective mass of the piston, A_p is the piston surface area, D_p is the clutch damping coefficient, P_{atm} is the atmospheric pressure, x_{p0} is the return spring preload. P_c is the centrifugal force [21,22] induced pressure generated from the rotation of the clutch assembly.

F_{res} is the displacement dependent resistance force. During the clutch fill, the resistance force comes from the return spring, thus the force F_{res} depends on the spring stiffness constant K_{cs}. During the clutch engagement, the resistance force is due to the squeezing of the clutch pack, and therefore, the resistance force F_{res} can be modeled as:

$$F_{res} = \begin{cases} K_{cs} \times (x_1 + x_{p0}) & (x_1 \le x_{fill}) \\ F_{en}(x_1 + x_{p0}) & (x_1 > x_{fill}) \end{cases} \tag{4.8}$$

where the function $F_{en}(x_1+x_{p0})$ include both spring force and the nonlinear clutch pack reaction force, x_{fill} is the clutch piston position at the end of the clutch fill.

F_{drag} is the piston seal drag force, which is dependent on the piston motion. It is modeled as:

$$F_{drag} = \begin{cases} \left[k_m (P_r + P_c) + c_m\right] \times sign(x_2) & (x_2 \neq 0) \\ F_{stick} & (x_2 = 0) \end{cases} \tag{4.9}$$

where k_m and c_m are constant, and F_{stick} is the static stick friction force from the Kanopp's stick-slip model [23]. Further detail of the mechanical dynamic model can be found in our recent work [20].

4.2.3 Modeling of the clutch chamber pressure dynamics

When the orifice between the high pressure port and the clutch chamber is open, the fluid will flow into the clutch chamber, which results in the pressure rise in the chamber. The pressure dynamics is modeled as:

$$\dot{P}_r = \frac{\beta(P_r)}{V}[Q(L_{spool}, P_r) - A_p x_2]$$

where V is the chamber volume, which is assumed constant due to small clutch piston displacement, and β is the effective bulk modulus.

As the clutch fill typically occurs in a low pressure range (1.68 bar to 1.97 bar) while the clutch engagement occurs in a much higher range, the air entrained in the oil could cause the bulk modulus variation. The variation is modeled with respect the pressure as [19]:

$$\beta(P_r) = \frac{\beta_e(1+10^{-5}P_r)^{1+1/\gamma_b}}{(1+10^{-5}P_r)^{1+1/\gamma_b} + 10^{-5}R(1-c_1P_r)(\beta_e/\gamma_b - 10^5 - P_r)} \tag{4.10}$$

where β_e is the bulk modulus in ideal fluid with no air entrained, γ_b is the ratio of specific heats for air, c_1 is the coefficient of air bubble volume variation due to the variation of the ratio of the entrained air and dissolved air content in oil, R is the entrained air content by volume in oil at atmosphere pressure. β_e, R, γ_b and c_1 are fixed when the oil temperature and pumping conditions are constant.

4.2.4. Overall System Dynamic Model

The overall clutch system dynamic model including the valve dynamics, the mechanical actuator dynamics, and the chamber pressure dynamics can be summarized as follows:

$$\begin{aligned}
\dot{L}_{spool} &= v_{spool} \\
\dot{v}_{spool} &= \frac{1}{M_{spool}}[F_{mag}(Vol) - K_{spring}(L_{spool} + L_{pre-load}) \\
&\quad - D_{spool}v_{spool} - A_{spool}P_r]
\end{aligned} \tag{4.11}$$

$$\dot{P}_r = \frac{\beta(P_r)}{V}[Q(L_{spool}, P_r) - A_p x_2] \tag{4.12}$$

$$\dot{x}_1 = x_2 \tag{4.13}$$

$$\begin{aligned}\dot{x}_2 = \frac{1}{M_p} \times [A_p \times (P_r + P_c - P_{atm}) - D_p x_2 \\ - F_{drag}(P_r + P_c, x_2) - F_{res}(x_1 + x_{p0})]\end{aligned} \tag{4.14}$$

Further investigation reveals that the time constant of the pressure reducing valve is far less than the time constant of the clutch actuation system pressure dynamics, which means that the dynamic behavior of the reducing valve can be neglected. This fact can be well exhibited from the experimental data shown in Figure 4.10(a) and (c). A step voltage is applied to the valve at 0.07 second. On the one hand, Figure 4.10 (c) shows the measurement of the flow rate through the valve opening orifice. Once the step signal is on, the valve quickly opens to its full orifice, which is reflected from the near step jump of the flow rate measurement close to 0.08 second and indicate that the valve time constant is around 10 ms. On the other hand, Figure 4.10(a) shows the pressure dynamics profile inside the clutch chamber. With a near step flow rate input shown in Figure 4.10(c), the pressure inside the clutch chamber slowly increases to its peak value in almost 0.4 second, which indicates the time constant to be around 320 ms in this case. This slow response is partially due to a low bulk modulus value at the low pressure.

Therefore, to simplify the control design, the proportional valve spool dynamics is converted into a static mapping,

$$L_{spool} = \frac{1}{K_{spring}} [F_{mag}(u) - K_{spring} \times L_{pre-load} - A_{spool} P_r] \tag{4.15}$$

Here, we denote $u = Vol$ as the control input to the proportional valve.

Therefore, the system dynamics (4.11-4.12) becomes:

$$\dot{P}_r = \frac{\beta(P_r)}{V} [Q(u, P_r) - A_p x_2] \tag{4.16}$$

$$\text{where} \quad Q(u,P_r)=\begin{cases} sign(P_h-P_r)C_d\sqrt{\dfrac{2|P_h-P_r|}{\rho}}A_{orifice}(L_{spool}), & L_{spool}(u,P_r)>0 \\ 0, & L_{spool}(u,P_r)=0 \\ -C_d\sqrt{\dfrac{2|P_r|}{\rho}}A_{dump}(L_{spool}), & L_{spool}(u,P_r)<0 \end{cases} \tag{4.17}$$

Finally the reduced order system dynamics include Eqs (4.13) - (4.17).

In addition, for a given flow rate q, the required control input u can also be determined based on Eqs (4.3), (4.4), (4.15) and (4.17). This relationship will be used in the next section and the mapping from q to u can be written as:

$$U(q,P_r)= \frac{Vol_{\max}}{i_{\max}-i_{\min}}\times\left[\frac{(L_{spool}K_{spring}+K_{spring}L_{pre-load}+A_{spool}P_r)}{K_f}-i_{\min}\right] \tag{4.18}$$

where

$$L_{spool}=\begin{cases} \dfrac{d_{spool}-\sqrt{d_{spool}^2-\dfrac{4q\cos(\theta)}{\pi sign(P_h-P_r)C_d\sqrt{\dfrac{2|P_h-P_r|}{\rho}}}}}{\sin(2\theta)}, & q>0 \\ 0, & q=0 \\ \dfrac{-d_{spool}+\sqrt{d_{spool}^2+\dfrac{4q\cos(\theta)}{\pi C_d\sqrt{\dfrac{2|P_r|}{\rho}}}}}{\sin(2\theta)}, & q<0 \end{cases} \tag{4.19}$$

Eq. (4.19) is to calculate the spool position L_{spool} corresponding to a specific valve opening orifice based on Eq. (4.3) and Eq. (4.4). The relationship between equation (4.17) and (4.18) can be written as $Q\{\ U(q, P_r), P_r\ \}= q$.

4.3. Robust Nonlinear Controller and Observer Design

4.3.1. Sliding Mode Controller Design for Pressure Control

The clutch system (4.13-4.17) is a third order nonlinear system. As both the control input u (the valve voltage) and the control output P_r (the chamber pressure) appear in the dynamic equation (4.16), the system has a nonlinear dynamics with relative degree 1 [24]. Eq. (4.13) and (4.14) are the system internal dynamics, the equilibrium point of which is asymptotically stable (The proof is straightforward, thus is omitted here). Therefore the nonlinear system is minimum phase [24]. Note that the internal dynamics in this application is a spring mass damper system, therefore the minimum phase feature also suggests that the whole system will be stabilized as long as the states other than the internal dynamics states could be stabilized. This unique feature suggests applying the sliding mode controller, which can ensure system robustness with a relatively low order controller design [24].

Define the tracking error e_2 as the difference between the desired pressure trajectory r and the actual measurement P_r.

$$e_2 = P_r - r \tag{4.20}$$

And define another error term e_1, the derivative of which is equal to e_2.

$$\dot{e}_1 = e_2 \tag{4.21}$$

With the pressure dynamics in (4.16), we have

$$\begin{aligned} \dot{e}_2 &= \dot{P}_r - \dot{r} \\ &= \frac{\beta(P_r)}{V}[Q(u,P_r) + \Delta_2(u,P_r) - A_p x_2] + \Delta_1(P_r) - \dot{r} \\ &= \frac{\beta(P_r)}{V} Q(u,P_r) - \frac{\beta(P_r)}{V} A_p x_2 - \dot{r} + \Delta_1(P_r) + \frac{\beta(P_r)}{V} \Delta_2(u,P_r) \end{aligned} \tag{4.22}$$

where $\Delta_1(P_r)$ represents the model uncertainty of the pressure dynamics (4.16), and $\Delta_2(u, P_r)$ represents the model uncertainty of the pressure reducing valve flow dynamics (4.17). Bounds of the uncertainty terms will be obtained experimentally in the later session.

Define the sliding surface S as:

$$S = k_1 e_1 + e_2 \tag{4.23}$$

where k_1 is a weighting parameter.

Then the controller can be designed as:

$$u = -U\{\frac{V}{\beta(P_r)} \times [k_1 e_2 - \frac{\beta(P_r) A_p}{V} x_2 - \dot{r}] - v_u, P_r\} \tag{4.24}$$

where U is defined in Eq. (4.18), v_u is a controller term to be designed later. As the piston velocity x_2 can not be measured directly due to the lack of a displacement and velocity sensor, an observer is needed to estimate x_1 and x_2. The estimated states can not only be fed back to the controller (4.24), but also used to evaluate the piston displacement and therefore the clutch fill status. The observer design for piston motion will be presented in the next session. With the observed x_2, the control input becomes:

$$\begin{aligned} u &= -U\{\frac{V}{\beta(P_r)} \times [k_1 e_2 - \frac{\beta(P_r) A_p}{V} \hat{x}_2 - \dot{r}] - v_u, P_r\} \\ &= -U\{\frac{V}{\beta(P_r)} \times [k_1 e_2 - \frac{\beta(P_r) A_p}{V} \times (x_2 + \Delta_3(\hat{x}_2)) - \dot{r}] - v_u, P_r\} \end{aligned} \tag{4.25}$$

where $\hat{x}_2$ is the estimate of x_2 and $\Delta_3(\hat{x}_2)$ is the estimation error.

Then the sliding surface becomes

$$\begin{aligned} \dot{S} &= k_1 \dot{e}_1 + \dot{e}_2 \\ &= k_1 e_2 + \dot{e}_2 \end{aligned} \tag{4.26}$$

By substituting Eq (4.22) and Eq (4.25) into (4.26), it becomes

$$\dot{S} = \frac{\beta(P_r)}{V} v_u + \Delta(u, P_r, \hat{x}_2) \tag{4.27}$$

where $\Delta(u, P_r, \hat{x}_2) = \Delta_1(P_r) + \frac{\beta(P_r)}{V} \Delta_2(u, P_r) + \frac{\beta(P_r) A_p}{V} \Delta_3(\hat{x}_2)$

With $V_{lp}=(1/2)S^2$ as the Lyapunov function for Eq (4.27), we have

$$\begin{aligned}\dot{V}_{lp} = S\dot{S} &= \frac{\beta(P_r)}{V} v_u S + \Delta S \\ &\le \frac{\beta(P_r)}{V} v_u S + |\Delta| \times |S|\end{aligned} \tag{4.28}$$

if $$\left|\frac{\Delta \times V}{\beta(P_r)}\right| \le \psi(P_r, \hat{x}_2) + \lambda_0 |v_u| \ , \tag{4.29}$$

where $\psi(P_r, \hat{x}_2)$ is a positive continuous function, and λ_0 is a real number in the $[0,1)$ interval.

Then v_u can be designed as:

$$v_u = -\gamma(P_r, \hat{x}_2) sign(S) \tag{4.30}$$

where $\gamma(P_r, \hat{x}_2)$ is the controller gain, and design $\gamma(P_r, \hat{x}_2) \ge \frac{\psi(P_r, \hat{x}_2)}{1-\lambda_0} + \gamma_0$, $\gamma_0 > 0$.

Substituting Eq. (4.29) and (4.30) into (4.28) gives [24]:

$$\begin{aligned}\dot{V}_{lp} &\le \frac{\beta(P_r)}{V} v_u S + |\Delta| \times |S| \\ &\le \frac{\beta(P_r)}{V} \times [-\gamma(P_r, \hat{x}_2) + \psi(P_r, \hat{x}_2) + \lambda_0 \gamma(P_r, \hat{x}_2)] |S| \\ &\le -\frac{\beta(P_r)}{V} \times \gamma_0 \times (1-\lambda_0) |S| \\ &< 0\end{aligned}$$

which proves the convergence of this controller design.

Finally, the controller is given as following:

$$u = -U\{\frac{V}{\beta(P_r)} \times [k_1 e_2 - \frac{\beta(P_r) A_p}{V} \times \hat{x}_2 - \dot{r}] + \gamma(P_r, \hat{x}_2) sign(S), P_r\} \tag{4.31}$$

In the real time implementation, to suppress the chattering problem, the *sign* function in (4.31) is approximated by a high slope saturation function as [24]

$$sign(S) = sat\left(\frac{S}{\sigma}\right)$$

where σ is a constant positive number. The control structure can therefore be summarized in Figure 4.4.

As shown in (4.31), implementation of the controller requires the uncertainty bound and the velocity estimation. A conservative uncertainty bound will make the controller gain γ too large, and thus result in chattering. Therefore a proper estimation of the model uncertainty is critical and will be presented in section 4. In addition, the piston velocity estimate $\hat{x}_2$ is actually a compensation term in the controller design (4.31), and it will influence the pressure tracking performance especially during the clutch fill, where the piston velocity is higher. Besides, the clutch fill status can also be evaluated based on the piston motion estimate. Therefore a piston motion observer is necessary and will be presented in the following section.

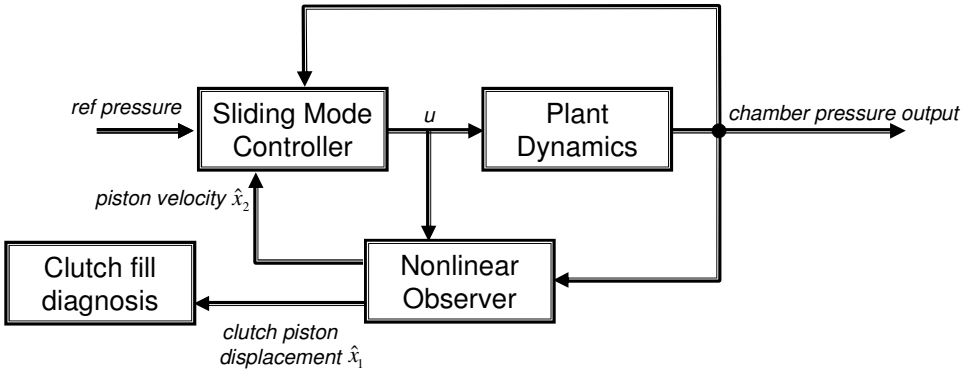

Fig. 4.4. Controller Design Structure

4.3.2. Observer Design

The observer is designed to estimate the clutch piston displacement x_1 and velocity x_2 given only the pressure measurement P_r. As shown below, given the unique system dynamics, the observer design can be transformed into a linear observer design problem.

During the clutch fill process, the piston velocity x_2 is nonzero and the drag force F_{drag} (Eq. 4.9) is only a function of the pressure. Also, the resistance force F_{res} (Eq. 4.8) is the return spring force and thus is linear as well. Suppose y is the measurement of the chamber pressure P_r. The observer for the clutch fill process is designed as:

$$\begin{aligned}
\dot{\hat{x}}_1 &= \hat{x}_2 + L_1 \times (\frac{V}{\beta(y)} \dot{y} - Q(u, y) + A_p \hat{x}_2) \\
\dot{\hat{x}}_2 &= \frac{1}{M_p}[A_p \times (y + P_c - P_{atm}) - D_p \hat{x}_2 - F_{drag}(y + P_c) \\
&\quad - K_{cs} \times (\hat{x}_1 + x_{p0})] + L_2 \times (\frac{V}{\beta(y)} \dot{y} - Q(u, y) + A_p \hat{x}_2)
\end{aligned} \tag{4.32}$$

Suppose the estimation error is denoted as

$$\begin{aligned}
\varepsilon_1 &= x_1 - \hat{x}_1 \\
\varepsilon_2 &= x_2 - \hat{x}_2
\end{aligned} \tag{4.33}$$

Combining (4.32) and (4.13-4.16), we have:

$$\begin{aligned}
\dot{\varepsilon}_1 &= \varepsilon_2 - L_1 (\frac{V}{\beta(y)} \dot{y} - Q(u, y) + A_p \hat{x}_2) \\
&= \varepsilon_2 - L_1 (-A_p x_2 + A_p \hat{x}_2) \\
&= \varepsilon_2 + L_1 A_p \varepsilon_2 \\
\dot{\varepsilon}_2 &= \frac{1}{M_p}[-D_p \varepsilon_2 - K_{cs} \varepsilon_1] + L_2 A_p \varepsilon_2
\end{aligned} \tag{4.34}$$

From which we can get:

$$\begin{bmatrix} \dot{\varepsilon}_1 \\ \dot{\varepsilon}_2 \end{bmatrix} = \begin{bmatrix} 0 & 1 + L_1 A_p \\ -\frac{K_{cs}}{M_p} & (L_2 A_p - \frac{D_p}{M_p}) \end{bmatrix} \begin{bmatrix} \varepsilon_1 \\ \varepsilon_2 \end{bmatrix} \tag{4.35}$$

Therefore the observer design problem becomes a linear observer design problem by incorporating the derivative of the pressure measurement. The estimation error will converge to zero if the observer gain L_1 *and* L_2 are selected so that the eigenvalues of the error dynamics (Eq 4.35) is on the left half plane. This will ensure the asymptotic stability of the observer error dynamics (Eq 4.35). Besides, the piston initial position might differ from the initial state of the observer, so the observer gain should be designed to enable fast error convergence as well.

During the clutch engagement, the resistance force F_{res} (Eq. 4.8) is nonlinear. However, the experimental calibration (to be shown in Figure 4.9) reveals that the wet clutch characteristic curve can be approximated with two straight lines. Therefore the observer

for clutch engagement can adopt the same structure as (4.32):

$$\begin{aligned}
\dot{\hat{x}}_1 &= \hat{x}_2 + L_1 \times (\frac{V}{\beta(y)} \dot{y} - Q(u, y) + A_p \hat{x}_2) \\
\dot{\hat{x}}_2 &= \frac{1}{M_p}[A_p \times (y + P_c - P_{atm}) - D_p \hat{x}_2 - F_{drag}(y + P_c) \\
&\quad - K_{en}(\hat{x}_1) \times (\hat{x}_1 + x_{p0})] + L_2 \times (\frac{V}{\beta(y)} \dot{y} - Q(u, y) + A_p \hat{x}_2)
\end{aligned} \tag{4.36}$$

where K_{en} is the stiffness parameter characterizing the clutch characteristic curve approximated by two straight lines.

Finally, as the observer design includes the derivative of the pressure measurement, in practice, the values of L_1 *and* L_2 are constrained to avoid the amplification of the measurement noise.

4.4. Model Identification and Uncertainty Bounds Estimation

The successful implementation of the sliding mode controller and the nonlinear observer depends on the precise characterization of system dynamics. Specifically, to avoid unnecessary high gain in the control design, which could cause chattering, a non-conservative bound of the unmodeled dynamics is critical. This section will thus focus on the dynamic model parameter identification and obtaining the uncertainty bounds for the identified model. Experimental setup will be described first, and the system parameters will be identified for the pressure reducing valve dynamics, the mechanical actuator dynamics, and the pressure dynamics respectively.

4.4.1. Experimental System Description

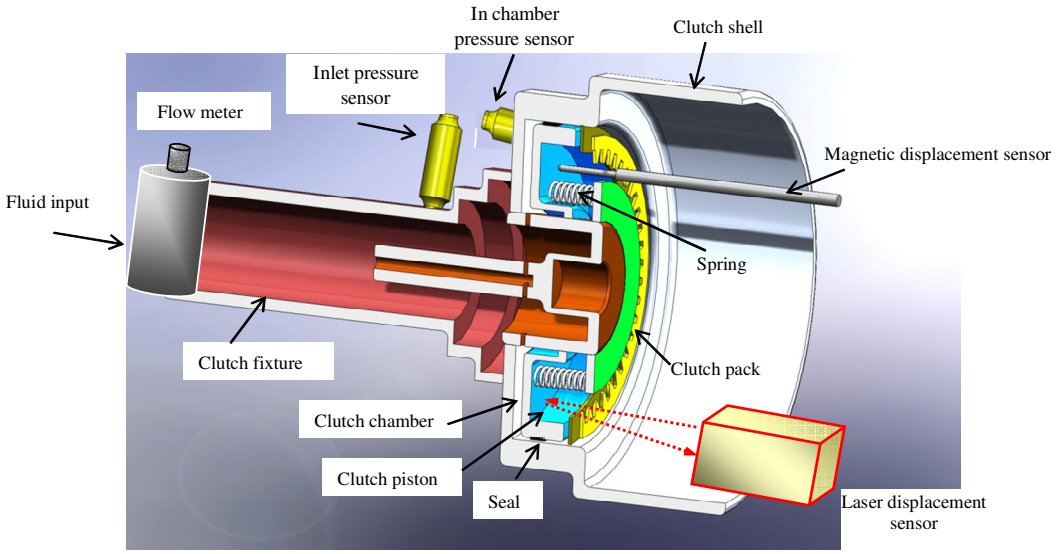

Fig. 4.5. Cross - section of the clutch assembly

A transmission clutch fixture as shown in Figure 4.2 has been designed and built. The clutch assembly is instrumented with several sensors as shown in Figure 4.5. The clutch piston displacement is measured by two different displacement sensors 180 degrees apart. A micro gauging differential variable reluctance transducer (MGDVRT) is mounted on one location of the clutch piston and a laser sensor is mounted 180 degree apart. Note that the displacement information will only be used for the dynamics modeling and control performance validation, but not for the feedback control. The only feedback signal used for clutch control is the pressure measurement. Given the compact structure of the clutch system and the small travel distance (1 mm) of the clutch piston, the displacement sensor must have a small size but high resolution (1.5 μm). The displacement sensors are calibrated with a micrometer to ensure accurate readings. The clutch system input pressure is measured using an Omega pressure sensor *PX209-300G5V* with measurement range from 0 to 20.7 *bar* and the resolution of 0.052 *bar*. The flow rate is measured using a Max Machinery *G015* flow meter with 0.15 to 15 *lpm* measurement range and 1.7*ms* time constant.

4.4.2. Pressure Reducing Valve Dynamic Model Identification

The valve dynamics identification includes two parts. One is to estimate the parameters in equation (4.15) for the spool position L_{spool}. The other one is to identify the function that relates the L_{spool} with the valve opening orifice.

For the proportional pressure reducing valve shown in Figure 4.3, the spool position is controlled by the coil magnetic force, the spring force, and the pressure force at the valve output port. Once a constant positive voltage is exerted on the valve, the magnetic force will counteract the spring force and push the valve to open. Then the pressure inside the clutch chamber will increase, which counteracts the magnetic force. When the pressure P_r in the chamber rises to a certain level, the orifice will be closed. For a given input voltage, there is a corresponding chamber pressure P_r. The spool equation (4.15) can therefore be formed for different pairs of P_r and voltage u.

$$\begin{aligned} K_f \times (\frac{i_{\max} - i_{\min}}{u_{\max}} u^1 + i_{\min}) - K_{spring} L_{pre-load} &= A_{spool} P_r^1 \\ &\vdots \\ K_f \times (\frac{i_{\max} - i_{\min}}{u_{\max}} u^n + i_{\min}) - K_{spring} L_{pre-load} &= A_{spool} P_r^n \end{aligned} \tag{4.37}$$

As the valve spring stiffness K_{spring} and the spool cross sectional area A_{spool} can be obtained from the manufacturing data, the unknown magnetic constant K_f and the spring pre-load $L_{pre\text{-}load}$ can be calibrated using the least square method from experimental measurement as shown in Figure 4.6. The horizontal axis in Figure 4.6 is the current value $((i_{\max} - i_{\min}) \times u / u_{\max} + i_{\min})$ corresponding to each control voltage u, and its vertical axis is the pressure force $A_{spool}P_r$. The magnetic constant K_f is the slope of the fitting line, and the preload $L_{pre\text{-}load}$ can be calculated from its intersection with the pressure axis.

With the above identified spool constants, the spool position can be calculated from equation (4.15) given a certain control input u. Note that calibrating the case of positive spool displacement is enough because negative spool position (clutch chamber connecting to the tank in Figure (4.3) can be obtained only by setting the valve input voltage u to zero due to the valve design. In addition, the function relating the spool

position L_{spool} to the orifice area $A_{orifice}$ can be identified using the flow rate together with the pressure measurement.

$$A_{orifice}(L_{spool}) = \frac{Q}{C_d \sqrt{\frac{2(P_h - P_r)}{\rho}}} \tag{4.38}$$

where Q is the flow in rate measured by the flow meter between the pressure reducing valve and the clutch chamber. The modeled spool position L_{spool} *vs* valve opening orifice area $A_{orifice}$ plot is shown in Figure 4.7. Different groups of experiments are conducted, and the data are all projected on Figure 4.7. Therefore the uncertainty bound $\Delta(L_{spool})$ can be determined through the experimental data.

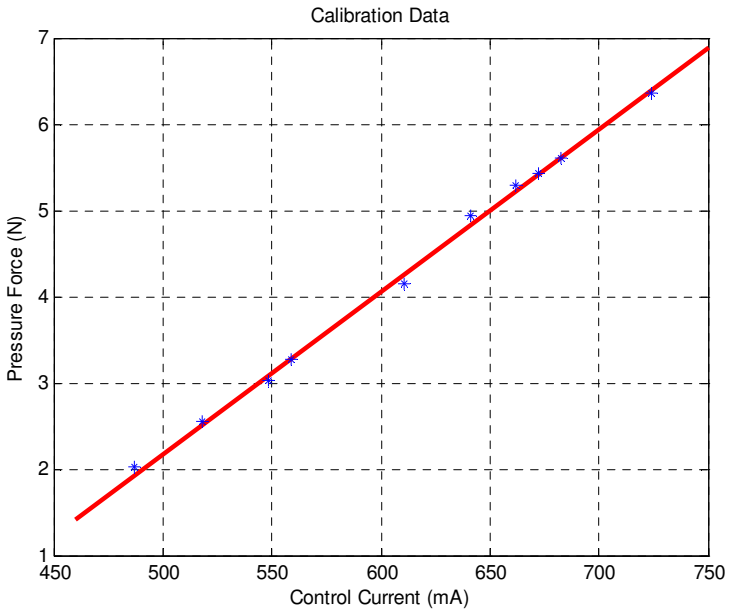

Fig. 4.6. Least square approximation of valve parameters

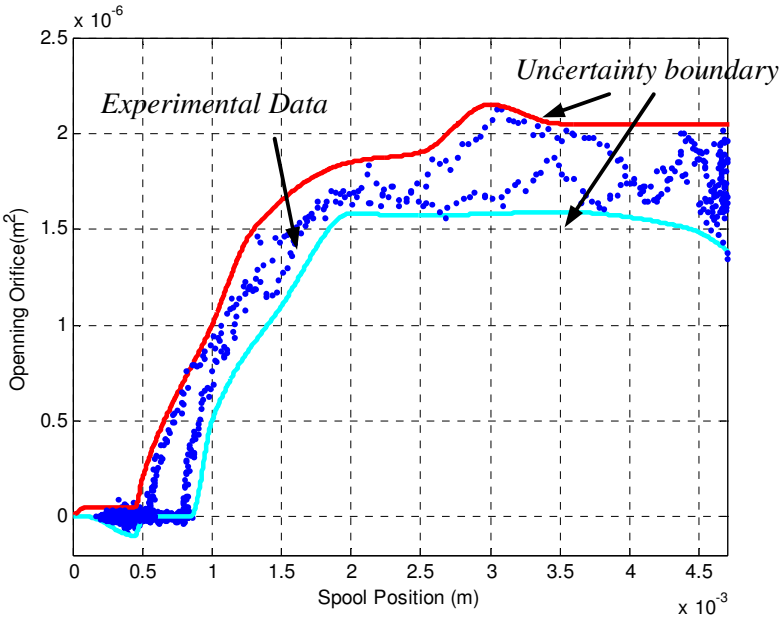

Fig. 4.7. The control valve spool position vs opening orifice area model and its uncertainty boundary

4.4.3. Mechanical Actuator Dynamics Model Identification

For the mechanical actuator model in Eq (4.13-4.14), the effective mass of the piston M_p, the piston surface area A_p, the return spring constant K_p, the preload distance of the return spring x_{p0}, the stick friction F_{stick} can be measured and calibrated as reported in reference [20]. The remaining model parameters, the damping coefficient D_p, and the piston seal drag force F_{drag} while the piston is moving, are identified using the least square iteration estimation approach [25]. The identified model is then compared with the experimental data using the input pressure profile shown in Figure 4.8(a), and the modeling error is shown in Figure 4.8(b). Further details of the clutch fill mechanical model identification can be found in our recent work [20].

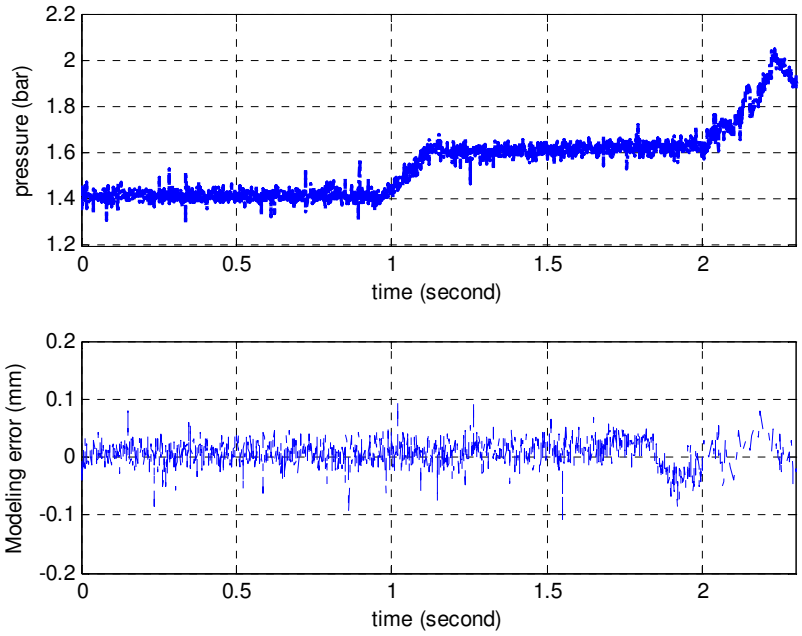

(a) Input pressure profile. (b) Displacement modeling error.

Fig. 4.8. Mechanical system identification model verification

In addition to the above mechanical actuator dynamics during clutch fill, the clutch pack displacement *vs* pressure characteristic curve is measured as shown in Figure 4.9. This curve is critical for the clutch engagement dynamics.

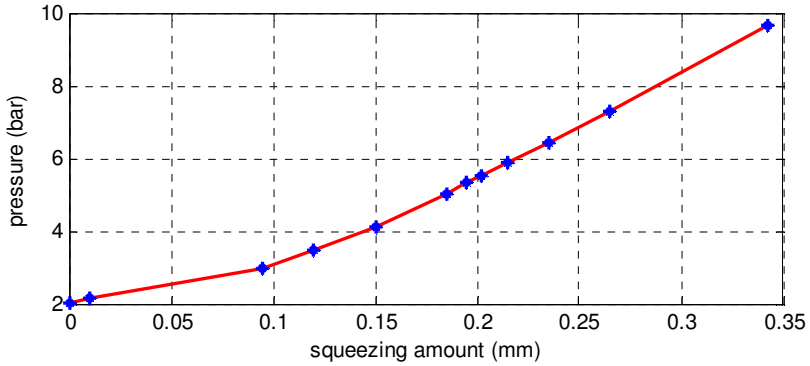

Fig. 4.9. The clutch characteristic curve. (The wet clutch pack squeezed displacement vs the corresponding pressure inside the clutch chamber)

4.4.4. Chamber Pressure Dynamics Model Identification

According to Eq. (4.16), the pressure dynamics is determined by the input flow rate and the output flow rate. The input flow rate is dependent on the valve dynamics identified

previously, and the output flow rate is calculated based on the measured piston displacement. Due to the rubber sealing and manufacturing tolerance, the friction around the circular piston is not necessarily balanced. This may cause the piston to twist around the shaft. Therefore it is necessary to measure the piston motion at different locations simultaneously and calculate the average piston displacement as shown in Figure 4.10(b). This observation is important for the dynamics modeling to detect when the clutch piston starts moving, which is crucial for the nonlinear observer estimation and the controller performance as will be explained later in section 4.5. The pressure dynamic model matching results are shown in Figure 4.10(a), and Figure 4.10(c) shows the flow rate into the clutch chamber. To characterize the model uncertainties, the pressure derivative error between the identified pressure dynamic model and multiple groups of representative experimental results are shown in Figure 4.11. The uncertainty bound of the pressure dynamic model can therefore be obtained.

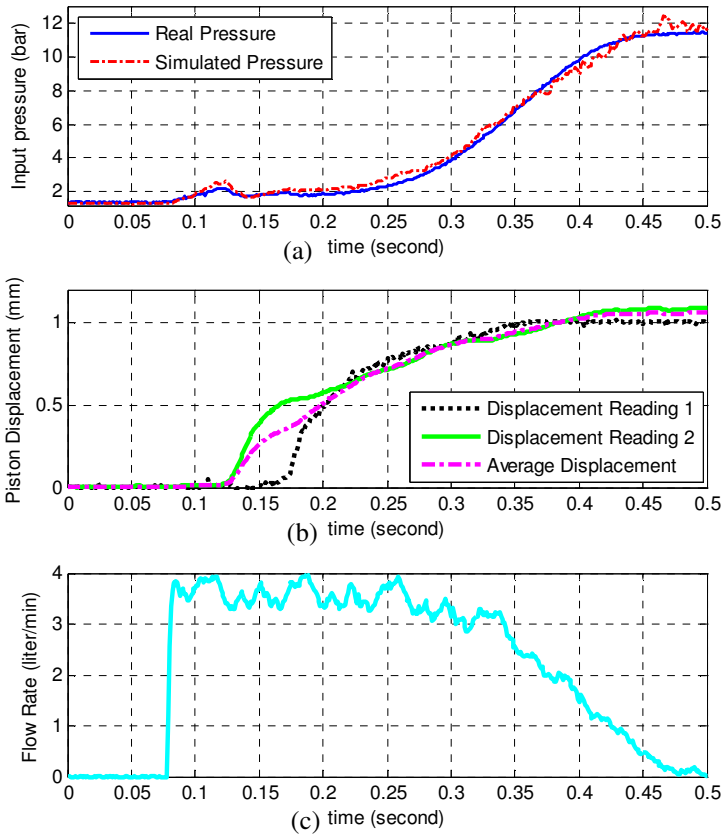

Fig. 4.10. Pressure dynamics model matching result

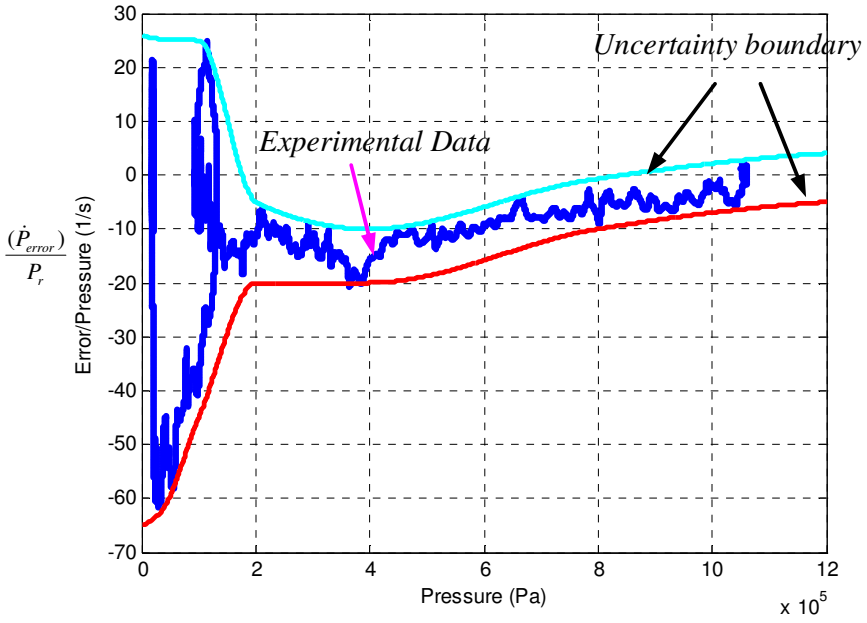

Fig. 4.11. Uncertainty bound of the pressure dynamics model

4.5. Experimental Results

In this section, experimental results are presented to validate the proposed control methods. A picture of the experimental setup is shown in Figure 4.12. The measured and identified parameter values are shown in Table 4.1.

The sliding mode controller together with the nonlinear observer is implemented on the clutch fixture. The continuous time controller is converted into a discrete controller with a sampling rate of $1ms$.

The observer estimation result is shown in Figure 4.13(a) comparing with the average displacement measured by the displacement sensors. As we only have pressure measurement in the real time feedback control, the clutch piston displacement information is not available directly. Then the observer displacement estimate could be used to diagnose the clutch fill status. For example, the clutch fill should finish within 250 ms and the piston should travel up to 0.7 mm at the end of the clutch fill. If the observer estimation at the end of clutch fill is not close the desired value, then further pressure control action is expected to amend the clutch fill status.

TABLE 4.1

PARAMETER VALUES FOR SYSTEM DYNAMICS

Symbol	Name	Value
M_p	clutch piston mass	0.4(kg)
x_{p0}	Clutch spring preload	1.5928 (mm)
D_p	Clutch piston damping	135.4 (N/m/s)
K_p	Clutch spring stiffness	242640 (N/m)
A_p	Clutch piston area	0.00628 (m^2)
V_0	Clutch chamber volume	4.02e-4 (m^3)
k_m	Piston drag force coefficient	0.001517 (m^2)
c_m	Piston drag force coefficient	5.22 (N)
K_{spring}	Valve spring stiffness	1087.6(N/m)
A_{spool}	Valve spool cross sectional area	5.0645e-006 (m^2)
K_f	Valve magnetic constant	22.7 (Tesla.m)
Vol_{max}	Maximum voltage for valve control	10 (volt)
γ_b	Ratio of specific heats for air	1.4
c_1	Coefficient of air bubble volume variation	0
ρ	Oil density	880 (kg/ m^3)
R	Entrained air content	6%
β_e	Effective bulk modulus of oil	17000 (bar)
k_s	Static friction coefficient	0.00153(m^2)
c_s	Static friction coefficient	5.26(N)
$L_{pre\text{-}load}$	Valve spool spring preload	6.7e-3 (m)
i_{min}	Minimum valve control current	250 (mA)
C_d	Discharge coefficient	0.7
i_{max}	Maximum valve control current	1280 (mA)

In practice, due to the linear approximation of the nonlinear clutch characteristic curve and the clutch pack wear, the mechanical model uncertainty during the clutch engagement is typically larger comparing to that during the clutch fill. A practical approach to maintain accurate estimation is to assign a larger L_2 gain (Eq. 4.36) during the clutch engagement, so that the pressure dynamics could dominate in the observer estimation. The effect of the initial state of the observer is shown in Figure 4.13 (b). Even with a 0.25 mm initial clutch position estimation error, the estimate converges to the actual value quickly. The effect of model uncertainties is investigated as well. Figure 4.14 shows the estimation results when the clutch return spring parameter K_p, the spring preload x_{p0}, the clutch damping coefficient D_p, the piston drag force coefficients k_m and

c_m, and the oil density are all perturbed by 5% . With a small L_2 gain for the clutch fill observer, the weighting on the pressure measurement is not enough to overcome the mechanical model error, and thus the estimation discrepancy during the clutch fill phase (from 0.1 to 0.3 second) is evident as shown in Figure 4.14 (a). The estimation can then converge during the clutch engagement due to a larger L_2 gain for the clutch engagement observer. Figure 4.14 (b) shows the estimation result if a larger L_2 gain is assigned for the clutch fill observer. However, in practice, the value of the L_2 gain is constrained. First, as the observer design has a derivative term, large observer gain may amplify the measurement noise. Second, increasing the gain L_2 will diminish the effect of the mechanical dynamics, which can prohibit the error convergence if the initial state error exists.

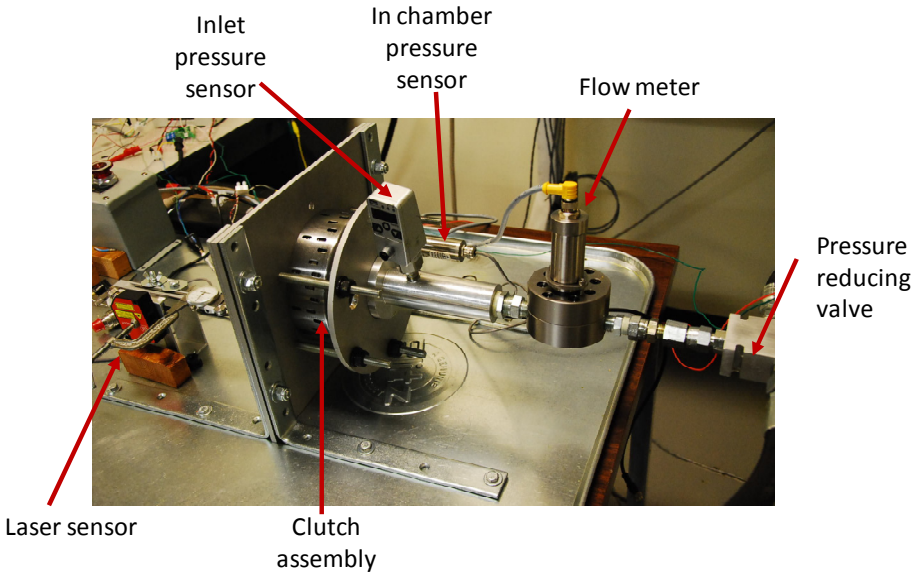

Fig. 4.12. The experimental setup for pressure based clutch actuation. (Only pressure is used in the real time feedback, and other sensors are installed for dynamic modeling purpose.)

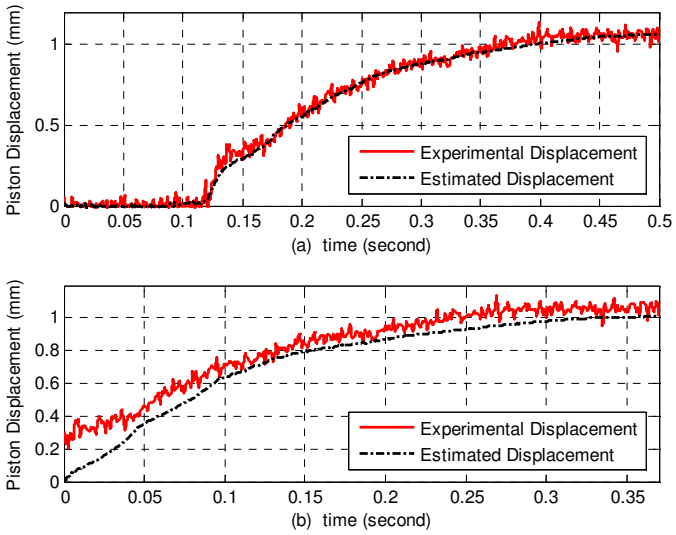

(a) Estimation with accurate initial state. (b) Estimation with inaccurate initial state

Fig. 4.13. The observer estimation results

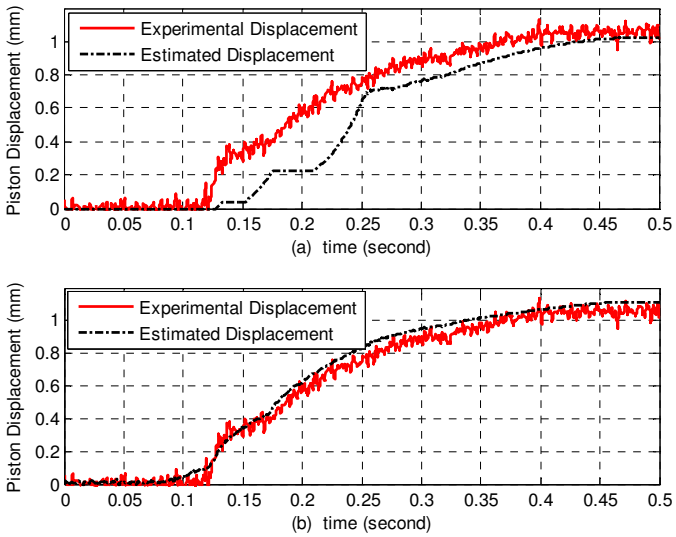

(a) Estimation with low L_2 gain in clutch fill. (b) Estimation with high L_2 gain in clutch fill

Fig. 4.14. The estimation with clutch fill mechanical dynamics perturbation

Figure 4.15 shows the pressure tracking result for clutch fill and clutch engagement. The initial pressure is at 1.68 bar, which is the critical pressure counteracting the spring preload. When the clutch fill starts, the pressure increases to 1.97 bar and then drops down to 1.9 bar. This pressure profile design is to enable the optimal clutch fill [20, 26]. During the clutch engagement, the pressure quickly rises to 7 bar to squeeze the clutch

pack. The pressure notch during engagement is to simulate the clutch slipping control. The control signal is shown in Figure 4.16 (a) and the flow in rate is shown in Figure 4.16 (b). The first peak flow rate corresponds to the clutch fill phase and the second one corresponds to the clutch engagement. During the clutch fill, the piston velocity is faster comparing with that during the clutch engagement. Therefore the flow out rate induced by the piston motion during the clutch fill is bigger, which needs more flow in rate to increase the pressure.

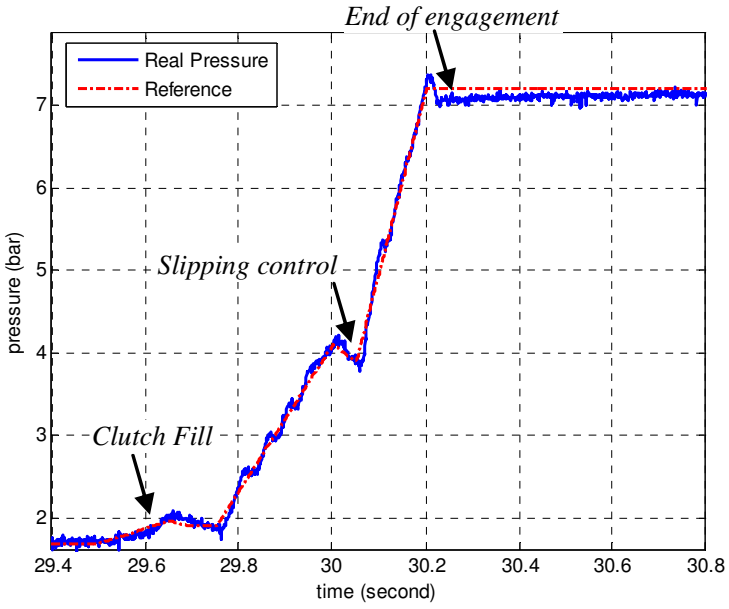

Fig. 4.15. Pressure tracking for clutch fill and clutch engagement

One of the challenges for the clutch fill pressure control is the sudden pressure drop once the clutch piston starts moving. Due to the rubber sealing and manufacturing tolerance, the friction around the piston may not be balanced. This may cause the piston to twist around the shaft, which means that the motion of the piston at different locations is not synchronized. When the pressure increases to certain level as shown in Figure 4.10(a), one part of the piston starts moving while the other part lags behind like what is shown in Figure 4.10(b). The twisting motion of the piston causes dynamic loading condition change and induces abrupt flow out from the chamber. This will further result in the sudden pressure drop. Because of the short duration of the clutch fill, the sudden pressure drop can easily lead to an unsuccessful clutch fill pressure tracking as shown in

Figure 4.17. To compensate the sudden flow out and therefore maintain pressure tracking during the dynamic loading transient, equal amount of fluid should flow in by increasing the control valve orifice. According to the controller design (Eq.4.31), under this scenario, there are two ways of ensuring sufficient control input. One is the accurate piston velocity estimation $\hat{x}_2$ and therefore the flow-out rate $A_p\hat{x}_2$, which could be translated to the required flow-in rate and thus the corresponding control input can be determined. The other is to assign a sufficiently large sliding mode gain γ so that enough control input will be exerted by multiplying the tracking error. In fact, it is always desirable to compensate the pressure drop through accurate piston velocity estimation because increasing the gain γ (Eq.4.31) can easily lead to the chattering effect. Figure 4.17(a) shows a much better tracking performance that can be attributed to the precise nonlinear observer and a precise dynamic model.

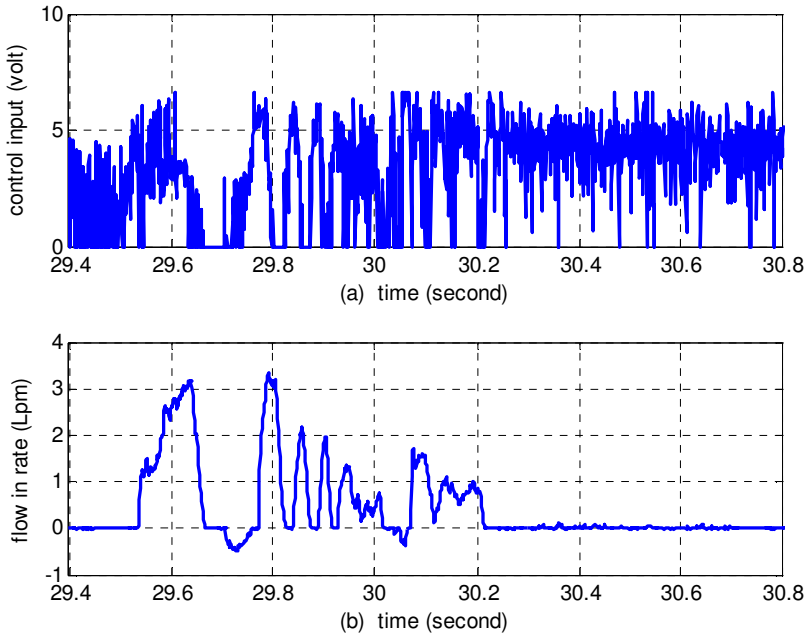

(a). Pressure control input for clutch fill and clutch engagement

(b). Flow rate for clutch fill and clutch engagement control

Fig. 4.16. Control input and the flow-in rate for clutch control

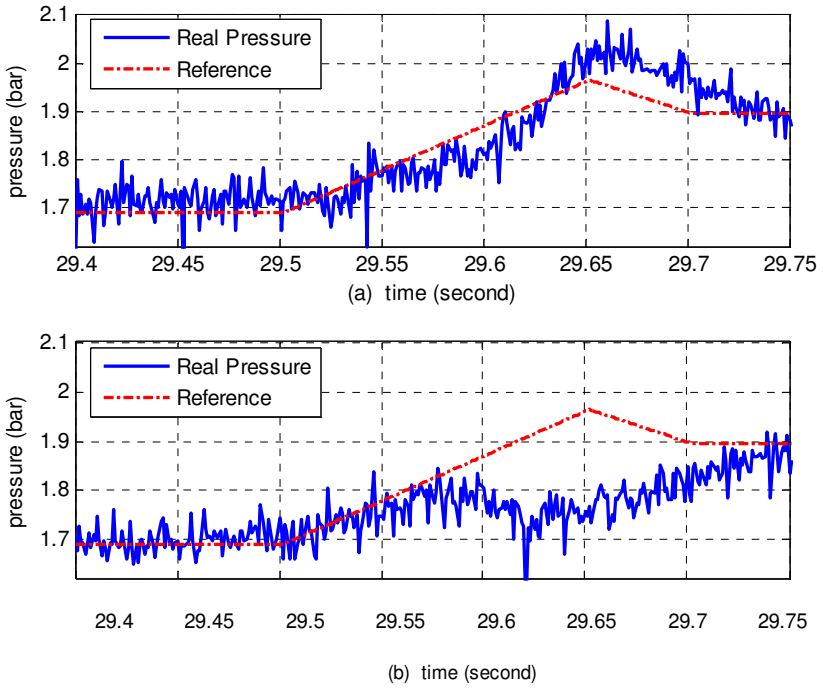

Fig. 4.17. Successful (a) and failed (b) pressure tracking during the clutch fill

The pressure chattering effect is shown in Figure 4.18. It is caused by a high sliding mode gain γ (Eq.4.31). In fact, the inappropriate high gain is mostly due to the conservative uncertainty bound of the clutch model. If the uncertainty bound is not well modeled, a large gain is then required, which will result in rapid control signal switching as shown in Figure 4.19(a) and Figure 4.19(b). The high frequency switching will excite the high frequency unmodeled dynamics and thus cause the chattering effect. Figure 4.19(b) shows the flow-in rate, which also exhibits the high frequency flow-in rate switching. The chattering effect is more severe in the high pressure range, where the hydraulic system is stiffer and thus more sensitive to the control command switching. Therefore, an appropriate sliding mode control gain should be selected based on the model uncertainty.

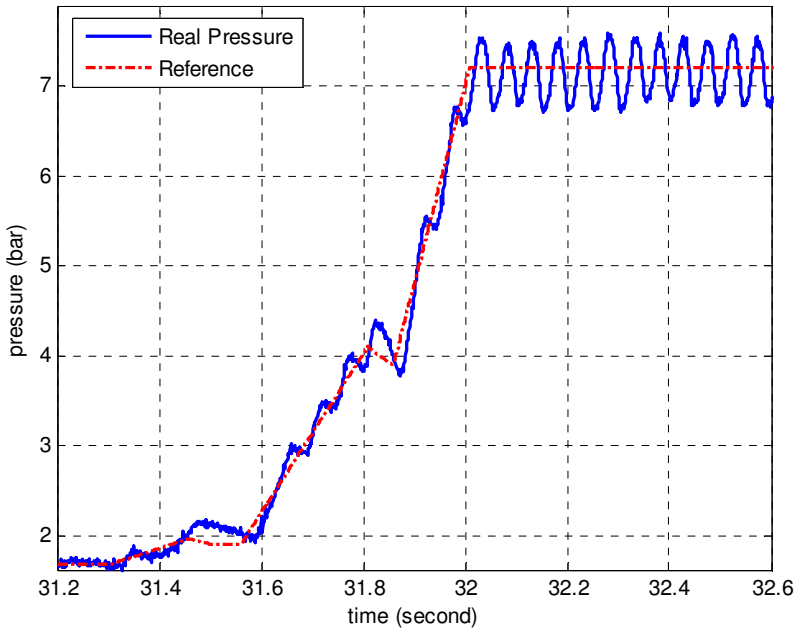

Fig. 4.18. Pressure chattering effect due to large uncertainty bound

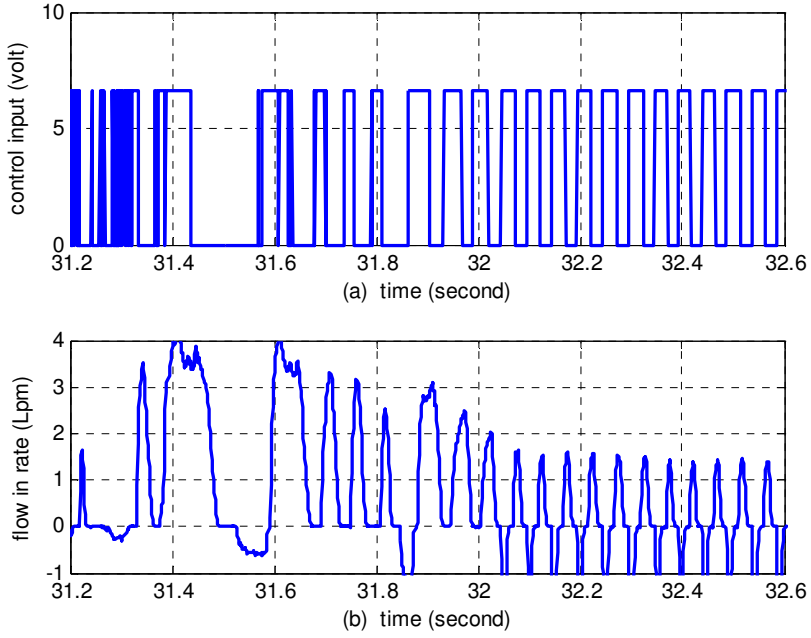

(a). Pressure control input for clutch fill and clutch engagement

(b). Flow rate for clutch fill and clutch engagement control

Fig. 4.19. Control input and flow rate data.

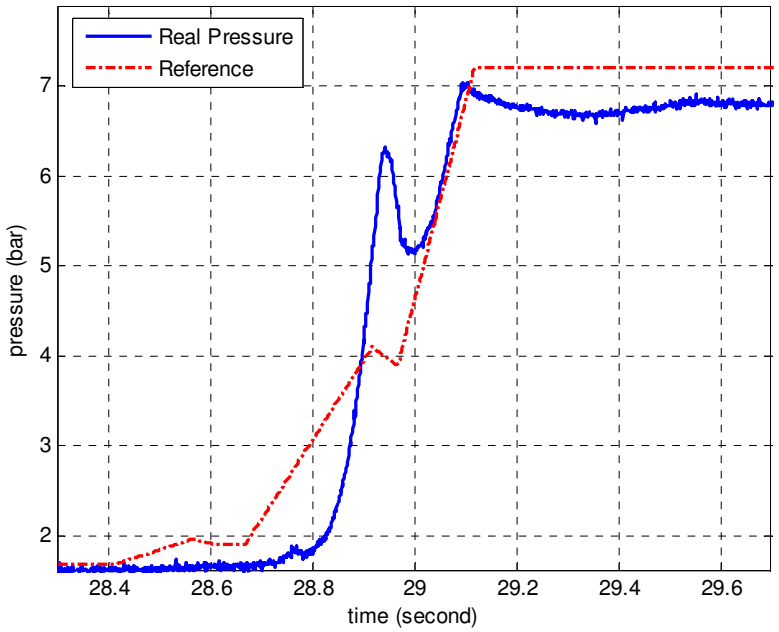

Fig. 4.20. Pressure tracking result for insufficient uncertainty bound estimate

We also tested the control performance when the uncertainty bound is too optimistic, which results in an insufficient sliding mode control gain to confine the actual uncertainty. Figure 4.20 shows the pressure tracking result in this case, where the tracking error doesn't converge. Figure 4.21 shows the corresponding control input and the flow rate.

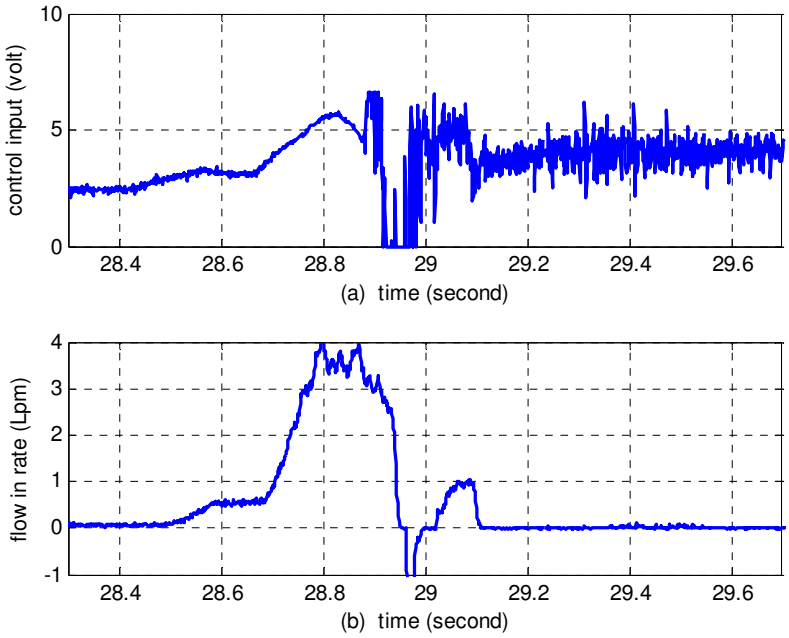

Fig. 4.21. Control signal and the flow rate for insufficient uncertainty bound estimate

4.6 Conclusion

This chapter presents a systematic approach for the pressure based clutch fill and engagement control of wet clutches in automatic, dual clutch, or hybrid transmissions. The clutch fill and engagement controls are critical for the clutch-to-clutch shift technology, which is the key enabler for fuel efficient, compact and low cost transmission designs. The main challenges of the pressure based clutch control design lie in the complex dynamics, the on/off behavior during the clutch fill phase, the pressure chattering effect induced by inappropriate control gain design, and the precise pressure tracking requirement during the dynamic loading condition transient. To address these challenges, first, a dynamic model capturing the bulk modulus variation and the piston motion wiggling effect is constructed based on extensive experimental results. A precise estimation of the bounds for unmodeled dynamics is also obtained. Then a sliding mode based robust controller is designed to track the desired pressure. To avoid chattering, the controller gain is designed based on the non-conservative uncertainty bound. To ensure precise tracking, an observer is designed to estimate the clutch piston motion, which is a necessary term in the controller structure to further alleviate the high gain demand. In addition, the observer estimation can also be used to diagnose the clutch fill status.

Finally, experimental results show the effectiveness of the proposed control methods. Future works include the investigation with a miniature pressure sensor, the model uncertainty calibration in various environments, and the vehicle test of the proposed control algorithm.

References in Chapter 4

[1] Wagner, G., "Application of Transmission Systems for Different Driveline Configurations in Passenger Cars". SAE Technical Paper 2001-01-0882.

[2] Lee, C.J., Hebbale, K.V. and Bai, S., "Control of a Friction Launch Automatic Transmission Using a Range Clutch". Proceedings of the 2006 ASME International Mechanical Engineering Congress and Exposition, Chicago, Illinois, 2006.

[3] Sun, Z. and Hebbale, K.V., "Challenges and opportunities in automotive transmission control". Proceedings of 2005 American Control Conference, Portland, OR, USA, June 8-10, 2005.

[4] Hebbale, K.V. and Kao, C.-K., "Adaptive Control of Shifts in Automatic Transmissions". Proceedings of the 1995 ASME International Mechanical Engineering Congress and Exposition, San Francisco, CA, 1995.

[5] Bai, S., Moses, R.L, Schanz, T. and Gorman, M.J. "Development of A New Clutch-to-Clutch Shift Control Technology". SAE Technical Paper 2002-01-1252.

[6] Marano, J.E, Moorman, S.P., Whitton, M.D., and Williams, R.L. "Clutch to Clutch Transmission Control Strategy". SAE Technical Paper 2007-01-1313.

[7] Han, W. and Yi, S.J., "A Study of Shift Control Using the Clutch Pressure Pattern in Automatic Transmission." Proc. Instn Mech. Engrs Part D: Journal of Automobile Engineering. Volume 217, Number 4/2003, pp 289-298.

[8] Zhang, Y., Chen, X., Zhang, X., Jiang, H., and Tobler, W., "Dynamic Modeling and Simulation of a Dual-Clutch Automated Lay-Shaft Transmission", ASME Journal of Mechanical Design Vol. 127, Issue. 2, pp. 302-307, March, 2005.

[9] T. Grewe, B. Conlon, and A. Holmes. Defining the General Motors 2-Mode Hybrid Transmission. SAE technical paper 2007-01-0273.

[10] S. Kim, J. Park, J. Hong, M. Lee and H. Sim. Transient control strategy of hybrid electric vehicle during mode change. SAE Technical Paper Series 2009-01-0228, 2009.

[11] M. Levin, et. al. Hybrid powertrain with an engine-disconnection clutch. SAE Technical Paper Series 2002-01-0930, 2002.

[12] Glielmo, L., Iannelli, L., Vacca, V., "Gearshift Control for Automated Manual Transmissions", IEEE/ASME Transactions on Mechatronics, Vol. 11, No.1, pp. 17-26, Feb., 2006.

[13] Langjord, H., Johansen, T., "Dual-Mode Switched Control of an Electropneumatic Clutch Actuator," IEEE/ASME Transactions on Mechatronics, in press, 2010.

[14] Montanari, M., Ronchi, F., Rossi, C., Tilli, A., Tonielli, A., "Control and Performance Evaluation of a Clutch Servo System With Hydraulic Actuation", Journal of Control Engineering Practice, Vol. 12, Issue 11, pp. 1369-1379, Nov, 2004.

[15] Horn, J., Bamberger, J., Michau, P., Pindl, S., "Flatness-based Clutch Control for Automated Manual Transmissions", Journal of Control Engineering Practice, Vol. 11, Issue 12, pp. 1353-1359, Dec., 2003.

[16] Sanada, K., Kitagawa, A., "A Study of Two-degree-of-freedom Control of Rotating Speed in an Automatic Transmission, Considering Modeling Errors of a Hydraulic System", Journal of Control Engineering Practice, Vol. 6, Issue 9, pp. 1125-1132, Dec., 1998.

[17] Gao, B., Chen, H., Sanada, K., Hu, Y., "Design of Clutch-Slip Controller for Automatic Transmission Using Backstepping," IEEE/ASME Transactions on Mechatronics, in press, 2010.

[18] Gao, B., Chen, H., Sanada, "A Reduced Order Nonlinear Clutch Pressure Observer for Automatic Transmission," IEEE Transactions on Control Systems Technology, Vol. 18, Issue.2, pp. 446-453, March., 2010.

[19] Yu, J., Chen, Z., and Lu, Y., " The Variation of Oil Effective Bulk Modulus With Pressure in Hydraulic Systems", Journal of Dynamic Systems, Measurement, and Control, Vol. 116, No. 1, pp. 146-150, March, 1994.

[20] Song, X., Mohd Zulkefli, A., and Sun, Z., "Automotive Transmission Clutch Fill Optimal Control: An Experimental Investigation", Proceedings of 2010 American Control Conference, Baltimore, MD, USA, June 30-July 2nd, 2010.

[21] Song, X., Sun, Z., Yang, X., Zhu, G., “Modeling, Control and Hardware-in-the-Loop Simulation of an Automated Manual Transmission”, Proc. Inst Mech. Engrs, Part D, Journal of Automobile Engineering, Vol. 224, pp.143-159, 2010.

[22] Song, X., Zulkefli, A., Sun, Z. and Miao, H., “Modeling, Analysis, and Optimal Design of the Automotive Transmission Ball Capsule System”, ASME Transactions on Journal of Dynamic Systems, Measurement and Control, Vol. 132, 021003, March, 2010.

[23] Karnopp, D., “Computer Simulation of Stick-Slip Friction in Mechanical Dynamic Systems”, Journal of Dynamic Systems, Measurement, and Control, Vol. 107, No. 1, pp. 100-103, March, 1985.

[24] Khalil, H., Nonlinear Systems, Third Edition, Pearson Education, Inc., 2002.

[25] Crassidis, J.L. and Junkins, J.L. “Optimal Estimation of Dynamic Systems”. Chapman and Hall/CRC Applied Mathematics and Nonlinear Science Series, CRC Express LLC, 2004.

[26] Miao, H., Sun, Z., Fair, J., Lehrmann, J., Harbin, S. “Modeling and Analysis of the Hydraulic System for Oil Budget in an Automotive Transmission”. Proceedings of ASME 2008 Dynamic Systems and Control Conference, Ann Arbor, Michigan, USA, Oct., 2008.

[27] Vasca, F., Iannelli, L., Senatore, A., Reale, G. , "Torque Transmissibility Assessment for Automotive Dry-Clutch Engagement," IEEE/ASME Transactions on Mechatronics, , no.99, pp.1-10, in press.

Chapter 5

The Clutch Level Design-- Design, Modeling and Control of a Novel Automotive Transmission Clutch Actuation System

The pressure based clutch control method introduced in Chapter 4 is expected to be robust and effective. However, the requirement for pressure sensor feedback inevitably increases cost and assembly complexity. For mass production, it is desirable to have a low cost and robust feedback mechanism without any sensor installed. Inspired by these requirements, an alternate clutch feedback control approach without sensor measurement is proposed in this chapter.

5.1 Introduction

The increasing demand of more fuel efficient automotive propulsion systems requires further improvement of the power transmission technologies. In recent years, many different types of transmissions, such as the six or more speeds automatic transmission, the dual clutch transmission, the automated manual transmission, and the electrically variable transmission have been developed by automotive manufacturers. Although different in design, they share common challenges on the smooth and efficient gear shift. The key issue to address is the precise and efficient operation of the clutch actuation system [1-2].

One example where a precise clutch actuation is critical is the clutch to clutch shift technology [3-6], which is the key enabler for a compact, low cost and efficient automatic transmission. The basic concept is to control the engagement and disengagement of the on-coming and off-going clutch packs to realize the gear shift [4]. To have a smooth shift, it is crucial to place the on-coming clutch piston at a pre-determined position before the shift, and this again highly depends on a precise and robust clutch control.

Due to the high power density of electro-hydraulic systems, the most common configuration is to use wet clutches with hydraulic actuated pistons in automatic and hybrid transmissions [7]. A schematic diagram of the hydraulic clutch actuation system is shown in Figure 5.1. Suppose initially the clutch is disengaged, then the piston is

separate from the clutch pack. Right before the clutch engagement, pressurized fluid will flow into the clutch chamber and push the clutch piston towards the clutch pack. This process is called clutch fill. At the end of clutch fill, high pressure fluid will continue flowing in and then push the piston to squeeze the clutch pack for clutch engagement to transfer power. It is crucial to have the piston arrive at the predetermined position at the end of clutch fill, otherwise the power transfer during the following engagement phase will be disturbed and therefore cause serious driveline vibration problem [2].

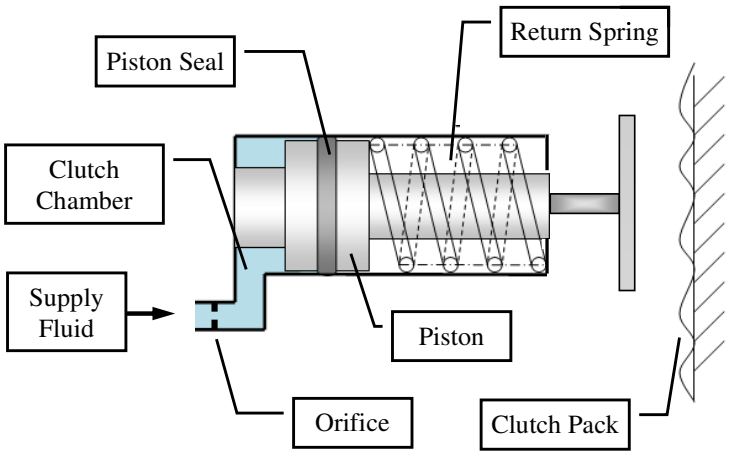

Figure 5.1 Schematic diagram of transmission clutch system

There are three main challenges associated with a precise clutch fill. First, the system is very sensitive. Even a small perturbation of the clutch fill displacement and fill time could easily cause an *over-fill* or an *under-fill* [2], which will degrade the shift quality. Second, the clutch piston typically travels 1~2 mm within 0.2 second during the clutch fill, which requires an accurate and swift actuation. Third, for mass production purpose, the clutch control system must be low cost, physically compact and robust. However, the traditional approach is in an open loop fashion due to the lack of a feedback sensor, which requires extensive calibration and also complicated upstream hydraulic control system. To address this problem, forming a feedback control loop is necessary. Ref [7] analyzes the unique nonlinear clutch actuation dynamics and proposes a sliding mode pressure based control method, which requires a pressure sensor in the clutch chamber. Different from Ref [7], in this chapter, an alternate clutch feedback control approach will be introduced, which relies on a new electro-hydraulic mechanism adopting the internal feedback concept [8] and enables a robust and precise control

without any sensor installed.

The new mechanism relays the clutch piston motion to the control spool position via a built-in hydra-mechanical feedback channel to achieve precise and robust piston motion without any feedback sensor. This design not only reduces the cost of forming an electronic controller, but also avoids the external nonlinear feedback controller synthesis considering the complex hydraulic clutch dynamics [7].

The rest of the chapter is organized as follows. Section 5.2 presents the system design and working principle of the new mechanism. Section 5.3 presents mechanical design of the new system and its dynamic modeling. To this end, simulation and experimental results are presented in section 5.4 to show the preciseness and robustness of the proposed system.

5.2 System Design and working principle

In this section, the proposed internal feedback clutch actuation system working principle will be presented first, and then its advantage over the conventional clutch actuation will be explained.

5.2.1 System design and working principle

Figure 5.2a shows the simplified schematic diagram of the proposed clutch actuation system, which mainly consists of two on/off valves, an internal feedback spool (IFS), a IFS return spring, a feedback channel and the clutch assembly. The internal feedback spool (IFS) controls the opening orifice between the supply pressure and the clutch chamber, and is the key component of the whole mechanism.

The following are the operating sequences of the system.

(1) When the clutch piston is at the initial disengaged position (Figure 5.2a), the on/off valve 1 connects the IFS orifice, A_{IFS}, to the fluid tank. The pressure inside the clutch chamber is low, so the clutch piston will be kept at the disengaged position by the return spring.

(2) When the clutch fill process begins, the on/off valve 1 is energized to connect the IFS orifice to the supply pressure. Pressurized fluid then enters the clutch chamber through the IFS orifice, counteracting the spring force and pushes the clutch piston to the right.

On the other side, the on/off valve 2 at the feedback exhaust port is closed to block the fluid inside the piston feedback chamber from flowing out to the tank. Therefore the clutch piston motion will squeeze the fluid in the piston feedback chamber to the IFS chamber through the feedback channel, which then drives the IFS upward (Figure 5.2b). As the IFS moves upward, the IFS orifice area gradually decreases. This restricts the flow through the IFS orifice which then slows down the pressure rise in the clutch chamber.

The clutch piston and the IFS continue to move in a synchronized fashion until the IFS orifice is cut off, which then separates the clutch chamber from the supply pressure. At the end of the clutch fill, the piston arrives at the final position just before engaging the clutch packs, and the IFS stops and the IFS orifice area is completely closed.

From the analysis above, it can be observed that the clutch piston displacement is fed back through the IFS orifice area, which regulates the fluid pressure inside the clutch chamber. This internal feedback structure ensures robust and precise motion of the clutch fill process. The feedback structure also guarantees a smoothly decreasing clutch piston velocity profile as it approaches the clutch fill final position.

(3) After the clutch fill, the clutch packs are ready to be engaged for torque transmission. When the clutch engagement starts, the clutch piston needs to be pushed further to squeeze the clutch. This can be realized by opening the on/off valve 2 at the exhaust port to release the fluid in the feedback chamber to the tank. As a result, the pressures in the piston feedback chamber and the IFS chamber will drop, and subsequently the IFS return spring can push the IFS downwards until the IFS orifice is fully open. The supply pressure, P_s, which now gets reconnected to the clutch chamber, will push the clutch piston further to squeeze the clutch packs.

(4) During the clutch disengagement, the clutch piston needs to move back to its initial position so that the clutch packs will be released. For that, the on/off valve 1 is de-energized to connect the IFS orifice to the low pressure tank. The return spring will then push the piston back to the disengaged position.

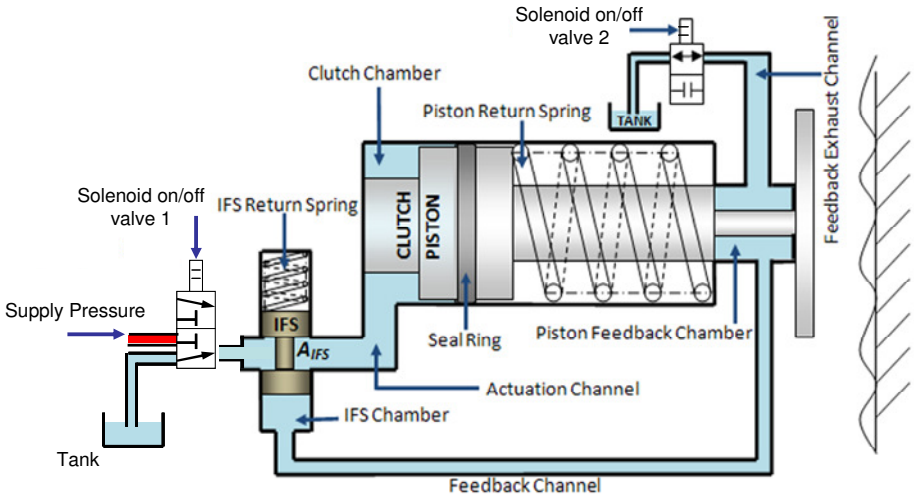

Figure 5.2a. Schematic diagram of the proposed clutch actuation control system

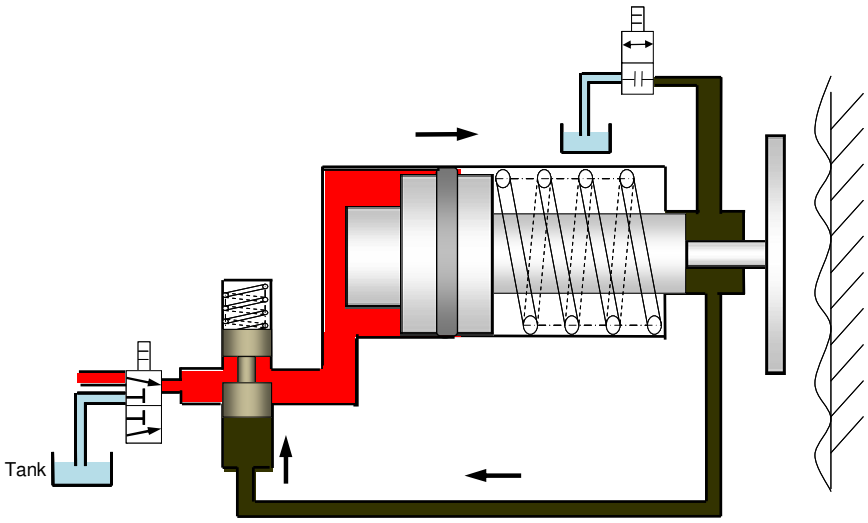

Figure 5.2b. Piston and IFS motion during clutch fill

Figure 5.2. IFS system design and working principle

5.5.2 Advantages of the new mechanism

The control block diagram of the IFS clutch actuation system is shown in Figure 5.3, which shows that the proposed mechanism consisting of the IFS, the clutch piston, and the on/off valve can be represented in a feedback loop.

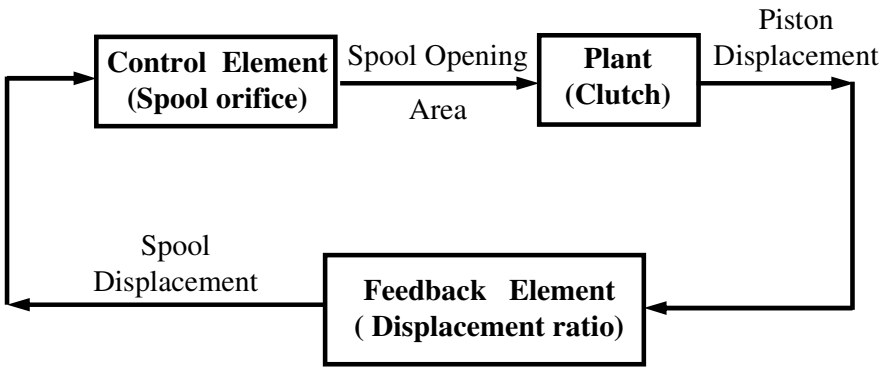

Figure 5.3. Feedback control diagram

There are two key merits of this new mechanism regarding the clutch control. First, instead of designing a nonlinear controller considering the complex nonlinear hydraulic dynamics, the proposed IFS clutch actuation system can realize a fast, precise and robust nonlinear control only by self-regulating the IFS spool orifice with the hydra-mechanical feedback rather than sensor measurement. The orifice area control automatically regulates the clutch chamber pressure and thus enables a smooth and precise clutch piston velocity and displacement profile. Second, ensuring a precise and robust clutch fill with the IFS system at the clutch level will enable the simplification of the upstream hydraulic control system including the control valves, the electronic control devices and their accessories [9]. This will not only improve the transmission system compactness, but can also alleviate the external control calibration efforts.

5.3 Mechanical Design and System Modeling

In this section, we will describe the IFS system mechanical design, targeting convenient assembly with the in production six speed automatic transmissions. Then based on the mechanical design, the dynamics model for the clutch fill process will be presented.

5.3.1 Mechanical System Design

The IFS mechanical system assembly shown in Figure 5.4 consists of the IFS body with chambers built inside, an IFS spool, a spring, two on/off valves and a clutch actuator. During the clutch fill, the pressure supply fluid will flow into the input chamber, passing the intermediate actuation chamber and the clutch orifice and finally reach the

clutch chamber (the path shown in solid red line in Figure 5.4). Note that the clutch orifice is a ring shaped long channel surrounding but not connecting to the feedback channel, and it's also connecting the intermediate actuation chamber and the clutch chamber. Once the high pressure fluid pushes the clutch piston forward, the piston will squeeze the fluid in the piston feedback chamber into the feedback channel and finally to the IFS chamber (the path shown in blue dashed line in Figure 5.4). Then the IFS piston will move to the left, counteracting the IFS spring and gradually closing the IFS orifice.

One of the most important design parameters is the IFS orifice, which is fabricated into a rectangular shaped slot. It acts as a crucial control variable that regulates the clutch chamber pressure by controlling the size of the IFS orifice area A_{IFS} with respect to the IFS spool displacement X_{IFS} during the clutch fill process. It determines the final clutch fill displacement, as the clutch piston will stop once the IFS orifice is cut off by the IFS spool. Therefore the orifice length should be designed according to the desired clutch fill final piston displacement.

5.3.2 IFS Modeling

The dynamics model of the IFS clutch control system includes the mechanical models of the clutch piston and the IFS spool, the pressure dynamics of the input pressure chamber, the intermediate actuation chamber, the clutch chamber, and the IFS chamber respectively. The piston feedback chamber is regarded as the same chamber as the IFS chamber because the feedback channel connecting these two are big enough to allow throttleless assumption.

The clutch and the IFS mechanical dynamics are described as

$$\begin{aligned} M_{pis}\ddot{X}_{pis} = (P_c + P_{cen})A_c - P_{IFS}A_{cb} - K_c(X_{pis} + X_{preload(pis)}) \\ - D_{pis}\dot{X}_{pis} - F_{drag}(P_c, \dot{X}_{pis}) \end{aligned} \tag{5.1}$$

$$\begin{aligned} M_{IFS}\ddot{X}_{IFS} = (P_{IFS} + P_{cen})A_{IFS} - K_{IFS}(X_{IFS} + X_{preload(IFS)}) \\ - D_{IFS}\dot{X}_{IFS} - F_{drag\_IFS}(\dot{X}_{IFS}) \end{aligned} \tag{5.2}$$

where M_{pis} is the clutch piston mass, X_{pis} is the clutch piston displacement, P_c is the clutch chamber pressure, P_{cen} is the average fluid centrifugal pressure as discussed in [10], A_c is the clutch piston area, A_{cb} is the clutch piston feedback area (the piston surface facing the piston feedback chamber), K_c is the clutch piston spring constant, $X_{preload(pis)}$ is the preload of the clutch piston spring, D_{pis} is the clutch damping coefficient. F_{drag} is the piston seal drag force, which is dependent on the piston motion. It is modeled as:

$$F_{drag} = \begin{cases} \left[k_m \left(P_c + P_{cen} \right) + c_m \right] \times sign\left(\dot{X}_{pis} \right) & (\dot{X}_{pis} \neq 0) \\ F_{stick} & (\dot{X}_{pis} = 0) \end{cases} \tag{5.3}$$

where k_m and c_m are constant, and F_{stick} is the static stick friction force from the Kanopp's stick-slip model [11]. Further detailed formulation of the mechanical dynamic model can be found in our recent work [12].

M_{IFS} is the IFS mass, X_{IFS} is the IFS displacement, P_{IFS} is the IFS/piston feedback chamber pressure, A_{IFS} is the IFS spool cross sectional area, K_{IFS} is the IFS spring constant, $X_{preload(IFS)}$ is the preload of the IFS spring and D_{IFS} is the IFS damping coefficient. In addition, the spool drag force F_{drag_IFS} is defined as:

$$F_{drag\_IFS} = \begin{cases} c_{m\_s} \times sign\left(\dot{X}_{IFS} \right) & (\dot{X}_{IFS} \neq 0) \\ F_{stick\_IFS} & (\dot{X}_{IFS} = 0) \end{cases} \tag{5.4}$$

where c_{m_s} is the spool friction constant, and F_{stick_IFS} is the static stick friction force of the IFS spool.

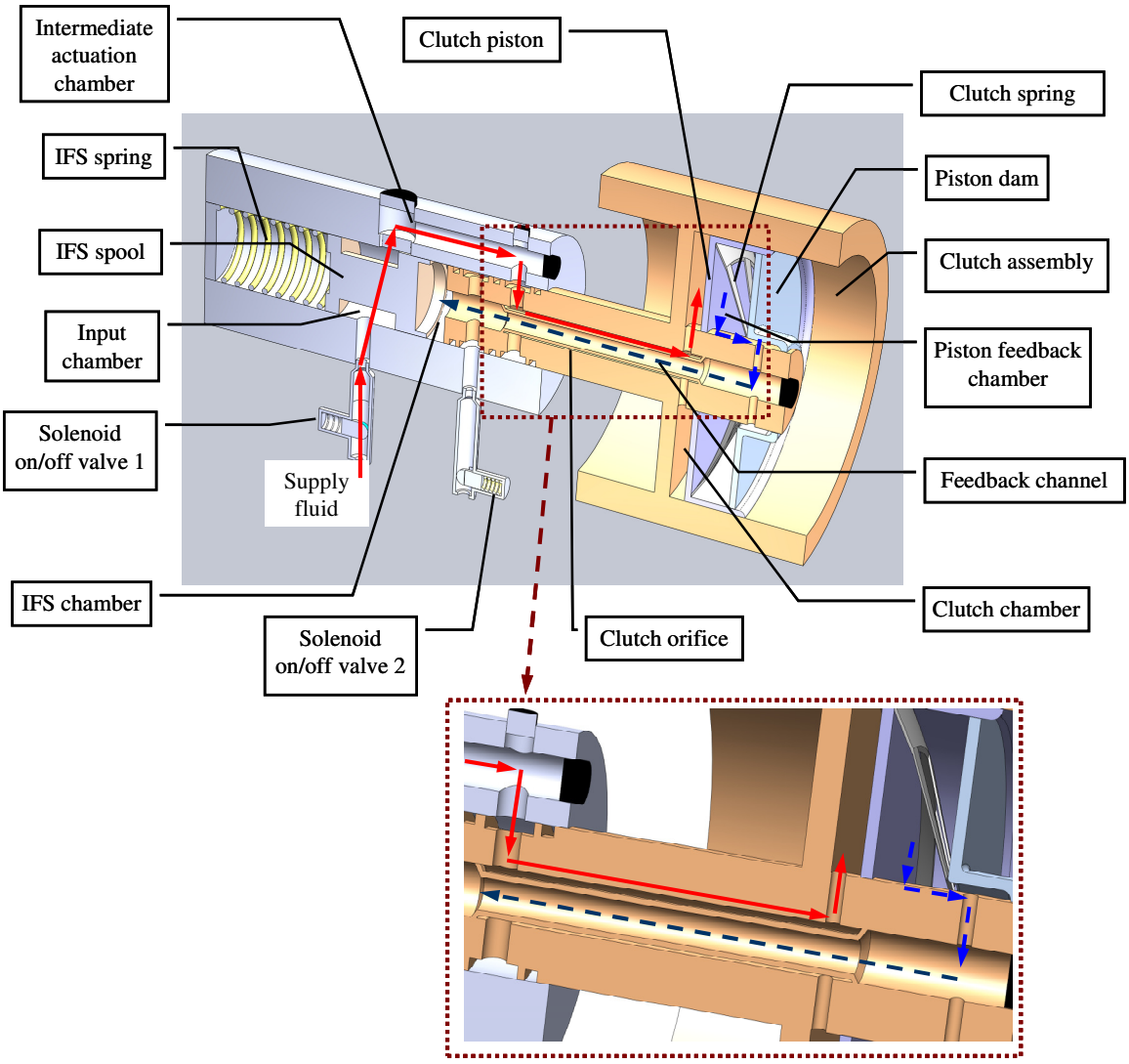

Fig 5.4. IFS system mechanical design drawing

The volumetric flow rates through the input chamber orifice, the intermediate actuation chamber orifice, and the clutch orifice can be described as

$$Q_{in} = A_{in} C_d \sqrt{\frac{2|P_s - P_{in}|}{\rho}} \cdot \mathrm{sgn}(P_s - P_{in}) \tag{5.5}$$

$$Q_{IFS} = A_{IFS} C_d \sqrt{\frac{2|P_{in} - P_m|}{\rho}} \cdot \mathrm{sgn}(P_{in} - P_m) \tag{5.6}$$

$$Q_c = A_c C_d \sqrt{\frac{2|P_m - P_c|}{\rho}} \cdot \mathrm{sgn}(P_m - P_c) \tag{5.7}$$

where C_d is the discharge coefficient, ρ is the transmission fluid density, P_s is the supply pressure, P_{in} is the input chamber pressure, P_m is the intermediate actuation chamber (Figure 5.4) pressure and P_c is the clutch chamber pressure. A_{in} is the orifice area between the supply channel and the input chamber, A_{IFS} is the IFS orifice opening area between the input chamber and the intermediate chamber, A_c is the ring shaped orifice between the intermediate chamber and the clutch chamber as shown in Figure 5.4. In particular, the IFS orifice area A_{IFS} keeps changing during clutch fill and is determined by the *IFS* spool displacement. It can be described as:

$$A_{IFS} = w \times (d - X_{IFS}) \tag{5.8}$$

where w is the slot width of the rectangular shaped IFS orifice, and d is the length of the slot orifice.

The pressure dynamics in the input chamber, the intermediate chamber, the clutch chamber and IFS chamber can be described as:

$$\dot{P}_{in} = \frac{\beta(P_{in})}{V_{in}}(Q_{in} - Q_{IFS}) \tag{5.9}$$

$$\dot{P}_m = \frac{\beta(P_m)}{V_m}(Q_{IFS} - Q_c) \tag{5.10}$$

$$\dot{P}_c = \frac{\beta(P_c)}{V_c}(Q_c - A_c \dot{X}_{pis}) \tag{5.11}$$

$$\dot{P}_{IFS} = \frac{\beta(P_{IFS})}{V_{IFS}}(A_{cb}\dot{X}_{pis} - A_{IFS}\dot{X}_{IFS}) \tag{5.12}$$

where V_{in} is the input chamber volume, V_m is the chamber volume of the intermediate actuation chamber, and V_c is the clutch chamber volume given by

$$V_c = V_{c0} + A_{pis} X_{pis} \tag{5.13}$$

where V_{c0} is the initial volume of the clutch chamber. In addition, V_{IFS} is the IFS chamber volume, which depends on the clutch piston and the IFS spool displacement and is given by:

$$V_{IFS} = V_{IFS0} + A_{IFS} X_{IFS} - A_{pis} X_{pis} \tag{5.14}$$

where V_{IFS0} is the initial value of the lumped IFS chamber, feedback channel and the piston feedback chamber volume before the clutch fill. In addition, the bulk modulus β is modeled as a function of the chamber pressure because the air entrained in the low pressure oil could cause the bulk modulus variation. The variation is modeled with respect the chamber pressure P_r (P_r may refer to any chamber pressure) as [13]:

$$\beta(P_r) = \frac{\beta_e (1+10^{-5} P_r)^{1+1/\gamma_b}}{(1+10^{-5} P_r)^{1+1/\gamma_b} + 10^{-5} R(1-c_1 P_r)(\beta_e / \gamma_b - 10^5 - P_r)} \tag{5.15}$$

where β_e is the bulk modulus in ideal fluid with no air entrained, γ_b is the ratio of specific heats for air, c_1 is the coefficient of air bubble volume variation due to the variation of the ratio of the entrained air and dissolved air content in oil, R is the entrained air content by volume in oil at atmosphere pressure. β_e, R, γ_b and c_1 are fixed when the oil temperature and pumping conditions are constant.

5.4. Simulation and Experimental Results

The designed internal feedback mechanism is fabricated for experimental verification. The internal channels are directly built inside the IFS body. The IFS clutch control test bed is shown in Figure 5.5. The main parts include a servo motor, an automotive transmission pump, a pilot-operated proportional relief valve, two on/off valves, a flow meter, two pressure sensors, a clutch mounting device/fixture, a displacement sensor, a power supply unit with servo amplifier and an XPC-target real time control system. In particular, one on/off valve controls the supply oil input into the clutch chamber, and the other controls the hydraulic oil injection into the internal feedback chamber for back pressure. In addition, as a note here, the sensors in the test bed are not used for the clutch control, but only for performance verification purpose. The IFS system operation requires no measurement feedback.

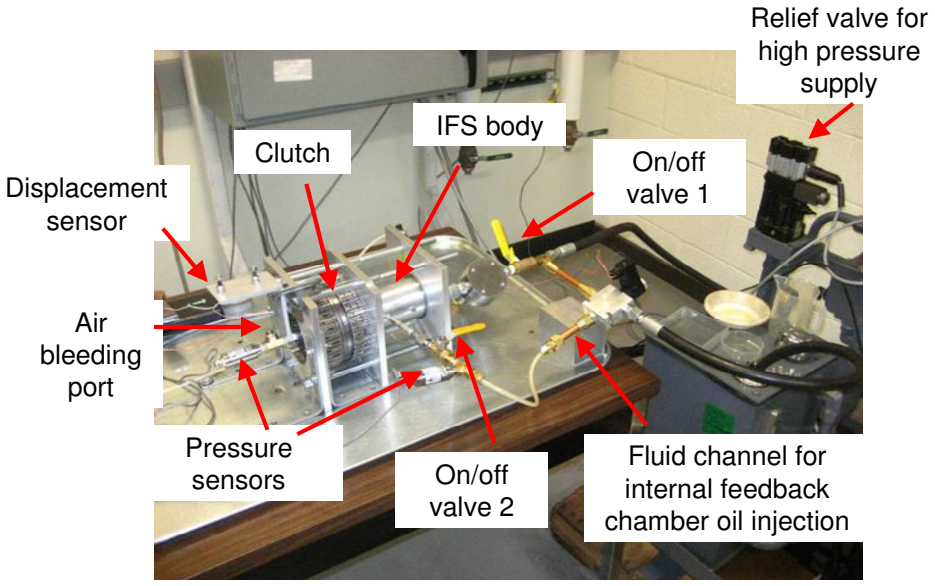

Figure 5.5. IFS clutch actuation test bed

The clutch fill experimental results are shown in Figure 5.6-Figure 5.9. The supply pressure is kept at 13 bar using a pressure relief valve. First, after injecting hydraulic oil into the internal feedback channel for back pressure, the internal feedback IFS chamber is cut off by the on/off valve 2. Then the on/off valve 1 connecting the supply pressure with the input chamber is switched to open, thus high pressure fluid can flow into the clutch chamber and then push the clutch piston to move. Over 30 groups of clutch fill tests are conducted and all of them show good repeatability. The clutch piston displacements from six representative tests are shown in Figure 5.6, which clearly shows that the displacement trajectories from different tests can almost overlap each other.

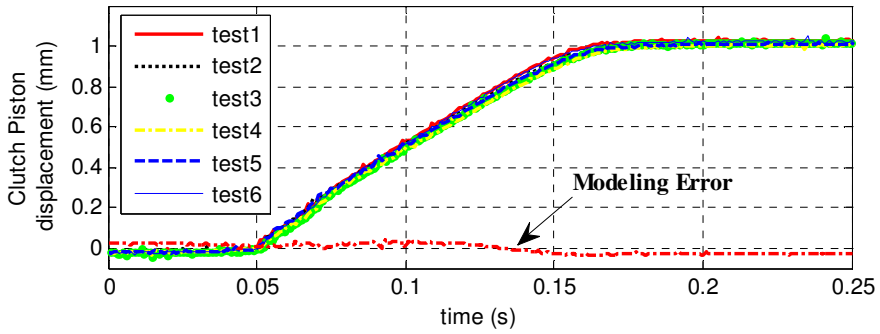

Figure 5.6. Multiple tests for clutch piston displacement and the dynamics modeling error of the clutch piston motion

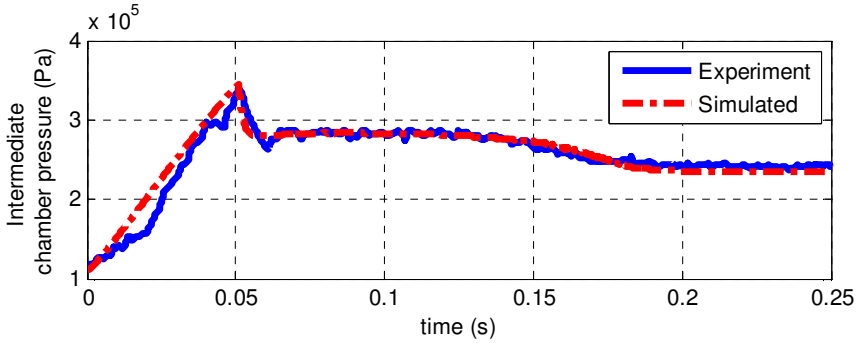

Figure 5.7. Intermediate actuation chamber pressure

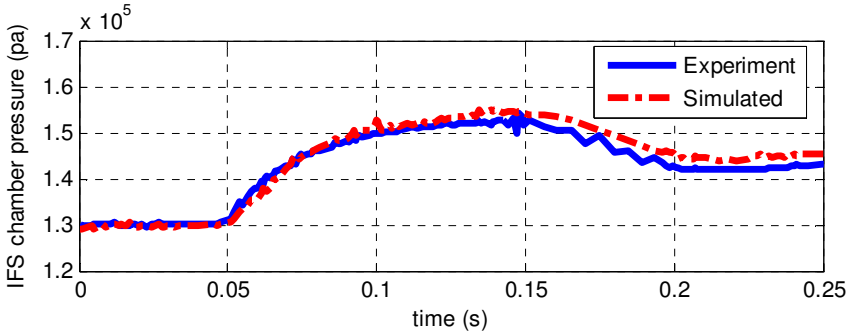

Figure 5.8. IFS chamber pressure

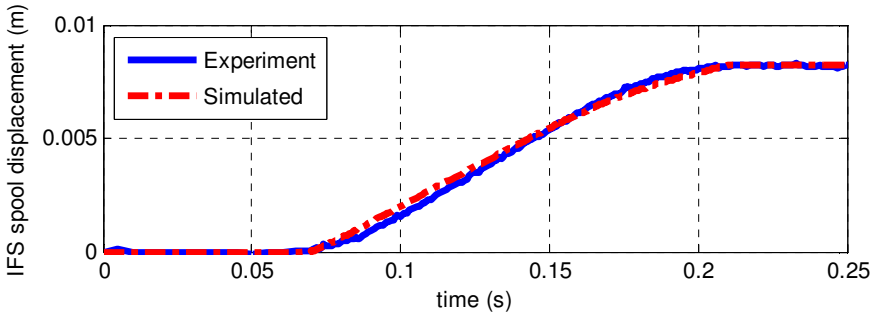

Figure 5.9. IFS spool displacement

At the start of the clutch fill process, the intermediate actuation chamber pressure quickly goes up due to the in-coming high pressure fluid as shown in Figure 5.7. At 0.05 seconds, the pressure in the intermediate actuation chamber (Figure 5.7) along with the clutch chamber is high enough to overcome the return spring force to push the clutch piston to move, then subsequently the clutch chamber pressure suddenly drops due to the piston motion induced out-flow. The pressure inside the clutch chamber is then kept in an appropriate level to keep moving the clutch piston forward. The pressure in the piston feedback and IFS chamber will then go up (Figure 5.8) due to the squeezing by the clutch piston, and thus push the IFS spool to close the IFS orifice. Once the IFS spool travels to the end and therefore cut off the IFS orifice as shown in Figure 5.9, the clutch piston stops at around 0.175 seconds. At the end of clutch fill, the clutch piston travels 1 mili-meter robustly as shown in Figure 5.6, which is exactly the desired clutch fill final displacement.

Finally, the system parameters are measured and identified as shown in Table I. The IFS system dynamics model built in Section III is then verified by simulation. The clutch piston motion dynamics modeling error is shown in Figure 5.6, and the dynamics modeling matching results for the intermediate actuation chamber pressure, the IFS chamber pressure and the IFS spool displacement are shown in Figures 5.7-5.9 respectively. It's assumed that the input on/off valve 1 in Figure 5.5 is opened 25% of the fully open orifice area in 250 mili-second. As can be seen, the dynamics model matches well with the experimental data and thus could be used for further design modification and analysis.

TABLE 5.1. SYSTEM PARAMETERS

Symbol	Name	Value
M_{pis}	clutch piston mass	0.4(kg)
$X_{preload(pis)}$	Clutch spring preload	4.15 (mm)
D_{pis}	Clutch piston damping	46926 (N/m/s)
K_c	Clutch spring stiffness	108899 (N/m)
A_c	Clutch piston front area	0.010681 (m^2)
A_{cb}	Clutch piston back area	0.010681 (m^2)
M_{IFS}	IFS spool mass	0.256 (kg)
K_{IFS}	IFS spring stiffness	1517.9(N/m)
A_{IFS}	IFS spool cross sectional area	0.000992 (m^2)
$X_{preload(IFS)}$	IFS spring preload	10.063 (mm)
D_{IFS}	IFS spool damping	438.96 (N/m/s)
k_m	Piston drag force coefficient	0.0016229 (m^2)
c_m	Piston drag force coefficient	50.927 (N)
k_s	Piston stick friction coefficient	0.0046229 (m^2)
c_s	Piston stick friction coefficient	122.927 (N)
c_{m_s}	IFS spool drag force coefficient	24.521 (N)
c_{stick_s}	IFS spool stick friction coefficient	26 (N)
w	Slot width of IFS orifice	1.988 (mm)
d	Length of the IFS slot orifice	7.3 (mm)
V_{in}	Input chamber volume	1.2455e-4 (m^3)
V_m	Intermediate chamber volume	1.8095e-5 (m^3)
V_{c0}	Clutch chamber initial volume	1.8277e-6 (m^3)
V_{IFS0}	IFS chamber initial volume	6.8e-4 (m^3)
A_{in}	Input chamber orifice area	2.4675e-5 (m^2)
A_{co}	Clutch chamber orifice area	1.5025e-5 (m^2)
γ_b	Ratio of specific heats for air	1.4
c_1	Coefficient of air bubble volume variation	-9.3e-6
ρ	Oil density	880 (kg/ m^3)
R	Entrained air content	7.5%
β_e	Effective bulk modulus of oil	17000 (bar)
C_d	Discharge coefficient	0.7

5.5. Conclusion

This chapter presents a novel transmission clutch actuation system with internal feedback. The internal feedback mechanism relays the clutch piston motion to the control spool position via a built-in feedback channel to achieve robust and precise clutch fill without any sensor measurement. The clutch fill process, which is traditionally

controlled in an open loop fashion due to the absence of a sensor, could therefore be controlled precisely using the internal feedback mechanism. The internal feedback system is designed for convenient assembly with the in-production automatic transmission by adding a few components, and is fabricated and tested in the clutch control test bed. Multiple tests demonstrate the accuracy and reliability of the clutch fill using the developed system, and the experimental and modeling results are presented. Future work includes more compact IFS system design and fabrication, the IFS orifice optimization for the optimal clutch fill, and finally the in-vehicle tests.

References in Chapter 5

[1] Wagner, G., "Application of Transmission Systems for Different Driveline Configurations in Passenger Cars". SAE Technical Paper 2001-01-0882.

[2] Sun, Z. and Kumar, H., "Challenges and opportunities in automotive transmission control". Proceedings of 2005 American Control Conference, Portland, OR, USA, June 8-10, 2005.

[3] Hebbale, K.V. and Kao, C.-K., "Adaptive Control of Shifts in Automatic Transmissions". Proceedings of the 1995 ASME International Mechanical Engineering Congress and Exposition, San Francisco, CA, 1995.

[4] Bai, S., Moses, R.L, Schanz, Todd and Gorman, M.J. "Development of A New Clutch-to-Clutch Shift Control Technology". SAE Technical Paper 2002-01-1252.

[5] Marano, J.E, Moorman, S.P., Whitton, M.D., and Williams, R.L. "Clutch to Clutch Transmission Control Strategy". SAE Technical Paper 2007-01-1313/

[6] Han, W. and Yi, S.J., "A Study of Shift Control Using the Clutch Pressure Pattern in Automatic Transmission." Proc. Instn Mech. Engrs vol. 217 Part D: J. Automobile Engineering. Volume 217, Number 4/2003, pp 289-298

[7] Song, X. and Sun, Z., "Pressure Based Clutch Control for Automotive Transmissions Using a Sliding Mode Controller", in press, IEEE Transactions on Mechatronics, 2011.

[8] Sun, Z., "Electro-Hydraulic Fully Flexible Valve Actuation System with Internal Feedback", ASME Transactions on Journal of Dynamic Systems, Measurement and Control, Vol. 131, 024502, March 2009.

[9] Miao, H., Sun, Z., Fair, J., Lehrmann, J., Harbin, S. "Modeling and Analysis of the Hydraulic System for Oil Budget in an Automotive Transmission". Proceedings of ASME 2008 Dynamic Systems and Control Conference, Ann Arbor, Michigan, USA, October 20-22, 2008

[10] Song, X., Sun, Z., Yang, X., Zhu, G., "Modeling, Control and Hardware-in-the-Loop Simulation of an Automated Manual Transmission", Proc. Inst Mech. Engrs, Part D, Journal of Automobile Engineering, Vol. 224, pp.143-159, 2010.

[11] Karnopp, D., “Computer Simulation of Stick-Slip Friction in Mechanical Dynamic Systems”, Journal of Dynamic Systems, Measurement, and Control, Vol. 107, No. 1, pp. 100-103, March, 1985.

[12] Song, X., Mohd Zulkefli, A., Sun, Z. and Miao, H., “Automotive Transmission Clutch Fill Control Using a Customized Dynamic Programming Method”, in press, ASME Transactions on Journal of Dynamic Systems, Measurement and Control, 2010.

[13] Yu, J., Chen, Z., and Lu, Y., “ The Variation of Oil Effective Bulk Modulus With Pressure in Hydraulic Systems”, Journal of Dynamic Systems, Measurement, and Control, Vol. 116, No. 1, pp. 146-150, March, 1994.

Chapter 6

The Driveline Level Design--Automated Manual Transmission (AMT) Optimal Clutch Engagement

Chapters 2 to Chapter 5 focus on the clutch level control. The control of the clutch actuation alone will not guarantee satisfactory performance of the whole power transmission system. Efficient and successful coordination with the driveline is another important factor. Failure in coordination will result in a less efficient or even perturbed power transmission. Therefore, in this chapter, the power transmission problem will be studied in the driveline level, by considering the clutch control and its coordination with driveline together. This study will be based on the automated manual transmission (AMT) optimal clutch engagement problem.

6.1. Introduction

The automated manual transmission (Figure 6.1) is a new type automatic transmission combining the benefits of both automatic and manual transmissions. A vehicle equipped with the automated manual transmission (AMT) should be operated in the same way as the automatic transmission, but the fuel economy should be highly improved comparing with the AT system. However, poorly designed AMT system will cause undesired vehicle vibration during gear shifts due to the torque interruption. This undesirable characteristic of the AMT system is actually the bottle neck for its wide application and competition with the automatic transmission system in the market. But this technical difficulty also brings in a great research opportunity, given the volatile fuel price and environmental concerns.

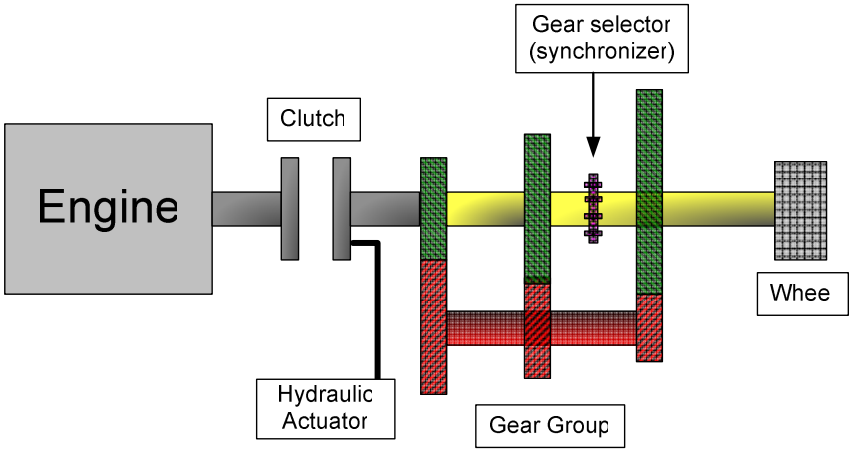

Figure 6.1. The AMT schematic diagram

The automated manual transmission [10-12] shares similar mechanical structure with the manual transmission system. Different from the manual transmission, the clutch and gearshift are controlled automatically by the AMT microcontroller. The most critical operation is the clutch launching and gearshift slipping control, which must satisfy several performance requirements: short gearshift duration and smooth gearshift with improved vehicle fuel efficiency.

To achieve those performance objectives, it is very important to build an effective dynamic model to study the dynamic characteristics of the AMT system. Moreover, it is also desirable to manage the control and motion strategy of the clutch engagement, which is the key factor for drivability and fuel consumption of the AMT system. The desired control method should result in smooth clutch engagement without lurch, and minimize energy loss due to the clutch slip for good fuel economy. In fact, in order to achieve these objectives, researches related to the clutch engagement during the gearshift phase have been widely explored. In [10], the control method to track reference clutch torque is presented to achieve the desirable performance. In [12], an approach for computing the desirable engine speed during gearshift is proposed. In [13], a neuro-fuzzy approach is implemented. In [14], a model based backstepping methodology is used to design the gearshift control in the AMT system.

However, in spite of the extensive literature on AMT control, the control methodology of the AMT system is still not mature for its wide applications. The main challenge lies in the clutch torque interruption during engagement and the coordination of

the engine and the transmission. To improve the control design and validation process, a practical model and rapid prototyping system is necessary. In this chapter, a Simulink AMT model is developed for AMT control strategy development and validation.

In addition, few papers have been published that offer a systematic approach to obtain the desired trajectory of the clutch torque input, which is the key for the minimal energy loss control. Reference [10] presents a method to control the clutch torque based upon the engine and the clutch reference velocities, but it doesn't provide the optimal clutch torque for smooth gearshift without vibration. Reference [15] provides a control strategy based on Linear Quadratic control, but the quadratic cost function used is not the actual energy loss cost function. In this chapter we will explore the possibility of using Dynamic Programming method to design the optimal clutch and engine velocity/torque trajectory during clutch engagement. Although the Dynamic Programming method requires tremendous computational throughput, it is capable of providing optimal solution based upon non-quadratic cost function and the given nonlinear dynamic model. Finally the optimal control generated from DP will be compared with regular non-optimal PID control.

This chapter is organized as follows. In Section 6.2, models of the driveline and the dry clutch are discussed. In Section 6.3, four different operating phases of the AMT are analyzed. The controllers corresponding to each phase are also presented. In addition, the possibility of using the Dynamic Programming method to generate the optimal clutch torque control input is investigated. Simulation results of the AMT system performance and the optimized clutch torque trajectory are presented in Section 6.4.

6.2. System Modeling

In this section, the dynamics of the driveline system and major subsystems of the AMT system are modeled. The clutch actuator model is well studied in Chapter 3 and thus will not be presented in detail here.

6.2.1 Driveline Modeling

The driveline dynamic modeling has been well studied in the literature [16-21]. Reference [2] presented a control oriented driveline dynamic model, which is adopted for

our development. The driveline is treated separately for clutch disk slipping condition, clutch disk engaged condition and gearshift synchronization condition. When the clutch disk is in the slipping operating condition, the driveline dynamics can be modeled as follows:

$$J_e\dot{\omega}_e = T_e - T_c(x_c)$$

$$[J_c + J_{eq}(i_g, i_d)]\dot{\omega}_c = T_c(x_c) - \frac{1}{i_g i_d}\left[k_{tw}\Delta\theta_{cw} + \beta_{tw}(\frac{\omega_c}{i_g i_d} - \omega_w)\right]$$

$$J_w\dot{\omega}_w = k_{tw}\Delta\theta_{cw} + \beta_{tw}(\frac{\omega_c}{i_g i_d} - \omega_w) - T_L(\omega_w) \tag{6.1}$$

$$\Delta\dot{\theta}_{cw} = \frac{\omega_c}{i_g i_d} - \omega_w$$

where J_e is the engine inertia, J_c is the clutch inertia, J_w is the wheel inertia, T_e is the engine torque, T_c is the clutch torque, ω_e is the engine rotational speed, ω_c is the clutch speed, ω_w is the wheel speed, x_c is the throwout bearing position. Furthermore, i_g is the gear ratio, i_d is the differential ratio, $J_{eq}(i_g, i_d)=J_m + (1/i_g^2)\times(J_{s1}+J_{s2}+(J_t/i_d^2))$, J_{s1} and J_{s2} are the inertias of the two disks connected to the synchronizer, J_m is the mainshaft inertia, J_t is the transmission gear box inertia, T_L is the load torque, θ_{cw} is the driveshaft torsional angle, k_{tw} is elastic stiffness coefficient, and β_{tw} is friction coefficients.

When the clutch is engaged, the engine speed and the clutch disk speed are the same. Then $\omega_e=\omega_c$ results in the driveline model as:

$$[J_e + J_c + J_{eq}(i_g, i_d)]\dot{\omega}_e = T_e - \frac{1}{i_g i_d}\left[k_{tw}\Delta\theta_{cw} + \beta_{tw}(\frac{\omega_c}{i_g i_d} - \omega_w)\right]$$

$$J_w\dot{\omega}_w = k_{tw}\Delta\theta_{cw} + \beta_{tw}(\frac{\omega_c}{i_g i_d} - \omega_w) - T_L(\omega_w) \tag{6.2}$$

$$\Delta\dot{\theta}_{cw} = \frac{\omega_c}{i_g i_d} - \omega_w$$

When the clutch disk is fully disengaged the engine flywheel, the gears are shifted, which

results in the rotational speed difference between the transmission gear shaft and the driveline shaft. The speed difference introduces friction between the collar gear and the synchronizer, which generates the synchronization torque T_s due to friction. By controlling the synchronization torque, the transmission shaft and gear shaft could be synchronized smoothly. During this synchronization process, there is no torque transmitted from the engine to the powertrain driveline. Thus the driveline dynamics during this process can be modeled as:

$$[J_c + J_{eq}(i_g, i_d)]\dot{\omega}_c = -\frac{T_s}{i_g}$$

$$J_w \dot{\omega}_w = T_s i_d - T_L(\omega_w) \tag{6.3}$$

Where T_s is the torque generated from the friction of the gear synchronizer.

6.2.2 Clutch Dynamics

The clutch packs are connected to the engine and the main shaft respectively (the clutch disk is connected to the main shaft and the flywheel disk is connected to the engine). The surfaces of the clutch packs are covered with friction material. The actuator controls the engagement and disengagement of the clutch pack on the engine flywheel and that on the main shaft. During a slipping close phase, the clutch disk on the main shaft is moved towards the flywheel disk until the friction between the two disks is high enough to transmit engine torque to the driveline. The clutch displacement position determines the direct normal force F_N between the flywheel disk and the clutch disk, and therefore the torque transmission capacity of the clutches. The relationship between the direct normal force and the torque transmission capacity is written as:

$$T_c = nF_N \mu R \tag{6.4}$$

where μ is the friction coefficient， n is the number of clutch packs, and R is the clutch mean radius.

When the clutch packs are in slipping phase, the transmitted clutch torque capacity is also the transmitted torque T_c, which is determined via a nonlinear relationship. In our simulation, the nonlinear characteristic of the clutch pack is based on the data reported by

[2]. When the clutches are in the engagement phase, the clutch torque T_c transmitted could be calculated directly from the driveline model for engagement phase. But if the calculated T_c is greater than the clutch torque transmission capacity, the clutch will slip. It should be noted that the nonlinear torque transfer characteristic is also influenced by the clutch temperature [22] and slip speed [23-24], but we will not consider these factors in the modeling of this chapter. This assumption will not affect the subsequent optimal clutch engagement design.

6.3. AMT Control System

The AMT system has four operating phases, which includes: engaged, slipping-open, synchronization, and slipping-close as shown in Figure 6.2. During ordinary operating conditions, the AMT is in the engaged phase, and the clutch is engaged. When a gearshift is requested based on the gearshift scheduling logic, the clutch pack on the main shaft moves away from the flywheel on the engine. And this case is considered as the slipping open phase. When the clutches are fully opened, a new gear can be engaged and the synchronization phase starts. The clutch disk and the mainshaft speed quickly change to a speed value corresponding to the new gear ratio due to the friction of the synchronizer. During the synchronization phase, the vehicle speed is assumed constant, and the engine speed also starts reducing. When the gearshift finishes, the slipping-close phase starts. In this phase, the clutch pack on the main shaft moves towards the fly wheel disk and then the clutch packs are squeezed. When the clutch and flywheel reach the same speed, they are locked up and a new engaged operating phase of the AMT starts.

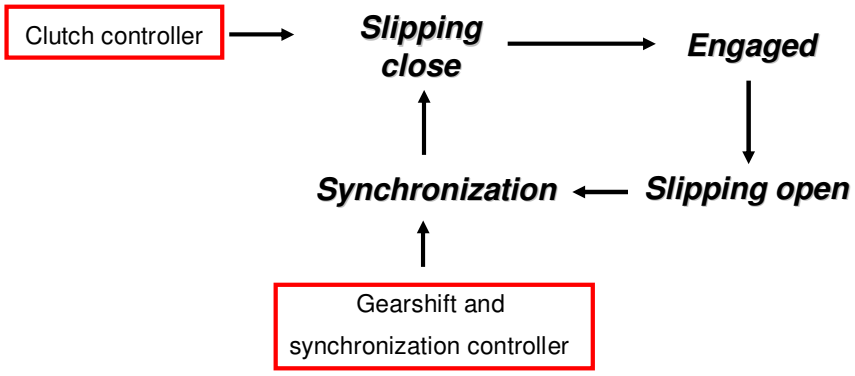

Figure 6.2. The clutch operation diagram

The control schematic diagram is shown in Figure 6.3. The main task of the

controllers is to control the engine speed and the clutch speed in order to meet the smooth clutch shift requirement.

6.3.1 Engine Control

The torque output of the engine is a function of the throttle and engine speed. The controlled engine torque in the simulation is determined by a pre-calibrated engine map, which is a look-up table with the throttle and the engine speed as inputs and the engine torque as output.

6.3.2 Gearshift Logic Control

The gearshift control logic determines the time to perform gearshift during a driving cycle for the best vehicle fuel economy. Some studies have been conducted to find the optimal gearshift strategies. Most of them are based on the vehicle speed and the amount of throttle. Once the gearshift command is initiated, the clutch starts disengaging and the appropriate gears will be shifted. In this chapter, the gearshift logic is implemented in a Stateflow finite state machine in Matlab/Simulink environment for a four gear AMT with gear ratios [2.393 1.450 1.000 0.677] from the first to the fourth gear.

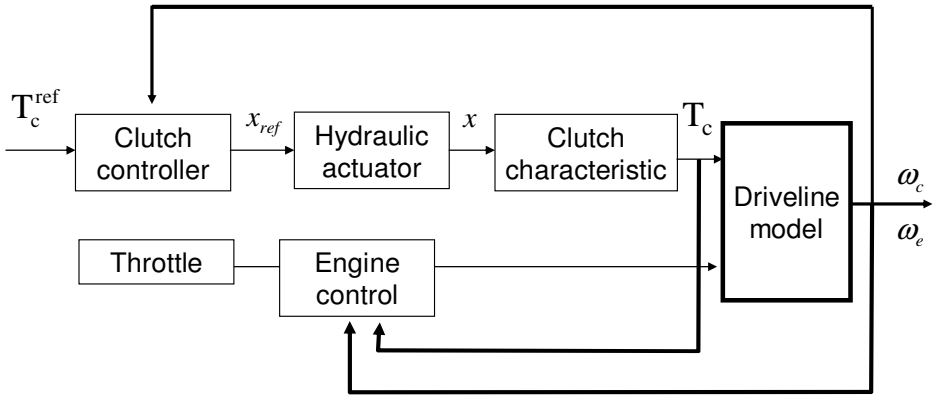

Figure 6.3. The control scheme of AMT system

6.3.3 Synchronization Control

During the synchronization phase, the clutches are disengaged, and no torque is transferred from the engine to the driveline system. The rotational speed of the gear to be connected to the driveline shaft is different from the driveline shaft rotational speed, and therefore needs to be synchronized. The synchronization is realized by controlling the friction torque between the new gear and the synchronizer collar gear, which is fixed on

the driveline shaft. The synchronization controller is realized by PID control presented in [13].

6.3.4 Clutch Control

The most important and difficult phase for the AMT operation is the slipping-close clutch engagement. Improper control of the clutch velocity and torque will lead to driveline vibration and bad fuel economy. Even worse, the energy loss during the clutch engagement generates heat and excessive heat could damage the clutch. The critical part for clutch control and operation is to control the displacement of the electrohydraulic actuator piston, which squeezes the clutch pack and therefore determines the clutch torque transferred to the driveline system. The transferred clutch torque together with the engine torque will affect the engine and clutch speed. Note that the speed difference between engine and clutch is proportional to the energy loss. Therefore, it is critical to have an optimal clutch and engine torque trajectories that enable a smooth and efficient torque transfer. In fact, although previous work [7] has been reported to design the optimal torque trajectory, the associated cost function is an approximation of the actual energy loss during clutch engagement. The main reason is due to the non-quadratic energy loss function, which is difficult to apply the LQR controller. Furthermore, to avoid driveline oscillation, not only do we need to consider the possible vibration at the end of clutch engagement, but also need to reduce the vibration during the entire process of clutch engagement. In addition, it is also important to ensure the smoothness of the reference clutch torque; otherwise it will be difficult for the controller to track. However, so far there is limited research work that takes all the above three criteria into account to generate optimal torque trajectory. In the later section, we will present a systematic way to obtain the optimal torque trajectory based on the Dynamic Programming method.

Before applying the dynamic programming method to the clutch slipping closing control, we first investigate the clutch system controllability, which determines the number of control inputs required to control the engine speed and clutch speed independently in order to meet the optimal clutch engagement requirement. If the clutch torque T_c is the only control input, based on the dynamic model (6.1) the controllability matrix is:

$$\begin{bmatrix} -1 & 0 & 0 & 0 \\ 1 & \dfrac{-\beta_{tw}}{\left(i_g i_d\right)^2} & C_{23} & C_{24} \\ 0 & \dfrac{\beta_{tw}}{\left(i_g i_d\right)} & C_{33} & C_{34} \\ 0 & \dfrac{1}{\left(i_g i_d\right)} & C_{43} & C_{44} \end{bmatrix} \tag{6.5}$$

Where

$$C_{23} = -\frac{-\beta_{tw}^2 - \beta_{tw}^2\left(i_g i_d\right)^2 + k_{tw}\left(i_g i_d\right)^2}{\left(i_g i_d\right)^4}$$

$$C_{24} = \frac{\beta_{tw}(-\beta_{tw}^2 - 2\beta_{tw}^2\left(i_g i_d\right)^2 + 2k_{tw}\left(i_g i_d\right)^2 - \left(i_g i_d\right)^4\beta_{tw}^2 + 2k_{tw}\left(i_g i_d\right)^4)}{\left(i_g i_d\right)^6}$$

$$C_{33} = -\frac{-\beta_{tw}^2 - \beta_{tw}^2\left(i_g i_d\right)^2 + k_{tw}\left(i_g i_d\right)^2}{\left(i_g i_d\right)^3}$$

$$C_{34} = -\frac{\beta_{tw}(-\beta_{tw}^2 - 2\beta_{tw}^2\left(i_g i_d\right)^2 + 2k_{tw}\left(i_g i_d\right)^2 - \left(i_g i_d\right)^4\beta_{tw}^2 + 2k_{tw}\left(i_g i_d\right)^4)}{\left(i_g i_d\right)^5}$$

$$C_{43} = -\frac{-\beta_{tw}[1+\left(i_g i_d\right)^2]}{\left(i_g i_d\right)^3}$$

$$C_{44} = -\frac{-(-\beta_{tw}^2 - 2\beta_{tw}^2\left(i_g i_d\right)^2 + k_{tw}\left(i_g i_d\right)^2 - \left(i_g i_d\right)^4\beta_{tw}^2 + k_{tw}\left(i_g i_d\right)^4)}{\left(i_g i_d\right)^5}$$

Note that the controllability matrix is not full rank (This fact is not intuitive but can be easily seen by simple matrix rank calculation). This indicates that the clutch speed and the engine speed cannot be controlled independently by the single control input T_c. With similar approach, it can be verified that the above controllability matrix is full rank and the system is controllable if T_e and T_c are both control inputs. Therefore, to efficiently control the energy loss and the driveline vibration, both T_e and T_c are regarded

as control inputs for the DP design.

6.3.5. Optimal Clutch and Engine Torque during the Clutch Engagement

In this section, we investigate the possibility of using the Dynamic Programming (DP) method to obtain the optimal torque trajectory during clutch engagement, and the result from DP will be used as a benchmark to compare with the result using the PID engagement controllers.

6.3.5.1 Formulation of the clutch engagement optimal control problem

To enable a smooth clutch engagement control, the clutch torque transmitted to the driveline system should not induce vibration. In fact, the most critical point is at the moment of the engagement. According to [2], to avoid the lurch problem, it is desirable that $\dot{\omega}_e(t_f^-) - \dot{\omega}_c(t_f^-)$ is as small as possible. Also, at final time t_f, the velocity difference between w_e and w_c must be zero to complete the engagement, and the clutch torque $T_c(t_f)$ is desirable to be larger than the load torque $T_L(t_f)$ to continue accelerating after engagement.

These requirements can be translated into a set of final state conditions that the system must satisfy:

$$\begin{aligned} &\min(\left|\dot{\omega}_e(t_f^-) - \dot{\omega}_c(t_f^-)\right|) \\ &\omega_e(t_f) - \omega_c(t_f) = 0 \\ &T_c(t_f) > T_L(t_f) \end{aligned} \tag{6.6}$$

where $\omega_e(t_f)$, $\omega_c(t_f)$ are the final state variables, and $T_c(t_f)$, $T_L(t_f)$ are the clutch torque control inputs and the load torque at the final state respectively.

Among the controls that can realize the clutch engagement, we would like to take the one that has minimum energy loss. The energy dissipated during the engagement can be written as:

$$E_d = \int_0^{t_f} (\omega_e(t) - \omega_c(t)) T_c(t) dt$$

In addition, to realize independent control of the ω_c and ω_e, the engine torque T_e is assumed to be controllable in the DP algorithm. The control inputs T_c and T_e obtained from the Dynamic Programming should be continuous and smooth enough to ease the future tracking control. Therefore the derivative of T_c and T_e is constrained to be a small value during the clutch engagement process. Moreover, this constraint on the clutch torque derivative also avoids high frequency input to the driveline system, and will therefore prohibit driveline system vibration [25-28] during the clutch engagement.

Now we are ready to formulate the clutch engagement control problem as an optimization problem based on the above control objectives. The cost function of the optimization problem is:

$$\begin{aligned} g = {} & \lambda_1 \int_0^{t_f} (\omega_e(t) - \omega_c(t)) T_c(t) dt + \lambda_2 \int_0^{t_f} [\dot{T}_c(t)]^2 dt \\ & + \lambda_3 \int_0^{t_f} [\dot{T}_e(t)]^2 dt + \lambda_4 \left| \dot{\omega}_e(t_f^-) - \dot{\omega}_c(t_f^-) \right| + \lambda_5 \left| \omega_e(t_f) - \omega_c(t_f) \right| \end{aligned} \tag{6.7}$$

In particular, the first term of the cost function ensures minimum energy dissipation during the clutch engagement process. And the second and third terms set constraints to the trajectory of the clutch torque and the engine torque to ensure smoothness. The last two terms will lead the system to reach the specified final conditions in the required time t_f. λ_1, λ_2, λ_3, λ_4 and λ_5 are the weighting factors.

As the cost function is not quadratic and the dynamic model is nonlinear, it is difficult to use traditional quadratic optimal control method to solve this problem. Therefore, we propose to apply the dynamic programming method to find the desired clutch and the engine speeds, or in other words, the optimal input clutch torque trajectory. A systematic solution to the above optimization problem can be determined recursively via Bellman's Dynamic Programming [8]. Since the system model is nonlinear, analytical solution cannot be obtained. Instead numerical solution will be provided. But first we need to discretize the system model to carry out the numerical Dynamic Programming method.

6.3.5.2 System model discretization

To alleviate the computational throughput for the Dynamic Programming, it is desirable to have a low order system model that captures the major system dynamics of

Eq (6.1). Therefore by assuming $\omega_c \equiv \omega_m \equiv i_g i_d \omega_w$, combining the vehicle inertia to the main shaft [2] leads to a 2nd order model. We use this reduced order model for our DP algorithm and the discretized 2nd order system model is as follows:

$$\omega_e(k+1) = \frac{[T_e(k) - T_c(k)]\Delta t}{J_e} + \omega_e(k) \tag{6.8}$$

$$\begin{aligned} \omega_c(k+1) &= \frac{[T_c(k) - T_L(k)]\Delta t}{J_v} + \omega_c(k) \\ &= \frac{[T_c(k) - Br(\frac{\omega_c}{i_g i_d})^2]\Delta t}{J_v} + \omega_c(k) \end{aligned} \tag{6.9}$$

where Δt refers to the sampling time interval, B is the resistance coefficient, r is the tire radius.

We define $N=T/\Delta t$ as the number of steps from the initial state to the final state. And the cost function (6.7) becomes:

$$\begin{aligned} g(x) = {} & \lambda_1 \sum_{k=1}^{N-1} [\omega_e(k) - \omega_c(k)] T_c(k) \Delta t + \lambda_2 \sum_{k=1}^{N-1} [T_c(k+1) - T_c(k)]^2 / \Delta t \\ & + \lambda_3 \sum_{k=1}^{N-1} [T_e(k+1) - T_e(k)]^2 / \Delta t + \lambda_5 \left| \omega_e(N) - \omega_c(N) \right| \\ & + \lambda_4 \left| \frac{\omega_e(N) - \omega_e(N-1)}{\Delta t} - \frac{\omega_c(N) - \omega_c(N-1)}{\Delta t} \right| \end{aligned} \tag{6.10}$$

Consequently, the optimal control problem is to find the optimal control inputs T_c and T_e to minimize the cost function

$$J(x) = \min_{u \in U} g(x) \tag{6.11}$$

6.3.5.3 Application of dynamic programming to the optimal clutch engagement control

In this section, the application of the conventional numeric Dynamic Programming for the clutch engagement control problem is discussed. To convert the Dynamic Programming into a finite computational problem, the standard method is to use the state space quantization [8-11]. By applying this approach, the state space is discretized into finite grids:

$$\begin{cases} \omega_c(k) \in \{\omega_c^1(k), \omega_c^2(k), \ldots \omega_c^j(k), \ldots \omega_c^L(k)\} \\ \omega_e(k) \in \{\omega_e^1(k), \omega_e^2(k), \ldots \omega_e^j(k), \ldots \omega_e^L(k)\} \end{cases} \tag{6.12}$$

Define $X(k)=[\omega_e(k), \omega_c(k)]^T$ and $X_{ij}(k)=[\omega^i{}_c(k), \omega^j{}_e(k)]$. Therefore, in each step, $\omega_e(k)$, $\omega_c(k)$ are discretized into L discrete values respectively, and $X(k)$ has $L \times L$ possible discrete values in the step k.

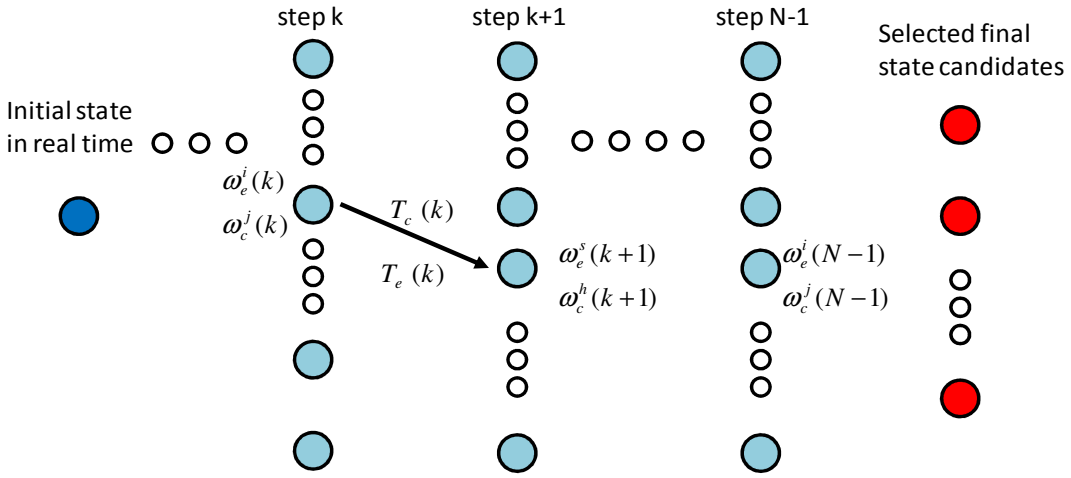

Figure 6.4. DP ALGORITHM

For the clutch engagement problem, the initial states are unknown because they depend on the driving condition. The final state of the clutch velocity ω_c is not specified either. To formulate this problem for the dynamic programming, we need to specify the final states first. As the final state value of the velocity difference ω_e-ω_c is required to be zero for clutch engagement, then the only final state value we need to specify is the clutch velocity ω_c. In fact, the range of $\omega_c(t_f)$ can be predetermined as the vehicle velocity range is restricted given specific gear shift ratio. Then the $\omega_c(t_f)$ range interval can be evenly partitioned into a number of discrete $\omega_c(t_f)$ values. During the Dynamic Programming searching process, the discrete states at step N-1 as shown in Figure 6.4 will choose the optimal final states respectively based on the cost function. In fact, as the driveline inertia is much larger than the engine inertia J_e, ω_c does not change much during the clutch engagement process comparing with the change of ω_e. Consequently in the DP searching process, the range of the state ω_c is restricted, and therefore the computation burden is alleviated.

The dynamic programming process ends at step 2 rather than step 1 as the initial

states are unknown. All the discretized states in step 2 will be assigned an optimal cost value and the corresponding optimal trajectory towards the final states. Then all the states and optimal trajectory will be stored in a look up table. During the real time driving, the initial states at the clutch engagement will be known. Therefore based on the initial state, we can select an optimal trajectory from the lookup table.

Then the spatial discretization yields the following general step of the Dynamic Programming algorithm:

Step N-1, **for** $1 \le i \le L$, **and for** $1 \le j \le L$,

$$J_{N-1}(\omega_e^i, \omega_c^j) = \min_{1 \le s \le L} \{ \lambda_5 [\omega_e^s(N) - \omega_c^s(N)]^2 + \lambda_4 [\frac{\omega_e^s(N) - \omega_e^j(N-1)}{\Delta t} - \frac{\omega_c^s(N) - \omega_c^j(N-1)}{\Delta t}]^2 \} \tag{6.13}$$

Step k, **for** $0 \le k < N-1$, **for** $1 \le i \le L$, **and for** $1 \le j \le L$

$$J_k(\omega_e^i, \omega_c^j) = \min_{\substack{1 \le s \le L \\ 1 \le h \le L}} \{ \lambda_1 [\omega_e(k) - \omega_c(k)] T_c(k) \Delta t + \lambda_2 [T_c^{s,h}(k+1) - T_c(k)] + \lambda_3 [T_e^{s,h}(k+1) - T_e(k)] + J_{k+1}(\omega_e^s(k+1), \omega_c^h(k+1)) \} \tag{6.14}$$

where $T_c(k)$ and $T_e(k)$ can be calculated from the equations (6.8) and (6.9) given specific $w^i_e(k)$, $w^j_c(k)$, $w^s_e(k+1)$, and $w^h_c(k+1)$. The optimal control policy minimizes of the cost in Equations (6.13) and (6.14).

6.4. Simulation Results and Case Study

In this section, we present simulation results of a few practical AMT operation cases for the automated manual transmission in Matlab/Simulink. The AMT modeling parameters are shown in Tab. 6.1.

TABLE 6.1. THE AMT SYSTEM DYNAMIC MODEL PARAMETERS

M_p	0.4 (kg)	ρ	813.79 (kg/ m^3)
x_{p0}	0.00357 (m)	r_{po}	63.9572 (mm)
K_p	151180 (N/m)	r_{pi}	43.0022 (mm)
D_p	30 (N/m/s)	r_{st}	37.3126 (mm)
A_p	0.00704 (m^2)	P_c	2.8164e4 (Pa)
α	1 (m/s)	T	1 (s)
V_0	0.00005(m^3)	Δt	0.02(s)
β	17000(bar)	$A_{orifice}$	3.407e-6 (m^2)
C_d	0.7	M	0.13
P_{atm}	1(bar)	n	3
J_e	0.2 kgm^2	R_a	0.065 (m)
i_d	3.94	J_w	133 kg.m2
J_c+J_{eq}	0.04kgm^2	β_{tw}	295 Nm/(rad/s)
k_{tw}	6200 Nm/rad		

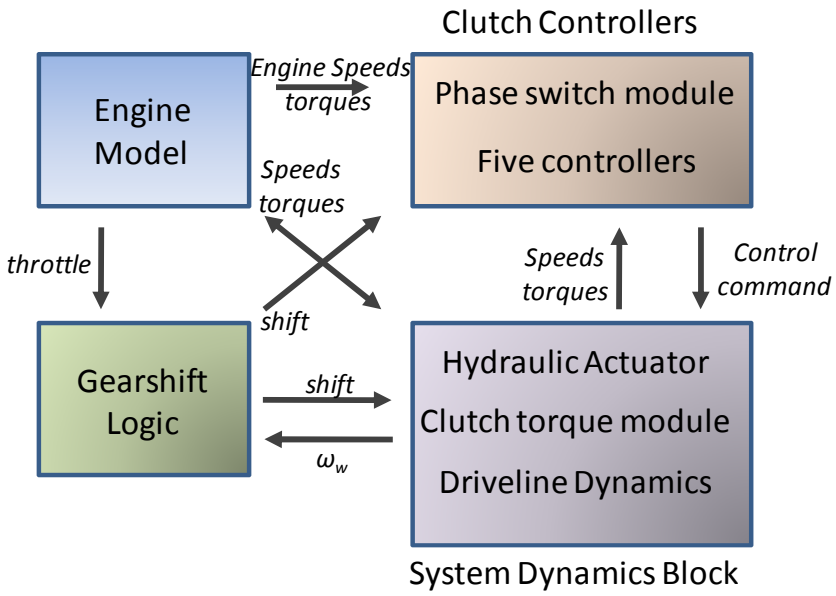

Figure 6.5. Simulink Model Blocks

Based on the mathematical system dynamic model, a simulation model is developed in the Matlab/Simulink environment. As shown in Figure 6.5, the Simulink model consists of four parts: the engine model, the gearshift logic model, the transmission

driveline model, and the transmission controller model.

The engine model provides the engine speed and torque based on the input throttle. The engine torque in the simulation is obtained from the pre-calibrated engine map, which is interpolated from a series of discrete throttle values and engine speed values.

The gearshift logic is programmed using the Stateflow in the Simulink, and is obtained based on the gearshift scheduling map, which provides the optimal gearshift schedule based upon the current vehicle speed and throttle. Once the gearshift command is initiated from the gearshift logic model, the clutch controller is triggered.

The clutch controllers include the engagement controller, the slipping opening controller, the synchronization controller, the go-to-slipping controller, and the slipping closing controller. The controllers switch between each other by triggering the proper controller in the specific operating phase. When no gearshift is requested, the engagement controller maintains a high pressure control signal to the hydraulic actuator to maintain the clutch engagement. Once the gearshift becomes active, the clutch control switches to the slipping opening controller and followed gearshift clutch controllers. This control sequence is carried out in our Simulink strategy by selecting the operating period right after the gearshift for different controllers and detecting the specific time period. On the one hand, the "detect change" function block in the Simulink is used to capture the gearshift request event. The starting time of the gearshift event t_s is recorded. On the other hand, the controller switching module implemented in the Simulink keeps updating the difference t_c - t_s between the current time t_c and t_s. As shown in Figure 6.6, when t_c - t_s is between 0 and 0.2 second, the slipping opening controller is activated and the input pressure control signal to the hydraulic actuator decreases to disengage the clutches. When t_c - t_s is greater than 0.2 and less than 0.4, the synchronization controller is triggered. When t_c - t_s is greater than or equal to 0.4 and less than 1.1, the controller switches to the go-to-slipping and then the slipping closing controller to engage the clutches. When t_c - t_s is greater than or equal to 1.1, the engagement controller is again activated to maintain the clutch engagement. In the future, if the new gearshift is requested, the starting time t_s is reset and the sequence repeats. As discussed before the hydraulic pressure controller implemented in Simulink is a combination of feedforward

and PID controllers.

The control signals generated from the AMT controller are then sent to the AMT transmission and the driveline system model block. This block is composed of the hydraulic clutch actuator dynamics model, the clutch torque physics module, and the driveline dynamics model. The clutch torque determination module simulates the clutch torque physical characteristic. The clutch torque is the sliding friction torque when the clutches are slipping; while it becomes static friction torque when the clutches are engaged. The clutch torque determination module will select different equations (Eq 6.1-Eq 6.3) to describe the different friction torques. The driveline dynamics block consists of the engagement driveline dynamics, the slipping closing dynamics and the synchronization. Similar to the controllers, the driveline dynamics also need to switch in different operating phases. The parts of the model that change with different AMT operating phases are implemented based on the event-control method. For instance, the commutation from the slipping-closing phase to the engaged phase is obtained with the event "$\omega_e=\omega_c$".

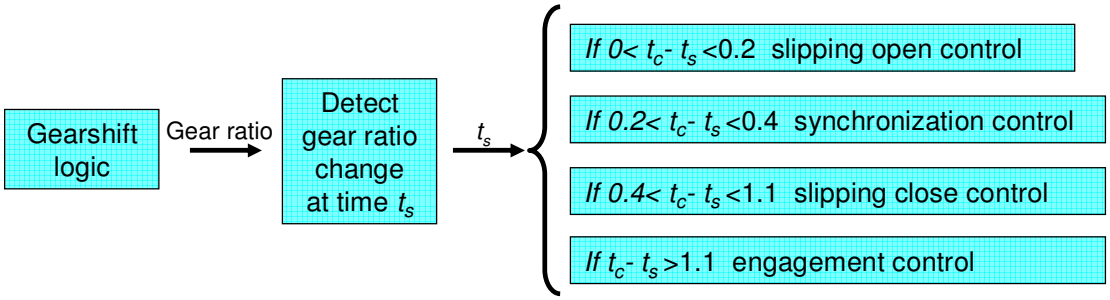

Figure 6.6. Controller Switch Logic

Figure 6.7 shows the engine throttle input and the gearshift scheduling for the simulation example. Figure 6.8 shows the corresponding simulation results. The gear ratio is shifted from 1 to 2, and later from 2 to 3. During each gearshift, the clutch torque first drops down to zero, and then stays for a while and finally goes up. The gearshift is realized when there is no clutch torque transferred. And the vehicle speed continuously increases.

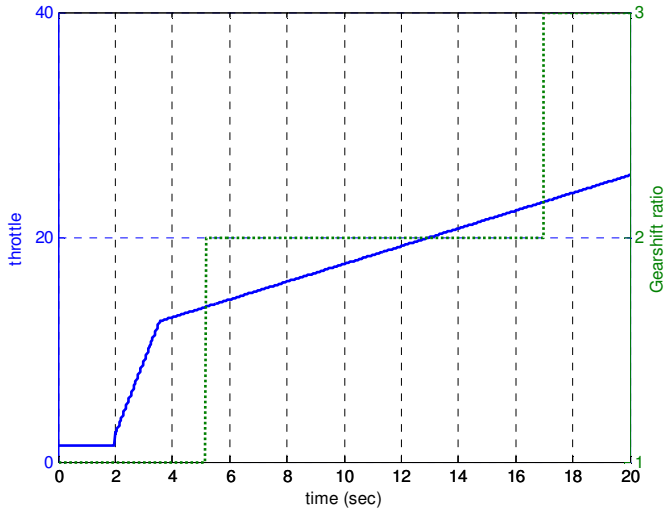

Figure 6.7. The throttle input and gearshift scheduling

We also conducted the simulation to obtain the optimal torque trajectory using the dynamic programming. The optimal velocity and the optimal torque trajectories are also compared with those obtained from the feedforward and PID control results in the Simulink simulation. To make a fair comparison, the initial conditions $\omega_{e\_initial}$ and $\omega_{c\_initial}$, which are defined as the speeds after synchronization and right before engagement, of both the optimal engagement and non-optimal engagement are the same. In addition, both of the engagements can be realized within the same time period. The gearshift is from gear 1 to 2. The simulation only shows the clutch synchronization and engagement process, which starts from the end of clutch disengagement and ends once the clutch plates are engaged. Figure 6.9 shows the trajectory of the clutch velocity ω_c and the engine velocity ω_e. The first 0.2 second is the synchronization phase. During the gear synchronization, the clutch plates are totally disengaged, and therefore no clutch torque T_c is transferred. The clutch velocity ω_c is dragged down by the driveline inertia during synchronization. On the other hand, the engine torque is assumed to be close to zero during synchronization, and the engine velocity ω_e does not change much during synchronization. Therefore the initial speed difference before the clutch engagement $\omega_{e\_initial}$-$\omega_{c\_initial}$ is larger than zero. During the clutch engagement phase, the clutch velocity does not change much due to the heavy inertia of the vehicle body, but the engine velocity ω_e decreases until the clutches are fully engaged. Figure 6.10 shows the

speed difference ω_e-ω_c. For the optimal engagement obtained from DP, the speed difference decreases during the clutch engagement. At the final time, the change of the speed difference becomes smaller as the derivative of ω_e is constrained to be close to that of ω_c near final time of the clutch engagement. Figure 6.11 shows the clutch torque T_c during the clutch engagement. Both of the clutch torque trajectories start from zero *Nm*. For the optimal clutch torque trajectory, the maximum torque difference in each step is limited to be smaller than 20 *Nm*. Figure 6.12 exhibits the engine torque T_e. The engine torque obtained from DP is required to be negative at the start of the clutch engagement, because otherwise the engine velocity will go up. The energy loss is compared in Figure 6.13. The energy loss trajectory shows the energy lost from the initial time to the current time t_1:

$$E_d(t_1) = \int_0^{t_1} (\omega_e(t) - \omega_c(t)) T_c(t) dt \tag{6.15}$$

We can see that at the end of the clutch engagement, the energy loss of the engagement using DP is almost half of the one produced by the PID controller. Therefore, to reduce energy loss, it is desirable to track the torque trajectories obtained from the Dynamic Programming. However, the computational throughput and lack of control means to precisely track the optimal trajectory make it difficult to be implemented into the current Simulink model. Our future research work will be focused on further reducing the computational throughput of the PD algorithm and developing effective control tools to track the optimal torque trajectories from DP.

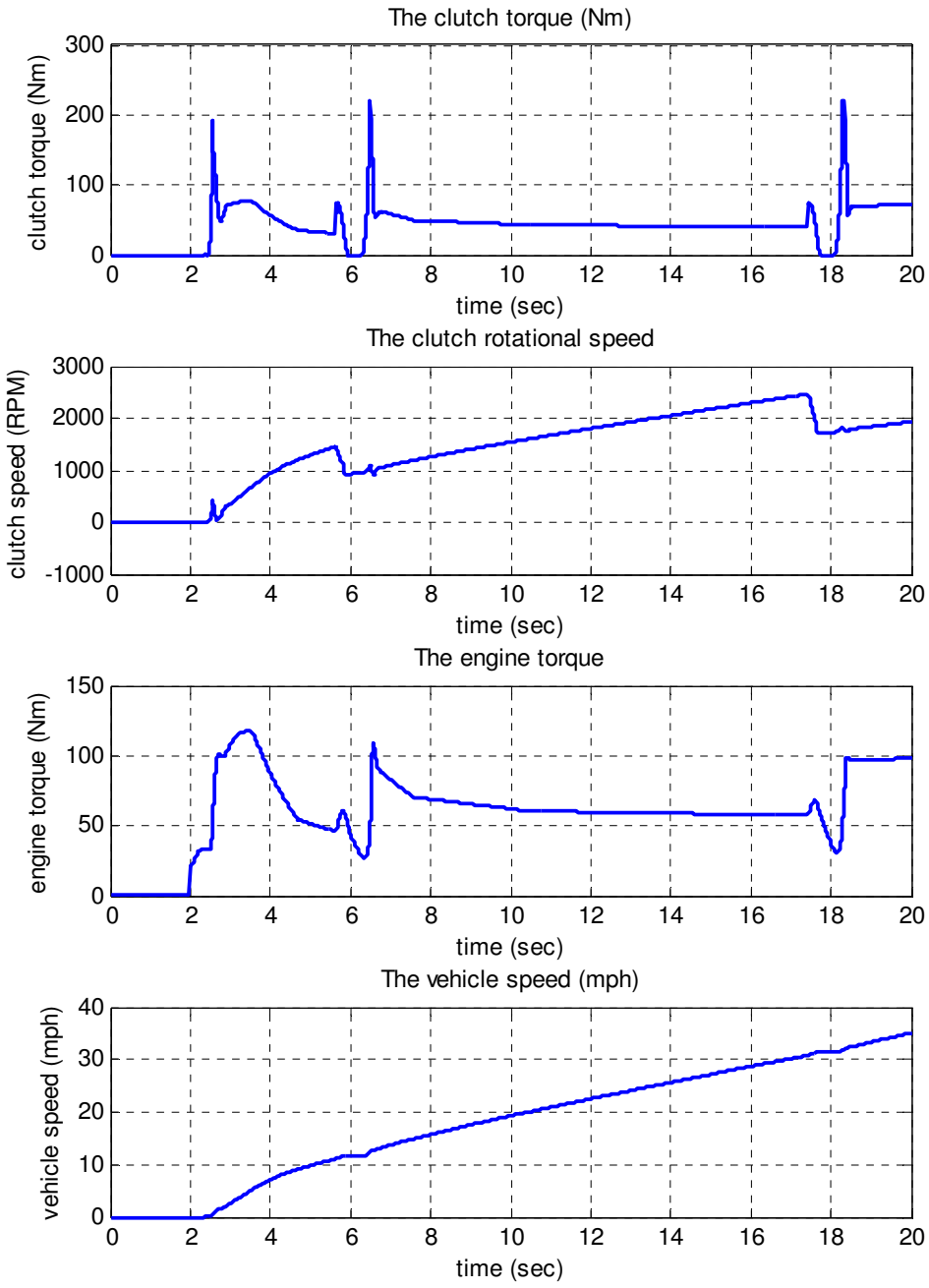

Figure 6.8. The AMT simulation results

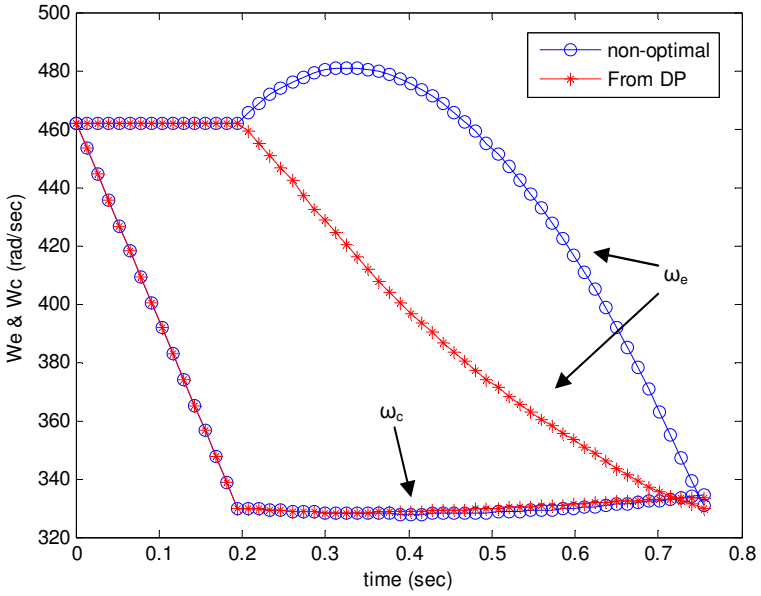

Figure 6.9. Trajectories of ω_c and ω_e

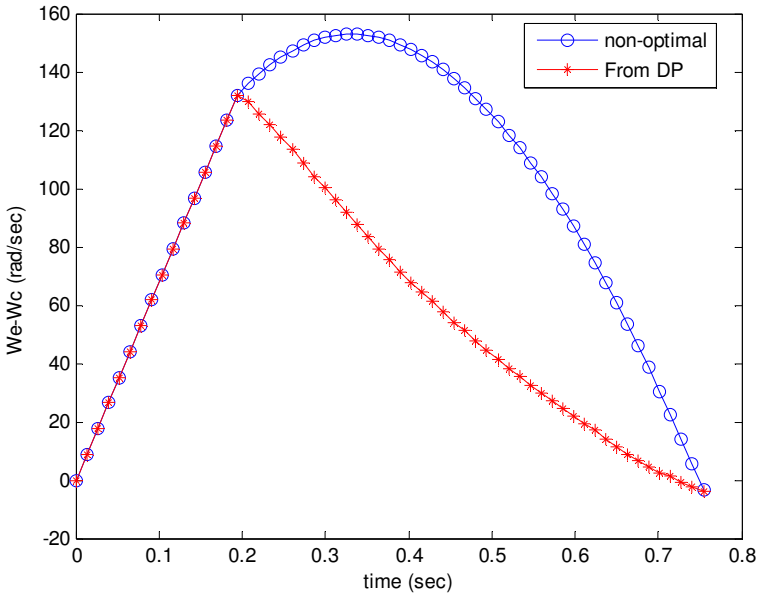

Figure 6.10. Optimal trajectory of $\omega_e - \omega_c$

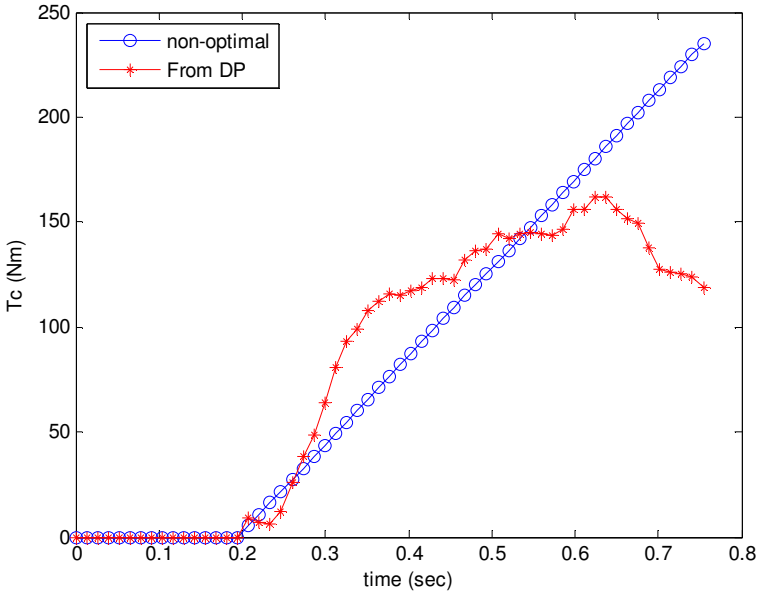

Figure 6.11. Optimal trajectory of T_c

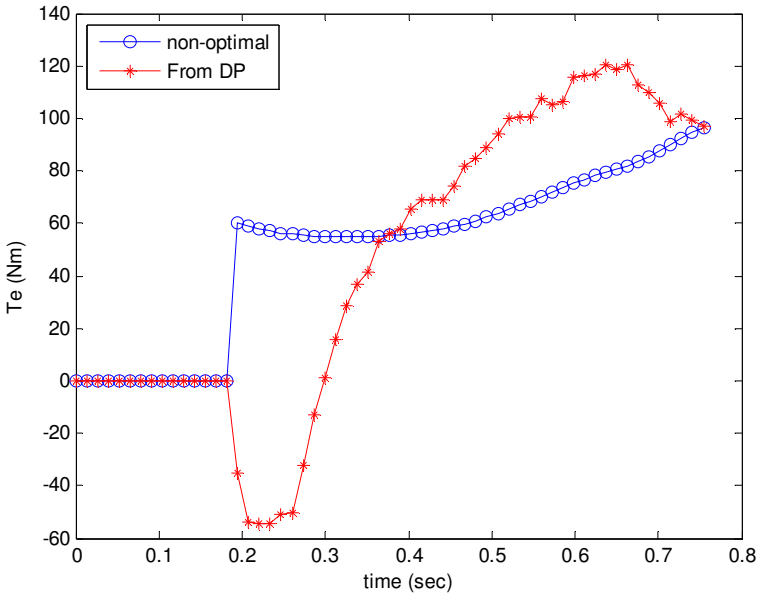

Figure 6.12. Optimal trajectory of T_e

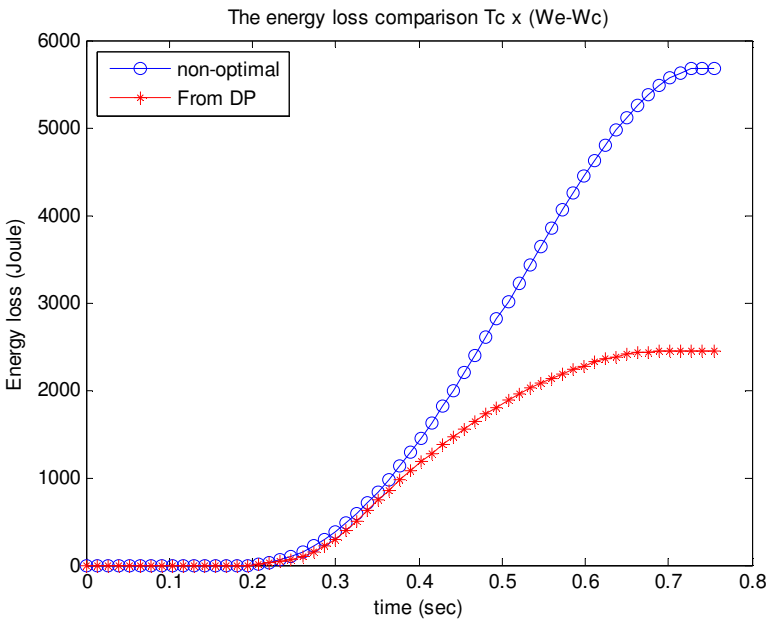

Figure 6.13. Energy loss comparison

6.5. Conclusion

This chapter presents a practical Simulink dynamic model with proper complexity for the AMT system. This AMT model provides adequate performance for AMT control development and validation. This is also a necessity for the rapid prototyping of an AMT controller. The developed AMT dynamic model also includes the driveline model, the engine model, the dry clutch and the hydraulic actuator models. An AMT gearshift control strategy is also developed that includes the gearshift control logic and the clutch control methodology. The developed AMT dynamic model and controller are realized in Simulink. Simulation validation results show that the developed AMT model, along with its controller, provides adequate complexity for control system simulation and development with proper throughput for real-time simulation. In addition, to realize an energy efficient and smooth clutch engagement, the dynamic programming method is used to generate the optimal clutch and engine torque control and it shows an almost 50% energy saving during the clutch engagement.

References In Chapter 6

[1] Sun, Z. and Hebbale, K., "Challenges and opportunities in automotive transmission control", Proceedings of 2005 American Control Conference, Portland, OR, pp. 3284-3289, June 8-10, 2005.

[2] Glielmo, L. Iannelli, L. Vacca, V. and Vasca, F. "Gearshift Control for Automated Manual Transmissions", IEEE/ASME Transactions on Mechatronics, VOL 11, No. 1, Feb., 2006.

[3] F. Garofalo, L. Glielmo, L. Iannelli, and F. Vasca, "Smooth engagement for automotive dry clutch" in Proc. 40th IEEE Conf. Decision and Control, Orlando, FL, 2001, pp. 529-534

[4] F. Amisano, G. Serra, and M. Velardocchia, "Engine control strategy to optimize a shift transient during clutch engagement," SAE Tech. Paper Series, no. 2001-01-0877, pp. 115–120, 2001.

[5] K. Hayashi, Y. Shimizu, S. Nakamura, Y. Dote, A. Takayama, and A. Hirako, "Neuro fuzzy optimal transmission control for automobile with variable loads," in Proc. IEEE Industrial Electronics, Control, and Instrumentation Conf., Maui, HI, 1993, vol. 1, pp. 430–434

[7] L. Glielmo, L. and F. Vasca, "Engagement Control for Automotive Dry Clutch", Proceedings of 2000 American Control Conference, Chicago, Illinois, pp. 1016-1017, June, 2000.

[8] Bellman, R., Dynamic Programming, Princeton University Press, New Jersey, 1957.

[9] Bellman, R. and Dreyfus, S., Applied Dynamic Programming, Princeton University Press, New Jersey, 1962.

[10] Bertsekas, D., Dynamic Programming and Optimal Control, Athena Scientific, 1995.

[11] Song, X., Zulkefli, A., Sun, Z. and Miao, H., "Transmission Clutch Fill Control Using A Customized Dynamic Programming Method". Proceedings of the 2008 ASME Dynamic System and Control Conference, DSC2008-2166, Ann Arbor, Michigan, 2008.

[12] H. Meritt, Hydraulic Control Systems, New York: Wiley, 1967.

[13] Luigi Glielmo , Luigi Iannelli, Vladimiro Vacca, Francesco Vasca, “Speed Control for Automated Manual Transmission with Dry Clutch”, 43rd IEEE Conference on Decision and Control, 1709—1714, Atlantis, Paradise Island, Bahamas, December 14-17, 2004

[14] http://www.adi.com/products_emu_pci.htm, 2009

[15] L. Glielmo and F. Vasca, “Optimal control of dry clutch engagement,” SAE Trans., J. Passenger Cars: Mech. Syst., vol. 6, no. 2000-01-0837, 2000.

[16] J. Slicker and R. N. K. Loh, “Design of robust vehicle launch control system,” IEEE Trans. Contr. Syst. Technol., vol. 4, no. 4, pp. 326–335, Jul. 1996.

[17] A. Bemporad, F. Borrelli, L. Glielmo, and F. Vasca, “Hybrid control of dry clutch engagement,” in Proc. European Control Conf., Porto, Portugal, 2001.

[18] H. Tanaka and H. Wada, “Fuzzy control of clutch engagement for automated manual transmission,” Veh. Syst. Dyn., vol. 24, pp. 365–376, 1995.

[19] Y. Lei, M. Niu, and A. Ge, “A research on starting control strategy of vehicle with AMT,” in Proc. FISITA World Automotive Congress, Seoul, Korea, 2000.

[20] A. Szadkowski and R. B. Morford, “Clutch engagement simulation: Engagement without throttle,” SAE Tech. Paper Series, no. 920766, 1992.

[21] J. Fredriksson and B. Egardt, “Nonlinear control applied to gearshifting in automated manual transmission,” in Proc. 39th IEEE Conf. Decision and Control, Sydney, Australia, 2000, pp. 444–449.

[22] F. Amisano, R. Flora, and M. Velardocchia, “A linear thermal model for an automotive clutch,” SAE Tech. Paper Series, no. 2000-01-0834, 2000.

[23] D. Centea, H. Rahnejat, and M. T. Menday, “The influence of the interface coefficient of friction upon the propensity to judder in automotive clutches,” Proc. Inst. Mech. Eng., vol. 213, pt. D, pp. 245–268, 1999.

[24] E. M. A. Rabeih and D. A. Crolla, “Intelligent control of clutch judder and shunt phenomena in vehicle drivelines,” Int. J. Veh. Des., vol. 17, no. 3, pp. 318–332, 1996

[25] DeLaSalle, S., Jansz, M., and Light, D. (1999), Design of a Feedback Control System for Damping of Vehicle Shuffle. Proceedings of the EAEC Conference, Barcelona, pp 278–284.

[26] Mo, C.Y., Beaumount, A.J., and Powell, N.N. (1996), SAE 960046, Active Control of driveability, pp 215–221.

[27] Baumann, J., Torkzadeh, D.D., Ramstein, A., Kienke, U., and Schelegl, Model-based predictive anti-jerk control T. Control Engineering Practice, 14, 259–266 (2006).

[28] Balfour, G., Dupraz, P., Ramsbottom, M., and Scotson, Diesel fuel injection control for optimum driveability SAE 2000-01-0265.

Chapter 7

The Propulsion System Level Design--Tracking Control of Periodic Signals with Varying Magnitude and Its Application To Hybrid Powertrain

A successful power transmission design should not only be able to operate efficiently and smoothly itself, but more importantly, it should also enable the power source energy efficient operation and reject the potential driveline vibration triggered by the power source. To be specific, the aggressive energy management of the hybrid powertrain and the HCCI combustion introduced previously both require a power transmission mechanism with efficient vibration rejection capability. As indicated in Chapter 1, vibration is one of the most difficult and important issue for propulsion and power transfer. In this thesis, we will propose control framework, which is expected to be effective solution for the energy efficient vibration reduction for a class of propulsion and power transfer system involving rotational motion. This framework will be explained based on the hybrid vehicle power train vibration reduction problem.

7.1. Introduction

The problem of tracking or rejecting signals generated by exogenous systems (exo-system) has been widely investigated and applied by researchers. One of the important research outcome for linear time invariant system is the internal model principle [1-2], which indicates that any feedback controller capable of tracking/ rejecting the specific signal/disturbance must embed a proper copy of the exo-system into the controller design. The problem in nonlinear setting is investigated in [3], and recent research work [4,5,6] explores the theory for linear time varying systems.

Based on the internal model principle, the repetitive controller [7] was proposed mainly for periodic signal tracking/rejection with only the period known. A delay with a positive feedback is embedded as an internal model in the repetitive control design. To enable real-world applications, the zero phase compensation [8] mechanism was

introduced to discrete repetitive control design, which greatly simplified the stabilizer design. With proper modification and robustness design [9], the discrete repetitive control has been widely used in many industrial applications.

However, the traditional repetitive control framework focuses on tracking/rejecting periodic signals without magnitude variation [8]. In fact, there exists a wide class of applications requiring tracking/rejecting varying magnitude periodic signals. The mathematical form of the periodic signals *d(t)* with amplitude variation is:

$$d(t) = f(t) \times p(t)$$

where *p(t)* is a periodic signal with period *T* ($p(t+T) = p(t)$), and *f(t)* is the magnitude variation function. A representative example of these applications is the vibration reduction in hybrid vehicle powertrain system [10].

As has been generally accepted in automotive industry, powertrain hybridization is one of the most promising approaches for reducing automobile fuel consumption and emissions [11]-[16]. The existing hybrid architectures include series hybrid [17]-[18], parallel hybrid [19] and power split hybrid [11]-[16]. The power split hybrid system, as shown in Figure 7.1, allows the engine power to be transmitted through both an electrical path and a mechanical path, and therefore improve the overall system efficiency. As a result of the optimized energy management, the internal combustion engine (ICE) will start or stop more frequently compared with conventional vehicles. During the engine start, however, significant torque pulsations will be generated due to the in-cylinder motoring/pumping pressure. The frequency of the engine torque pulsation is proportional to the engine speed, and the pulsation at low speed range resonates with the driveline dynamics and therefore leads to undesirable driveline vibration [10] as shown in Figure 7. 2. Similarly the engine firing pulse, especially for advanced combustion with a short combustion duration, such as homogenous charge compression ignition (HCCI) [20]-[21], will exhibit large torque pulsations and have the same issue for triggering driveline vibrations. To reduce the vibration, the energy management strategy needs to avoid certain operating conditions at the cost of sacrificing fuel economy. Therefore, it is desirable to remove or compensate the engine torque pulsations and broaden its range of

operation to further improve vehicle fuel efficiency. Conventional approach is to add damping such as a torque converter, which results in energy loss. A promising approach is by controlling the electrical motor (MG2 shown in Figure 7.1) to track or reject the engine torque pulsation [8], as shown in Figure 7.1. Due to the stroke by stroke motion of the internal combustion engine, the engine torque pulsation is naturally dependent on the rotational-angle of the ICE. As shown in Figure 7.2 a), the torque pulsation is periodic with respect to the rotational angle, but becomes aperiodic in the time domain (shown in Figure 7.2 b)) as the engine speed varies. This unique feature suggests treating the problem in the angle domain, in which the period of the torque pulsation becomes invariant and the generating dynamics could be derived by leveraging on the signal periodicity. In this chapter, we propose to apply the internal model based repetitive control framework to reject the pulsation. The merit of using an internal model controller here is its ability to reject different kinds of engine torque oscillation, the exact trajectory of which is unknown in advance. However, due to the cost and accuracy concerns of the sensors, it is desirable to feedback the drive shaft speed oscillation instead of the torque vibration. As will be shown in the later section, the vibration of the drive shaft speed has the same frequency feature as the torque vibration, but its amplitude changes continuously. This unique feature again raises the necessity of looking into the tracking control for the periodic but amplitude varying signal.

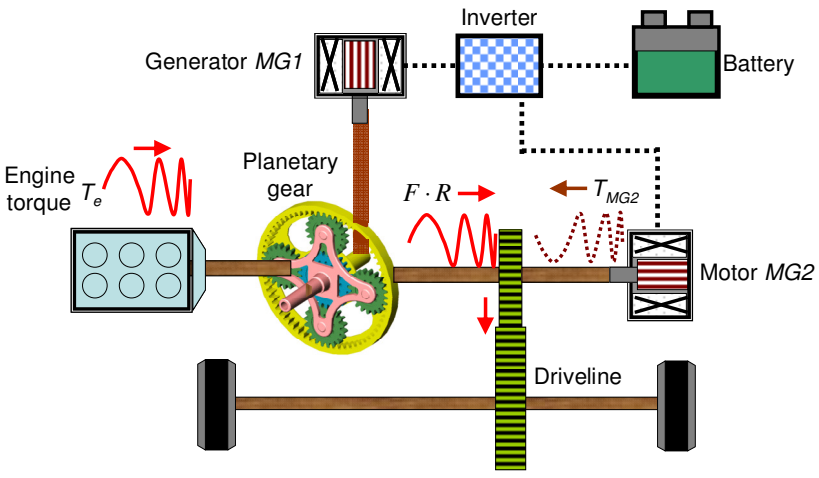

Figure 7.1. Schematic Diagram of Hybrid Powertrain

As will be revealed in the following section, the generating dynamics of the magnitude varying periodic signal could be time varying, instead of being time invariant as those for purely periodic signal. Thus the traditional repetitive control design mechanism, which mainly treats time invariant generating dynamics, will not ensure asymptotic tracking performance. Therefore, a new framework for controlling magnitude varying periodic signals needs to be developed. More interestingly, in the hybrid powertrain problem, the magnitude variation for the velocity oscillation to be rejected is due to the integration of the torque vibration with varying frequency, and thus its generating dynamics needs to be specially derived. Furthermore, as will be shown in this chapter, as the hybrid powertrain vibration problem is treated in the angle domain to gain the signal periodicity, the actuator plant dynamics need to be converted to the angle domain as well, which will result in a time varying (actually angle varying) plant dynamics.

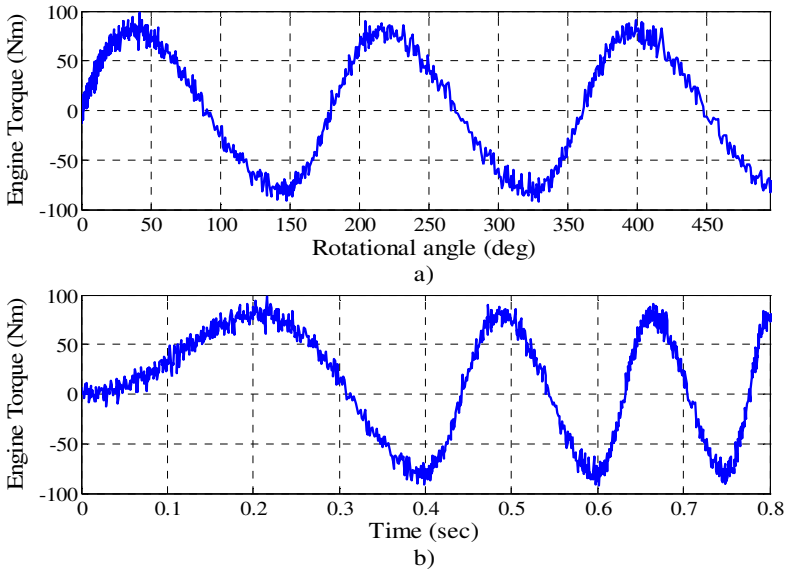

Figure 7.2. Engine Torque Oscillation in Time and Angle Domain

To sum up, the problem defined above is the tracking/rejection control of a magnitude varying periodic signal/disturbance with a time varying plant dynamics. Interestingly, together with the generating dynamics and the control framework presented in this chapter, our recently developed time varying repetitive control design method [4]

provides an effective tool to solve the above defined problem. The rest of this chapter is organized as follows. Section 7.2 analyzes the generating dynamics for periodic signal with amplitude variation. Section 7.3 formulates the hybrid powertrain vibration reduction problem as a amplitude changing periodic disturbance rejection problem. Section 7.4 presents the controller design for the hybrid vehicle vibration reduction. Section 7.5 shows the controller design process and the simulation results. Conclusion is provided in section 7.6.

7.2. Tracking Control of Periodic Signal with Time-Varying Amplitude

In this section, we will analyze the generating dynamics of the periodic signals with amplitude change, where the period T and the magnitude variation are known a priori. It is well known from Fourier series that the periodic signal $p(t)$ with period T can be expressed by infinite combinations of harmonic signals, and therefore the finite order polynomial can not generate such $p(t)$. But in discrete time, by taking advantage of the periodicity [6],

$$p(k) = p(k-N) \tag{7.1}$$

where k is the current discrete time step, $N=T/\Delta t$ is the discrete time period and Δt is the sampling time internal.

The generating dynamics can therefore be written as:

$$\Lambda(z) = 1 - z^{-N} \tag{7.2}$$

with the left-shift operator z, ie. $z[p](k)=p(k+1)$.

Following the similar approach, we can also derive the discrete generating dynamics for the magnitude varying periodic signal $d(t)$.

Theorem 7.1. If the amplitude change of the periodic signal follows a trajectory describing by $f(t)$, where t is the time variable, then the discrete generating dynamics of this signal will be:

$$\Lambda(z) = 1 - z^{-N} \frac{f(k+N)}{f(k)} \tag{7.3}$$

Proof: The periodicity of the signal yields

$$\frac{d(k)}{f(k)} = \frac{d(k)z^{-N}}{f(k-N)} \tag{7.4}$$

then we can have

$$[1 - \frac{f(k)z^{-N}}{f(k-N)}]d(k) = 0 \tag{7.5}$$

which yields

$$[1 - z^{-N} \frac{f(k+N)}{f(k)}]d(k) = 0 \tag{7.6}$$

therefore the generating dynamics will be

$$\Lambda(z) = 1 - z^{-N} \frac{f(k+N)}{f(k)} \tag{7.7}$$ ■

The generating dynamics (7.3) is time varying, as *f(k+N)/f(k)* is not constant. Figure 7.3 shows the commonly used internal model controller structure in repetitive control, where $A^{-1}B$ is the plant model, and the feedback loop formed by PQ^{-1} and $G^{-1}F$ is the internal model controller. In the discrete repetitive control [6] for linear time invariant plant, PQ^{-1} is z^{-N}, and $G^{-1}F$ is 1, thus the feedback internal model controller will be exactly the generating dynamics (7.2). However, in case of the time varying generating dynamics (7.7), directly embedding the generating dynamics (7.7) by assigning $PQ^{-1} = z^{-N} \frac{f(k+N)}{f(k)}$ and $G^{-1}F$ as 1 will not yield asymptotic performance, even if the plant $A^{-1}B$ is linear time invariant. The fundamental reason is due to the time varying PQ^{-1}. This argument can be better explained by the following lemma [4]:

Lemma 7.1 [4]: For the internal model structure in Figure 7.3, the necessary condition for internal model controller to yield asymptotic performance is to satisfy the following condition:

$$(G^{-1}FPQ^{-1}A^{-1}B - A^{-1}BPQ^{-1}G^{-1}F)[u] = 0 \tag{7.8}$$

where *G, F, P, Q* are the internal model controller parameters, and $A^{-1}B$ is the plant dynamics.

Proof: see [4].

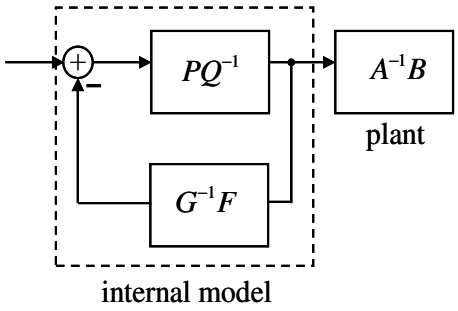

Figure 7.3. Internal Model Controller Construction

Lemma 7.1 indicates that the necessary condition for the internal model controller to yield asymptotic performance is the swapping between the controller and the plant dynamics model. If the generating dynamics is time varying like (7.7), its corresponding internal model controller parameter $G^{-1}FPQ^{-1}$ will be time varying as well. So even if the plant dynamics $A^{-1}B$ is linear time invariant, condition (7.8) can not be met if the internal model controller is obtained by embedding the generating dynamics only. [4] proposes an algorithm to construct the repetitive controller for periodic signal and time varying plant by embedding both the generating dynamics and the plant dynamics. With proper formulation in the following section, this method can also be applied to design the tracking control of magnitude varying periodic signal. In what follows, an example of rejecting amplitude varying periodic signal is introduced, and its repetitive controller is synthesized.

7.3. Application of Amplitude Varying Periodic Signal Repetitive Control On Hybrid Powertrain Vibration Reduction

In this section, the hybrid powertrain dynamics and its vibration caused by engine starting and stopping is analyzed. The vibration signal to reject is shown to be periodic with varying amplitude. The generating dynamics is then derived and the appropriate controller design method will be discussed.

7.3.1 Formulation of the Vibration Rejection Problem

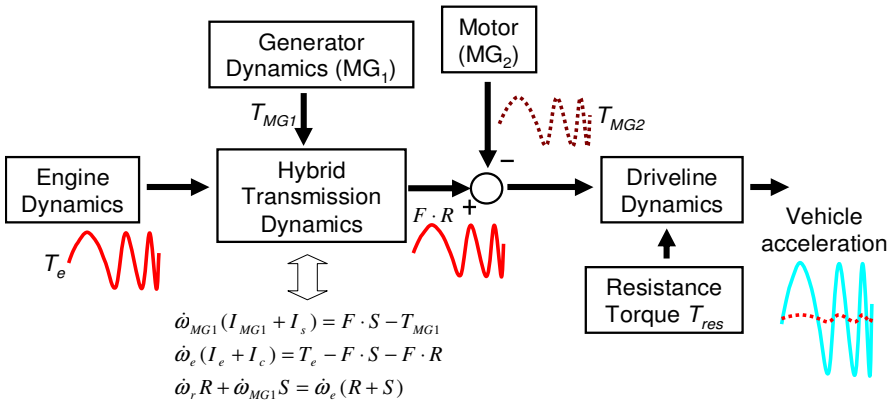

Figure 7.4. Block Diagram of the Hybrid System

Figure 7.4 shows the block diagram of the hybrid powertrain system in Figure 7.1. During the engine start, significant torque pulsations will be generated due to the in-cylinder motoring/pumping pressure. As shown in Figure 7.4, the engine torque T_e and the generator (MG1) torque T_{MG1} are combined through a hybrid transmission planetary gear set, which outputs the torque $F{\cdot}R$. The torque $F{\cdot}R$, together with the motor torque T_{MG2}, is the input to the vehicle driveline. The hybrid powertrain dynamics is shown as the following [11]:

$$\begin{aligned}
&\dot{\omega}_{MG1}(I_{MG1}+I_s) = F\cdot S - T_{MG1}\\
&\dot{\omega}_e(I_e+I_c) = T_e - F\cdot S - F\cdot R\\
&\dot{\omega}_r\left(\frac{R_{tire}^2}{K}m + I_{MG2}K + I_rK\right) = (T_{MG2}+F\cdot R)K - T_{res}
\end{aligned} \tag{7.9}$$

where $\omega_{MG1}, \omega_e, \omega_r$ are the rotational speed of the motor *MG1*, the engine, and the ring gear [13] respectively, and here we assume the ring gear speed ω_r is equal to the drive shaft rotational speed. I_r, I_s and I_c are the inertias of the ring gear, the sun gear and the carrier gear. I_{MG1}, I_{MG2} and I_e are the inertias of the motor *MG1*, motor *MG2* and the

engine respectively. F is the internal force on the pinion gear and m is the vehicle mass. K is the final driven ratio, and T_{res} is driveline and wheel resistance torque.

Equation (7.9) indicates that, the planetary gear set based hybrid transmission adds the flexibility [11] of power management of the engine and generator/motor, but directly transfers the engine torque T_e to the driveline without vibration damping in between [8]. The engine torque pulsation due to the pumping pressure will be directly transferred to the driveline, and will result in driveline vibration [8]. This problem becomes severe at low engine speed. First, the frequency of the engine torque pulsation is proportional to the engine speed, and the low oscillating frequency at low engine speed resonates with the driveline dynamics. Second, the engine motoring during engine starting will generate larger engine torque pulsation than its normal operation, and therefore will cause significant driveline vibration. However, the low speed engine operation is inevitable. In hybrid vehicles, engine starting and stopping should occur frequently to switch power sources and therefore provide better fuel economy. The Toyota Automotive research group [8] unveiled this problem in Toyota Prius hybrid powertrain, and their proposed solution is to control the motor torque in an open loop fashion to compensate the vibration, which is certainly not the most effective way.

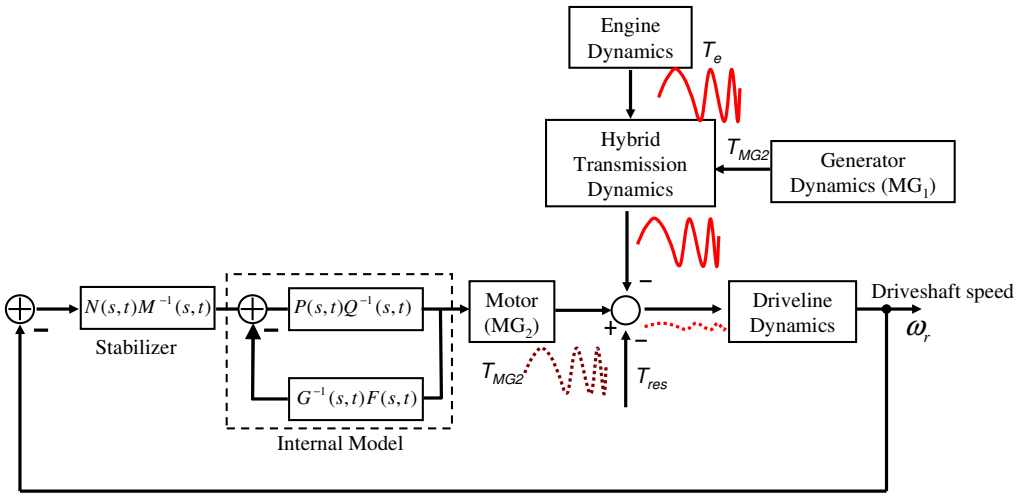

Figure 7.5. Control Block Diagram for vibration reduction

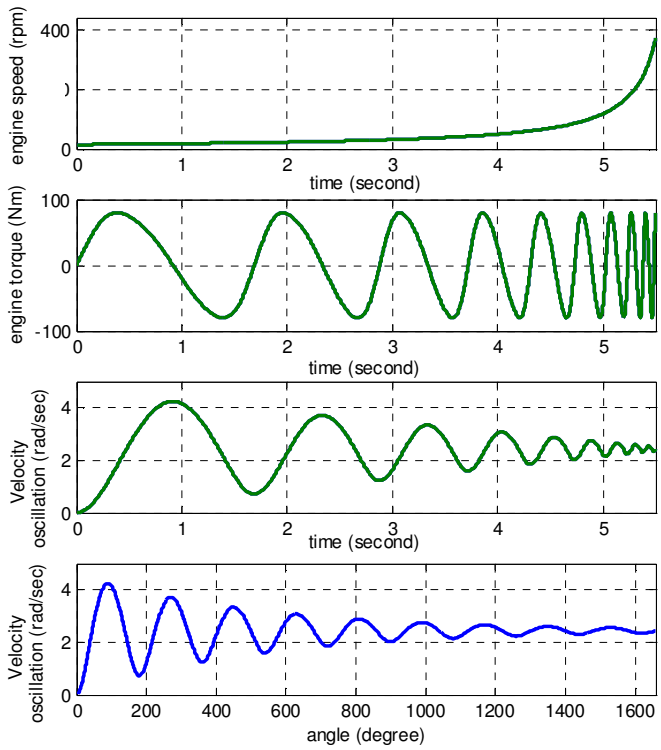

Figure 7.6. Magnitude Varying Periodic Velocity Variation

In this chapter, we propose to reject the disturbance with an internal model controller. Interestingly, due to the stroke by stroke motion of the internal combustion engine, the engine torque pulsation is naturally dependent of the rotational-angle θ of the ICE. As shown in Figure 7.2 a), the torque pulsation is periodic with respect to the engine rotational angle θ, but becomes aperiodic in the time domain (shown in Figure 7.2 b)) as the engine speed varies. While it is generally difficult to derive the generating dynamics for an arbitrary aperiodic signal, this unique feature suggests treating the problem in the angle domain, in which we can take advantage of the periodicity to obtain the generating dynamics. Since in practice the torque oscillation is difficult to measure and note that the torque pulsation results in speed vibration, we use the drive shaft rotational speed as the feedback control variable as shown in Figure 7.5. The speed vibration, which is mathematically the integration of the torque pulsation, is still aperiodic in the time domain. But different from the torque pulsation, it is periodic with varying magnitude in the angle domain. This fact can be better illustrated by Figure 7.6. As the frequency of

the acceleration A becomes higher and higher, the magnitude of the velocity V becomes smaller. The mathematical meaning is that the integration of the signal with varying frequency decreases as the frequency goes up. To construct the internal model controller, we first need to derive its generating dynamics of the velocity oscillation signal.

Theorem 7.2: If $\frac{dV}{dt} = A$, and A is periodic with respect to the rotational angle but aperiodic with respect to time, then the discrete generating dynamics in the angle domain for signal V is

$$\Lambda(z,k) = 1 - z^{-1} - z^{-N}\frac{\omega_e(k)}{\omega_e(k+N)} + z^{-(N+1)}\frac{\omega_e(k+1)}{\omega_e(k+N+1)} \tag{7.10}$$

where N is the period of the discrete periodic signal A in the angle domain.

Proof: Noting that $\frac{dV}{dt} = A$, which implies:

$$\frac{dV(\theta)}{d\theta}\frac{d\theta}{dt} = A, \tag{7.11}$$

where θ is the engine rotational angle. As

$$\frac{d\theta}{dt} = \omega_e(\theta) \tag{7.12}$$

Substitute Eq.(7.12) to equation (7.11) yields

$$\omega_e(\theta)\frac{dV(\theta)}{d\theta} = A \tag{7.13}$$

As A is periodic in the rotational angle domain, $\omega_e(\theta)\frac{dV(\theta)}{d\theta}$ is periodic with respect to θ as well. Therefore,

$$\omega_e(k)\frac{dV(k)}{d\theta} = \omega_e(k-N)\frac{dV(k-N)}{d\theta} \tag{7.14}$$

Replacing the derivative term in Eq.(14) by discrete approximation yields

$$\omega_e(k)\frac{z-1}{\Delta\theta z}V(k) = z^{-N}\omega_e(k)\frac{z-1}{\Delta\theta z}V(k) \tag{7.15}$$

After proper transformation, we can get

$$\omega_e(k)\frac{z-1}{\Delta\theta z}V(k) = z^{-N}\omega_e(k)\frac{z-1}{\Delta\theta z}V(k) \tag{7.16}$$

which yields

$$[1 - z^{-1} - z^{-N}\frac{\omega_e(k)}{\omega_e(k+N)} + z^{-(N+1)}\frac{\omega_e(k+1)}{\omega_e(k+N+1)}]V(k) = 0 \quad \blacksquare$$

Remark: Note that the sampling step k corresponds to each sampling instant of θ, instead of time t. N is the number of sampling times in one period. ω_e is the engine rotational speed. Also note that the generating dynamics depends on the engine rotational speed ω_e. As the speed ω_e is changing with time, the generating dynamics (7.10) is actually time varying (actually angle varying, but in this chapter we do not specifically discriminate these two terminologies). In addition, the order of the generating dynamics is N+1, which is one order higher than the signal sampling rate per period cycle.

7.4. Rotational Angle Based Control

As generating dynamics of the vibration signal is derived in the angle domain, the actuator dynamics needs to be converted to the angle domain as well. In this section, we will show the construction of the actuator dynamics in the angle domain.

7.4.1 Plant Dynamics Model

As analyzed in section 7.3, the drive shaft rotational velocity is fed back to form the feedback loop as shown in Figure 7.5.

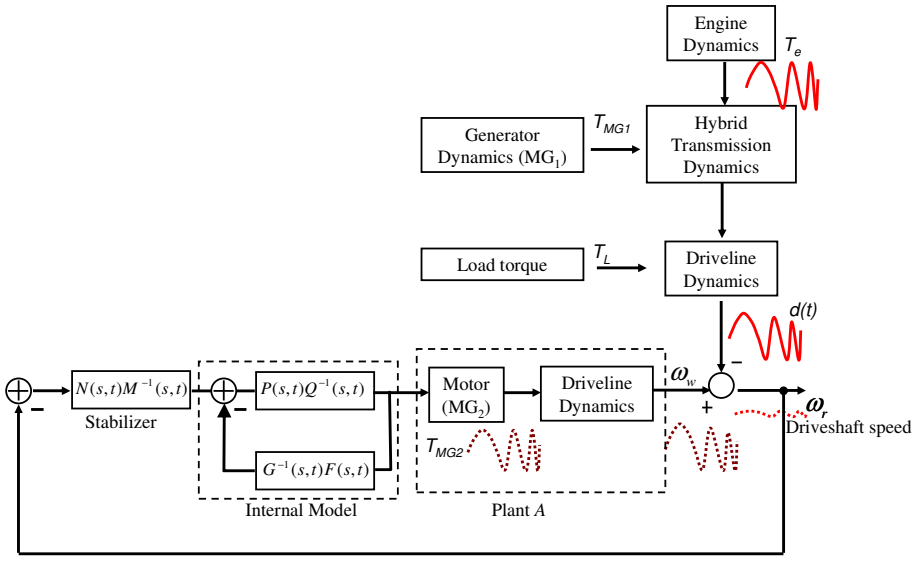

Figure 7.7. Transformed Control Block Diagram for vibration reduction

To aid the controller synthesis, the block diagram in Figure 7.5 can be transformed into that in Figure 7.7. From Figure 7.7, we can clearly see that the disturbance to be rejected is the driveline velocity vibration signal *d(t)*, and the plant dynamics (plant *A*) is the motor dynamics together with the driveline dynamics. The control objective is to generate the corresponding motor torque so that the output ω_w of the plant *A* (Figure 7.7) can compensate the disturbance speed *d(t)*, and therefore the drive shaft rotational speed ω_r is free of vibration. The motor for vibration reduction in this chapter is selected to be a DC motor, and the plant *A* dynamics (motor together with the driveline dynamics) can be modeled as:

$$
\begin{aligned}
\dot{i} &= -\frac{R}{L} i - \frac{K_b}{L} \omega_m + \frac{1}{L} u \\
\dot{\omega}_m &= \frac{K_m}{J} i - \frac{K_f}{J} \omega_m - \frac{1}{KJ}\left[k_{tw} \Delta\theta_{cw} + \beta_{tw} \left(\frac{\omega_m}{K} - \omega_w \right) \right] \\
J_w \dot{\omega}_w &= k_{tw} \Delta\theta_{cw} + \beta_{tw} \left(\frac{\omega_m}{K} - \omega_w \right) - \eta \omega_w \\
\Delta\dot{\theta}_{cw} &= \frac{\omega_m}{K} - \omega_w
\end{aligned}
\tag{7.17}
$$

where u is the control input voltage, i is the motor current, K_b, K_m, R and L are the motor dynamic constant, ω_m is the motor rotational speed, ω_w is speed output from the plant *A* as shown in Figure 7.7, $J = I_{MG2} + I_r$ as defined in (9), J_w is the vehicle driveline inertia,

θ_{cw} is the driveshaft torsional angle, k_{tw} is elastic stiffness coefficient, β_{tw} is friction coefficients, and η is the driveline damping coefficient. Here we assume the total driveline resistance torque T_{res} is a combination of the load torque T_L and the damping torque $\eta\omega_w$. The load torque T_L is assumed constant during the engine start/stop period due to the short engine start/stop duration. The model can be further reduced by assuming the rigidity of the driveline shaft and thus $\omega_m = \omega_w$. Therefore the dynamics model becomes:

$$\begin{aligned} \dot{i} &= -\frac{R}{L}i - \frac{K_b}{L}\omega_w + \frac{1}{L}u \\ \dot{\omega}_w &= \frac{1}{(KJ + J_w)} \times (KK_m i - KK_f \omega_w - \eta\omega_w) \end{aligned} \tag{7.18}$$

Which can be translated into the state space form as :

$$\begin{aligned} \dot{x}(t) &= \bar{A}x(t) + \bar{B}u(t) \\ y(t) &= \bar{C}x(t) \\ e(t) &= \bar{C}x(t) + d(t) \end{aligned} \tag{7.19}$$

where

$$\bar{A} = \begin{bmatrix} -\frac{R}{L} & -\frac{K_b}{L} \\ \frac{KK_m}{(KJ + J_w)} & -\frac{KK_f + \eta}{(KJ + J_w)} \end{bmatrix},\ \bar{B} = \begin{bmatrix} \frac{1}{L} \\ 0 \end{bmatrix},\ \bar{C} = \begin{bmatrix} 0 \\ 1 \end{bmatrix},\ x = \begin{bmatrix} i \\ \omega_w \end{bmatrix},$$

where $d(t)$ is the disturbance to be rejected, whose generating dynamics in the angle domain is Eq (7.10) .

7.4.2 Conversion of the Plant Model to Angle Domain

As the problem is to be investigated in the angle domain, and also because the generating dynamics (7.10) is derived in angle domain, the plant model (7.19) should also be converted into the rotational angle domain [4] as:

$$\begin{aligned}
\frac{d\bar{x}(\theta)}{d\theta} &= \frac{1}{\bar{\omega}_e(\theta)}\bar{A}\bar{x}(\theta) + \bar{B}\frac{1}{\bar{\omega}_e(\theta)}\bar{u}(\theta) \\
\bar{y}(\theta) &= C\bar{x}(\theta) \\
\bar{e}(\theta) &= C\bar{x}(\theta) + \bar{d}(\theta)
\end{aligned} \tag{7.20}$$

Note that d is periodic with respect to the engine rotational angle $\theta(t)$ and $\theta(t)$ is defined as $\theta(t) = \int_{t_0}^{t} \omega_e(\tau)d\tau$. Clearly the model (7.20) is linear angle varying. In this chapter we still call system (7.20) linear time varying system as the system remains same if the operator θ is replaced by operator t. It can be verified that system (7.20) is uniformly controllable and observable [4]. For implementation, it is sampled at evenly discrete angle intervals $\theta(k)$, $\theta(k+1)$,…, and the rotational domain discrete system model can be formed as [4]:

$$\begin{aligned}
x(k+1) &= F(k)x(k) + G(k)u(k) \\
e(k) &= H(k)x(k) + d(k)
\end{aligned} \tag{7.21}$$

where k+1 denotes the sampling angle instant $\theta(k+1)$, and $F(k) = e^{\bar{A}T}(k)$ with $G(k) = (e^{\bar{A}T}(k) - I)\bar{A}^{-1}\bar{B}$, when matrix $\bar{A}$ is non-singular.

7.4.3 Internal Model Controller Design

In order to apply our recently developed controller design [4] via I/O representation, we need to transform the state space model (7.21) to polynomial fraction representation [20]. To do so, we briefly introduce the definitions on polynomial differential operator (*PDO*) (see [20]).

Definition 7.1: Denote the one step delay operator z^{-1}. The left polynomial differential operator (*PDO*) of degree n, $P(z, k)$, is defined as:

$$P(z,k) = a_n(k)z^{-n} + \cdots + a_1(k)z^{-1} + a_0(k) \tag{7.22}$$

where $a_i(k)$ are bounded and nonzero functions of k for k>0. If $a_0(k)$=1 for all k, then the above left *PDO* is termed as *monic*.

The Input/Output (I/O) representation of the discrete state space mode (7.21) can then be derived following the method in [4] as:

$$y(k) = A(z,k)^{-1} B(z,k)u(k) + d(k) \tag{7.23}$$

Where *A(z,k)* and *B(z,k)* are two *PDO*s defined as (7.22).

We recall our recently developed results [4] for the time varying tracking control design:

Proposition 1: [4] Consider plant model (7.21) and exogenous signal model (7.10). The controller structure is shown in Figure 7.7. Design *G(z,k)=A(z,k)*, and *F(z,k)=B(z,k)*. If *PDO P(z,k)*, *Q(z,k)*, *N(z,k)* and *M(z,k)* satisfy the following conditions:

$$A(z,k)Q(z,k) + B(z,k)P(z,k) = \Lambda(z,k)Q(z,k) \tag{7.24}$$

$$\Lambda(z,k)Q(z,k)\bar{M}(z,k) + B(z,k)P(z,k)\bar{N}(z,k) = A_s(z,k) \tag{7.25}$$

where $A_s(z,k)$ is exponentially stable *PDO*, and

$$\bar{M}(z,k) = Q^{-1}(z,k)M(z,k)$$

$$\bar{N}(z,k) = Q^{-1}(z,k)N(z,k)$$

Then the asymptotic performance is achieved, i.e., $\lim_{k\to\infty} \omega_w(k) = 0$.

Note that *M(z,k)* and *N(z,k)* are the stabilizing controllers shown in Figure 7.7. For more information about the controller design theory, please refer to [4].

TABLE 7. 1. PARAMETER VALUES OF THE DYNAMIC MODEL

R	2 ohms	J	32.9 kg.m^2
L	0.05 henrys	J_w	133 kg.m^2
K_m	150 Nm/amp	β_{tw}	295 Nm
k_{tw}	6200 Nm/rad	K_b	50 V/(rad/s)
K_f	0.5 Nm/(rad/s)	R_a	0.065 m
η	49.5 Nm/(rad/s)	K	3.9

7.5. Simulation Results

In this section, we present the simulation results of applying the angle based time-varying repetitive control together with the generating dynamics (7.10) to compensate for the engine torque pulsation in the hybrid powertrain. The idea is to control the motor in the hybrid powertrain to generate the appropriate torque to counteract the engine torque pulsation so that driveline vibration can be suppressed. Heavy duty DC motor parameters have been selected for the dynamics model for preliminary investigation as shown in Table 1.

Due to the stroke by stroke motion, the pulsation disturbance *d* is periodic in the angle domain. To precisely represent *d*, we use 23 samples for sampling rate per period cycle, and therefore the generating polynomial (7.10) for the disturbance *d* is given by

$$\Lambda(z,k) = 1 - z^{-1} - z^{-23}\frac{\omega_e(k)}{\omega_e(k+23)} + z^{-24}\frac{\omega_e(k+1)}{\omega_e(k+24)} \tag{7.26}$$

Now, given the plant dynamics model (7.23) and the generating dynamics model $\Lambda(z,k)$ (7.26), The controller design follows two steps [4].

Step1: Solve *P(z,k)* and *Q(z,k)* to satisfy condition (7.24).

Setp 2: Solve $\bar{M}(z,k)$ and $\bar{N}(z,k)$ to meet condition (7.25).

The internal model controller in Figure 7.7 can therefore be constructed. The high order generating polynomial (7.26) inevitably enforces the high order internal model and stabilizing controller. The order of $P(z,k)Q^{-1}(z,k)$ in the internal model unit is 23 and the order of the stabilizer $N(z,k)M^{-1}(z,k)$ is 24. The high order controller is then simulated in Matlab/Simulink.

Finally, Figure 7.8 and Figure 7.9 show the simulation results. Here the control target is to control the system to track the driveshaft speed oscillation. Then the difference between the tracking result and the speed oscillation will be the output of the disturbance rejection. Thus the better the tracking result, the smaller the oscillation will be. Two controller design methods are compared. The first one is designed using the traditional repetitive control internal model generating dynamics (Eq 7.10), and the

second controller is designed based on our approach proposed in this chapter. Figure 7.8 shows the tracking result for a smooth engine start (the engine speed increases slowly). Figure 7.8(b) and Figure 7.8(c) compares the tracking result of magnitude varying periodic disturbance signal (the drive shaft speed oscillation), using the traditional repetitive control generating dynamics Eq (7.2) and that using Eq (7.10) derived in this chapter respectively. The traditional approach does not guarantee asymptotic performance, but the tracking error is not evident here. This is because the magnitude change of the oscillation velocity is related to the variation rate of the engine speed. As a slowly varying engine speed ω_e (Figure 7.8(a)) results in slow magnitude change of the driveshaft oscillation speed, the loss of tracking using the traditional repetitive control approach is not apparent. However, Figure 7.9 shows the tracking result for a steep engine start. Figure 7.9(b) clearly shows a significant tracking error using the traditional repetitive control internal model generating dynamics, while the tracking result in Figure 7.9 (c) clearly exhibits the asymptotic tracking performance using our proposed controller with the generating dynamics [10].

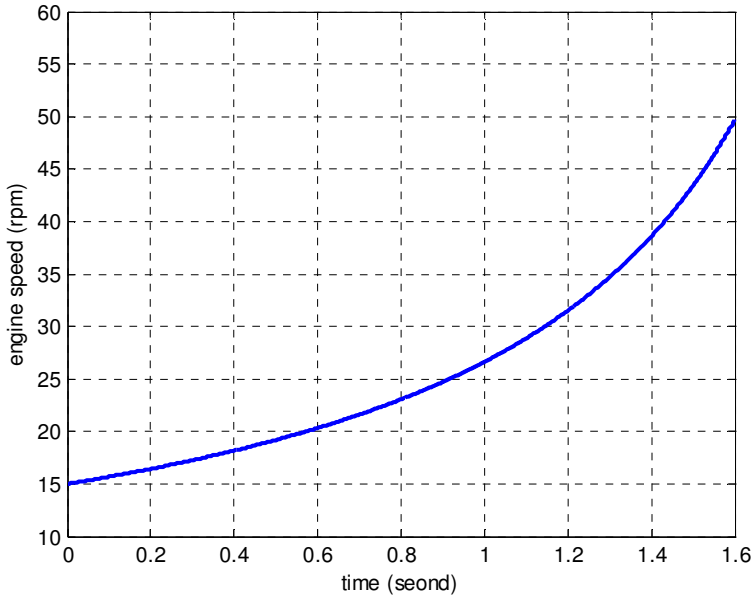

Figure 7.8(a). Engine Speed Profile

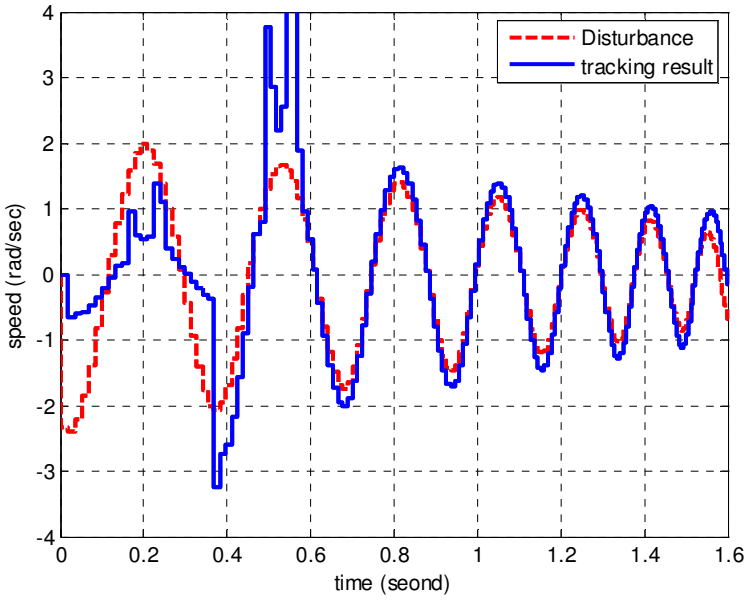

Figure 7.8(b). Tracking Result Using the Generating Dynamics From Traditional Repetitive Control

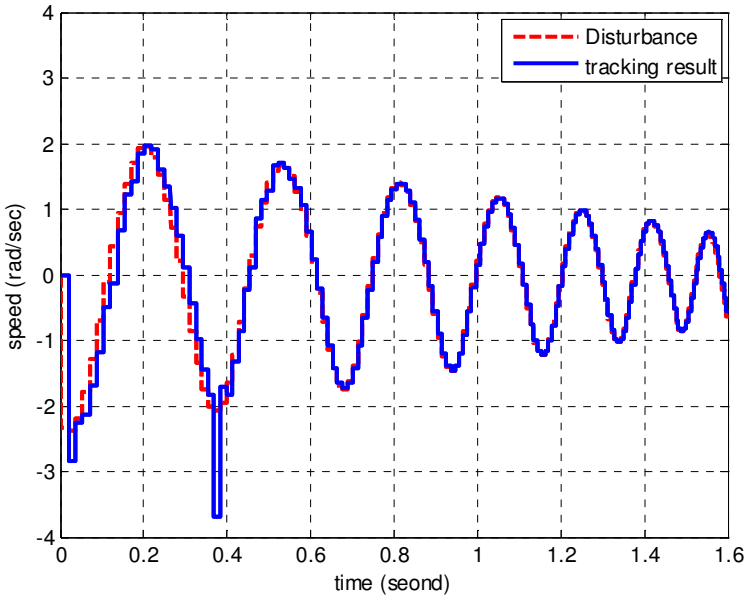

Figure 7.8(c). Tracking Result Using the Developed Generating Dynamics

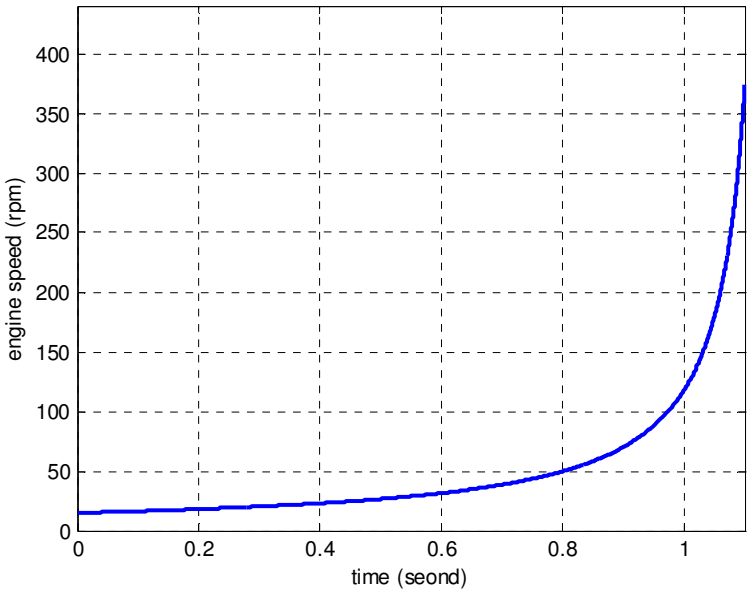

Figure 7.9 (a). Steep Engine Speed Profile

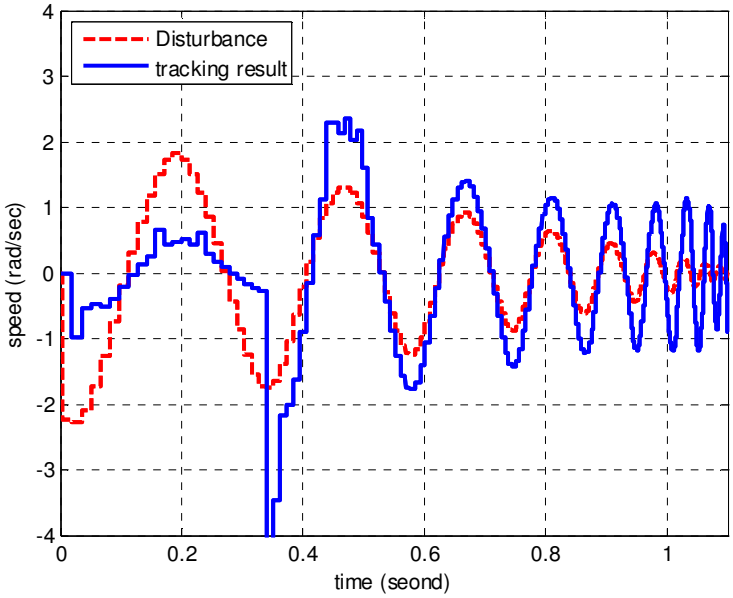

Figure 7.9(b). Tracking Result Using the Generating Dynamics From Traditional Repetitive Control

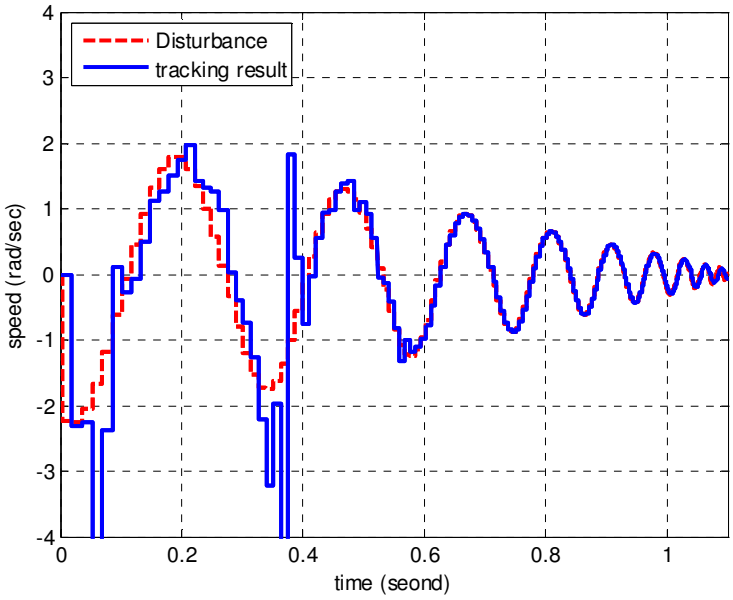

Figure 7.9(c). Tracking Results Using the Developed Generating Dynamics

7.6. Conclusion

This chapter presents the tracking or rejection of periodic signals with varying peak to peak magnitude. The generating dynamics for this kind of signals are first derived. Moreover, this chapter reveals that the traditional repetitive control framework will no longer ensure asymptotic performance with time varying generating dynamics, and a recently developed time varying repetitive control framework could be used for the controller design. In addition, as an example of applying the tracking control of this unique signal, the hybrid vehicle powertrain vibration reduction problem is introduced. The generating dynamics of the vibration disturbance is derived and a rotational angle based time varying repetitive control design framework is applied. Simulation results show that the proposed control method is a promising solution. Future work will be the robustness investigation of the proposed controller, and its experimental implementation.

References In Chapter 7

[1] B.A. Francis. The internal model principle of control theory. SIAM Journal of Control, vol. 15 (3), pp. 486-505, 1977.

[2] B.A. Fancis, and W.M. Wonham. The internal model principle of control theory. Automatica, vol. 12 (5), pp. 457-465, 1976.

[3] A. Isidori, C.I. Byrnes, Output regulation of nonlinear systems, IEEE Transactions on Automatic Control 35 (2) (1990), 131-140

[4] Z. Sun, Z. Zhang, and T.-C. Tsao. Trajectory tracking and disturbance rejection of linear time-varying systems: input/output representation. Systems and Control Letters, vol. 58 (6): 452-460, 2009.

[5] S. Hara, Y. Yamamoto, T. Omata, and M. Nakano. Repetitive control systems: a new type servo system for periodic exogenous signals. IEEE Transactions on Automatic Control, 33(7):659-668, 1988.

[6] M. Tomizuka, T.-C. Tsao, and K.-K. Chew. Analysis and synthesis of discrete-time repetitive controllers. ASME Transactions on Journal of Dynamic Systems, Measurement and Control, 111: 353-358, 1989.

[7] T.-C. Tsao and M. Tomizuka. Robust adaptive and repetitive digital tracking control and application to hydraulic servo for noncircular machining. ASME Transactions on Journal of Dynamic Systems, Measurement and Control, 116 (1):24-32, 1994.

[8] S. Tomura, Y. Ito, K. Kamichi, and A. Yamanaka. Development of vibration reduction motor control for series-parallel hybrid system. In SAE Technical Paper Series 2006-01-1125, 2006.

[9] J. Meisel. An Analytical Foundation for the Toyota Prius THS-II Powertrain with a Comparison to a Strong Parallel Hybrid-Electric Powertrain. SAE technical paper 2006-01-0666.

[10] T. Grewe, B. Conlon, and A. Holmes .Defining the General Motors 2-Mode Hybrid Transmission. SAE technical paper 2007-01-0273.

[11] J. Liu, and H. Peng. Modeling and control of a power-split hybrid vehicle. IEEE Transactions on Control Systems Technology, vol. 16 (6) pp. 1242-1251, 2008.

[12] P. Pisu, G. Rizzoni G. A comparative study of supervisory control strategies for hybrid electric vehicles. IEEE Transactions on Control Systems Technology, Vol. 15, no. 3, pp. 506-518, 2007.

[13] M. Ducusin, S. Gargies, and C. Mi. Modeling of a series hybrid electric high-mobility multipurpose wheeled vehicle. IEEE Transactions on Vehicular Technology, Vol. 56, no. 2, pp. 557-565, 2007.

[14] Y. J. Kim, Z. Filipi. Series hydraulic hybrid propulsion for a light truck - optimizing the thermostatic power management. SAE paper 2007-24-0080, 2008 SAE Transactions, Journal of Engines.

[15] T. Goro, et al. Development of the hybrid system for the Saturn VUE hybrid. SAE technical paper 2006-01-1502.

[16] S. Kim, J. Park, J. Hong, M. Lee and H. Sim. Transient control strategy of hybrid electric vehicle during mode change. In SAE Technical Paper Series 2009-01-0228, 2009

[17] M. Levin, et. al. Hybrid powertrain with an engine-disconnection clutch. In SAE Technical Paper Series 2002-01-0930, 2002.

[18] T. Kuo. Valve and fueling strategy for operating a controlled auto-ignition combustion engine. In SAE 2006 Homogeneous Charge Compression Ignition Symposium, pp. 11-24, San Ramon, CA, 2006.

[19] T. Kuo, Z. Sun, J. Eng, B. Brown, P. Najt, J. Kang, C. Chang, and M. Chang. Method of HCCI and SI combustion control for a direct injection internal combustion engine. U.S. patent 7,275,514, 2007.

[20] K.S. Tsakalis, P.A. Ioanou, Linear Time-Varying Systems: Control and Adaptation, in: Advances in Industrial Control, Prentice Hall, Englewood Cliffs, NJ, 1993

[21] A.Ichikawa, H.Katayama, Output regulation of time-varying systems, IEEE Transactions on Automatic Control 35 (2) (1990) 131-140

[22] Z. Zhang, A. Serrani, The linear periodic output regulation problem, Systems & Control Letters 55(7) (200) 518-529

Chapter 8

The Propulsion System Level Design—Robust Stabilizer Design for Linear Parameter Varying (LPV) Internal Model Control System

8.1 Introduction

The hybrid vehicle engine start/stop torque oscillation rejection problem is introduced in the previous chapter. The engine output torque is aperiodic in the time domain, but is periodic with respect to the engine rotational angle. Similarly, the induced driveline speed oscillation is periodic with magnitude variation in the angle domain. To take advantage of these unique characteristics with respect to angular displacement, we convert the plant model into the rotational-angle domain. The converted plant dynamics model is shown as follows: (refer to Chapter 7 for detail)

$$\begin{aligned} \frac{dx(\theta)}{d\theta} &= \frac{1}{\omega_e(\theta)}\bar{A}x(\theta) + \bar{B}\frac{1}{\omega_e(\theta)}u(\theta) \\ y(\theta) &= \bar{C}x(\theta) \\ e(\theta) &= \bar{C}x(\theta) + d(\theta) \end{aligned} \tag{8.1}$$

Here ω_e is the engine rotational speed, and $\bar{A}$, $\bar{B}$, $\bar{C}$ are the original *LTI* plant dynamics matrices. d is the output disturbance signal, which should be rejected so that the error e will converge to zero. As a result, the original time domain *LTI* plant model becomes Linear Parameter Varying (*LPV*) with respect to the engine speed ω_e in the angle domain. Therefore the problem considered is to reject a disturbance signal for linear parameter varying (*LPV*) system. In this chapter, we will treat the LPV system tracking/rejection problem in a general form, which can potentially be applied to other applications beyond the automotive field as well.

As an important topic in control theory, tracking/rejecting a class of reference/disturbance signals, which are generated by an exogenous system (exo-system), has been widely studied in the past several decades. The resulted controller can enable a

wide class of applications where the reference/disturbance signal may not be measurable but their generating dynamics are known. A well known principle to solve these kind of problems is the internal model principle (refer the explanation in *LTI*[1-2], *LTV* [5-7], and nonlinear [4] settings respectively), which expresses the fact that a suitable copy (internal model) of the exogenous signal model to generate the required input *u* must be embedded in the *LTI* [8-10] feedback control loop in order to solve the tracking/rejecting problem. For *LTI* systems, an internal model can be designed solely based on the generating dynamics of the exogenous signal.

However, the internal model controller design for parameter varying system is not as well studied as that for linear time invariant case. The major difficulty is that directly embedding the disturbance generating dynamics will no longer guarantee asymptotic performance for linear parameter varying system [5]. To achieve asymptotic performance, we need to study the reference tracking or disturbance rejection problem in the *LTV* setting. This extension is not trivial, as the internal model-based design in *LTV* settings is still an open area of investigation, and the design method of constructing time-varying internal model units to achieve asymptotic performance is limited.

Recently [5] proposes a new design methodology for the construction of a time-varying internal model, which enables the internal model-based control for *LTV* systems. Specifically, the SISO *LTV* plant subject to exogenous signals in the state space form as Eq (8.1) can be converted into the I/O representation [5] as

$$y = A^{-1}(s,t)B(s,t)[u] + d \tag{8.2}$$

where y is the tracking error, u is the control input and d is the exogenous signal, and $B(s,t)$ is a polynomial differential operator [3] (which is different from the state matrix $\overline{B}$ in Eq (8.1), and $A^{-1}(s,t)$ is an inverse operator of a polynomial [3] differential operator $A(s,t)$. The disturbance signal *d(t)*, to be tracked or rejected, satisfies the following generating polynomial:

$$\Lambda(s,t)[d] = 0$$

where $\Lambda(s,t)$ is the time varying generating dynamics describing the disturbance signal d.

As shown in Figure 8.1 [5], the internal model consists of two time-varying subsystems connected in a feedback fashion. Specifically, controllers $P(s,t)Q^{-1}(s,t)$ and $G^{-1}(s,t)F(s,t)$ are responsible for constructing the time-varying internal model, while controller $N(s,t)M^{-1}(s,t)$ is the stabilizer unit. The idea behind this design is that a self-excitation mechanism has to be embedded in the feedback loop so that it drives the plant to compensate the persistent and bounded signal *d(t)* when output error *e(t)* converges to zero. In specific, the proposed design includes the following two ingredients:

Step 1: When the input u_{st} to the internal model is zero (the stabilizer is inactive), the signal $-d$ is generated in the feedback loop (that is, u_d=-d).

Step 2: Embedding a copy of the plant model and combining the result of Step 1, it enforces that the output of the internal model u is indeed the desired input to keep *e(t)* identically at zero.

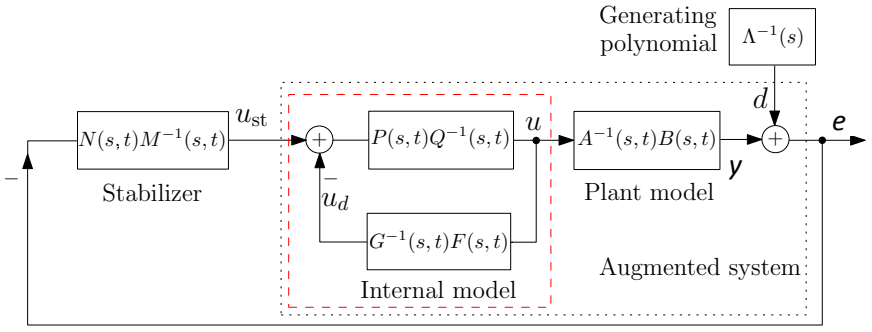

Figure 8.1. Block diagram of the feedback controller from [5].

Once an appropriate internal model unit is designed, the tracking/disturbance rejection problem is then converted to a stabilization problem, which basically requires a stabilizer design to stabilize the augmented system including the internal model and the plant dynamics. Few stabilizer synthesis methods for the time varying internal model control system are available. Ref [5, 37] introduces the design approach using the time varying pole-placement technique. However, as the pole-placement stabilizer is very sensitive to model uncertainties especially in the time varying setting, it's hard to realize

the time varying internal model controller in the experiment. That's why limited experimental results have ever been reported yet. Therefore, a robust stabilizer design for the time varying internal model based control is crucial, but currently is still unavailable. This is because the internal model based control [5, 37] usually contains high order dynamics to embed the generating dynamics of a wide class of signals, and the key challenge is how to stabilize the high order internal model system with a low order stabilizer in a robust fashion.

To address this problem, in this thesis, a low order and computationally efficient robust stabilizer is proposed. The low order yet robust control synthesis is enabled by the unique characteristic of the internal model system stabilization problem. The controller is then applied for a hydraulic dynamometer system and tested for pressure tracking. Finally the experimental studies will be presented to demonstrate its effectiveness.

8.2 Existing Linear Parameter Varying System Control Design Methods

The augmented system including the original plant and the internal model in Figure 8.1 is essentially a Linear Parameter Varying system (*LPV*) (refer to Chapter 7 for detail). We can assume the varying parameter ω_e can be measured in real time. For a general *LPV* dynamical system, the robust control techniques have been studied extensively in the past two decades [11-43], and the fundamental approach is to obtain the controller by solving a series of finite Linear Matrix Inequalities (*LMI*s) [12] optimization. However, directly applying the general robust *LPV* techniques to the internal model stabilizer design will result in a very high order stabilizer, which is not only computationally intensive for off-line synthesis but also induce high on-line computational cost. In what follows a literature on *LPV* control techniques will be surveyed, the challenges of applying it to the internal model problem will be further revealed, and finally approaches to address these challenges will be proposed.

The *LPV* system notion is first introduced in [11]. The preliminary approach to study *LPV* system gain scheduling resorts to the design of a sequence of linear time invariant controllers and then interpolate among them. But this approach cannot guarantee stability performance except for slowly varying parameters. Then more

systematical approaches based on linear Lyapunov function with fixed Lyapunov matrix were proposed later [22-24]. The Lyapunov stability condition can then be transformed into the so called linear matrix inequality (*LMI*) conditions using Schur complements [12], such that the *LPV* controller can be designed by solving a set of *LMI* convex optimization problems. This control synthesis method is applicable if the parameter can be measured in real time, and could be formulated to characterize robust stability and performance. However, according to [25], the approach in [12] is very conservative because it allows arbitrary rate of variation of the parameters. Ref [25] therefore proposes a method based on parameter dependent Lyapunov function, which allows the incorporation of the rate of parameter variation and therefore offers less conservative control design. In addition, different variations [28-32] of *LPV* control approaches addressing specific problems have been proposed since then as well.

Here a representative robust *LPV* control synthesis method proposed in [34] is described as follows:

Consider the *LPV* plant governed by

$$\begin{aligned} \dot{x} &= A(\omega_e)x + B_1(\omega_e)d + B_2(\omega_e)u \\ e &= C_1(\omega_e)x + D_{11}(\omega_e)d + D_{12}(\omega_e)u \\ y &= C_2(\omega_e)x + D_{21}(\omega_e)d \end{aligned} \tag{8.3}$$

where d is the disturbance, e is the control error. There exists a gain-scheduled output-feedback controller enforcing internal stability and a bound γ on the L_2 gain of the closed loop system, whenever there exist parameter-dependent symmetric matrices $Y(\omega_e)$ and $X(\omega_e)$ [34] such that for all the parameter ω_e within its bounded range the following infinite-dimensional *LMI* problem holds:

$$\begin{bmatrix} N_X & 0 \\ 0 & I \end{bmatrix}^T \begin{bmatrix} \dot{X} + XA + A^T X & XB_1 & C_1^T \\ B_1^T X & -\gamma I & D_{11}^T \\ C_1 & D_{11} & -\gamma I \end{bmatrix} \begin{bmatrix} N_X & 0 \\ 0 & I \end{bmatrix} < 0 \tag{8.4}$$

$$\begin{bmatrix} N_Y & 0 \\ 0 & I \end{bmatrix}^T \begin{bmatrix} \dot{Y} + YA^T + AY & YC_1^T & B_1 \\ C_1 Y & -\gamma I & D_{11} \\ B_1^T & D_{11}^T & -\gamma I \end{bmatrix} \begin{bmatrix} N_Y & 0 \\ 0 & I \end{bmatrix} < 0 \tag{8.5}$$

$$\begin{bmatrix} X & I \\ I & Y \end{bmatrix} > 0 \tag{8.6}$$

where N_X and N_Y designate any bases of the null spaces of $[C_2 \; D_{21}]$ and $[\, B_1^T \; D_{12}^T]$, respectively. Then the robust *LPV* stabilizer can be formed based on *X*, *Y* and the original plant state matrices. For computer design purpose, one needs to transfer the infinite dimensional *LMI*s in the parameter space into finite *LMI*s. The commonly used method is introduced in [12]. First the parameter space is discretized, and then a series of *LMI*s can be formed for each discrete parameter. The corresponding local controller can therefore be calculated based on each *LMI*, and the final *LPV* controller can be obtained from the interpolation of these discrete controllers

Although ensuring strong robust stability, the above method is very computational intensive. The stabilizer order needs to be the same as the order of the system dynamics to be stabilized. In the case of the time varying internal model control, the system to be stabilized is the augmented system, which includes the plant and the internal model dynamics. As the parameter varying internal model designed in Figure 8.1 is usually high order due to the embedded generating dynamics of a wide class of signals, the stabilizer design using the traditional *LPV* control framework will result in a very high order stabilizer, which is not only undesirable for on-line implementation but is also computational intensive for off-line controller solver. Although methods [37-40] to reduce the controller order for a general *LPV* system have been proposed, the orders reduced are limited and the methods cannot guarantee a feasible solution due to the non-convex formulation. In addition, the output together with partial state feedback introduced in [41] cannot be applied to the internal model control synthesis either as the state feedback will not be zero even when the tracking error converges to zero. To address this high order stabilizer issue for *LPV* internal model control, as a key contribution in this chapter, a unique parameter dependent gain based *LPV* stabilizer

design method is proposed to stabilize the high order internal model controller. The main advantage of this controller is its low order yet robust nature (in fact zero order), which not only limits the off-line control synthesis computational effort, but also enable efficient on-line implementation.

8.3 Robust Stabilization for *LPV* Internal Model Controller

8.3.1 Preliminaries

For a regular *LPV* control synthesis problem, there are three key issues that one need to address:

(1). How to formulate the closed loop stability condition into convex Linear Matrix Inequalities (LMIs) to enable the controller synthesis.

(2). How to embed the L_2 induced norm constraint to enable robust control design in the *LMI* constraints.

(3). How to efficiently solve the convex *LMI*s spanning the whole parameter variation space.

The three issues above will be addressed in this chapter for the linear parametric varying internal model control problem. For convenient explanation, some preliminary definitions on the *LPV* systems will be explained in the following.

Definition 8.1. Shur Complement:

The symmetric block matrix $M = \begin{bmatrix} V & U^T \\ U & R \end{bmatrix} > 0$ if and only if $R > 0$ and $V - U^T R^{-1} U > 0$. Here $V - U^T R^{-1} U$ is called the Shur Complement of the matrix *M*.

Definition 8.2. Quadratic stability with constant Lyapunov matrix

Consider a general *LPV* system

$$\begin{aligned} \dot{x} &= A(\omega)x + B(\omega)u \\ y &= C(\omega)x + D(\omega)u \end{aligned} \tag{8.7}$$

where ω is the time varying parameter vector. If there exists a constant positive definite matrix Y, such that

$$A^T(\omega)Y + YA(\omega) < 0 \tag{8.8}$$

then the system is quadratically stable.

Note that the matrix Y here is constant. The Lyapunov condition (8.8) can then be transformed into *LMI* equation, from which the matrix Y can be solved. It has the merit of enabling computationally efficient controller synthesis, but in most cases the controllers designed are very conservative.

Definition 8.3. Quadratic stability with parameter dependent Lyapunov matrix

Similar to the previous definition, consider an *LPV* system, if there exists a parameter dependent positive definite matrix $Y(\omega)$, such that

$$Y\ (\omega)[A(\omega)] + [A(\omega)]^T Y(\omega) + \sum_{i=1}^{s} \dot{\omega}_i \frac{\partial Y(\omega)}{\partial \omega_i} < 0 \tag{8.9}$$

then the system is quadratically stable.

where ω_i is the scalar elements in the parameter vector ω, and s is the dimension of the vector. In this case, the Lyapunov matrix $Y(\omega)$ is parameter dependent with respect to ω. This stability condition alleviates the conservativeness comparing with a constant Lyapunov matrix, but may increase the off-line computational cost.

Definition 8.4. Closed loop *LPV* system γ performance problem:

Consider a regular *LPV* system in the state space form (8.7) above, the output controller can be written as:

$$\begin{aligned} \dot{x}_k &= A_K(\omega)x_k + B_K(\omega)y \\ u &= C_K(\omega)x_k + D_K(\omega)y \end{aligned} \tag{8.10}$$

And the closed loop system is denoted as:

$$\begin{aligned} \dot{x}_{clp} &= A_{clp}(\omega)x_{clp} + B_{clp}(\omega)d \\ e &= C_{clp}(\omega)x_{clp} + D_{clp}(\omega)d \end{aligned} \tag{8.11}$$

Here d is the external reference or disturbance, and e is the tracking/rejecting error.

Then the *LPV* synthesis γ performance problem is described as [25]:

Given a performance level $\gamma>0$, the LPV synthesis γ-performance problem is solvable if there exists a continuously differentiable parameter dependent Lyapunov matrix $Y(\omega)>0$ such that

$$\begin{bmatrix} A_{clp}^T(\omega)Y(\omega) + Y(\omega)A_{clp}(\omega) + \sum_{i=1}^{s}(\omega_i \frac{\partial Y}{\partial \omega_i}) & Y(\omega)B_{clp}(\omega) & C_{clp}^T(\omega) \\ B_{clp}^T(\omega)Y(\omega) & -\gamma I & D_{clp}^T(\omega) \\ C_{clp}(\omega) & D_{clp}(\omega) & -\gamma I \end{bmatrix} < 0 \tag{8.12}$$

Then the induced L_2 norm of the closed loop system (8.11) is less than γ, that is: $\|e\|_2 < \gamma\|d\|_2$. Where s is the number of time varying parameters, and ω_i is each individual parameter in the parameter vector. Note that the Lyapunov matrix $Y(\omega)$ and the controller matrix A_k, B_k, C_k and D_k are the unknown variables that we need to solve. The key is to find the corresponding design variables to satisfy the Linear Matrix Inequality (*LMI*) (8.12).

8.3.2 Parameter Dependent Input Gain Injection Problem Formulation

Consider a regular *MIMO* linear parameter varying system

$$\begin{aligned} \dot{x} &= A(\omega)x + B(\omega)u \\ y &= C(\omega)x \end{aligned} \tag{8.13}$$

where ω is the varying parameter vector.

Assuming the controller is

$$u = K(\omega)y = K(\omega)C(\omega)x \tag{8.14}$$

where $K(\omega)$ is input injection gain, which is a single column vector. Then the closed loop system becomes:

$$\begin{aligned} \dot{x}_{clp} &= [A(\omega) + B(\omega)K(\omega)C(\omega)]x_{clp} \\ y &= Cx_{clp} \end{aligned} \tag{8.15}$$

Definition 8.5: Quadratic stability with parameter dependent input gain injection

If the closed loop *LPV* system (8.15) with input gain injection is quadratically stable, then the following closed loop Lyapunov function should be solvable with a positive definite parameter dependent Lyapunov matrix $Y(\omega)$ and a time varying input injection control gain $K(\omega)$

$$Y(\omega)[A(\omega) + B(\omega)K(\omega)C(\omega)] + [A(\omega) + B(\omega)K(\omega)C(\omega)]^T Y(\omega) + \sum_{i=1}^{s} \dot{\omega}_i \frac{\partial Y(\omega)}{\partial \omega_i} < 0 \tag{8.16}$$

Note that only Y and K are unknown variables in the inequality above.

However, the LMI equation above is not convex, so that typically it's hard to obtain Y and K. This fact can be seen from the expanded Lyapunov based *LMI* equation: (here all the parameters are time varying, so we omit the notion of ω):

$$YA + YBKC + A^T Y + (BKC)^T Y + \sum_{i=1}^{s} \dot{\omega}_i \frac{\partial Y(\omega)}{\partial \omega_i} < 0 \tag{8.17}$$

Since Y and K are both variables to be determined, we cannot formulate this *LMI* into a convex LMI optimization problem due to the unavoidable variables (Y and K) crossing terms $YBKC$ and $(BKC)^T Y$. Thus the control design under this formulation is not solvable. This fact is also well explained in [35, 36].

8.3.3 Time Varying Internal Model Stabilization Using Input Gain Injection

Comparing with a dynamic controller, applying the input gain injection control to the time varying internal model control problem does offer great merits. First, using a sequence of time varying control gains instead of the dynamic controller with multiple orders, the on-line control implementation becomes more computational efficient.

Second, the number of parameters to be calculated off-line is much less. Essentially the input injection control gain is a time varying vector whose dimension is equal to the dimension of the augmented system, while the dynamic controller consists of time varying state space matrices, which have much more parameters to be determined.

Although the input gain injection synthesis is a non-convex optimization problem for a general *LPV* system as discussed in previous session, it is possible to formulate the time varying internal model stabilization into a convex optimization with input gain injection. This is because the augmented system (the internal model + plant) to be stabilized contains the virtual dynamics (the internal model), which offers great flexibility in the parameter dependent input gain injection design. In particular, the position and number of the inputs into the internal model are flexible and this flexibility could be incorporated into the control synthesis formulation.

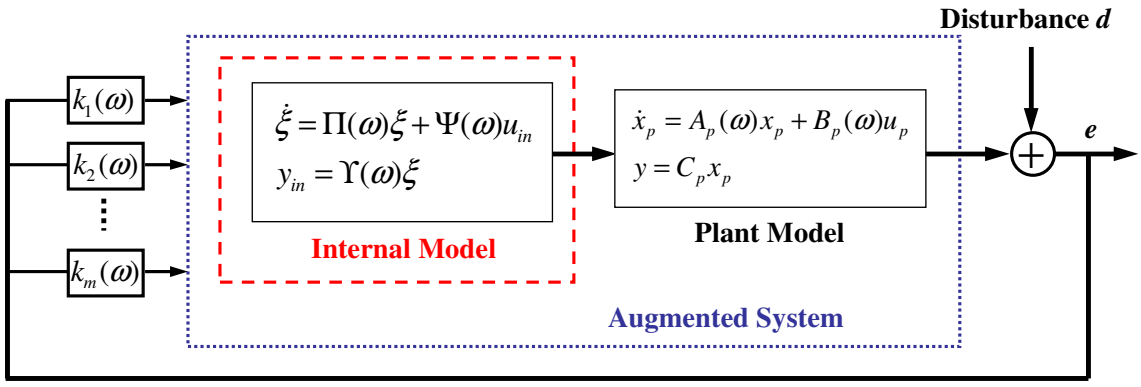

Figure 8.2. Stabilizer construction for internal model control system

Consider the augmented system (internal model + plant) shown in the Figure 8.2, suppose the *SISO* plant dynamics is described as:

$$\begin{aligned} \dot{x}_p &= A_p(\omega)x_p + B_p(\omega)u_p \\ y &= C_p x_p \end{aligned} \tag{8.18}$$

The plant dynamics can be transformed into the observer canonical form as:

$$\begin{aligned} \dot{x}_{op} &= A_{op}(\omega)x_{op} + B_{op}(\omega)u_p \\ y &= C_{op}x_{op} \end{aligned} \tag{8.19}$$

Here we assume the plant is of order n.

The internal model is constructed in a feedback fashion by two interconnected blocks as shown in Figure 8.1. Assume the interconnected m-th order internal model dynamics in I/O form (Figure 8.1) could be finally transformed into the state space from represented as:

$$\begin{aligned} \dot{\xi} &= \Pi(\omega)\xi + \Psi(\omega)u_{in} \\ y_{in} &= \Upsilon(\omega)\xi \end{aligned} \tag{8.20}$$

Then the augmented system (internal model + plant dynamics) could be written as:

$$\begin{aligned} \dot{X}_{aug} &= A_{aug}(\omega)X_{aug} + B_{aug}(\omega)u \\ y &= C_{aug}X_{aug} \end{aligned} \tag{8.21}$$

where $A_{aug}(\omega) = \begin{bmatrix} A_{op}(\omega) & B_{op}(\omega)\Upsilon(\omega) \\ 0_{m\times m} & \Pi(\omega) \end{bmatrix}$

$$B_{aug}(\omega) = \begin{bmatrix} \mathrm{B}_{11} = B_{op} & \mathrm{B}_{12} \\ \mathrm{B}_{21} & \mathrm{B}_{22} \end{bmatrix}$$

$$C = \begin{bmatrix} C_{op} & 0_{1\times m} \end{bmatrix}.$$

$X_{aug} = \begin{bmatrix} x_{op} & \xi \end{bmatrix}^T$ is the state vector of the augmented system of the order $n+m$. x_{op} is the original plant dynamics state, and ξ is the internal model states.

Here B_{aug} is a ($n+m$) by ($n+m$) square matrix. B_{11} is determined by the plant dynamics as:

$$\mathrm{B}_{11} = B_{op}$$

B_{12}, B_{21}, and B_{22} are to be determined. In other words, in B_{aug}, the first block matrix B_{11} comes from the plant dynamics and is fixed, while others (B_{12}, B_{21}, and B_{22}) are still flexible and can be assigned arbitrarily as they are in the virtual internal model. The higher the internal model order is, the more entries are to be determined in the B_{aug} matrix, which also means more flexibility in the control design.

To enable the time varying gain synthesis, we choose the entries of B_{aug} in the following way:

$$\mathrm{B}_{12} = [\mathrm{O}_{n\times m}],\ \mathrm{B}_{21} = [\mathrm{O}_{m\times n}],\quad \mathrm{B}_{22} = I_{m\times m}$$

where B_{12} is designed as a n by m zero matrix, B_{21} is a m by n zero matrix, and B_{22} is a m by m identity matrix.

So the B_{aug} matrix for the augmented system becomes:

$$B_{aug}(\omega) = \begin{bmatrix} B_{op} & \mathrm{O}_{m\times n} \\ \mathrm{O}_{n\times m} & I_{m\times m} \end{bmatrix} \tag{8.22}$$

Then if there exists a parameter dependent gain vector $K(\omega)$, which can stabilize the closed loop augmented system:

$$\dot{X}_{aug} = A_{aug}(\omega)X_{aug} + B_{aug}(\omega)K(\omega)C_{aug}X_{aug} \tag{8.23}$$

then the stabilizer design is successful.

As mentioned in the previous session, the key difficulty of the time varying input gain injection control synthesis is its non-convex LMI equations due to the cross multiplication of the design variables. The following technique will remove this constraint by taking advantage of the virtual internal model structure.

Now suppose we can choose the structure of the time varying gain K as:

$$K = \begin{bmatrix} k_1 \\ \vdots \\ k_n \\ k_{n+1} \\ \vdots \\ k_{n+m} \end{bmatrix} = \begin{bmatrix} 0 \\ \vdots \\ 0 \\ k_{n+1} \\ \vdots \\ k_{n+m} \end{bmatrix} \tag{8.24}$$

which means the first n elements of the gain K are forced to be zero. Here n is the dimension or order of the plant dynamics, and m is the order of the internal model. In general, the internal model order should be much higher than that of the plant order.

And define $\bar{B}_I = \begin{bmatrix} 1 & & & \\ & \ddots & & \\ & & \ddots & \\ & & & 1 \end{bmatrix}_{(n+m)\times(n+m)} = I_{(n+m)\times(n+m)}$

which is a $(n+m)$ by $(n+m)$ identity matrix.

It can be verified that

$$B_{aug}(\omega)K(\omega) = \bar{B}_I K(\omega) \tag{8.25}$$

Then if there exists a time varying gain vector $K(\omega)$, which can stabilize the following closed loop augmented system:

$$\dot{X}_{aug} = A_{aug}(\omega)X_{aug} + \bar{B}K(\omega)C_{aug}X_{aug} = A_{aug}(\omega)X_{aug} + K(\omega)C_{aug}X_{aug} \tag{8.26}$$

equally means that the designed control gain $K(\omega)$ can stabilize the original closed loop system (8.23).

Therefore, we translate the time varying gain synthesis for system (8.23) to the time varying injection gain design for system (8.26).

Then the above closed loop Lyapunov based LMI equation (8.17) can be written as:

$$YA_{aug} + YKC_{aug} + A_{aug}^T Y + (KC_{aug})^T Y + \sum_{i=1}^{s} \dot{\omega}_i \frac{\partial Y(\omega)}{\partial \omega_i} < 0 \tag{8.27}$$

$$==> YA_{aug} + YKC_{aug} + A_{aug}^T Y + C_{aug}^T K^T Y + \sum_{i=1}^{s} \dot{\omega}_i \frac{\partial Y}{\partial \omega_i} < 0 \tag{8.28}$$

$$==> YA_{aug} + YKC_{aug} + A_{aug}^T Y + C_{aug}^T (YK)^T + \sum_{i=1}^{s} \dot{\omega}_i \frac{\partial Y(\omega)}{\partial \omega_i} < 0 \tag{8.29}$$

Suppose $L=YK$

$$==> \quad YA_{aug} + LC_{aug} + A_{aug}^T Y + C_{aug}^T L^T + \sum_{i=1}^{s} \dot{\omega}_i \frac{\partial Y(\omega)}{\partial \omega_i} < 0 \tag{8.30}$$

Note that there exists no design variable (Y and L) multiplication crossing terms in Eq (8.30), thus the linear matrix inequality (8.30) above is convex. Using the interior point optimization method, the variable Y and L can be obtained. Then the control vector $K(\omega)$ can be derived as:

$$K(\omega) = Y(\omega)^{-1} L(\omega)$$

Remark: As shown in the derivation above, by selecting the specific B_{aug} matrix and K vector, the non-convex optimization problem can be transformed into a convex optimization problem. The problem left is how to formulate and constrain the optimization such that the first n elements of the designed K vector from Eq (8.31) below are zero.

8.3.4 LMI Formulation To Synthesize Parameter Dependent Input Injection Gain Vector $K(\omega)$

The proposed approach is to design a time varying gain vector whose first n elements are zero. As K is essentially an LMI inequality variable and obtained from the multiplication of two *LMI* variables (Eq 8.31),

$$K(\omega) = Y(\omega)^{-1} L(\omega) = \begin{bmatrix} k_1 \\ \vdots \\ k_n \\ k_{n+1} \\ \vdots \\ k_{n+m} \end{bmatrix} \tag{8.31}$$

there is no guarantee that the K obtained from the LMI optimization would have the feature required. In fact, currently there is no method to directly synthesize a K whose

first n elements are zero. Therefore, in the following, we will propose an indirect approach based on two consecutive steps as listed in the following:

(1). The first step is to embed n uncertainty terms Δ_1 up to Δ_n in the first n elements of the control gain vector K (Eq 8.31), such that a small perturbation on the time varying injection gains will still stabilize the closed loop system.

(2). The second step is to constrain the maximum value of the first n elements of the K vector, such that the maximum absolute value of k_1 up to k_n will not exceed max ($|\Delta_1|$) up to max ($|\Delta_n|$). Thus even if k_1 to k_n are non-zero from the control synthesis but are enforced to be zero in the real time implementation, the system will still be stable.

In the following further details about the two steps synthesis approach will be presented.

<u>*Step 1*</u>: ***Embedding uncertainty term in the control gain matrix:***

Consider the augmented linear parameter varying system (8.21), assuming the control input is

$$u_{aug} = [K(\omega) + \Delta_K]y = [K(\omega) + \Delta_K]C_{aug}(\omega)X_{aug} \tag{8.32}$$

where $\Delta_K = \begin{bmatrix} \Delta_1 \\ \vdots \\ \Delta_n \\ 0 \\ \vdots \\ 0 \end{bmatrix}$

Note the uncertainty terms are only embedded in the first n rows.

Then the closed loop system (8.26) becomes:

$$\dot{X}_{aug} = [A_{aug}(\omega) + \left(K(\omega) + \begin{bmatrix} \Delta_1 \\ \vdots \\ \Delta_n \\ 0 \\ \vdots \\ 0 \end{bmatrix} \right) C_{aug}(\omega)] X_{aug}$$

$$= [A_{aug}(\omega) + K(\omega) C_{aug}(\omega) + \begin{bmatrix} \Delta_1 \\ \vdots \\ \Delta_n \\ 0 \\ \vdots \\ 0 \end{bmatrix} C_{aug}(\omega)] X_{aug} \tag{8.33}$$

Theorem 8.1: If the following linear matrix inequality holds:

$$YA_{aug} + YKC_{aug} + Y \begin{bmatrix} \Delta_1 \\ \vdots \\ \Delta_n \\ 0 \\ \vdots \\ 0 \end{bmatrix} C_{aug} + {A_{aug}}^T Y + (KC_{aug})^T Y + {C_{aug}}^T \begin{bmatrix} \Delta_1 \\ \vdots \\ \Delta_n \\ 0 \\ \vdots \\ 0 \end{bmatrix}^T Y + \sum_{i=1}^{s} \dot{\omega}_i \frac{\partial Y(\omega)}{\partial \omega_i} < 0 \tag{8.34}$$

for the uncertainty value spanning the whole range of [Δ_{1min}, Δ_{1max}] , [Δ_{2min}, Δ_{2max}] … and [Δ_{nmin}, Δ_{nmax}], then the closed loop system Eq (8.26) will be quadratically stable even with the perturbation Δ_K in the input injection control gain *K*.

Proof: Omitted. The proof is similar to the above *LMI* Lyapunov matrix formulation in Eq (8.27). ■

However, in the optimization of the *LMI* Eq (8.34), we need to consider all the uncertainties within the uncertainty range. This may involve intensive computation. Fortunately, it is only necessary to consider the minimum and maximum value of the uncertainty interval. This argument can be formally described as the following:

Theorem 8.2. Suppose

$$f(\Delta_K) = YA_{aug} + YKC_{aug} + Y\Delta_K C_{aug} + A_{aug}^T Y + (KC_{aug})^T Y + C_{aug}^T \Delta_K^T Y + \sum_{i=1}^{s} \dot{\omega}_i \frac{\partial Y(\omega)}{\partial \omega_i}$$

If $\max\{f(\Delta_{K\max}), f(\Delta_{K\min})\} < 0$, then $f(\Delta_K) < 0$ for any $\Delta_K \in [\Delta_{K\min}, \Delta_{K\max}]$.

Proof: The proof is straightforward due to the affine property of the uncertainty vector Δ_K. ■

Therefore it is only necessary to consider the maximum and minimum value of the uncertainty boundary in the controller synthesis optimization, and all the control gain perturbation within the uncertainties range can stabilize the closed loop system (8.26).

Step 2: ***Constraining the size of the first n elements in the parameter dependent input injection control gain K(ω).***

Now step 1 ensures that the system can be stabilized even though the parameter dependent control gain K is perturbed by Δ_K. Then if the maximum absolute value of k_1 up to k_n designed in *LMI* optimization are non-zero but does not exceed max ($|\Delta_1|$) up to max ($|\Delta_n|$), the system will still be stable even if k_1 to k_n are set to be zero in the real time control. Two methods (Theorem 8.3a and 8.3b) are proposed to realize the gain constraint. They can constrain the norm individually, and either one could be used in the controller synthesis (The synthesis results shown in this thesis is based on 8.3a). We will present the following two theorems for constraining the norm of k_1, and similarly k_2 to k_n could be constrained in the same fashion.

Theorem 8.3 (a): For each discrete step i in the LMI optimization,, the Lyapunov matrix Y and the variable vector L should satisfy all the following linear matrix inequalities:

$$\begin{bmatrix} \alpha_1 \lambda & G_1 \\ G_1^T & Y \end{bmatrix} > 0, \quad Y > \alpha_1 I, \quad \begin{bmatrix} -\lambda_L I & L^T \\ L & -I \end{bmatrix} < 0, \tag{8.35}$$

where $G_1 = [1 \quad 0 \quad ... \quad 0 \quad 0]$, then k_1 is smaller than $\lambda\sqrt{\lambda_L}$. ■

Proof: As $k_1 = G_1 Y^{-1} L$, we can first constrain the norm of $G_1 Y^{-1}$ and L separately, then the two norm of k_1 will be constrained as well.

From $\begin{bmatrix} -\lambda_L I & L^T \\ L & -I \end{bmatrix} < 0$, by shur complement:

$$==> -\lambda_L + L^T L < 0$$

$$==> L^T L < \lambda_L$$

$$==> \|L\|_2 < \sqrt{\lambda_L}$$

To prove $\|G_1 Y^{-1}\|_2 < \lambda$, note that : $Y > \alpha_1 I$

$$==> Y^{-1} < \frac{1}{\alpha_1} I$$

$$==> Y^{-1} Y^{-1} < \frac{1}{\alpha_1} Y^{-1}$$

$$==> G_1 Y^{-1} Y^{-1} G_1^T < \frac{1}{\alpha_1} G_1 Y^{-1} G_1^T$$

Then if:

$$\frac{1}{\alpha_1} G_1 Y^{-1} G_1^T - \lambda < 0$$

$$==> G_1 Y^{-1} Y^{-1} G_1^T - \lambda < 0$$

$$==> \|G_1 Y^{-1}\|_2 < \lambda$$

Therefore, according to Cauchy-Schwarz inequality, having the above *LMI* constraints will ensure:

$$\|k_1\|_2 = \|G_1 Y^{-1} L\|_2 \le \|G_1 Y^{-1}\|_2 \|L\|_2 < \lambda \sqrt{\lambda_L} \quad . \blacksquare$$

Theorem 8.3 (b): For each discrete step *i* in the LMI optimization,, the Lyapunov matrix *Y* and the variable vector *L* should satisfy all the following linear matrix inequalities:

$$\begin{bmatrix} \lambda_1 & G_1 \\ G_1^T & Y \end{bmatrix} > 0, \quad \begin{bmatrix} -\lambda_2 I & L^T \\ L & -Y \end{bmatrix} < 0, \tag{8.36}$$

where $G_1 = [1 \quad 0 \quad ... \quad 0 \quad 0]$, then k_1 is smaller than $\sqrt{\lambda_1 \lambda_2}$. ■

Proof: From $\begin{bmatrix} -\lambda_2 I & L^T \\ L & -Y \end{bmatrix} < 0$, by shur complement:

$$==> -\lambda_2 + L^T Y^{-1} L < 0$$

$$==> \left\| Y^{-1/2} L \right\|_2 < \sqrt{\lambda_2}$$

In addition, from $\begin{bmatrix} \lambda_1 & G_1 \\ G_1^T & Y \end{bmatrix} > 0$

$$==> \lambda_1 - G_1 Y^{-1} G_1^T > 0$$

$$==> G_1 Y^{-1} G_1^T < \lambda_1$$

$$==> \left\| G_1 Y^{-1/2} \right\|_2 < \sqrt{\lambda_1}$$

Therefore, according to Cauchy-Schwarz inequality, having the above *LMI* constraints will ensure:

$$\left\| k_1 \right\|_2 = \left\| G_1 Y^{-1} L \right\|_2 = \left\| G_1 Y^{-1/2} Y^{-1/2} L \right\|_2 \le \left\| G_1 Y^{-1/2} \right\|_2 \left\| Y^{-1/2} L \right\|_2 < \sqrt{\lambda_1 \lambda_2} \quad . \blacksquare$$

8.3.5 Robust Input Gain Injection Controller Design

In this section, the robust control gain design considering the system model uncertainty will be presented. Both the unstructured and structured uncertainty could be embedded into the stabilizer synthesis. We will first discuss embedding the unstructured

uncertainty (unmodeled dynamics) into the parameter dependent input gain injection synthesis.

As shown in Figure 8.3, the plant model uncertainty is considered at the output side.

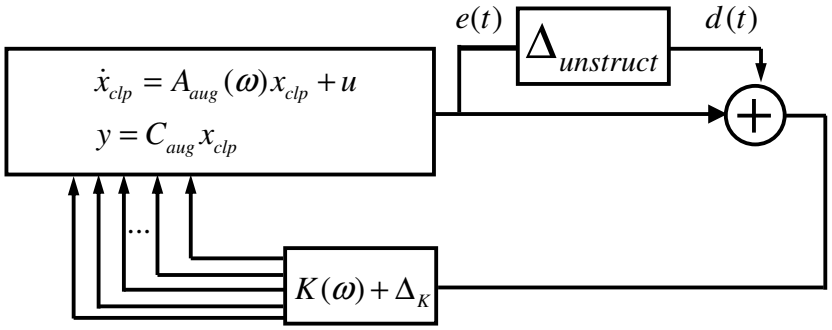

Figure 8.3. Control loop with unstructured plant dynamics uncertainty

Now according to the small gain theorem, if $\|\Delta_{unstruct}\|_\infty \le 1/\gamma$, then the induced L_2 norm between e and d in Figure 8.3 should satisfy: $\|e\|_2 / \|d\|_2 < \gamma$ for robust stability.

So the key problem is to formulate the appropriate conditions to constrain the induced L_2 norm and also enable the closed loop controller design based on a convex *LMI*.

The closed loop system shown in Figure 8.3 can be represented as:

$$\begin{bmatrix} \dot{x}_{clp} \\ e(t) \end{bmatrix} = \begin{bmatrix} A_{aug} + KC_{aug} + \Delta_K^T C_{aug} & K + \Delta_K^T \\ C_{aug} & 0 \end{bmatrix} \begin{bmatrix} x_{clp} \\ d(t) \end{bmatrix} \tag{8.37}$$

In the following theorem and its proof, for presentation convenience, A_{aug} and C_{aug} are denoted as A and C respectively.

Theorem 8.4: If the following linear matrix inequality holds,

$$\begin{bmatrix} YA+YKC+Y\Delta_K C+A^T Y+(KC)^T Y+C^T\Delta_K^T Y+\sum_{i=1}^{s}\dot{\omega}_i\frac{\partial Y(\omega)}{\partial\omega_i} & Y(K+\Delta_K) & C^T \\ (K+\Delta_K)^T Y & -\gamma I & 0 \\ C & 0 & -\gamma I \end{bmatrix} < 0 \tag{8.38}$$

then

(1). The nominal closed loop system is exponentially stable.

(2). The induced L_2 norm between e and d is smaller than γ, thus the system is robustly stable. ■

Proof: (1). See the appendix in this chapter.

In addition to the unstructured uncertainty, the plant structured parameter uncertainty can be considered as well in the controller synthesis. If the boundary of the parametric uncertainty Δ_S can be obtained in the experiment, then embedding the structured uncertainty in the control design can alleviate the design conservativeness comparing with using the unstructured uncertainty alone. The linear structured uncertainty can be formulated as a LMI shown below. The proof is straightforward thus is omitted.

$$\begin{bmatrix} \begin{pmatrix} Y(A+\Delta_S)+YKC+Y\Delta_K C+(A+\Delta_S)^T Y \\ +(KC)^T Y+C^T\Delta_K^T Y+\sum_{i=1}^{s}\dot{\omega}_i\frac{\partial Y(\omega)}{\partial\omega_i} \end{pmatrix} & Y(K+\Delta_K) & C^T \\ (K+\Delta_K)^T Y & -\gamma I & 0 \\ C & 0 & -\gamma I \end{bmatrix} < 0 \tag{8.39}$$

8.3.6 Additional Control Gain Constraints

Two additional constraints can be added as well to improve the controller performance and avoid saturation. First, the magnitude of the control gain $K(\omega)$ should be restricted in the controller synthesis optimization to avoid control saturation. Second,

constraints could be set for the Lyapunov matrix $Y(\omega)$ in Eq (8.38) to ensure fast convergence rate.

Constraining the size of the input injection control gain K(ω).

Theorem 8.5: For each discrete step *i*, the Lyapunov matrix *Y* should satisfy the following linear matrix inequality together with the conditions in Theorem 8.3:

$$\begin{bmatrix} Y & I \\ I & \lambda_Y I \end{bmatrix} > 0, \tag{8.40}$$

Then the 2 norm in the input gain vector *K* is smaller than $\lambda_Y \sqrt{\lambda_L}$. ■

Proof: See appendix in this chapter. ■

Controlling the Stabilizer Convergence Rate:

For each discrete step *i*, the Lyapunov matrix *Y* should satisfy:

$$\alpha_1 I < Y < \alpha_2 I \tag{8.41}$$

$$YA_{aug} + YKC_{aug} + A_{aug}^T Y + (KC_{aug})^T Y + \sum_{i=1}^{s} \dot{\omega}_i \frac{\partial Y(\omega)}{\partial \omega_i} < -cI$$

Then the state transition of the nominal closed loop system (8.26) will satisfy:

$$\left\| X_{clp}(t) \right\|^2 < \frac{\alpha_2}{\alpha_1} \left\| X_{clp}(0) \right\|^2 \exp\left[-\frac{c}{\alpha_2} t \right]$$

The proof is omitted as the conditions above are commonly used for exponential convergence.

8.4 Experimental Investigation and Results

In the experimental study, the engine start torque oscillation rejection will be simulated in the hydraulic dynamometer system. As the engine pumping torque pulse is a frequency varying signal, whose frequency is proportional to the engine speed (see

details in Chapter 7), the loading torque with similar shape should be generated by the hydraulic actuator to compensate the torque vibration from the engine. As the pressure difference in the dynamometer hydraulic system is closely related to the loading torque, for experiment convenience, we define the control target as the pressure tracking of a chirp signal. The frequency of the chirp signal will change and go up quickly to simulate the situation in the engine start. So the key is to design a time varying internal model controller and its stabilizer to track this signal with varying frequency.

The hydrostatic dynamometer system consists of a hydraulic control system, a 4 cylinder diesel engine and a number of sensing devices. A detailed photograph of the main hardware in the hydrostatic dynamometer system is shown in Figure 8.4(a). The hydraulic system of the hydrostatic dynamometer is shown in Figure 8.4(b). The main hydraulic components are: a boost pump and an engine load (EL) pump/motor (both are variable displacement piston pumps), a load-sensing control (LSC) valve (proportional valve), and a high-speed control (HSC) valve (two-stage pilot valve, shown in the bottom right corner of Figure 8.4(b)).

In the load-sensing feedback loop, the LSC valve regulates the inlet (operating) pressure of the EL pump/motor P_{in} in Figure 8.4(b) to hold a constant value. In the engine loading/motoring loop, the HSC valve, as the primary actuator, controls the outlet pressure of the EL pump/motor P_{out}. The displacement adjustment mechanism, as the secondary actuator, controls the displacement of the EL pump/ motor. Since the dynamometer torque is a function of the displacement and pressure drop, and also we can keep the inlet pressure P_{in} nearly constant, generating a frequency varying torque output can be translated into the outlet pressure regulation to generate frequency varying outlet pressure pulses. And this is exactly the target in the following experiments.

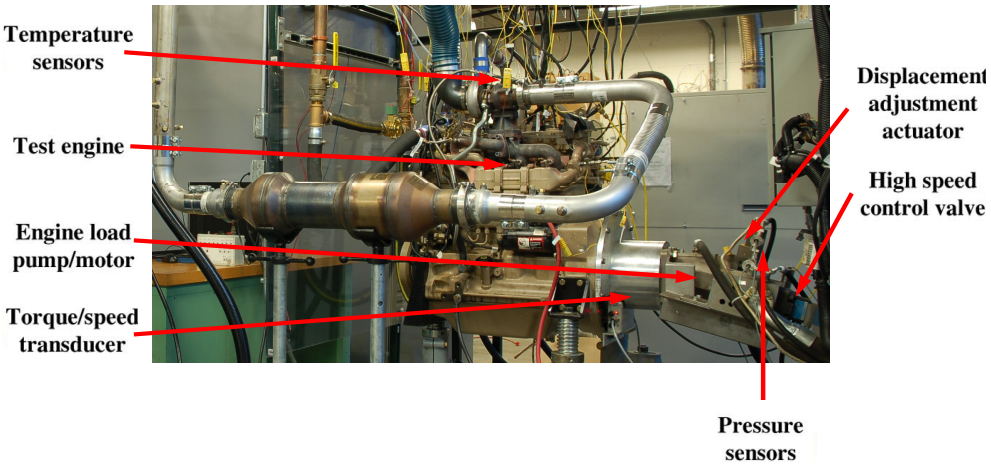

Figure 8.4 (a). Picture of hydrostatic dynamometer system

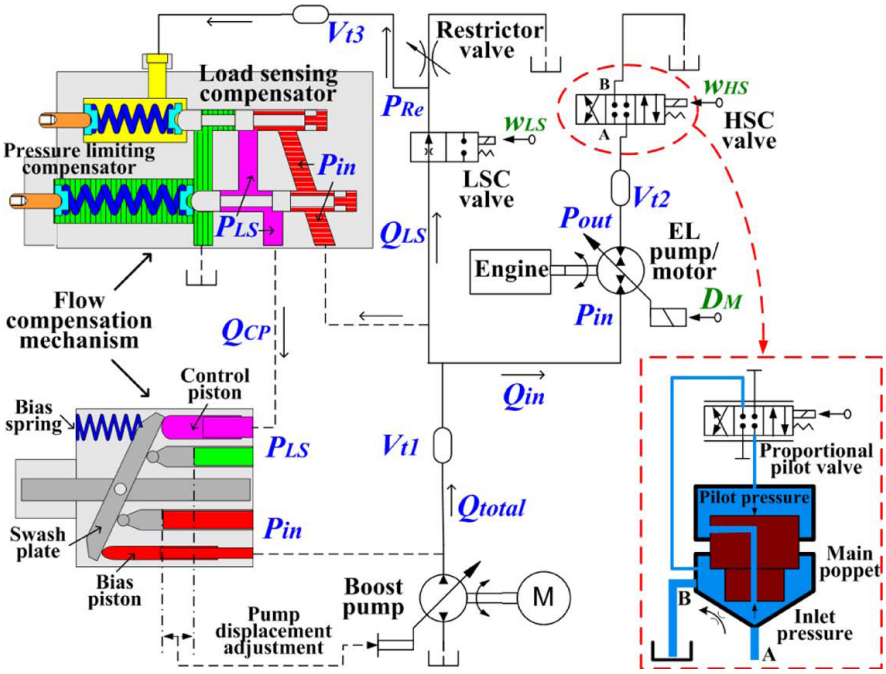

Figure 8.4 (b). Schematic diagram of the hydrostatic dynamometer

8.4.1 System Dynamics Modeling and Controller Design

The hydraulic system dynamics model includes a first order pilot operated valve model and a first order pressure dynamics. The second order model can be written as:

$$\dot{L} = -\tau L + b_L u$$
$$\frac{V}{\beta}\dot{P} = W_L H - C_d \sqrt{\frac{2P}{\rho}} A_u(L) \tag{8.42}$$

where L is the valve spool displacement, τ is the inverse of the valve time constant, b_L is the valve voltage/orifice coefficient, β is the bulk modulus of the hydraulic oil, V is the chamber volume, W_L is the rotational speed of the engine load (EL) pump/motor, H is the EL pump/motor displacement, ρ is the hydraulic oil density, $A_u(L)$ is the orifice function. The first order valve dynamics is a simplification of the pilot operated proportional control valve. The plant model is a nonlinear because of the multiplication of the state P and L. However, if P could be treated as a parameter measured on-line, then the system could be regarded as a quasi linear parameter varying (*LPV*) system.

The reference signal to be tracked is a chirp signal with a varying frequency $\omega(t)$. This kind of signal can be modeled as an exo-system [5]:

$$S(t) = \begin{bmatrix} 0 & \omega(t) \\ -\omega(t) & 0 \end{bmatrix} \tag{8.43}$$

with the reference signal $\omega(t)$ as the time varying parameter.

Both the exo-system model and the plant dynamics need to be transformed into the observer canonical form to enable the time varying internal model design. The transformed plant model can be written as:

$$\begin{aligned} \dot{x}_{o1} &= -a_1 x_{o1} + x_{o2} \\ \dot{x}_{o2} &= \frac{\beta\tau}{V} W_L H - a_0 x_{o1} + b_0 u \\ y &= x_{o1} \end{aligned} \tag{8.44}$$

where

$$b_0 = \beta \times RHS / V^2 \sqrt{\tau \dot{P} + \tau^2 P}\ ,\ a_1 = \tau\ ,\ a_0 = 0\,, \tag{8.45}$$

y is the output pressure.

And the exo-system in the observer canonical form is

$$S_O(t) = \begin{bmatrix} -\alpha_1(t) & 1 \\ -\alpha_0(t) & 0 \end{bmatrix} \tag{8.46}$$

where

$$\alpha_1(t) = -\frac{\dot{\omega}(t)}{\omega(t)} \text{ and } \alpha_0(t) = \omega^2(t) + \frac{\ddot{\omega}(t)\omega(t) - \dot{\omega}^2(t)}{\omega^2(t)} \tag{8.47}$$

In addition, the $W_L H$ in Eq (8.44) is assumed to be constant and known, so a feed-forward input $u_d = -\frac{\beta\tau}{b_0 V} W_L H$ is used to compensate the constant term. Then the control input u in Eq (8.44) becomes $u=u_d+u_{st}$, with u_{st} denoting the control input from the *LPV* stabilizer.

The time varying internal model can therefore be designed and the augmented system (the internal model + plant dynamics) can be written as:

$$\begin{aligned} \dot{X}_{aug}(t) &= A_{aug}(t) X_{aug}(t) + B_{aug}(t) u_{st} \\ Y_{aug}(t) &= C_{aug} X_{aug}(t) \end{aligned} \tag{8.48}$$

where

$$A_{aug}(t) = \begin{bmatrix} -a_1(t) & 1 & 0 & 0 \\ -a_0(t) & 0 & b_0(t)\gamma_1(t) & b_0(t)\gamma_2(t) \\ 0 & 0 & 0 & 1 \\ 0 & 0 & \varphi_1(t) & \varphi_2(t) \end{bmatrix} \tag{8.49}$$

$$\varphi_1 = -a_0 - b_0(-\dot{q}_0 / q_0^2) - p_0 b_0 / q_0 - \dot{a}_1 \text{ and } \varphi_2 = -a_1 - b_0 / q_0 \tag{8.50}$$

$$\gamma_1 = -\dot{q}_0 / q_0^2 + p_0 / q_0, \ \gamma_2 = 1/q_0 \tag{8.51}$$

$$q_0 = b_0 / (\alpha_1 - a_1), \ p_0 = (\alpha_0 - a_0)/(\alpha_1 - a_1) + \dot{b}_0 / b_0 \tag{8.52}$$

To enable robust stabilizer design, the B_{aug} matrix in Eq(8.48) is designed as

$$B_{aug}(t) = \begin{bmatrix} 0 & 0 & 0 & 0 \\ 0 & b_0(t) & 0 & 0 \\ 0 & 0 & 1 & 0 \\ 0 & 0 & 0 & 1 \end{bmatrix} \tag{8.53}$$

Note that b_0 is the only non-zero and non-unit term. In this case, instead of enforcing both the first two gains k_1 and k_2 in the control gain K to be zero, it is only necessary to constrain the k_1 to be zero. That is:

$$K_{aug} = \begin{bmatrix} k_1 \\ k_2 \\ k_3 \\ k_4 \end{bmatrix} = \begin{bmatrix} 0 \\ k_2 \\ k_3 \\ k_4 \end{bmatrix} \tag{8.54}$$

And Δ_K for the control gain synthesis is

$$\Delta_K = [\Delta_1 \quad 0 \quad 0 \quad 0]^T \tag{8.55}$$

To see this point, define

$$\bar{B}_I = \begin{bmatrix} 1 & 0 & 0 & 0 \\ 0 & 1 & 0 & 0 \\ 0 & 0 & 1 & 0 \\ 0 & 0 & 0 & 1 \end{bmatrix} = I_{4\times 4} \tag{8.56}$$

It can be verified that

$$\bar{B}_I \begin{bmatrix} 0 \\ k_2 \\ k_3 \\ k_4 \end{bmatrix} = B_{aug}(t) \begin{bmatrix} 0 \\ k_2 / b_0 \\ k_3 \\ k_4 \end{bmatrix} \tag{8.57}$$

From which we can see that if K_{aug} in Eq(8.54) can stabilize

$$\dot{X}_{aug} = A_{aug}(\omega) X_{aug} + \bar{B}_I K_{aug} C_{aug} X_{aug} \tag{8.58}$$

equally means that the designed control gain $\begin{bmatrix} 0 & k_2/b_0 & k_3 & k_4 \end{bmatrix}^T$ can stabilize the closed loop system of (8.48)

$$\dot{X}_{aug} = A_{aug}(t)X_{aug} + B_{aug}(t)KC_{aug}X_{aug} \tag{8.59}$$

In other words, after obtaining $\begin{bmatrix} 0 & k_2 & k_3 & k_4 \end{bmatrix}^T$ from the optimization based control synthesis for the closed loop system (8.59), the real time time-varying control gain could be set to be $\begin{bmatrix} 0 & k_2 / b_0 & k_3 & k_4 \end{bmatrix}^T$.

So the target for the *LPV* synthesis is to design the time varying input injection gain whose first element is zero to stabilize the augmented system (8.48) in a robust fashion.

8.4.2 Experimental Results and Discussion

The system dynamics (Eq. 8.42) has been identified for the second order hydraulic system. It's hard to use a second order model to precisely describe the pressure together with the valve dynamics covering a wide frequency range. In particular, to have the model simulation match the experimental data, the τ in Eq (8.42) needs to be small for high frequency input and large for low frequency input. While using a higher order model will give better model matching result, it will induce control design complexity. So in the controller synthesis, we use a small τ (τ =12) , which will make the dynamic model imprecise for low frequency region. However, the uncertainty in the second order model can also be a test for the robustness of the control method.

The time varying internal model is first designed, and the time varying stabilizer gains are synthesized as shown in Figure 8.5 based on the proposed design method in Sec. 8.3. It can be seen that the gain k_1 is constrained into a fairly small value comparing with k_2 and k_4. Δ_K in Eq (8.55) for K_{aug} (Eq. 8.54) is chosen to be in the interval from [-200 0 0 0]^T to [200 0 0 0]^T, which can bound the gain k_1 throughout the parameter range shown in Figure 8.5. Therefore setting k_1 to be zero in the real time implementation will not destabilize the system.

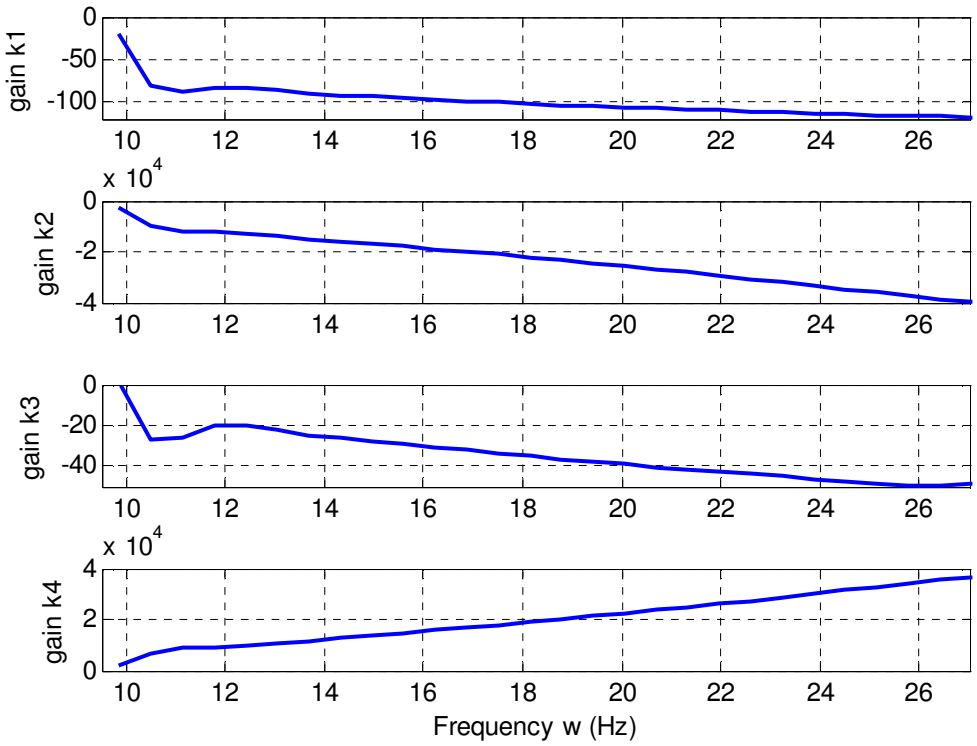

Figure 8.5 Time varying input injection gains

The designed time varying internal model together with the stabilizer is then implemented in the hydro-dynamometer system. Three groups of experiments are shown from Figure 8.6 to Figure 8.8.

In the first group, the reference signal frequency variation rate is 4.8 Hz/sec, and the frequency is changing from 10 Hz to 25Hz in nearly three seconds as shown in Figure 8.6(a). The tracking error converges fast within the two cycles as shown in Figure 8.6(b). The control input shown in Figure 8.6(c) presents a frequency varying control command with magnitude variation even in the steady states. As mentioned earlier, it's hard to use the second order model to describe the system dynamics covering a wide frequency range, and the model uncertainties are inevitable. Nevertheless, the successful pressure tracking and stabilization results shown in Figure 8.6 indicates the robustness of the time varying stabilizer design. To further study the stabilizer robustness, we add 20% perturbation to

the parameter b_0 in the internal model (Eq 8.49), and the system can still be stabilized and exhibit similar tracking results as shown in Figure 8.6.

In the second test, the b_0 in Eq (8.45) is further perturbed by 4 times of its original value and therefore the internal model designed (8.49) has larger perturbation comparing with the first group of experiment. We first let the system track a reference with slower frequency variation of 0.79 Hz/sec. Figure 8.7 shows the pressure tracking results of a chirp signal with varying frequency between 10 Hz to 29.75 Hz in 25 second. The signal frequency variation can be observed from Figure 8.7(a), which also shows that the controlled pressure converges to the reference pressure slowly at the initial stage. The slow convergence is mainly due to the internal model parameter perturbation. Figure 8.7 (b) and (c) present the zoom-in view of tracking result for one second at two different frequency ranges, which clearly indicates the frequency difference. The control command shown in Figure 8.7(d) again exhibits the magnitude varying feature of the input.

In the third experiment, the b_0 in Eq (8.45) is still perturbed the same amount as the second test (four times of its original value), but the tracking reference signal is the same as the first group of experiment, which has a much faster frequency variation rate of 4.8Hz/sec. As shown in Figure 8.8(a), the controller can no longer maintain good tracking results as it does in the slow frequency varying case (Figure 8.7). This is because the faster frequency variation rate (4.8 Hz/sec *vs* 0.79Hz/sec) will affect $\alpha_1(t)$ and $\alpha_0(t)$ in Eq (8.47) and subsequently q_0 and γ_2 in Eq (8.52) and Eq (8.51), which will then amplify the effect of the perturbation of $b_0(t)$ in the internal model Eq (8.49).

Therefore, we can conclude that the stabilizer is robust since the model uncertainty and small perturbation will not cause instability. For large parameter perturbation, the system can keep reasonable tracking for smooth frequency varying, but the error starts diverging in the case of aggressive frequency variation.

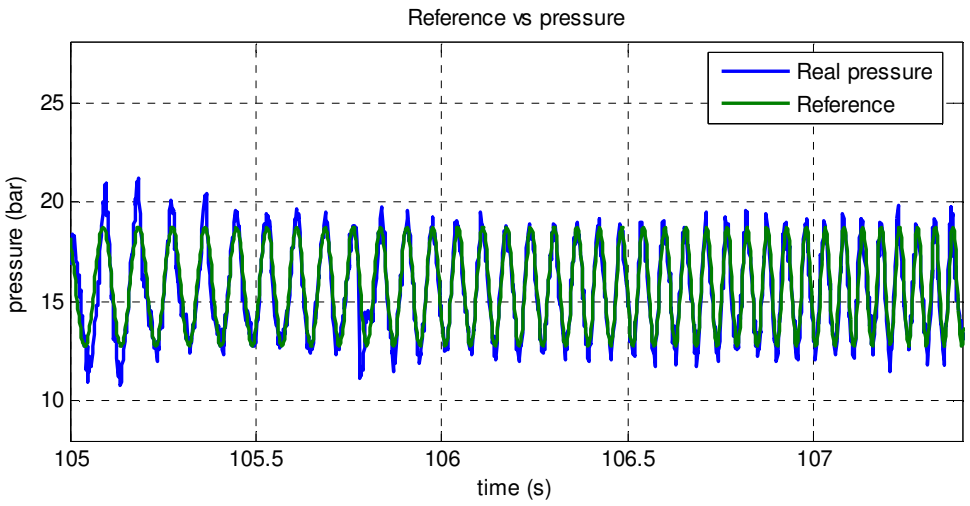

Figure 8.6 (a). Pressure tracking with 4.8Hz/sec frequency variation rate

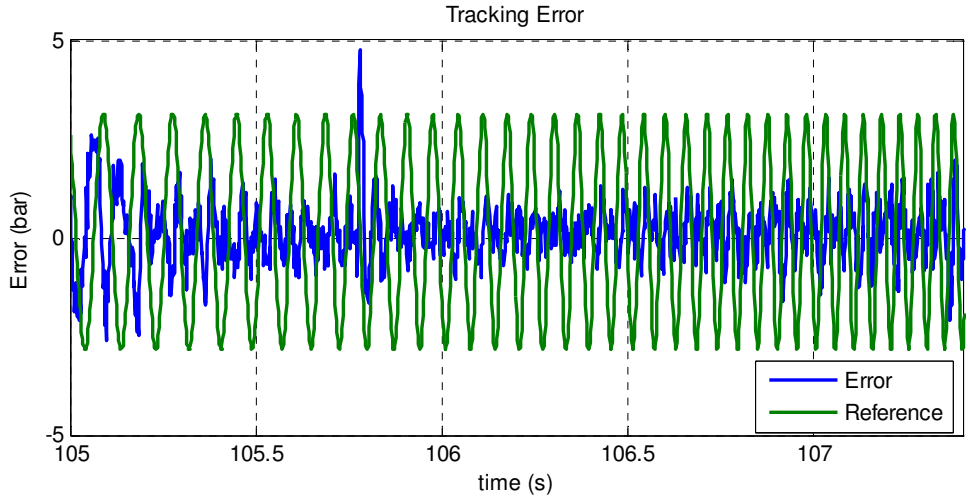

Figure 8.6 (b). Pressure tracking error *vs* shifted reference

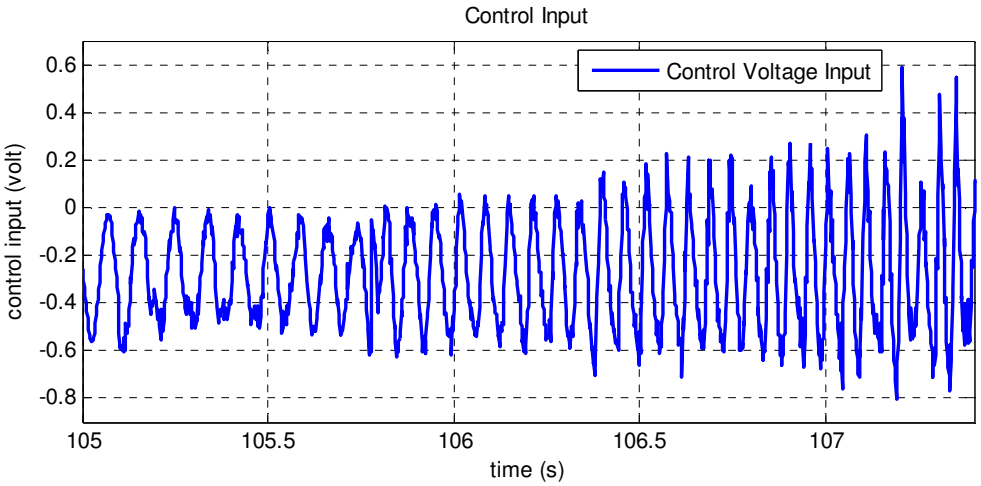

Figure 8.6 (c). Valve control voltage input

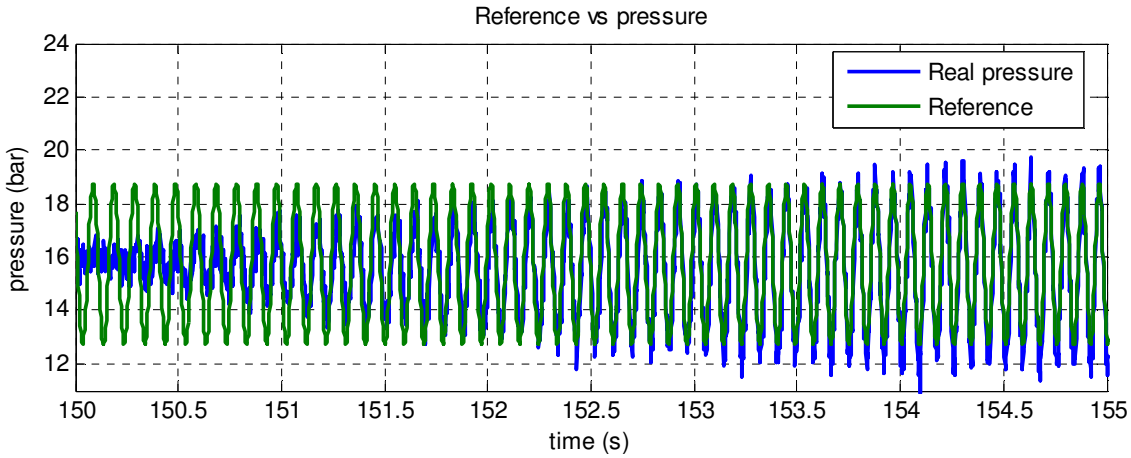

Figure 8.7 (a). Zoom-in view of pressure tracking at the start with 0.79Hz/sec frequency variation

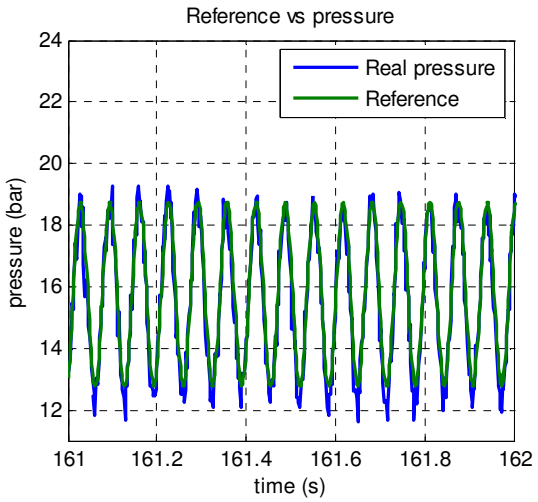

Figure 8.7 (b). zoom-in view at 161 sec

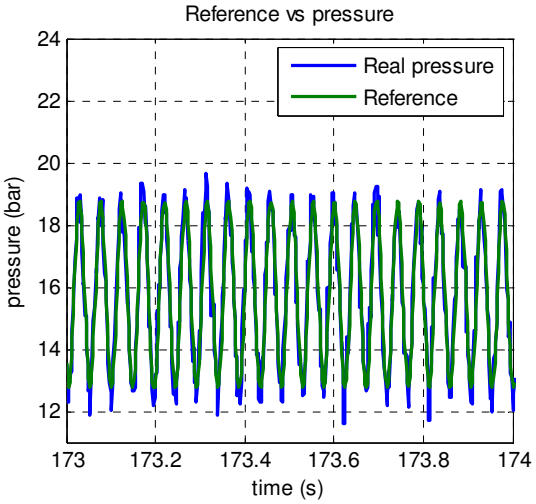

Figure 8.7 (c). zoom-in view at 173 sec

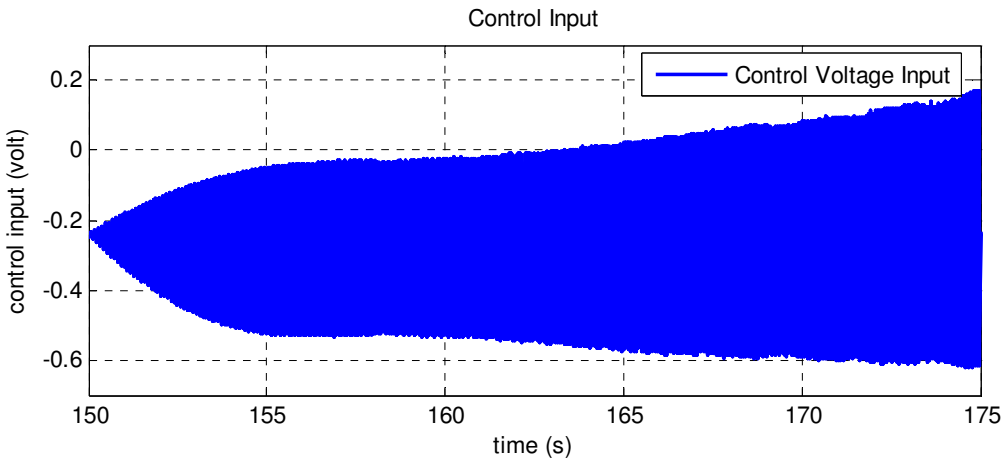

Figure 8.7 (d). Valve control input for pressure tracking with 0.79Hz/sec frequency variation rate

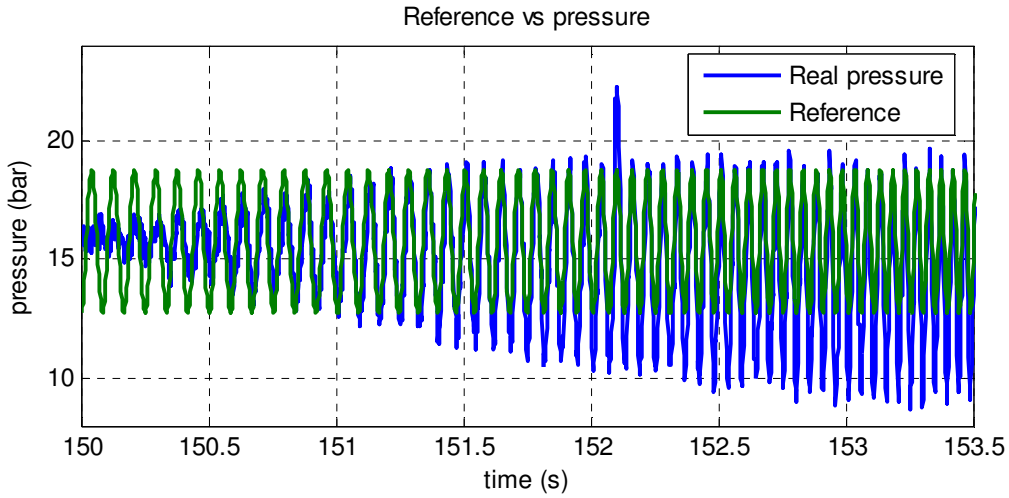

Figure 8.8 (a). Tracking failure for aggressive frequency variation reference due to parameter perturbation

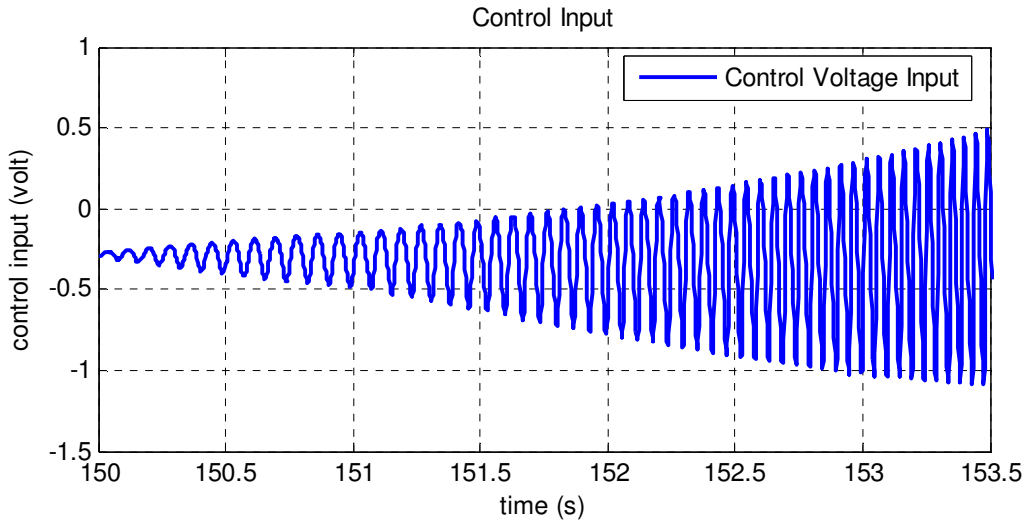

Figure 8.8 (b). Valve control input

TABLE 8.1. SYSTEM PARAMETERS

Symbol	Description	Quantity
β	**effective bulk modulus**	**1.3e9 (Pa)**
V	**chamber volume**	**2e-4 (m^3)**
R_{HS}	$R_{HS}=C_d A_{HS}(\rho)^{1/2}$ **(m^3/sec/$Pa^{1/2}$)**	**1.05e-5**
H	**EL pump displacement**	**107 (cc/rev)**

8.5 Conclusion

As a conclusion, the problem defined in this chapter is the tracking/rejection control of a periodic signal/disturbance for a linear parameter varying (*LPV*) plant dynamics based on the internal model principle. A low order and computationally efficient robust stabilizer design for the *LPV* internal model control is still an open problem and not available previously. A promising approach is proposed to solve this problem, which is the key contribution in this chapter. The proposed method is enabled by the unique dynamics characteristic of the internal model system, and translates a non-convex controller synthesis into a convex optimization based control design. To this end, experiments are conducted to verify the proposed control methodology using the hydrostatic dynamometer system, and the synthesized controller is shown to be efficient, low order, and robust.

8.6 Appendix in Chapter 8:

Proof for Theorem 8.4

Proof: (1). By Shur complement, the *LMI* (8.40) above can be converted into the following Riccati equation:

$$YA + YKC + Y\Delta_K C + A^T Y + (KC)^T Y + C^T \Delta_K^T Y + \sum_{i=1}^{s} \dot{\omega}_i \frac{\partial Y(\omega)}{\partial \omega_i}$$

$$+ \frac{1}{\gamma} C^T C + \frac{1}{\gamma} Y(K + \Delta_K)(K + \Delta_K)^T Y < 0$$

As $\frac{1}{\gamma} C^T C + \frac{1}{\gamma} Y(K + \Delta_K)(K + \Delta_K)^T Y$ is positive semi-definite, then

$$YA + YKC + Y\Delta_K C + A^T Y + (KC)^T Y + C^T \Delta_K^T Y + \sum_{i=1}^{s} \dot{\omega}_i \frac{\partial Y(\omega)}{\partial \omega_i} < 0$$

So the nominal closed loop system is quadratically stable, which equally means exponential stability in the linear time varying case. ■

Proof: (2):

Define the Lyapunov function for closed loop system (8.39) as $V(x_{clp}) = x_{clp}{}^T Y x_{clp}$

$$\dot{x}_{clp} = (A + KC + \Delta_K C) x_{clp} + (K + \Delta_K^T) d(t)$$

The time derivative of the Lyapunov function *V* is

$$\frac{d}{dt} V(x_{clp}) = x_{clp}{}^T \left[YA + YKC + Y\Delta_K C + A^T Y + (KC)^T Y + C^T \Delta_K^T Y + \sum_{i=1}^{s} \dot{\omega}_i \frac{\partial Y(\omega)}{\partial \omega_i} \right] x_{clp}$$
$$+ x_{clp}{}^T Y(K + \Delta_K^T) d(t) + d^T(t)(K + \Delta_K^T)^T Y x_{clp}$$

As

$$YA + YKC + Y\Delta_K C + A^T Y + (KC)^T Y + C^T \Delta_K^T Y + \sum_{i=1}^{s} \dot{\omega}_i \frac{\partial Y(\omega)}{\partial \omega_i}$$

$$< -\frac{1}{\gamma} C^T C - \frac{1}{\gamma} Y(K + \Delta_K)(K + \Delta_K)^T Y$$

$$\Rightarrow \frac{d}{dt} V(x_{clp}) < x_{clp}{}^T \left[-\frac{1}{\gamma} C^T C - \frac{1}{\gamma} Y(K + \Delta_K)(K + \Delta_K)^T Y \right] x_{clp} + x_{clp}{}^T Y(K + \Delta_K^T) d(t) + d^T(t)(K + \Delta_K^T)^T Y x_{clp}$$

$$\Rightarrow \frac{d}{dt} V(x_{clp}) < x_{clp}{}^T \left[-\frac{1}{\gamma} C^T C - \frac{1}{\gamma} Y(K + \Delta_K)(K + \Delta_K)^T Y \right] x_{clp} - \gamma d^T(t) d(t) + \gamma d^T(t) d(t) + x_{clp}{}^T Y(K + \Delta_K^T) d(t) + d^T(t)(K + \Delta_K^T)^T Y x_{clp}$$

$$\Rightarrow \frac{d}{dt} V(x_{clp}) < -\left[\begin{array}{l} \gamma d^T(t) d(t) - x_{clp}{}^T Y(K + \Delta_K^T) d(t) - d^T(t)(K + \Delta_K^T)^T Y x_{clp} \\ + x_{clp}{}^T \frac{1}{\gamma} Y(K + \Delta_K)(K + \Delta_K)^T Y x_{clp} \end{array} \right] + \gamma d^T(t) d(t) - \frac{1}{\gamma} x_{clp}{}^T C^T C x_{clp}$$

$$\Rightarrow \frac{d}{dt} V(x_{clp}) < -\left[\sqrt{\gamma} d(t) - \frac{1}{\sqrt{\gamma}} (K + \Delta_K)^T Y x_{clp} \right]^T \left[\sqrt{\gamma} d(t) - \frac{1}{\sqrt{\gamma}} (K + \Delta_K)^T Y x_{clp} \right] + \gamma d^T(t) d(t) - \frac{1}{\gamma} x_{clp}{}^T C^T C x_{clp}$$

Integrate both sides:

$$\Rightarrow 0 < V < -\left\| \sqrt{\gamma} d(t) - \frac{1}{\sqrt{\gamma}} (K + \Delta_K)^T Y x_{clp} \right\|_2^2 + \gamma \left\| d(t) \right\|_2^2 - \frac{1}{\gamma} \left\| e(t) \right\|_2^2$$

Therefore $\dfrac{\left\| e(t) \right\|_2}{\left\| d(t) \right\|_2} < \gamma$

Therefore the system will be robustly stable if the L_2 norm of the unstructured uncertainty is less than $1/\gamma$. ■

Proof for Theorem 8.5

Proof: From Theorem 8.3 (a), we have already proved that $\|L\|_2 < \sqrt{\lambda_L}$.

In addition, as $\begin{bmatrix} Y & I \\ I & \lambda_Y I \end{bmatrix} > 0$, by shur complement,

$==> Y^{-1} < \lambda_Y I$

$==> x^T Y^{-1} x < x^T \lambda_Y x$, where x is any vector belonging to R^n.

$==> \|Y^{-1}\|_{i2} \|x\|_2^2 < \lambda_Y \|x\|_2^2$

$==> \|Y^{-1}\|_{i2} < \lambda_Y$

where $\|Y^{-1}\|_{i2}$ is the induced matrix two norm.

Therefore, according to the induced matrix norm consistency condition, $\|K\|_2 = \|Y^{-1}L\|_2 < \|Y^{-1}\|_{i2} \|L\|_2 < \lambda_Y \sqrt{\lambda_L}$. ■

References in Chapter 8

[1] B.A. Francis. The internal model principle of control theory. SIAM Journal of Control, vol. 15 (3), pp. 486-505, 1977.

[2] B.A. Fancis, and W.M. Wonham. The internal model principle of control theory. Automatica, vol. 12 (5), pp. 457-465, 1976.

[3] K.S. Tsakalis, P.A. Ioanou, Linear Time-Varying Systems: Control and Adaptation, in: Advances in Industrial Control, Prentice Hall, Englewood Cliffs, NJ, 1993

[4] A. Isidori, C.I. Byrnes, Output regulation of nonlinear systems, IEEE Transactions on Automatic Control 35 (2) (1990), 131-140

[5] Z. Sun, Z. Zhang, and T.-C. Tsao. Trajectory tracking and disturbance rejection of linear time-varying systems: input/output representation. Systems and Control Letters, vol. 58 (6): 452-460, 2009.

[6] A.Ichikawa, H.Katayama, Output regulation of time-varying systems, IEEE Transactions on Automatic Control 35 (2) (1990) 131-140

[7] Z. Zhang, A. Serrani, The linear periodic *output regulation problem, Systems & Control Letters 55(7) (200) 518-529*

[8] S. Hara, Y. Yamamoto, T. Omata, and M. Nakano. Repetitive control systems: a new type servo system for periodic exogenous signals. IEEE Transactions on Automatic Control, 33(7):659-668, 1988.

[9] M. Tomizuka, T.-C. Tsao, and K.-K. Chew. Analysis and synthesis of discrete-time repetitive controllers. ASME Transactions on Journal of Dynamic Systems, Measurement and Control, 111: 353-358, 1989.

[10] T.-C. Tsao and M. Tomizuka. Robust adaptive and repetitive digital tracking control and application to hydraulic servo for noncircular machining. ASME Transactions on Journal of Dynamic Systems, Measurement and Control, 116 (1):24-32, 1994.

[11] Shamma, J. S., & Athans, M. (1990). Analysis of nonlinear gain scheduled control systems. IEEE Transactions on Automatic Control, AC-35(8), 898-907.

[12] Rugh, W. J. and Jeff S. Shamma (2000). Research on gain-scheduling. Automatica, 36, 1401-1425.

[13] Packard, A. (1994). Gain-scheduling via linear fractional transformations. Systems and Control Letters, 22, 79-92.

[14] Reichert, R. (1992). Dynamic scheduling of modern-robust-control autopilot designs for missiles. IEEE Control Systems Magazine, 12(5), 35-42.

[15] Rugh, W. J. (1983). Linearization about constant operating points: An input-output viewpoint. Proceedings of the IEEE conference on decision and control, San Antonio, TX (pp. 1165-1169).

[16] Rugh, W. J. (1991). Analytical framework for gain-scheduling. IEEE Control Systems Magazine, 11(1), 79-84.

[17] Shahruz, S. M., & Behtash, S. (1992). Design of controllers for linear parameter-varying systems by the gain scheduling technique. Journal of Mathematical Analysis and Applications, 168(1), 195-217.

[18] Shamma, J. S., & Athans, M. (1991). Guaranteed properties of gain scheduled control of linear parameter-varying plants. Automatica, 27(3), 898-907.

[19] Shamma, J. S., & Cloutier, J. R. (1992). Trajectory scheduled missile autopilot design. Proceedings of the first IEEE conference on control applications, Dayton, OH, September.

[20] Shamma, J. S., & Xiong, D. (1999). Set-valued methods for linear parameter varying systems. Automatica, 35(6), 1081-1089.

[21] Stilwell, D. J., & Rugh, W. J. (2000). Stability preserving interpolation methods for the synthesis of gain scheduled controllers. Automatica, 36(5), 665-671.

[22] P. Apkarian and P. Gahinet, “A convex characterization of gainscheduled H_inf controllers,” IEEE Trans. Automat. Contr., vol. 40, pp. 853–864 and p. 1681, May 1995.

[23] G. Becker, A. Packard, D. Philbrick, and G. Balas, “Control of parametrically-dependent linear systems: A single quadratic Lyapunov approach,” in Proc. Amer. Contr. Conf., San Fransisco, CA, 1993, pp. 2795–2799.

[24] P. Apkarian, P. Gahinet, and G. Becker, “Self-scheduled H_inf control of linear parameter-varying systems: A design example,” Automatica, vol. 31, pp. 1251–1261, Sept. 1995.

[25] F. Wu, X. Yang, A. Packard, and G. Becker, “Induced L2-norm control for LPV system with bounded parameter variations rates,” in Proc. Amer. Contr. Conf., Seattle, WA, 1995, pp. 2379–2383.

[26] P. Gahinet, P. Apkarian, and M. Chilali, “Parameter-dependent Lyapunov functions for real parametric uncertainty,” IEEE Trans. Automat. Contr., vol. 41, pp. 436–442, 1996.

[27] E. Feron, P. Apkarian, and P. Gahinet, “Analysis and synthesis of robust control systems via parameter-dependent Lyapunov functions,” IEEE Trans. Automat. Contr., vol. 41, pp. 1041–1046, July 1996.

[28] G. Becker, “Parameter-dependent control of an under-actuated mechanical system,” in Proc. IEEE Conf. Decision Contr., 1995.

[29] P. Apkarian, “On the discretization of LMI-synthesized linear parameter varying controllers,” Automatica, vol. 33, pp. 655–661, 1997.

[30] P. Gahinet and P. Apkarian, “A linear matrix inequality approach to H_inf control,” Int. J. Robust and Nonlinear Contr., vol. 4, pp. 421–448, 1994.

[31] P. Gahinet, “Explicit controller formulas for LMI-based H1 synthesis,” in Proc. Amer. Contr. Conf., 1994, pp. 2396–2400.

[32] G. Becker, “Additional results on parameter-dependent controllers for LPV systems,” in IFAC World Congr., San Fransisco, CA, 1996.

[33] S. Boyd and L. El Ghaoui, “Method of centers for minimizing generalized eigenvalues,” Linear Algebra Applicat., vol. 188, pp. 63–111, Apr. 1992.

[34] P. Apkarian and R. Adams, “Advanced gain-scheduling techniques for uncertain systems,” in Proc. Amer. Contr. Conf., June 1997, pp 3331–3335.

[35] V.L.Syrmos, C.T. Abdallah, P. Dorato, and K. Grigoriadis, “Static Output Feedback—A Survey,” in Automatica.,ol.33, No.2, pp125-137, 1997.

[36] A.I. Zecevic and D.D.Siljak, “Design of Robust Static Output Feedback for Large-scale Systems,” in IEEE Trans. Automat. Contr., vol. 49, No.11, pp. 2040–2044, Nov 2004.

[37] Zhang, Z., and Sun, Z., 2010. “A novel internal model based tracking control for a class of linear time-varying systems”. ASME Journal of Dynamic Systems, Measurement and Control, 132(1), pp. 011004–1–10.

[38] El Ghaoui, L. and P. Gahinet (1993). Rank minimization under LMI constraints: a framework for output feedback problems. In Proc. European Control. Co& Groningen, pp. 1176-1179.

[39] Grigoriadis, K. M. and R. E. Skelton (1993). Low-order control design for LMI problems using alternating projection methods. In Proc. 31st Allerton Conf on Communication, Control and Computing, Urbana-Champaign, IL. pp. 231-240.

[40] Grigoradis, K. M., & Skelton, R. E. (1996). Low-order control design for LMI problems using alternating projection methods. Automatica, 32(8), 1117 ‑ 1125.

[41] L.H.Lee, Identification and Robust Control of Linear Parameter Varying Systems, Ph.d. dissertation, Department of Mechanical Engineering, University of California at Berkeley (1997).

Chapter 9

Conclusion, Contributions Summary and Future Work

9.1 Conclusion

In conclusion, this thesis focuses on the design, dynamic analysis and control methodologies, which can enable the smooth and efficient power transmission for conventional, hybrid and future automotive propulsion systems. We formulate the problem in three levels: the basic clutch level, the intermediate driveline level and the entire propulsion system level. The critical research problems are revealed for each level, and the resolving design and control solutions are proposed accordingly.

First, for the clutch level, to realize a precise and efficient clutch actuation, the enabling approaches are presented in two categories: open loop and closed loop clutch control. The open loop actuation considers the consistent initial condition and the clutch fill process optimization. In the closed loop case, the solutions are further divided into two groups: the feedback control with sensor measurement and the closed loop control without sensor feedback. Second, for the driveline level, optimal driveline coordination is formulated into a nonlinear optimization problem, which is solved using the Dynamic Programming. Finally, for the propulsion system level, the power source start/stop torque pulses rejection is treated as a disturbance rejection using the time varying internal model framework. Two critical issues are addressed. One is the tracking control of the periodic signal with magnitude variation, and the other is the low order and robust stabilizer design for the time varying internal model controller. Both of them are the fundamental issues for the internal model control framework, and the research outcome can be potentially applied to other applications beyond the automotive field as well.

9.2 Contributions Summary

The contributions of this thesis span from the control applications to the fundamental control theory. Application wise, this thesis formulates the smooth and efficient power transmission design and control problem in three levels, and proposes

design, dynamics analysis and control methodologies to address the critical challenges in each level respectively. For control theory, a robust and low order stabilizer synthesis method is proposed to enable reference tracking/disturbance rejection based on linear time varying internal model principle. This thesis addresses one of the most crucial issues in the linear time varying internal model control synthesis, which enables experimental investigation of the internal model controller in the *LTV* setting.

9.2.1 Contributions in power transmission applications:

(1). Formulate the consistent initial condition control into an optimal ball capsule shape design using Dynamic Programming. Provide the mathematical derivation of the unique asymmetric valve orifice, which is not available in the literature. Reveal that the system dynamic instability is the key to realize fast response.

(2). Formulate the optimal clutch fill problem, and propose a novel customized dynamic programming method. The method can successfully avoid the stiff hydraulic dynamics which otherwise will cause intensive optimization computation for the control design. It can also avoid the interpolation error and the unreachable discrete states associated with the conventional DP. Experiments conducted to verify the control scheme.

(3). This thesis is the first research summary systematically documenting the analysis of the unique dynamics of the "wet" clutch actuation. It presents a systematic approach for controlling the "wet" clutch with only pressure feedback. More specifically, first, several unique phenomena of the "wet" clutch dynamics are revealed and are used to guide the robust control (sliding mode + observer) design. This makes the proposed control method more effective for this type of clutch system. Second, while directly applying the sliding mode controller may cause chattering, two approaches to constrain the feedback gain are applied and proved to be effective in the experiment. Finally, a nonlinear observer is designed to estimate the clutch motion with only pressure measurement.

(4). Propose a novel clutch control mechanism to realize closed loop control with no electronic sensor measurement. The feedback is realized by a built-in hydra-mechanical structure, and would ensure clutch fill preciseness and robustness comparing with pure

open loop control. Prototype was fabricated, dynamics model built, and experimental tests exhibit reliable and precise results.

(5).The optimal mathematical descriptions for smooth driveline coordination and slipping heat minimization formulated. Propose applying Dynamic Programming to solve the optimal engagement for automated manual transmission, which involves non-quadratic cost function and nonlinear dynamics. Comparing with existing suboptimal solution with quadratic cost function approximations, the results obtained are closer to the optimal solution.

(6). Apply the angle based repetitive control to fulfill the energy efficient vibration rejection for hybrid vehicle. The engine torque disturbance characteristics analyzed, and the corresponding controller synthesis provided.

9.2.2 Contributions in control theory:

(1). Based on the time varying internal model principle, formulate the tracking control of a unique group of signals, the periodic signal with magnitude variation. Derive its generating dynamics, and provide the asymptotic tracking control design.

(2). Solves a fundamental bottleneck problem in the linear time varying internal model control theory by proposing a novel low order robust stabilizer design. Convert the control synthesis conditions into a sequence of Linear Matrix Inequality (*LMI)* constraints, which could be solved efficiently by optimization algorithms. The significant impact is to enable the experimental realization of the linear time varying internal model control. The research results could potentially enable a wide class of control design based on linear time varying internal model principle, such as the repetitive control for linear time varying system.

9.3 Future Work

The future work will be outlined based on the three levels. First, for the clutch level, the designed ball capsule system (Chapter 2) is expected to be fabricated and tested in the experiment. Both the optimal design results and the derived asymmetric valve orifice equation should be verified from the experimental study. In addition, although the

optimal clutch fill (Chapter 3), the pressure based closed loop clutch actuation (Chapter 4) and the hydra-mechanical feedback clutch mechanism design (Chapter 5) have been evaluated with solid experimental data, the in-vehicle tests are expected to further demonstrate their effectiveness and robustness in different working environments. What's more, further design optimization on the novel hydra-mechanical feedback based clutch mechanism (Chapter 5) is expected. For example, the size of the system could be smaller to make it compact for transmission assembly. Second, for the driveline level design, the current Dynamic Programming based optimal coordination design (Chapter 6) is relatively computational intensive, therefore the study on the more computational efficient optimization method could be the research work in the next step. For the propulsion system level design, research on the angle based repetitive control for linear time varying plant using the proposed parameter dependent gain injection stabilizer (Chapter 8) will be the study for the next step. This control synthesis further requires extending the current continuous time *LPV* stabilizer design method to the discrete case, and then implementing the high order time varying repetitive controller for the experimental setup.

Bibliography[1]

- A.I. Zecevic and D.D.Siljak, "Design of Robust Static Output Feedback for Large-scale Systems," in IEEE Trans. Automat. Contr., vol. 49, No.11, pp. 2040–2044, Nov 2004.
- A. Isidori, C.I. Byrnes, Output regulation of nonlinear systems, IEEE Transactions on Automatic Control 35 (2) (1990), 131-140
- A. Bemporad, F. Borrelli, L. Glielmo, and F. Vasca, "Hybrid control of dry clutch engagement," in Proc. European Control Conf., Porto, Portugal, 2001.
- A. Szadkowski and R. B. Morford, "Clutch engagement simulation: Engagement without throttle," SAE Tech. Paper Series, no. 920766, 1992.
- A.Ichikawa, H.Katayama, Output regulation of time-varying systems, IEEE Transactions on Automatic Control 35 (2) (1990) 131-140
- Bai, S., Moses, R.L, Schanz, Todd and Gorman, M.J. "Development of A New Clutch-to-Clutch Shift Control Technology". SAE Technical Paper 2002-01-1252.
- Bellman, R., 1957, Dynamic Programming, Princeton University Press, New Jersey.
- Bellman, R. and Dreyfus, S., 1962, Applied Dynamic Programming, Princeton University Press, New Jersey.
- Bertsekas, D., Dynamic Programming and Optimal Control, Athena Scientific, 1995.
- Baumann, J., Torkzadeh, D.D., Ramstein, A., Kienke, U., and Schelegl, Model-based predictive anti-jerk control T. Control Engineering Practice, 14, 259–266 (2006).
- Balfour, G., Dupraz, P., Ramsbottom, M., and Scotson, Diesel fuel injection control for optimum driveability SAE 2000-01-0265.
- B.A. Francis. The internal model principle of control theory. SIAM Journal of Control, vol. 15 (3), pp. 486-505, 1977.
- B.A. Fancis, and W.M. Wonham. The internal model principle of control theory. Automatica, vol. 12 (5), pp. 457-465, 1976.

[1] The numbered references in each chapter refer to the reference lists at the end of each chapter, and the cumulative bibliography here summarizes all the cited work throughout the thesis.

- Crassidis, J.L. and Junkins, J.L. “Optimal Estimation of Dynamic Systems”. Chapman and Hall/CRC Applied Mathematics and Nonlinear Science Series, CRC Express LLC, 2004.
- Daekyun Kim, Huei Peng, Shushan Bai, and Joel M. Maguire. “Control of Integrated Powertrain with Electronic Throttle and Automatic Transmission.” IEEE Transactions on Control Systems Technology, Vol. 15, Issue 3, pp. 474 – 482, May 2007
- De Madrid, A.P. Dormido, S., and Morilla, F., “Reduction of the Dimensionality of Dynamic Programming: A Case Study,” Pro. Of 1999 American Control Conference, pp 2852-2856, June 1999
- D. Centea, H. Rahnejat, and M. T. Menday, “The influence of the interface coefficient of friction upon the propensity to judder in automotive clutches,” Proc. Inst. Mech. Eng., vol. 213, pt. D, pp. 245–268, 1999.
- DeLaSalle, S., Jansz, M., and Light, D. (1999), Design of a Feedback Control System for Damping of Vehicle Shuffle. Proceedings of the EAEC Conference, Barcelona, pp 278–284.
- E. Feron, P. Apkarian, and P. Gahinet, “Analysis and synthesis of robust control systems via parameter-dependent Lyapunov functions,” IEEE Trans. Automat. Contr., vol. 41, pp. 1041–1046, July 1996.
- El Ghaoui, L. and P. Gahinet (1993). Rank minimization under LMI constraints: a framework for output feedback problems. In Proc. European Control. Co& Groningen, pp. 1176-1179.
- E. M. A. Rabeih and D. A. Crolla, “Intelligent control of clutch judder and shunt phenomena in vehicle drivelines,” Int. J. Veh. Des., vol. 17, no. 3, pp. 318–332, 1996
- F. Garofalo, L. Glielmo, L. Iannelli, and F. Vasca, “Smooth engagement for automotive dry clutch” in Proc. 40th IEEE Conf. Decision and Control, Orlando, FL, 2001, pp. 529-534

- F. Amisano, G. Serra, and M. Velardocchia, “Engine control strategy to optimize a shift transient during clutch engagement,” SAE Tech. Paper Series, no. 2001-01-0877, pp. 115–120, 2001.
- F. Amisano, R. Flora, and M. Velardocchia, “A linear thermal model for an automotive clutch,” SAE Tech. Paper Series, no. 2000-01-0834, 2000.
- F. Wu, X. Yang, A. Packard, and G. Becker, “Induced L2-norm control for LPV system with bounded parameter variations rates,” in Proc. Amer. Contr. Conf., Seattle, WA, 1995, pp. 2379–2383.
- Gautschi, W., 1997. Numerical Analysis: An Introduction, Birkhauser Boston
- Gao, B., Chen, H., Sanada, K., Hu, Y., “Design of Clutch-Slip Controller for Automatic Transmission Using Backstepping,” IEEE/ASME Transactions on Mechatronics, in press, 2010.
- Gao, B., Chen, H., Sanada, “A Reduced Order Nonlinear Clutch Pressure Observer for Automatic Transmission,” IEEE Transactions on Control Systems Technology, Vol. 18, Issue.2, pp. 446-453, March., 2010.
- G. Becker, “Additional results on parameter-dependent controllers for LPV systems,” in IFAC World Congr., San Fransisco, CA, 1996.
- G. Becker, “Parameter-dependent control of an under-actuated mechanical system,” in Proc. IEEE Conf. Decision Contr., 1995.
- G. Becker, A. Packard, D. Philbrick, and G. Balas, “Control of parametrically-dependent linear systems: A single quadratic Lyapunov approach,” in Proc. Amer. Contr. Conf., San Fransisco, CA, 1993, pp. 2795–2799.
- Glielmo, L. Iannelli, L. Vacca, V. and Vasca, F. “Gearshift Control for Automated Manual Transmissions”, IEEE/ASME Transactions on Mechatronics, VOL 11, No. 1, Feb., 2006.
- Grigoriadis, K. M. and R. E. Skelton (1993). Low-order control design for LMI problems using alternating projection methods. In Proc. 31st Allerton Conf on Communication, Control and Computing, Urbana-Champaign, IL. pp. 231-240.
- Grigoradis, K. M., & Skelton, R. E. (1996). Low-order control design for LMI problems using alternating projection methods. Automatica, 32(8), 1117 – 1125.

- Han, W. and Yi, S.J., "A Study of Shift Control Using the Clutch Pressure Pattern in Automatic Transmission." Proc. Instn Mech. Engrs vol. 217 Part D: J. Automobile Engineering. Volume 217, Number 4/2003, pp 289-298
- Hairer, E., Wanner, G., 1996. Solving Ordinary Differential Equations II (second edition), Springer Series in Computational Mathematics
- Hebbale, K.V. and Kao, C.-K., "Adaptive Control of Shifts in Automatic Transmissions". Proceedings of the 1995 ASME International Mechanical Engineering Congress and Exposition, San Francisco, CA, 1995.
- Horn, J., Bamberger, J., Michau, P., Pindl, S., "Flatness-based Clutch Control for Automated Manual Transmissions", Journal of Control Engineering Practice, Vol. 11, Issue 12, pp. 1353-1359, Dec., 2003.
- H. Meritt, Hydraulic Control Systems, New York: Wiley, 1967.
- H. Tanaka and H. Wada, "Fuzzy control of clutch engagement for automated manual transmission," Veh. Syst. Dyn., vol. 24, pp. 365–376, 1995.
- http://www.adi.com/products_emu_pci.htm, 2009
- I. Kolamanovsky, I. Siverguina, and B. Lygoe, "Optimization of Powertrain Operating Policy for Feasibility Assessment and Calibration: Stochastic Dynamic Programming Approach," Proceedings of the American Control Conference, Anchorage, AK, pp 1425-1430, May 8-10, 2002
- J.M. Kang, I. Kolmanovsky and J.W. Grizzle, "Dynamic Optimization of Lean Burn Engine Aftertreatment." ASME Transactions on Journal of Dynamic Systems, Measurement, and Control, Vol. 123/153, pp. 153-160, June 2001
- John, H. and Lapidus, L., "Aspects of the Forward Dynamic Programming Algorithm", I&EC Process Design and Development, 1968.
- J. Liu, and H. Peng. Modeling and control of a power-split hybrid vehicle. IEEE Transactions on Control Systems Technology, vol. 16 (6) pp. 1242-1251, 2008.
- J. Fredriksson and B. Egardt, "Nonlinear control applied to gearshifting in automated manual transmission," in Proc. 39th IEEE Conf. Decision and Control, Sydney, Australia, 2000, pp. 444–449.

- J. Meisel. An Analytical Foundation for the Toyota Prius THS-II Powertrain with a Comparison to a Strong Parallel Hybrid-Electric Powertrain. SAE technical paper 2006-01-0666.
- J. Slicker and R. N. K. Loh, "Design of robust vehicle launch control system," IEEE Trans. Contr. Syst. Technol., vol. 4, no. 4, pp. 326–335, Jul. 1996.
- K. Hayashi, Y. Shimizu, S. Nakamura, Y. Dote, A. Takayama, and A. Hirako, "Neuro fuzzy optimal transmission control for automobile with variable loads," in Proc. IEEE Industrial Electronics, Control, and Instrumentation Conf., Maui, HI, 1993, vol. 1, pp. 430–434
- Karnopp, D., "Computer Simulation of Stick-Slip Friction in Mechanical Dynamic Systems", Journal of Dynamic Systems, Measurement, and Control, Vol. 107, No. 1, pp. 100-103, March, 1985.
- Khalil, H., Nonlinear Systems, Third Edition, Pearson Education, Inc., 2002.
- K.S. Tsakalis, P.A. Ioanou, Linear Time-Varying Systems: Control and Adaptation, in: Advances in Industrial Control, Prentice Hall, Englewood Cliffs, NJ, 1993
- Larson, R. and Casti, J., 1978, Principles of Dynamic Programming: Basic Analytical and Computational Methods, Marcel Dekker Inc., New York and Basel.
- Lee, C.J., Hebbale, K.V. and Bai, S., "Control of a Friction Launch Automatic Transmission Using a Range Clutch". Proceedings of the 2006 ASME International Mechanical Engineering Congress and Exposition, Chicago, Illinois, 2006.
- Langjord, H., Johansen, T., "Dual-Mode Switched Control of an Electropneumatic Clutch Actuator," IEEE/ASME Transactions on Mechatronics, in press, 2010.
- L. Glielmo, L. and F. Vasca, "Engagement Control for Automotive Dry Clutch", Proceedings of 2000 American Control Conference, Chicago, Illinois, pp. 1016-1017, June, 2000.
- Luigi Glielmo , Luigi Iannelli, Vladimiro Vacca, Francesco Vasca, "Speed Control for Automated Manual Transmission with Dry Clutch", 43rd IEEE Conference on Decision and Control, 1709—1714, Atlantis, Paradise Island, Bahamas, December 14-17, 2004

- L. Glielmo and F. Vasca, "Optimal control of dry clutch engagement," SAE Trans., J. Passenger Cars: Mech. Syst., vol. 6, no. 2000-01-0837, 2000.
- L.H.Lee, Identification and Robust Control of Linear Parameter Varying Systems, Ph.d. dissertation, Department of Mechanical Engineering, University of California at Berkeley (1997).
- Miao, H., Sun, Z., Fair, J., Lehrmann, J., Harbin, S. "Modeling and Analysis of the Hydraulic System for Oil Budget in an Automotive Transmission". Proceedings of ASME 2008 Dynamic Systems and Control Conference, Ann Arbor, Michigan, USA, October 20-22, 2008
- Montanari, M., Ronchi, F., Rossi, C., Tilli, A., Tonielli, A., "Control and Performance Evaluation of a Clutch Servo System With Hydraulic Actuation", Journal of Control Engineering Practice, Vol. 12, Issue 11, pp. 1369-1379, Nov, 2004
- Mo, C.Y., Beaumount, A.J., and Powell, N.N. (1996), SAE 960046, Active Control of driveability, pp 215–221.
- M. Levin, et. al. Hybrid powertrain with an engine-disconnection clutch. SAE Technical Paper Series 2002-01-0930, 2002.
- M. Tomizuka, T.-C. Tsao, and K.-K. Chew. Analysis and synthesis of discrete-time repetitive controllers. ASME Transactions on Journal of Dynamic Systems, Measurement and Control, 111: 353-358, 1989.
- M. Ducusin, S. Gargies, and C. Mi. Modeling of a series hybrid electric high-mobility multipurpose wheeled vehicle. IEEE Transactions on Vehicular Technology, Vol. 56, no. 2, pp. 557-565, 2007.
- Manring, N., 2005, Hydraulic Control Systems, John Wiley & Sons, Hoboken, New Jersey.
- M. Levin, et. al. Hybrid powertrain with an engine-disconnection clutch. In SAE Technical Paper Series 2002-01-0930, 2002.
- Marano, J.E, Moorman, S.P., Whitton, M.D., and Williams, R.L. "Clutch to Clutch Transmission Control Strategy". SAE Technical Paper 2007-01-1313/

- P. Pisu, G. Rizzoni G. A comparative study of supervisory control strategies for hybrid electric vehicles. IEEE Transactions on Control Systems Technology, Vol. 15, no. 3, pp. 506-518, 2007.
- Packard, A. (1994). Gain-scheduling via linear fractional transformations. Systems and Control Letters, 22, 79-92.
- P. Apkarian and P. Gahinet, "A convex characterization of gain scheduled H_inf controllers," IEEE Trans. Automat. Contr., vol. 40, pp. 853–864 and p. 1681, May 1995.
- P. Apkarian, P. Gahinet, and G. Becker, "Self-scheduled H_inf control of linear parameter-varying systems: A design example," Automatica, vol. 31, pp. 1251–1261, Sept. 1995.
- P. Apkarian and R. Adams, "Advanced gain-scheduling techniques for uncertain systems," in Proc. Amer. Contr. Conf., June 1997, pp 3331–3335.
- P. Apkarian, "On the discretization of LMI-synthesized linear parameter varying controllers," Automatica, vol. 33, pp. 655–661, 1997.
- P. Gahinet and P. Apkarian, "A linear matrix inequality approach to H_inf control," Int. J. Robust and Nonlinear Contr., vol. 4, pp. 421–448, 1994.
- P. Gahinet, "Explicit controller formulas for LMI-based H1 synthesis," in Proc. Amer. Contr. Conf., 1994, pp. 2396–2400.
- P. Gahinet, P. Apkarian, and M. Chilali, "Parameter-dependent Lyapunov functions for real parametric uncertainty," IEEE Trans. Automat. Contr., vol. 41, pp. 436–442, 1996.
- Rugh, W. J. and Jeff S. Shamma (2000). Research on gain-scheduling. Automatica, 36, 1401-1425.
- Reichert, R. (1992). Dynamic scheduling of modern-robust-control autopilot designs for missiles. IEEE Control Systems Magazine, 12(5), 35-42.
- Rugh, W. J. (1983). Linearization about constant operating points: An input-output viewpoint. Proceedings of the IEEE conference on decision and control, San Antonio, TX (pp. 1165-1169).
- Rugh, W. J. (1991). Analytical framework for gain-scheduling. IEEE Control Systems Magazine, 11(1), 79-84.

- Shamma, J. S., & Athans, M. (1990). Analysis of nonlinear gain scheduled control systems. IEEE Transactions on Automatic Control, AC-35(8), 898-907.
- Shahruz, S. M., & Behtash, S. (1992). Design of controllers for linear parameter-varying systems by the gain scheduling technique. Journal of Mathematical Analysis and Applications, 168(1), 195-217.
- Shamma, J. S., & Athans, M. (1991). Guaranteed properties of gain scheduled control of linear parameter-varying plants. Automatica, 27(3), 898-907.
- Shamma, J. S., & Cloutier, J. R. (1992). Trajectory scheduled missile autopilot design. Proceedings of the first IEEE conference on control applications, Dayton, OH, September.
- Shamma, J. S., & Xiong, D. (1999). Set-valued methods for linear parameter varying systems. Automatica, 35(6), 1081-1089.
- Stilwell, D. J., & Rugh, W. J. (2000). Stability preserving interpolation methods for the synthesis of gain scheduled controllers. Automatica, 36(5), 665-671.
- S. Boyd and L. El Ghaoui, "Method of centers for minimizing generalized eigenvalues," Linear Algebra Applicat., vol. 188, pp. 63–111, Apr. 1992.
- S. Hara, Y. Yamamoto, T. Omata, and M. Nakano. Repetitive control systems: a new type servo system for periodic exogenous signals. IEEE Transactions on Automatic Control, 33(7):659-668, 1988.
- S. Tomura, Y. Ito, K. Kamichi, and A. Yamanaka. Development of vibration reduction motor control for series-parallel hybrid system. In SAE Technical Paper Series 2006-01-1125, 2006.
- Song, X., Zulkefli, A., Sun, Z. and Miao, H., "Transmission Clutch Fill Control Using A Customized Dynamic Programming Method", Proceedings of the 2008 ASME Dynamic System and Control Conference, DSCC 2008-2166, Ann Arbor, Michigan, 2008.
- Song, X., Zulkefli, A., Sun, Z. and Miao, H., "Modeling, Analysis, and Optimal Design of the Automotive Transmission Ball Capsule System", ASME Transactions on Journal of Dynamic Systems, Measurement and Control, Vol. 132, 021003, March, 2010.

- Song, X., Sun, Z., Yang, X., Zhu, G., "Modeling, Control and Hardware-in-the-Loop Simulation of an Automated Manual Transmission", Proc. Instn Mech. Engrs Part D: Journal of Automobile Engineering, Vol. 224, No. 2, pp.143-160, 2010.
- Song, X., Mohd Zulkefli, A., and Sun, Z., "Automotive Transmission Clutch Fill Optimal Control: An Experimental Investigation", Proceedings of 2010 American Control Conference, Baltimore, MD, USA, June 30-July 2nd, 2010.
- Song, X. and Sun, Z., "Pressure Based Clutch Control for Automotive Transmissions Using a Sliding Mode Controller", in press, IEEE Transactions on Mechatronics, 2011.
- Song, X., Mohd Zulkefli, A., Sun, Z. and Miao, H., "Automotive Transmission Clutch Fill Control Using a Customized Dynamic Programming Method", in press, ASME Transactions on Journal of Dynamic Systems, Measurement and Control, 2010.
- Song, X., Zulkefli, A., Sun, Z. and Miao, H., "Transmission Clutch Fill Control Using A Customized Dynamic Programming Method". Proceedings of the 2008 ASME Dynamic System and Control Conference, DSC2008-2166, Ann Arbor, Michigan, 2008.
- Sanada, K., Kitagawa, A., "A Study of Two-degree-of-freedom Control of Rotating Speed in an Automatic Transmission, Considering Modeling Errors of a Hydraulic System", Journal of Control Engineering Practice, Vol. 6, Issue 9, pp. 1125-1132, Dec., 1998.
- Sun, Z., "Electro-Hydraulic Fully Flexible Valve Actuation System with Internal Feedback", ASME Transactions on Journal of Dynamic Systems, Measurement and Control, Vol. 131, 024502, March 2009.
- Sun, Z. and Hebbale, K., "Challenges and Opportunities in Automotive Transmission Control", Proceedings of 2005 American Control Conference, Portland, OR, USA, June 8-10, 2005.
- S. Tomura, Y. Ito, K. Kamichi, and A. Yamanaka. Development of vibration reduction motor control for series-parallel hybrid system. In SAE Technical Paper Series 2006-01-1125, 2006.

- S. Kim, J. Park, J. Hong, M. Lee and H. Sim. Transient control strategy of hybrid electric vehicle during mode change. In SAE Technical Paper Series 2009-01-0228, 2009
- T. Kuo. Valve and fueling strategy for operating a controlled auto-ignition combustion engine. In SAE 2006 Homogeneous Charge Compression Ignition Symposium, pp. 11-24, San Ramon, CA, 2006.
- T. Kuo, Z. Sun, J. Eng, B. Brown, P. Najt, J. Kang, C. Chang, and M. Chang. Method of HCCI and SI combustion control for a direct injection internal combustion engine. U.S. patent 7,275,514, 2007.
- T. Goro, et al. Development of the hybrid system for the Saturn VUE hybrid. SAE technical paper 2006-01-1502.
- T. Grewe, B. Conlon, and A. Holmes. Defining the General Motors 2-Mode Hybrid Transmission. SAE technical paper 2007-01-0273.
- T.-C. Tsao and M. Tomizuka. Robust adaptive and repetitive digital tracking control and application to hydraulic servo for noncircular machining. ASME Transactions on Journal of Dynamic Systems, Measurement and Control, 116 (1):24-32, 1994.
- V.L.Syrmos, C.T. Abdallah, P. Dorato, and K. Grigoriadis, “Static Output Feedback—A Survey,” in Automatica.,ol.33, No.2, pp125-137, 1997.
- Vasca, F., Iannelli, L., Senatore, A., Reale, G. , "Torque Transmissibility Assessment for Automotive Dry-Clutch Engagement," IEEE/ASME Transactions on Mechatronics, , no.99, pp.1-10, in press.
- Wagner, G., “Application of Transmission Systems for Different Driveline Configurations in Passenger Cars”. SAE Technical Paper 2001-01-0882.
- Yu, J., Chen, Z., and Lu, Y., “ The Variation of Oil Effective Bulk Modulus With Pressure in Hydraulic Systems”, Journal of Dynamic Systems, Measurement, and Control, Vol. 116, No. 1, pp. 146-150, March, 1994.
- Y. Lei, M. Niu, and A. Ge, “A research on starting control strategy of vehicle with AMT,” in Proc. FISITA World Automotive Congress, Seoul, Korea, 2000.

- Y. J. Kim, Z. Filipi. Series hydraulic hybrid propulsion for a light truck - optimizing the thermostatic power management. SAE paper 2007-24-0080, 2008 SAE Transactions, Journal of Engines.
- Zhang, Y., Chen, X., Zhang, X., Jiang, H., and Tobler, W., "Dynamic Modeling and Simulation of a Dual-Clutch Automated Lay-Shaft Transmission", ASME Journal of Mechanical Design Vol. 127, Issue. 2, pp. 302-307, March, 2005.
- Z. Sun, Z. Zhang, and T.-C. Tsao. Trajectory tracking and disturbance rejection of linear time-varying systems: input/output representation. Systems and Control Letters, vol. 58 (6): 452-460, 2009.
- Z. Zhang, A. Serrani, The linear periodic output regulation problem, Systems & Control Letters 55(7) (200) 518-529
- Z. Zhang, A. Serrani, The linear periodic output regulation problem, Systems & Control Letters 55(7) (200) 518-529
- Zhang, Z., and Sun, Z., 2010. "A novel internal model based tracking control for a class of linear time-varying systems". ASME Journal of Dynamic Systems, Measurement and Control, 132(1), pp. 011004–1–10.